Investigating the role of Histone Post Translational Modifications in yeast Stationary Phase

A dissertation presented for the degree of Doctor of Philosophy, in the Faculty of Science, Trinity College Dublin by

Zain Mohammedfaowzi Baazeem

February 2026

Moyne Institute of Preventive Medicine

Department of Microbiology

School of Genetics and Microbiology

Trinity College Dublin

University of Dublin

Declaration

I declare that this thesis has not been submitted as an exercise for a degree at this or any other university and it is entirely my own work, except where it is duly acknowledged in the text.

I agree to deposit this thesis in the University's open-access institutional repository or allow the library to do so on my behalf, subject to Irish Copyright Legislation and Trinity College Library conditions of use and acknowledgement.

I consent to the examiner retaining a copy of the thesis beyond the examining period.



Zain Baazeem

30-09-2025

Summary

The aim of this thesis was to determine how the chromatin modifications, histone H2B ubiquitination (H2Bub) and H3 K36 methylation (H3K36me), influence the development and maintenance of cellular quiescence in the yeast, *Saccharomyces cerevisiae*. Single and double mutants deficient for H2Bub (*htb-K123RΔ*) and H3K36me (*hht-K36AΔ*) were therefore characterised during growth into stationary phase, during which time cellular quiescence normally develops. The aim was to test the hypothesis that H2Bub and H3K36me are required to ensure the proper transcriptional pathways occur to establish quiescent cells and maintain their transcriptional silencing and survival in the absence of glucose.

A clear growth delay was seen due to loss of H3K36me, whereas even slower proliferation and lower final cell densities in rich medium were seen in the double mutant. However, glucose uptake was unaffected in any of the mutants. Hypersensitivity to DNA damage, cell wall stress, and osmotic shock was shown by the double mutant in stationary phase.

All core histone proteins levels were similar to wild-type levels in each mutant during exponential growth and at the diauxic shift. However, H3 was abnormally elevated in stationary phase double mutant cells suggesting H2Bub and H3K36me contribute to correct histone stoichiometry after prolonged glucose depletion. Increased linker histone H1 (Hho1p) levels were seen during exponential growth in all mutants, suggesting that in transcriptionally active conditions these marks normally restrain H1 abundance. Together, these data suggest a role for H2Bub and H3K36me in maintaining correct chromatin structure during growth into stationary phase.

High H3K14ac, H4ac4, and H3K9ac during exponential growth and repression of these marks in stationary phase was seen in wild-type cells. However, elevated H3K14ac and H4Ac4 levels were seen in all mutants during exponential growth, indicating hyperacetylation when H2Bub and/or H3K36me are lost. Furthermore, in stationary phase, the double mutant fails to repress these marks, indicating defective establishment of a repressed chromatin state occurs in the absence of both H2Bub and H3K36me.

Stationary-phase development was perturbed in all mutants. However, a bias toward increased quiescent (Q) cell formation was seen in the H2Bub-deficient mutant and the population of

quiescent cells that were formed showed progressive viability loss over time. Conversely, the non-quiescent (NQ) cells formed in the H2Bub-deficent mutant showed increased survival. This suggests a role for H2Bub in potentially opposing apoptosis in quiescent cells and promoting apoptosis in the non-quiescent cell population. Conversely, H3K36me loss resulted in a bias toward elevated NQ cell formation and reduced viability in both Q and NQ pools. A blurred Q/NQ identity was seen in the double mutant highlighting synergistic disruption of the chromatin-governed quiescence program.

RNA-Seq analysis of day 7 purified quiescent cells revealed that the H3K36me-deficient mutant showed the greatest numbers of up and downregulated genes compared to the H2Bub-deficient mutant. However, the impact upon gene activation and repression in the H3K36me-deficient mutant was reduced when the site for H2Bub was additionally mutated in the double mutant. This suggests a dominant role for H3K36me in governing activation and repression of gene transcription in quiescent cells and that H2Bub contributes to the de-repression and repression of transcription evident in the absence of H3K36me.

Overall, the data suggest that there is a complex non-additive epistasis occurring between H2Bub and H3K36me which is required to properly remodel chromatin in quiescence and correctly regulate transcription.

Acknowledgements

In the name of God, the Most Merciful, the Most Compassionate. I begin by expressing my deepest gratitude to Almighty Allah for granting me strength, patience, and countless blessings throughout this journey. Without His guidance, none of this would have been possible.

My deepest thanks go to my supervisor, Prof. Alastair Fleming, for his unwavering support, guidance, and kindness. His encouragement, wisdom, and humanity have shaped not only this thesis but also my personal and academic growth. I will remain forever grateful for his mentorship.

I am sincerely thankful to Dr. Karsten Hokamp for his invaluable guidance with data analysis, and to my thesis committee Dr. Carsten Kröger, Dr. Siobhán O'Brien, and Dr. Máire Ní Leathlobhair for their constructive feedback and encouragement. My thanks also go to Dr. Marta Martins, Head of Department, for her continued support.

Special appreciation is due to the Moyne Institute office and technical staff, whose kindness and help created a supportive environment, especially during my illness and recovery. I am also grateful to all Fleming lab members and the Microbiology Department for their friendship and assistance.

To my dear friends Kevin Mercurio, Rebecca Owens, Cian McNulty, Xuyuan Guo, Dr. Reham Al-Najjar, and Dr. Hala Al-Layas thank you for being my family away from home and for bringing joy and strength to this journey.

On a personal level, I am eternally indebted to my parents, Mohammedfawzi Baazeem and Awatif Azizalurahman, for their prayers, love, and unwavering support, and to my siblings Rami, Zouhar, Reham, and Anfal for their encouragement and care. My nieces and nephews Toleen, Leen, Joudi, Wateen, Lateen, Lareen, Ahmed, Lojain, and Mouna have been a constant source of joy. My heartfelt thanks to my brother Rami, my soulmate throughout my postgraduate journey since Brisbane, Australia. You have been my inspiration and my role model.

I also extend my gratitude to Khamael Khamis and Amani Al-suwayni for their encouragement throughout this journey.

I am grateful to King Abdulaziz University, Saudi Arabia, for financial support, with special thanks to Prof. Ibrahim Ali Al-Zahrani, Dr. Hashim Felemban, Dr. Ammar Basabrin and Dr. Mohammed Al-Hashimi and to the Royal Embassy of Saudi Arabia in Dublin for their assistance.

Finally, my heartfelt thanks to Dr.Yasmin Adel Ali Fergani for her encouragement and guidance.

This thesis is not only my effort but also a reflection of the love, support, and inspiration I have received from so many wonderful people. To each of you, I offer my deepest gratitude.

Dedication

To God Almighty, for granting me strength, patience, and wisdom.

To my late grandmother—may God bless her soul—whose dream of higher education continues to inspire me.

To my parents, for instilling in me the values of education, perseverance, and hard work.

To my brothers, sisters, and their children, for their constant love and encouragement.

To my supervisor, Prof. Alastair Fleming, for his invaluable guidance, support, and inspiration throughout this journey.

And to myself, for the perseverance and resilience that made this achievement possible.

I am proud of you.



ZAIN M BAAZEEM

Conferences

1. Baazeem ZM. and Fleming AB. 2025, (March 2-5th). Investigating the role of histone post translational modifications in yeast stationary phase. Poster Presentation at 17th European Conference on Fungal Genetics (ECFG17) Convention Centre Dublin, Ireland.
2. Baazeem ZM. and Fleming AB. 2024, (August 11-15th). Investigating the role of histone post translational modifications in yeast stationary phase. Poster Presentation at 12th edition of the International Mycological Congress, held in Maastricht, The Netherlands.
3. Baazeem ZM. and Fleming AB. 2023, (June 1st). Attended at DAPI at University College Dublin (UCD) in Ireland.
4. Baazeem ZM. and Fleming AB. 2023, (June 22nd). Investigating the role of histone post translational modifications in yeast stationary phase. Poster Presentation at the IFS (Irish FungalSociety) Annual Conference at Dublin College University (DCU) in Ireland.
5. Baazeem ZM. and Fleming AB. Attended at Lumivero Virtual Conference for data statistical analysis. 2023 (September 27-28th).
6. Baazeem ZM. and Fleming AB. 2022, (December 8th). Investigating the role of histone post translational modifications in yeast stationary phase. Poster presentation SGM Xmas social at the Atrium of the Smurfit Institute of Genetics at Trinity College Dublin (TCD) in Ireland.
7. Baazeem ZM. and Fleming AB. Attended at NK Cell Therapy Workshop Proteintech online event. Awarded by Proteintech Group. 2024 (July 9th).
8. Baazeem ZM. and Fleming AB. Attended at University Biological Safety Workshop. 2022 (June 15th) University Safety Officer (Biological Hazards) Trinity College of Dublin.

Table of Contents

Declaration ..... *ii*

Summary ..... *iii*

Acknowledgements ..... *v*

Dedication ..... *vii*

Conferences ..... *viii*

List of Tables ..... *xvi*

Index of Figures ..... *xviii*

Chapter 1 ..... *1*

Introduction *1*

1.1 Overview **2**

1.2 Historical background and Importance of Chromatin Structure **2**

1.3 The core histones **4**

1.4 Histone post-translational modifications (PTMs) **6**

1.5 Chromatin as a regulator of Gene Expression **8**

1.5.1 ATP-dependent chromatin remodelling 9

1.5.2 Chromatin and Transcription 10

1.6 Transcriptional Control in Yeast **11**

1.6.1 Gene Promoters in Yeast 11

1.6.2 Initiation, Elongation, Termination of transcription 13

i. Initiation of Transcription 13

ii. Elongation 13

iii. Termination 13

1.7 Mediator Complex **14**

1.8 The role of histone H2B ubiquitylation and histone H3 methylation in transcription **14**

1.8.1 Histone H2B monoubiquitylation 14

1.8.2 Mechanism of H2B Ubiquitylation 15

1.8.3 Role of H2Bub in transcription elongation: 16

1.9 Histone methylation in yeast **17**

1.9.1 The role of H3 lysine 36 methylation during transcription 18

1.10 The PAF Complex as a Multifunctional Regulator of RNA Polymerase II Transcription **19**

1.10.1 PAF Regulation through Interaction with Pol II Elongation Machinery and Promoter-Associated Transcription Factors 20

1.10.2 The PAF Complex's Role in H2B Monoubiquitylation 20

1.11 Yeast Stationary Phase **21**

1.11.1 Distinct Cell Populations: Quiescent (Q) and Non-Quiescent (NQ) 22
1.11.2 Implications of Studying Q and NQ Cells 23
1.12 Chromatin Remodelling During the Stationary Phase in Yeast 24
1.13 The Aim of This Research 25
1.14 The specific objectives: 25
Chapter 2 27
Materials & Methods 27
2.1 Chemicals, reagents and growth media 27
2.1.1 Chemicals and reagents 27
2.1.2 Growth media 27
2.1.3 Yeast extract, peptone, dextrose broth and media 28
2.2 Yeast strains 28
2.2.1 Yeast culture conditions 28
2.3 Growth Curve and Final Cell Density 30
2.4 Microscope images of the yeast cells (Cell morphology) 30
2.5 Growth 'Spot' Tests 31
2.6 Fractionation of stationary phase cultures 31
2.6.1 Preparation of Percoll density gradient 31
2.6.2 Density gradient separation of yeast cultures 32
2.7 Western blot analysis 33
2.7.1 Protein Extraction 33
2.7.2 Bradford Assay 34
2.7.3 SDS-Polyacrylamide gel electrophoresis (SDS-PAGE) 35
2.7.3.1 Preparation of protein samples for SDS-PAGE 35
2.7.3.2 Preparation and running of SDS-PAGE 35
2.7.4 Western Blot 36
2.7.4.1 Detection of protein antigens 37
2.8 Isolation of RNA 39
2.8.1 RNA Extraction 39
2.8.1.1 Ethanol Precipitation 40
2.8.1.2 Determination of nucleic acid concentration 40
2.8.2 RNA-Seq 41
2.9 Statistical analysis 43
Chapter 3 44
Characterisation of mutants deficient for 44
histone H2B monoubiqitylation and H3 lysine 36 methylation 44
3.1 Introduction 45
3.2 Results 47

3.2.1 Confirmation of wild-type, *htb-K123RΔ, hht-K36AΔ,* and *K123R-K36AΔ* strains 47
3.2.2 Section 1: Phenotypic characterisation of wild-type and mutants during growth into stationary phase. 48
3.2.2.1 Single and double mutants deficient for H2Bub and H3K36me show distinct phenotypes 48
3.2.2.2 Analysis of growth in liquid media containing glucose 48
3.2.2.3 Analysis of cell density during entry into stationary phase 49
3.2.2.4 Measuring Glucose Depletion in Yeast Growth 50
3.2.2.5 Analysis of cell viability during the stationary phase 51
3.2.2.6 Analysing *htb-K123RΔ,hht-K36AΔ* and *K123R-K36AΔ* mutant cell morphology 52
3.2.3 Section 2: Testing for phenotypes in exponential and stationary phase cells by challenging cells in various 'spot tests' 53
3.2.3.1 Analysis of temperature sensitivity 54
3.2.3.2 Analysis of the ability to grow on different carbon sources 55
3.2.3.3 Analysis of growth on a non-fermentable carbon source 56
3.2.3.4 Analysis of responses to DNA damage caused by camptothecin. 57
3.2.3.5 Analysis of the growth response to the DNA-damaging agent, methyl methane sulfonate 58
3.2.3.6 Analysis of the growth response to DNA-damaging agent, hydroxy urea 59
3.2.3.7 Analysis of sensitivity to caffeine 60
3.2.3.8 Analysis of sensitivity to oxidative stress 62
3.2.3.9 Analysis of sensitivity to Osmotic and Ionic Stress Response 63
3.2.3.10 Analysis of sensitivity to Chemical Stress 64
3.2.4 Section 3: Investigating the transcriptional and chromatin landscape in wild-type and mutants during growth into stationary phase: 65
3.2.4.1 Investigating RNA Pol II levels in unseparated mutant cells during SP. 66
3.2.4.2 Regulation of PAF1 Complex During Growth into SP 68
3.2.4.3 Analysing Core Histone Levels as Cells Grow into Stationary Phase (SP) 70
3.2.4.4 Analysis of Hho1p Abundance During Stationary Phase (SP) 71
3.2.4.5 Histone acetylation levels during exponential growth and stationary phase in wild-type and histone modification-deficient yeast mutants. 74
3.2.4.6 Analysis of H3K4ac4, H3K14ac and H3K9ac levels 74
3.2.4.7 Analysis of H4K16 and H3K56 acetylation levels: 76
3.2.4.8 Examining the regulators of histone acetylation as cells enter SP 77
3.2.4.9 Histone H4 serine 10-phosphate Expression Dynamics during entry into SP. 78
3.2.4.10 Regulation of the Histone Variant H2A.Z (Htz1p) Levels in exponential and SP cells 80

3.3 Summary of main findings 81

3.4 Discussion 83

Chapter 4 89

Analysis of wild-type, htb-K123RΔ, hht-K36AΔ, and K123R-K36AΔ mutants during growth into stationary phase 90

4.1 Introduction 91

4.2 Results 92
4.2.1 Percoll-gradient centrifugation to separate quiescent (Q) and non-quiescent (NQ) cells 92
4.2.2 Exponential phase wild-type and mutants did not form two cell populations 94
4.2.3 The gradients were fractionated to isolate the two populations 95

4.2.4 Cell morphology of unseparated, Q cell and NQ cells in *htb-K123R*Δ, *hht-K36A*Δ, and *K123R-K36A*Δ strains during SP 98

4.3 Summary of Main Findings 101
4.3.1 *htb-K123R*Δ Mutant 101
4.3.2 *hht-K36A*Δ Mutant 102
4.3.3 *K123R-K36A*Δ Double Mutant 102

4.4 Discussion 102

Chapter 5 105

Analysis of global transcription during development of cellular quiescence in htb-K123RΔ, hht-K36AΔ, and K123R-K36AΔ mutants 106

5.1 Introduction 106

5.2 Results 108
5.2.1 RNA Quality Assessment 108
5.2.2 Principal Component Analysis (PCA) of RNA-Seq Data 110
5.2.3 Heatmap Analysis 112
5.2.4 R-squared (R^2) Regression Analysis 114

5.3 Gene Expression Changes in the Exponential Phase 114
5.3.1 Levels of upregulation in Mutant Strains During Exponential Phase 116

5.4 Gene Ontology (GO) Analysis of *htb-K123R*Δ Upregulated Genes 117
5.4.1 Gene Ontology (GO) Analysis of *hht-K36A*Δ Upregulated Genes 119
5.4.2 Gene Ontology (GO) Analysis of *K123R-K36A*Δ Upregulated Genes 122
5.4.3 Venn Diagram to show unique and shared upregulated genes in exponentially growing H2Bub and H3K36me-deficient mutants 125
5.4.4 Analysis of Gene Downregulation in Mutant Strains in exponential phase 126
5.4.5 Gene ontology analysis of genes downregulated in different mutants during exponential phase 128
5.4.6 Venn Diagram Analysis of downregulated Genes 133

5.5 Summary 134

5.6 Gene Expression Changes at the Diauxic shift 136
5.6.1 Analysis of genes upregulated in the Mutant Strains at the Diauxic Shift 137
5.6.2 Scatterplot Analysis of Upregulated Genes in different mutants in Diauxic Shift 138

5.7 Gene Ontology (GO) Analysis of *htb-K123R* Upregulated Genes 140
5.7.1 Gene Ontology (GO) Analysis of *hht-K36A*Δ Upregulated Genes 142
5.7.2 Gene Ontology (GO) Analysis of *K123R-K36A*Δ Upregulated Genes 144
5.7.3 Venn Diagram Analysis of upregulated Genes 149
5.7.4 Genes downregulated in the mutant strains during Diauxic Phase 150
5.7.5 Gene Ontology (GO) Analysis of *htb-K123R*Δ downregulated Genes 152
5.7.6 Gene Ontology (GO) Analysis of *hht-K36A*Δ downregulated Genes 154
5.7.7 Gene Ontology (GO) Analysis of *K123R-K36A*Δ downregulated Genes 157
5.7.8 Venn Diagram Analysis of downregulated Genes 160

5.8 Summary 161

5.9 Gene Expression Changes in Day-7 Quiescent Cells 162

5.9.1 Analysis of genes upregulated in Mutant Strains During Quiescent Phase....163

5.10 Gene Ontology (GO) Analysis of *htb-K123RΔ* Upregulated Genes 165

5.10.1 Gene Ontology (GO) Analysis of *hht-K36A*Δ Upregulated Genes 168

5.10.2 Gene Ontology (GO) Analysis of *K123R-K36A*Δ Upregulated Genes 171

5.10.3 Venn Diagram Analysis of upregulated Genes 174

5.11 Analysis of genes downregulated in day-7 quiescent cells 175

5.11.1 Gene Ontology (GO) Analysis of *htb-K123R*Δ downregulated Genes 176

5.11.2 Gene Ontology (GO) Analysis of *hht-K36A*Δ downregulated Genes 180

5.11.3 Gene Ontology (GO) Analysis of *K123R-K36A*Δ downregulated Genes 182

5.11.4 Venn Diagram Analysis of downregulated Genes 186

5.12 Summary 187

5.13 Discussion 188

5.13.1 Transcriptional Regulation During Exponential Phase 189

5.13.2 Transcriptional Regulation During Diauxic Shift 190

5.13.3 Transcriptional Regulation During Quiescence 191

5.14 Implications 193

5.15 Limitations 193

5.16 Future Directions 193

5.17 Conclusion 194

Chapter 6 195

Transcriptional Reprogramming by Histone Modification in Yeast Across Growth Transitions 196

6.1 Introduction 196

6.2 Transcriptional changes between growth phases 199

6.2.1 Results of analysis of gene expression in wild-type, *htb-K123R*Δ*, hht-K36A*Δ, and the double mutant *K123R-K36A*Δ at the diauxic shift (Dix) compared to transcription of each strain during exponential phase. 199

Figure 6.1: Time-course analysis of RNA-Seq data. RNA-Seq data at diauxie and in day 7 quiescent wild-type and mutant cells were compared to their own exponential phase RNase-Seq data. 199

6.2.2 Assessing changes in the levels of gene expression during the diauxic shift (Dix) in wild-type and histone mutant backgrounds relative to exponential phase. 201

6.3 Overlap of the upregulated genes in each strain during diauxic shift (Dix) 203

6.3.1 Overlap in the downregulated genes of each strains during diauxic shift (Dix) 204

6.3.2 Analysis of the genes uniquely upregulated and downregulated during the diauxic shift in the *htb-K123RΔ* deletion strains 206

6.3.3 Analysis of genes uniquely upregulated and downregulated during the diauxic shift in the *hht-K36A*Δ deletion strains 207

6.3.4 Analysis of the genes uniquely upregulated and downregulated during the diauxic shift in the *K123R-K36A*Δ deletion strains 208

6.4 Gene ontology analysis of upregulated genes in wild-type cells during the transition from Exponential Phase to the Diauxic Shift 209

6.4.1 Gene ontology analysis of downregulated genes in wild-type cells during the Exponential Phase to Diauxic Shift 210
6.4.2 Gene ontology analysis of upregulated genes in the *htb-K123R*Δ Mutant during the transition from Exponential Phase to the Diauxic Shift. 212
6.4.3 Gene ontology analysis of downregulated genes in the *htb-K123R*Δ Mutant during the Exponential Phase to Diauxic Shift. 214
6.4.4 Gene ontology analysis of upregulated genes in the *hht-K36A*Δ Mutant during the Exponential Phase to Diauxic Shift. 215
6.4.5 Gene ontology analysis of downregulated genes in the *hht-K36A*Δ Mutant during the Exponential Phase to Diauxic Shift. 217
6.4.6 Gene ontology analysis of upregulated genes in the *K123R-K36A*Δ Double Mutant during the Exponential Phase to Diauxic Shift. 219
6.4.7 Gene ontology analysis of downregulated genes in the *K123R-K36A*Δ Double Mutant during the Exponential Phase to Diauxic Shift. 221

6.5 Analysis of gene expression in wild-type, *htb-K123RΔ, hht-K36AΔ,* and the double mutant *K123R-K36AΔ* in quiescent day 7 (Q-D7) cells compared to transcription during exponential phase 223

6.5.1 Analysing transcription levels of the total number of genes upregulated and downregulated at the Quiescence relative to exponential phase levels of transcription in wild-type and histone mutants. 225
6.5.2 Comparison of the upregulated genes of each strain evident in quiescent cells relative to exponentially growing cells 226

6.6 Comparison of the downregulated genes of each strain evident in quiescent cells relative to exponentially growing cells 227

6.6.1 Comparison of the genes uniquely upregulated and downregulated in quiescent *htb-K123R*Δ deletion strains relative to transcription in quiescent wild-type cells 229
6.6.2 Comparison of the genes uniquely upregulated and downregulated in quiescent *hht-K36A*Δ deletion strains relative to transcription in quiescent wild-type cells 229
6.6.3 Comparison of the genes uniquely upregulated and downregulated in quiescent *K123R-K36A*Δ deletion strains relative to transcription in quiescent wild-type cells 230

6.7 Gene ontology analysis of upregulated genes in the wild-type cells during the transition from Exponential Phase to cell Quiescence. 231

6.7.1 Gene ontology analysis of downregulated genes in the wild-type cells during the Exponential Phase to Quiescence Day 7 (Q-D7). 233
6.7.2 Gene ontology analysis of upregulated genes in the *htb-K123R*Δ Mutant during the Exponential Phase to Quiescence Day 7 (Q-D7). 234
6.7.3 Gene ontology analysis of downregulated genes in the *htb-K123R*Δ Mutant during the Exponential Phase to Quiescence Day 7 (Q-D7) 236
6.7.4 Gene ontology analysis of upregulated genes in the *hht-K36A*Δ Mutant during the Exponential Phase to Quiescence Day 7 (Q-D7). 237
6.7.5 Gene ontology analysis of downregulated genes in the *hht-K36A*Δ Mutant during the Exponential Phase to Quiescence Day 7 (Q-D7) 239
6.7.6 Gene ontology analysis of upregulated genes in the *K123R-K36A*Δ Double Mutant during the Exponential Phase to Quiescence Day 7 (Q-D7). 241
6.7.7 Gene ontology analysis of downregulated genes in the *K123R-K36A*Δ Double Mutant during the Exponential Phase to Quiescence Day 7 (Q-D7). 242

6.8. Discussion 244

6.8.1 Transcriptional Reprogramming in Histone Mutants During the Diauxic Shift and quiescence (Q-D7) 244

6.9 Differential Gene Expression Reveals Stage-Specific Adaptations 247

6.9.1 Comparative Analysis of Upregulated and Downregulated Genes in wild-type Yeast During Diauxic Shift and quiescent day 7 (Q-D7) 247

6.9.2 Comparative Analysis of Upregulated and Downregulated Genes in *htb-K123R*Δ mutant Yeast During Diauxic Shift and quiescent day 7 (Q-D7) 248

6.9.3 Comparative Analysis of Upregulated and Downregulated Genes in *hht-K36A*Δ mutant Yeast During Diauxic Shift and quiescent day 7 (Q-D7) 249

6.9.4 Comparative Analysis of Upregulated and Downregulated Genes in *K123R-K36A*Δ double *mutant* Yeast During Diauxic Shift and quiescent day 7 (Q-D7) 250

6.10 Summary of Main Findings 253

6.10.1 Widespread Transcriptional Deregulation in Histone Mutants. 253

6.10.2 Unique and Overlapping Gene Regulation. 253

6.10.3 Functional and Metabolic Dysregulation. 254

6.10.4 Intricate Functional Relationship Between Histone Modifications 254

6.10.5 Chromatin state evidence 254

Chapter 7 256

Final Discussion 256

7.1 Global Transcriptional Reprogramming in Response to Metabolic Transition 257

7.2 The Diauxic Shift 257

7.3 Quiescence entry (Day 7) 258

7.4 Unique and Overlapping Gene Regulation: Dissecting the Roles of H2B K123ub and H3 K36me 259

7.4.1 Diauxic Shift 259

7.4.2 Quiescence entry (Day 7) 260

7.5 Gene Ontology Analysis: A Detailed Functional Interpretation 261

7.5.1 GO Analysis of the Diauxic Shift 262

7.5.2 GO Analysis of Quiescence entry (Day 7) 263

7.6 Implications for Quiescence and Long-Term Viability 263

7.7 Conclusions and Future Directions 264

References 265

Appendix 278

List of Tables

Table 1.1: shows the core histone proteins……...5

Table 2.1: Yeast strains used in this research……...……28

Table 2.2: Antibodies used in western immunoblotting……..36

Table 5.1:Differential Gene Expression in Mutant Strains During the Exponential Phase……...106

Table 5.2: List of genes commonly up-regulated Exponential Phase *htb-K123R*Δ compared to wild-type.…….……..…….109

Table 5.3: List of genes commonly up-regulated during Exponential Phase in *hht-K36A*Δ compared to wild-type.…….…….…….112

Table 5.4: List of genes commonly up-regulated during Exponential Phase in *K123R-K36A*Δ compared to wild-type.…….…….…….114

Table 5.5: List of genes commonly down-regulated during Exponential Phase in *htb-K123R*Δ compared to wild-type …….……..119

Table 5.6: List of genes commonly down-regulated during Exponential Phase in *hht-K36A*Δ compared to wild-type…….……...……122

Table 5.7: List of down-regulated genes enriched for GO term indicated during Exponential Phase in *K123R-K36A*Δ compared to wild-type.……...……123

Table 5.8: Differential Gene Expression in Mutant Strains During the Diauxic Shift…….....127

Table 5.9: List of genes commonly up-regulated during diauxic shift in *htb-K123R*Δ compared to wild-type.....131

Table 5.10: List of genes commonly up-regulated during diauxic shift in *hht-K36A*Δ compared to wild-type.…….……..133

Table 5.11: List of genes commonly up-regulated during diauxic shift in *K123R-K36A*Δ compared to wild-type…….…….……..136

Table 5.12: List of genes commonly down-regulated during diauxic shift in *htb-K123R* compared to wild-type.…….……..……...…….142

Table 5.13: List of genes commonly down-regulated during diauxic shift in *hht-K36A* compared to wild-type.…….…..145

Table 5.14: List of genes commonly down-regulated during diauxic shift in *K123R-K36A*Δ compared to wild-type.…….……..147

Table 5.15: Differential Gene Expression in Mutant Strains During the Quiescent Phase……..……151

Table 5.16: List of genes up-regulated during Quiescent cells Day 7 in *htb-K123R*Δ compared to wild-type…….……..……..154

Table 5.17: List of genes up-regulated during Quiescent cells Day 7 in *hht-K36A*Δ compared to wild-type……..……..157

Table 5.18: List of genes up-regulated during Quiescent cells Day 7 in *K123R-K36A*Δ compared to wild-type…….…….……..160

Table 5.19: List of genes commonly down-regulated during Quiescent cells Day 7 in *htb-K123R*Δ compared to wild-type…….…….……...165

Table 5.20: List of genes down-regulated during Quiescent cells Day 7 in *hht-K36A*Δ compared to wild-type…….……..168

Table 5.21: List of genes down-regulated during Quiescent cells Day 7 in *K123R-K36A*Δ compared to wild-type…….……..171

Table 6.1: Shows the numbers of genes more than 2-fold up and down-regulated in each strain at diauxie compared to transcription in that same strain at exponential phase……186

Table 6.2: Shows the numbers of genes more than 2-fold up and down-regulated in each strain in day-7 quiescent cells compared to transcription at exponential phase……...….208

Index of Figures

Figure 1.1: Figure showing the nucleosome crystal structure ……..…….……3

Figure 1.2: Diagram represented DNA arranged into chromatin..…….…..4

Figure 1.3: The structure of the core nucleosome.…….....……..……..5

Figure 1.4: Schematic showing examples of various histone PTMs. ……6

Figure 1.5: Schematic overview of the main histone post-translational modifications (PTMs)…….7

Figure 1.6: The histone code hypothesis……8

Figure 1.7: ATP-dependent chromatin remodeler mechanism……..…9

Figure 1.8: Eukaryotic Gene Regulation: Transcription and Initiation……12

Figure 1.9: Schematic showing regulation of histone post-translational modifications……..14

Figure 1.10: Role of H2Bub during transcription elongation. ……...……16

Figure 1.11: Role of H3K36me during transcription elongation……..…...…18

Figure 1.12: The transition to the stationary phase involves distinct growth phases……..…21

Figure 1.13: Diagram depicting the quiescent (Q) and non-quiescent (NQ) cell populations formed during Stationary phase…….…….22

Figure 2.1: Schematic of fractionation of stationary phase cultures……31

Figure 2.2: Schematic of Protein Extraction. This figure was created using BioRender…..…32

Figure 2.3: Schematic of SDS-Polyacrylamide gel and western blot……..……35

Figure 2.4: Schematic of RNA extraction……...……38

Figure 2.5: RNA sample preparation for RNA-Seq analysis……...……39

Figure 2.6: Schematic showing the main steps in RNA-Sequencing……...……40

Figure 3.1: Western blot analysis to confirm the strains used in this study…….……44

Figure 3.2: Growth Analysis on glucose and doubling time of Mutant and Wild-Type Strains……..…….45

Figure 3.3: Analysis of cell density after 24h growth in YPD…….…46

Figure 3.4: Growth and Glucose Consumption Among Wild-Type and Mutant Strains…….47

Figure 3.5: Analysis of cell viability in wild-type, *htb-K123R*Δ*, hht-K36A*Δ, and *K123R-K36A*Δ mutant strains over 7 days in YPD medium……...…..……48

Figure 3.6: Cell images of wild-type, *htb-K123R*Δ*, hht-K36A*Δ and *K123R-K36A*Δ mutant cells……...49

Figure 3.7: Temperature sensitivity growth tests of exponentially growth (Exp) and stationary phase (SP) growing cultures on plates……..…50

Figure 3.8: Growth tests of exponentially growing (Exp) and stationary phase (SP) cultures on plates with different carbon sources……51

Figure 3.9: Serial ten-fold dilution growth tests on a non-fermentable carbon source (Acetic acid) of exponentially growing (Exp) and stationary phase (SP) cultures……...……52

Figure 3.10: Testing response to DNA damage of exponential (Exp) and stationary phase (SP) cells……..……53

Figure 3.11: Serial ten-fold dilution growth tests of (Exp) and (SP) cultures on plates containing the DNA damaging reagent, MMS…….……54

Figure 3.12: Serial ten-fold dilution growth tests to DNA-damaging reagent Hydroxyurea (HU) of exponentially growth (Exp) and stationary phase (SP) cultures…….……55

Figure 3.13: Testing cell sensitivity to the Caffeine of exponentially growth (Exp) and stationary phase (SP) cultures……..……56

Figure 3.14: Testing cell sensitivity to osmotic and oxidative stress of exponentially growth (Exp) and stationary phase (SP) cultures…….……57

Figure 3.15: Testing cell sensitivity to osmotic and Ionic stress of exponentially growth (Exp) and stationary phase (SP) cultures……..……..58

Figure 3.16: Testing cell sensitivity to Chemical stress (formamide) of exponentially growth (Exp) and stationary phase (SP) culture……...……59

Figure 3.17: RNAP II CTD phosphorylation levels in wild-type and mutant yeast strains across different growth phases…….……62

Figure 3.18: Western blot analysis of PAF1 protein levels……..……63

Figure 3.19: Western blot analysis of core histone protein levels ……...……65

Figure 3.20: Western blot analysis of Hho1p protein levels……..……..……67

Figure 3.21: Western blot analysis of histone acetylation……69

Figure 3.22: Western blot analysis of histone acetylation ……...……70

Figure 3.23: Western blot analysis of Gcn5p and Rpd3p protein levels……..……72

Figure 3.24: Western blot analysis of HS10P protein levels……73

Figure 3.25: Western blot analysis of H2A.Z (Htz1p) levels……...……75

Figure 4.1: Separation of Day 7 cultures into quiescent Q and non-quiescent cell NQ populations……...……86

Figure 4.2: Separation of Day 14 cultures into quiescent Q and non-quiescent cell NQ populations……..…….86

Figure 4.3: Exponential phase cells do not form two populations following Percoll-gradient centrifugation……...……87

Figure 4.4: The gradients were fractionated to isolate the two populations day 7……...……89

Figure 4.5: The gradients were fractionated to isolate the two populations day 14…….……90

Figure 4.6: Day 7, Q, and NQ cells morphology…….……92

Figure 4.7: Day 14, Q, and NQ cells morphology……...……93

Figure 5.1: The diagram illustrates the timing of RNA isolation……...……..99

Figure 5.2: Assessment of RNA Quality from Yeast Strains During Exponential Phase ….101

Figure 5.3: Principal Component Analysis (PCA) of RNA-Seq data……103

Figure 5.4: Heatmap of Gene Expression Profiles Across Different Experimental Conditions……..……104

Figure 5.5: R^2 Regression Analysis of RNA-Seq Data……..……105

Figure 5.6: Total Genes Significantly Upregulated in Each Mutant Compared to Wild-Type During Exponential Phase……..……107

Figure 5.7: Gene Ontology (GO) analysis of upregulated genes in the *htb-K123R*Δ mutant strain……..…….110

Figure 5.8: Gene Ontology (GO) analysis of upregulated genes in the *hht-K36A*Δ mutant strain……..…….113

Figure 5.9: Gene Ontology (GO) analysis of upregulated genes in the combined *K123R-K36A*Δ mutant strain……..……115

Figure 5.10: Venn diagram illustrating the overlap and uniqueness of upregulated genes among the three mutant strains compared to the wild-type……116

Figure 5.11: Total genes significantly downregulated in each mutant compared to wild-type ……...…….118

Figure 5.12: Gene ontology terms for downregulated genes in *htb-K123R*Δ……120

Figure 5.13: Gene ontology terms for downregulated genes in *hht-K36A*Δ……...……123

Figure 5.14: Venn diagram illustrating the overlap and uniqueness of downregulated genes among the three mutant strains compared to the wild-type……124

Figure 5.15: Genes showing more than a two-fold Up and Down regulated During the Diauxic Shift……..……128

Figure 5.16: Total Genes Significantly Upregulated in Each Mutant Compared to wild-type During Diauxic shift (Dix)…….……129

Figure 5.17: Gene Ontology (GO) analysis of upregulated genes in the *htb-K123R*Δ mutant strain……...……132

Figure 5.18: Gene Ontology (GO) analysis of upregulated genes in the *hht-K36A*Δ mutant strain……...……134

Figure 5.19: Gene Ontology (GO) analysis of upregulated genes in the combined *K123R-K36A*Δ mutant strain ……..…137

Figure 5.20: Venn diagram illustrating the overlap and uniqueness of upregulated genes among the three mutant strains compared to the wild-type.……...……138

Figure 5.21: Total Genes Significantly Downregulated in Each Mutant Compared to wild-type During Diauxic shift..…….……140

Figure 5.22: Gene Ontology (GO) analysis of downregulated genes in the *htb-K123R*Δ mutant strain……...……143

Figure 5.23: Gene Ontology (GO) analysis of downregulated genes in the *hht-K36A*Δ mutant strain……...……146

Figure 5.24: Gene Ontology (GO) analysis of downregulated genes in the *K123RK36A*Δ mutant strain……...……148

Figure 5.25: Venn diagram illustrating the overlap and uniqueness of upregulated genes among the three mutant strains compared to the wild-type……149

Figure 5.26: Total Genes Significantly Upregulated in Each Mutant Compared to wild-type During Quiescent Phase……...……..……152

Figure 5.27: Gene Ontology (GO) analysis of upregulated genes in the *htb-K123R*Δ mutant strain……...……155

Figure 5.28: Gene Ontology (GO) analysis of upregulated genes in the *hht-K36A*Δ mutant strain……...……158

Figure 5.29: Gene Ontology (GO) analysis of upregulated genes in the combined *K123R-K36A*Δ mutant strain……..……161

Figure 5.30: Venn diagram illustrating the overlap and uniqueness of upregulated genes among the three mutant strains compared to the wild-type ……...……162

Figure 5.31: Total Genes Significantly Downregulated in Each Mutant Compared to wild-type During Quiescent Phase…….……163

Figure 5.32: Gene Ontology (GO) analysis of downregulated genes in the *htb-K123R*Δ mutant strain……...……166

Figure 5.33: Gene Ontology (GO) analysis of downregulated genes in the *hht-K36A*Δ mutant strain……...……169

Figure 5.34: Gene Ontology (GO) analysis of downregulated genes in the *K123R-K36A*Δ mutant strain……...……172

Figure 5.35: Venn diagram illustrating the overlap and uniqueness of downregulated genes among the three mutant strains compared to the wild-type ……...…173

Figure 6.1: Time-course analysis of RNA-Seq data…….…..185

Figure 6.2: Total number of genes up and down regulated at diauxic shift in each strain compared to when that strain is exponentially growing……187

Figure 6.3: Average up and down regulation of gene transcription in wild-type and mutants at diauxic shift compared to exponential phase……...…..189

Figure 6.4: Venn diagram of upregulated genes……...….191

Figure 6.5: Venn diagram to identification of common and unique downregulated genes...191

Figure 6.6: Unique and shared transcriptional profiles in *htb-K123RΔ* during diauxic shift compared to exponential phase for upregulated and down regulated……....192

Figure 6.7: Unique and shared transcriptional profiles in yeast deletion in *hht-K36AΔ* mutants during exponential phase compared to diauxic shift in wild-type cells for upregulated and down regulated…….…...……..193

Figure 6.8: Unique and shared transcriptional profiles in yeast deletion in *K123R-K36AΔ* mutants during exponential phase compared to diauxic shift in wild-type cells for upregulated and down regulated…….……...194

Figure 6.9: GO analysis of genes upregulated in wild-type cells at the diauxic shift compared to exponential phase……...196

Figure 6.10: GO analysis of genes downregulated in wild-type cells at the diauxic shift compared to exponential phase……...…..…….197

Figure 6.11: GO analysis of genes upregulated in *htb-K123R*Δ cells at the diauxic shift compared to exponential phase…….….199

Figure 6.12: GO analysis of genes downregulated in *htb-K123R*Δ cells at the diauxic shift compared to exponential phase……..…200

Figure 6.13: GO analysis of genes upregulated in *hht-K36A*Δ cells at the diauxic shift compared to exponential phase……..202

Figure 6.14: GO analysis of genes downregulated in *hht-K36A*Δ cells at the diauxic shift compared to exponential phase…….….203

Figure 6.15: GO analysis of genes upregulated in *K123R-K36A*Δ cells at the diauxic shift compared to exponential phase……..…205

Figure 6.16: GO analysis of genes downregulated in *K123R-K36A*Δ cells at the diauxic shift compared to exponential phase……..206

Figure 6.17: Total number of genes for treatment transcriptional profiles in yeast deletion mutants conducted differential gene expression analysis……..….208

Figure 6.18: Average up and down regulation of gene transcription in wild-type and mutants in day 7 quiescent cells compared to exponential phase cells…….……...210

Figure 6.19: Venn diagram of upregulated genes across different quiescent conditions…...212

Figure 6.20: Venn diagram of downregulated genes in quiescent cells……..……...212

Figure 6.21: Unique and shared transcriptional profiles in *htb-K123R*Δ yeast deletion mutants during exponential phase compared to Quiescence cell Day 7 in wild-type cells for upregulated and down regulated……..……...213

Figure 6.22: Unique and shared transcriptional profiles in *hht-K36A*Δ yeast deletion mutants during exponential phase compared to Quiescence cell Day 7 in wild-type cells for upregulated and down regulated……..……...…214

Figure 6.23: Unique and shared transcriptional profiles in *K123R-K36A*Δ yeast deletion mutants during exponential phase compared to Quiescence cell Day 7 in wild-type cells for upregulated and down regulated……...…..215

Figure 6.24: GO analysis of genes upregulated in wild-type cells at the exponential phase compared to Quiescence day 7 (QD7)…… ……...……...…216

Figure 6.25: GO analysis of genes downregulated in wild-type cells at the exponential phase compared to Quiescence day 7 (QD7)… ……..218

Figure 6.26: GO analysis of genes upregulated in *htb-K123R*Δ cells at the exponential phase compared to Quiescence day 7 (QD7)…… ……..219

Figure 6.27: GO analysis of genes downregulated in *htb-K123R*Δ cells at the exponential phase compared to Quiescence day 7 (QD7)…… ……...…….221

Figure 6.28: GO analysis of genes upregulated in *hht-K36A*Δ cells at the exponential phase compared to Quiescence day 7 (QD7)…… ……..….222

Figure 6.29: GO analysis of genes downregulated in *hht-K36A*Δ cells at the exponential phase compared to Quiescence day 7 (QD7)…… ……...……...….224

Figure 6.30: GO analysis of genes upregulated in *K123R-K36A*Δ cells at the exponential phase compared to Quiescence day 7 (QD7)…… ……..….225

Figure 6.31: GO analysis of genes downregulated in *K123R-K36A*Δ cells at the exponential phase compared to Quiescence day 7 (QD7)…… ……227

Figure 6.32: Venn diagram showing the total number of genes treatment bound in various yeast strains under Total-Dix treatment……...……..229

Figure 6.33: Venn diagram showing the total number of genes treatment bound in various yeast strains under QD7-Total treatment……...….229

Figure 6.34: Gene regulation wild-type-Exp-Dix VS Exp-QD7 Up and Downregulated….230

Figure 6.35: Gene regulation *htb-K123R*Δ -Exp-Dix VS Exp-QD7 Up and Downregulated……...231

Figure 6.36: Gene regulation *hht-K36A*Δ -Exp-Dix VS Exp-QD7 Up and Downregulated..232

Figure 6.37: Gene regulation *K123R-K36A*Δ -Exp-Dix VS Exp-QD7 Up and Downregulated……...233

Figure 6.38: Gene Ontology (GO) analysis of genes differentially expressed in the comparison of Exp vs. Dix for up and downregulated……..….234

Figure 6.39: Gene Ontology (GO) analysis of genes differentially expressed in the comparison of Exp vs. QD7 for up and downregulated…….……235

Chapter 1

Introduction

1.1 Overview

Chromatin is a highly organised nucleoprotein complex located in the nucleus of eukaryotic cells and plays a central role in genome integrity and gene regulation. DNA is packaged into chromatin by wrapping around histone proteins to form nucleosomes, which are the fundamental structural units of chromatin. Chromatin exists in either an open (euchromatin) or closed (heterochromatin) conformation, which determines the accessibility of the underlying DNA. Transitions between these states are critical for the regulation of transcription, replication, DNA repair, and chromatin inheritance. The dynamic nature of chromatin enables eukaryotic cells to modulate gene expression in response to developmental and environmental cues. Interconversion between euchromatin and heterochromatin occurs through nucleosome remodelling and is mediated by post-translational histone modifications and chromatin associated regulatory factors.

1.2 Historical background and Importance of Chromatin Structure

The fundamental organisation of chromatin was first described by (Kornberg, 1974), who demonstrated that chromatin consists of repeating DNA–protein units later termed nucleosomes. Each nucleosome comprises approximately 147 base pairs of DNA wrapped around a histone octamer containing two copies of the core histones H2A, H2B, H3, and H4. Subsequent electron microscopy studies confirmed nucleosomes as the basic structural units of chromatin. This discovery provided the first mechanistic insight into how eukaryotic genomes are compacted within the nucleus while remaining accessible for essential processes such as transcription and replication.

Early studies revealed that nucleosomes impede access to DNA but that this barrier can be modulated by histone modifications and chromatin-remodelling complexes. The X-ray crystal structure of the nucleosome at 2.8 Å resolution reported by (Mäder *et al.*, 1997) elucidated histone–DNA interactions at the molecular level (Fig. 1.1). Subsequent studies identified histone acetylation as a modification that weakens histone–DNA interactions, thereby increasing chromatin accessibility to transcription factors and RNA polymerase (Grunstein, 1997). Collectively, these findings established chromatin as an active regulator of gene expression rather than a passive DNA-packaging scaffold (Fig. 1.2).

The chromatin structure was first uncovered by (Kornberg, 1974). In his groundbreaking work, Kornberg demonstrated that chromatin consists of repeating units of DNA and histones, later known as nucleosomes. In these units, approximately 147 base pairs of DNA are wrapped around a histone octamer comprising two of each of the four core histones, H2A, H2B, H3 and H4. The structure identified by Kornberg was later confirmed through other studies employing electron microscopy, establishing nucleosomes as the fundamental structural units of chromatin. This discovery marked the first detailed understanding of how eukaryotic cells package their DNA into the relatively small nucleus while still allowing processes like transcription and replication through controlled access to genetic information. Early research showed that nucleosomes act as a physical barrier to transcription and replication but could be modulated by specific histone modifications and chromatin remodelling complexes. For example, the X-ray crystal structure of the nucleosome at 2.8 Å resolution by (Mäder *et al.*, 1997) provided a detailed molecular understanding of histone-DNA interactions (Fig. 1.1). (Grunstein, 1997) and subsequent researchers identified acetylation as a specific histone modification that reduces the interaction between histones and DNA. This reduction increases chromatin accessibility to transcription factors and RNA polymerase. These early evidences suggested that chromatin was not merely a passive structure but actively influenced gene expression (Fig. 1.2).

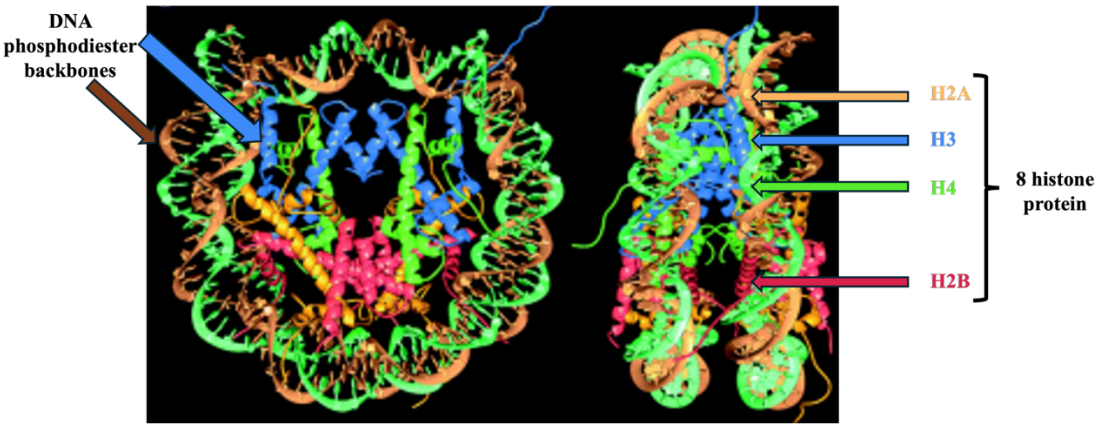


Figure 1.1: Figure showing the nucleosome crystal structure: ribbon traces for the 146-bp DNA phosphodiester backbones (brown and turquoise) and eight histone protein main chains (blue: H3; green: H4; yellow: H2A; red: H2B. (Mäder *et al.*, 1997)

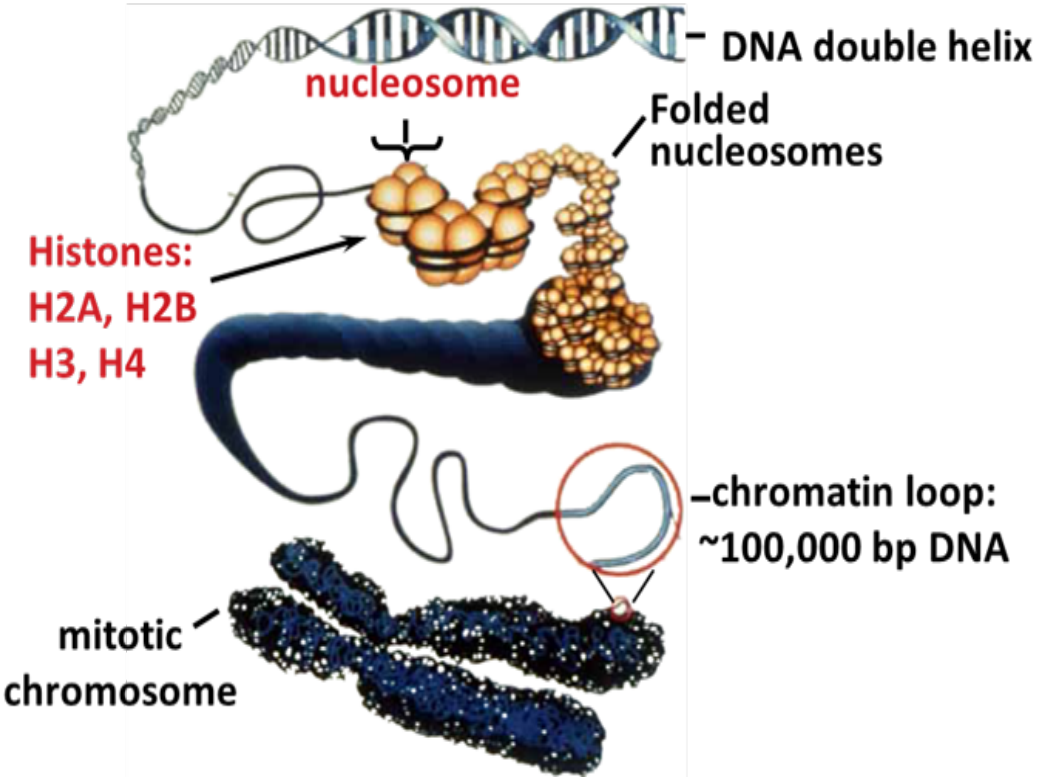


Figure 1.2: Diagram represented DNA arranged into chromatin. Each nucleosome contains two copies of the H3, H4, H2A, and H2B histone proteins. The DNA connecting nucleosomes is where histone H1 binds to form the chromosome and further compacts DNA within the nucleus**.** This figure was uploaded by (Lewin, 2004).

1.3 The core histones

The four core histones making up the nucleosome octamer are known as H2A, H2B, H3 and H4 (Table 1.1). They all share the same fundamental structure comprising a structured globular domain and a flexible N-terminal tail. Studies have shown that the core histones are well conserved in all eukaryotes (Claude, 2022). Together, these small, basic histones combine into an octamer of a single (H3-H4) two tetramer and two H2A-H2B dimers (Fig. 1.3). There are approximately fourteen regions of contact with the histone proteins and DNA, causing the nucleosome to form a very stable DNA-protein complex (Mäder *et al.*, 1997).

Properties of the histone proteins		
Histone	**Molecular weight (Da)**	**Number of amino acids residues**
H1	**21.1**	**223**
H2A	**15.3**	**129**
H2B	**14**	**125**
H3	**15.3**	**135**
H4	**11.3**	**102**

Table 1.1 Properties of the core histone proteins. The lists of four core histone proteins (H1, H2A, H2B, H3, and H4), molecular weight (Daltons, Da), and number of amino acid residues.

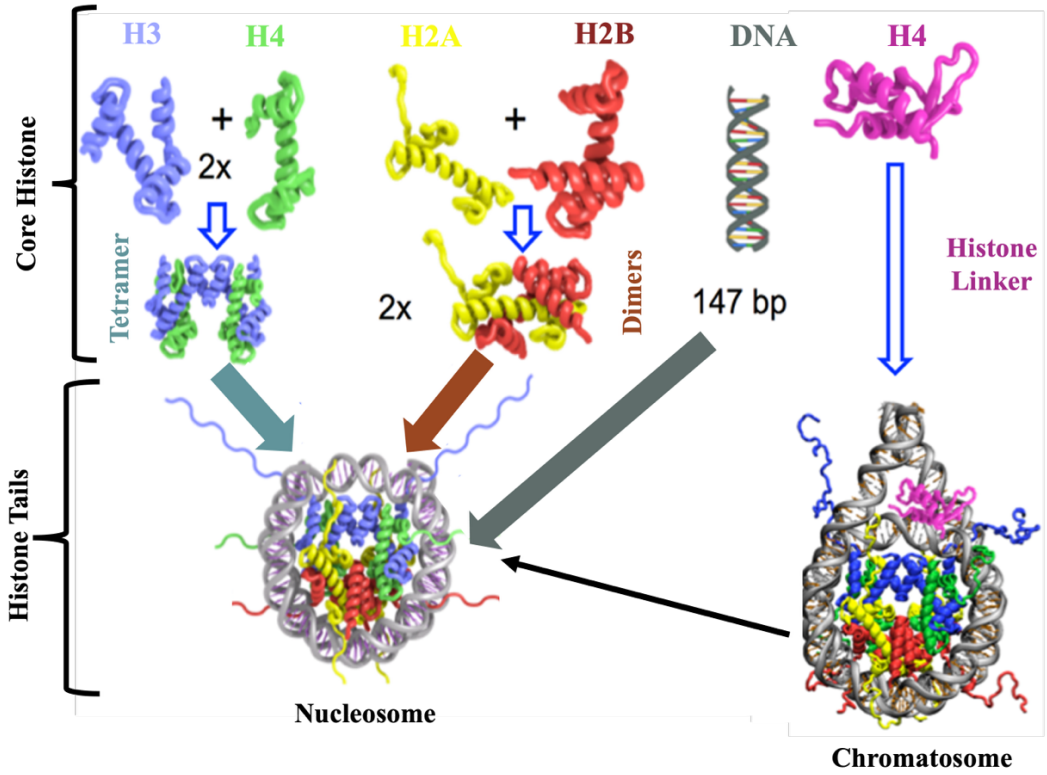


Figure 1.3: The structure of the core nucleosome. High-resolution crystal structure of the nucleosome. The DNA fibre is wrapped around a tetramer of H3 (blue) and H4 (green), along with two H2A (yellow) and H2B (red) dimers. The globular domain of histone H1 (pink) binds the nucleosome at the dyad. (Draizen *et al.*, 2016).

1.4 Histone post-translational modifications (PTMs)

By modifying the interaction between histones and DNA, histone PTMs play a central role in chromatin regulation. These modifications influence chromatin accessibility and function (Strahl and Allis, 2000). The flexible N-terminal tails of histones are where many of these modifications occur (Fig. 1.4). The modifications in the N-terminal tails include acetylation, which is the addition of acetyl groups to lysine residues. Acetylation (AC) is typically associated with transcriptional activation (Grunstein, 1997). Acetylation of histones helps in neutralization of the positive charge on histones, which results in a reduction of their affinity for DNA and creates a more open chromatin conformation. Histone acetyltransferases are the enzymes (HATs) involved in adding acetyl groups. The histone deacetylases (HDACs), on the other hand, remove them (Struhl, 1998).

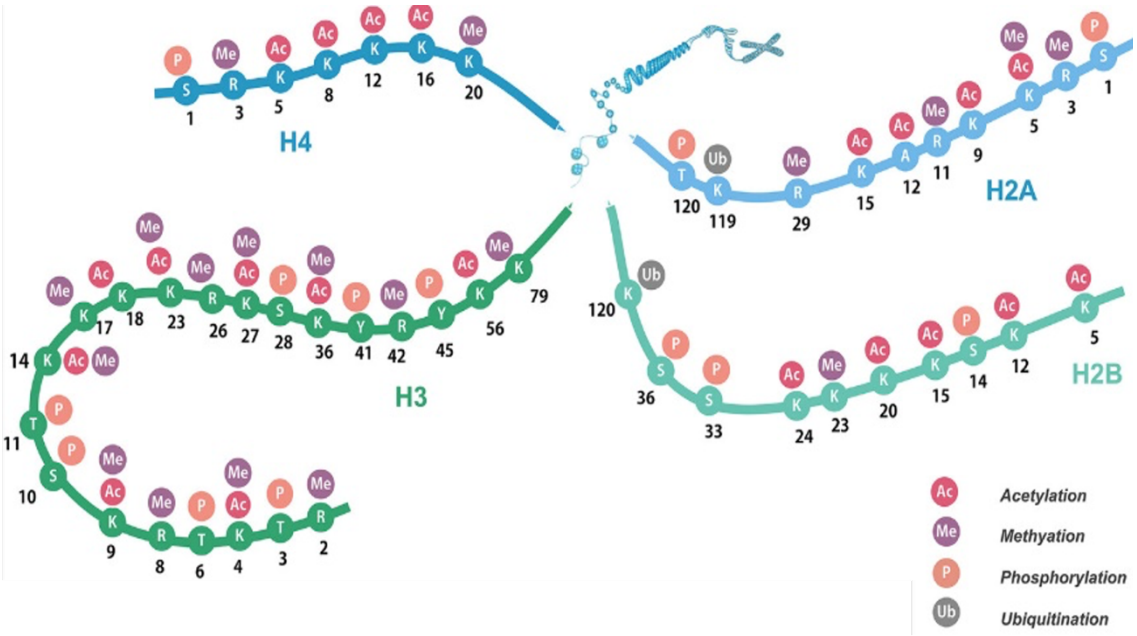


Figure 1.4: Schematic showing examples of various histone PTMs. Acetylation (Ac), phosphorylation (P), methylation (Me), and ubiquitylation (Ub) of the core histone proteins indicated. This figure was uploaded by (Grigoreva *et al.*, 2024).

Another common PTM is the methylation (Me) of histones. In methylation, there is the addition of methyl groups to lysine or arginine residues. The methylation of histones can either activate or repress gene expression depending on the site of modification. For example, H3K4 methylation helps transcription activation, while H3K27 methylation is associated with gene silencing (Strahl and Allis, 2000).

Addition of phosphate groups to serine, threonine, or tyrosine residues is also a type of PTM called phosphorylation (P). It is often involved in DNA damage response and chromatin condensation during mitosis (Rogakou *et al.*, 1998). On some occasions, there is the attachment of ubiquitin to histone proteins, and this PTM is called ubiquitination (Ub). Ubiquitination plays a key role in transcriptional regulation, DNA repair, and histone turnover (Sun and Allis, 2002). It has been shown that monoubiquitylation of H2B is also required for the methylation of H3K4 and H3K79. A less well-understood modification called Sumoylation (Sumo) has been generally associated with transcriptional repression and chromatin compaction (Zhang and Reinberg, 2001) (Fig. 1.5). These histone PTMs have been shown to influence chromatin structure and function (Strahl and Allis, 2000).

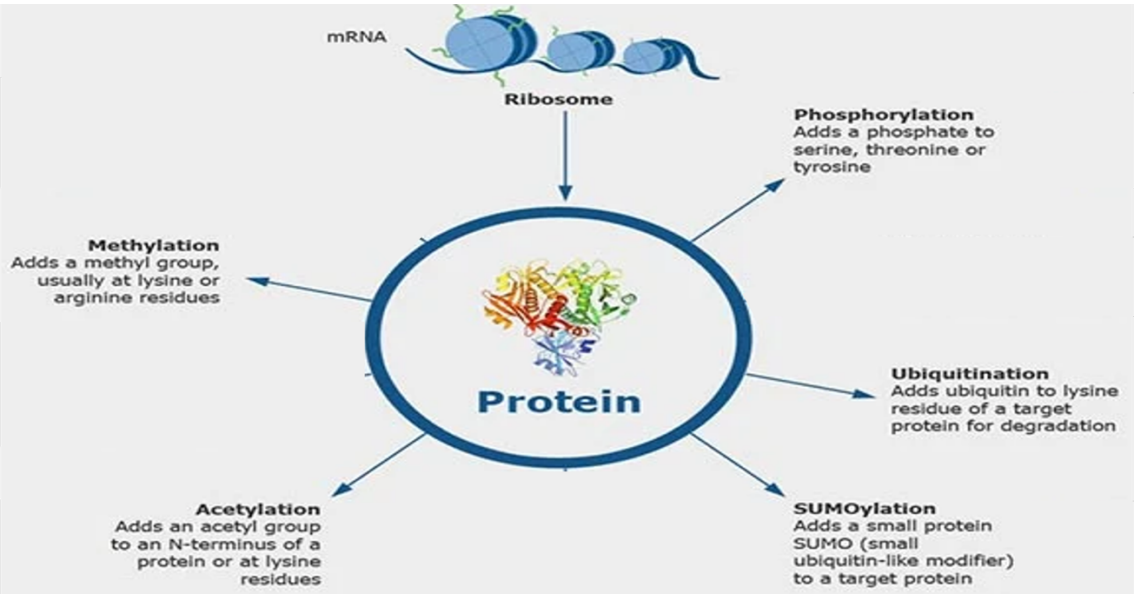


Figure 1.5: Schematic overview of the main histone post-translational modifications (PTMs), including acetylation (Ac), methylation (Me), phosphorylation (P), Sumoylation (Sumo) and ubiquitination (Ub). These modifications occur on the N-terminal tails of histone proteins and regulate chromatin structure and gene expression by changing histone-DNA interactions. PTMs serve as signals

for the recruitment of chromatin-associated proteins that mediate transcriptional activation or repression (Rogakou *et al.*, 1998).

1.5 Chromatin as a regulator of Gene Expression

Due to its ability to switch between more compact and more open structures, chromatin can act as a gatekeeper of gene expression. Post-translational modifications of histones, such as acetylation, methylation, phosphorylation, and ubiquitination, are the regulators of this switch and thus, influence transcription. These post-translational modifications can therefore either promote or repress the transcription of specific genes.

The "histone code" hypothesis proposes that these histone modifications function as a code which is deposited upon chromatin by the 'writers', is read by different 'reader' proteins which then bring about the effect (Fig. 1.6). (Strahl and Allis, 2000). The 'erasers' can then remove the PTMs to re-set the code.

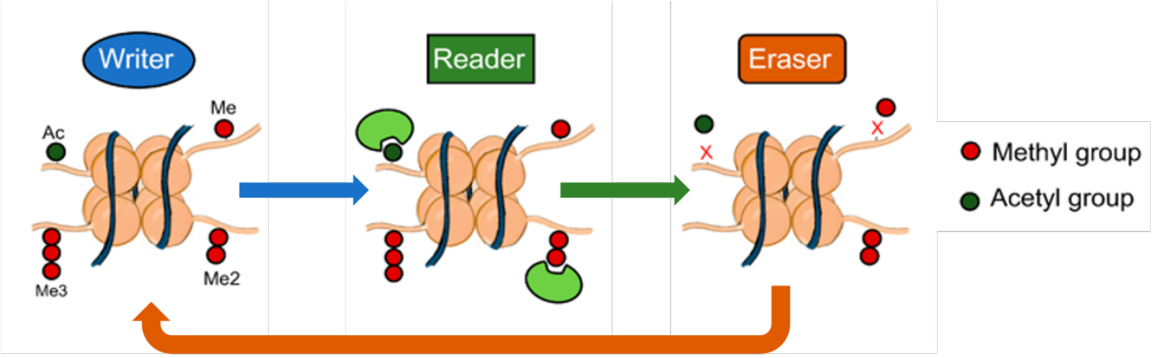


Figure 1.6: The histone code hypothesis. The diagram illustrates the core principle of the Histone Code Hypothesis. This hypothesis proposes that specific combinations of chemical modifications on histone proteins, create a "code" that is read by other proteins to control gene expression without altering the underlying DNA sequence. Writer: Enzyme add specific histone protein, Eraser: Enzyme remove these modification and Reader: protein recognize and bind modification. Methyl group (Me): (Me3, Me2) indicates the level of methylation (tri-methyl, di-methyl), which can have different effects based on its

location. Acetyl group (Ac): Acetylation is generally associated with opening chromatin and activating gene expression (Allis and Jenuwein, 2016).

1.5.1 ATP-dependent chromatin remodelling

The regulation of cellular gene expression, and DNA replication and repair, can also be controlled by a mechanism whereby ATP hydrolysis is utilised by chromatin remodelling complexes to modify the positioning of nucleosomes (Fig. 1.7). These complexes can also alter histone-DNA interactions or can replace canonical histones with variants by utilizing the energy from ATP hydrolysis (Cairns *et al.*, 1996).

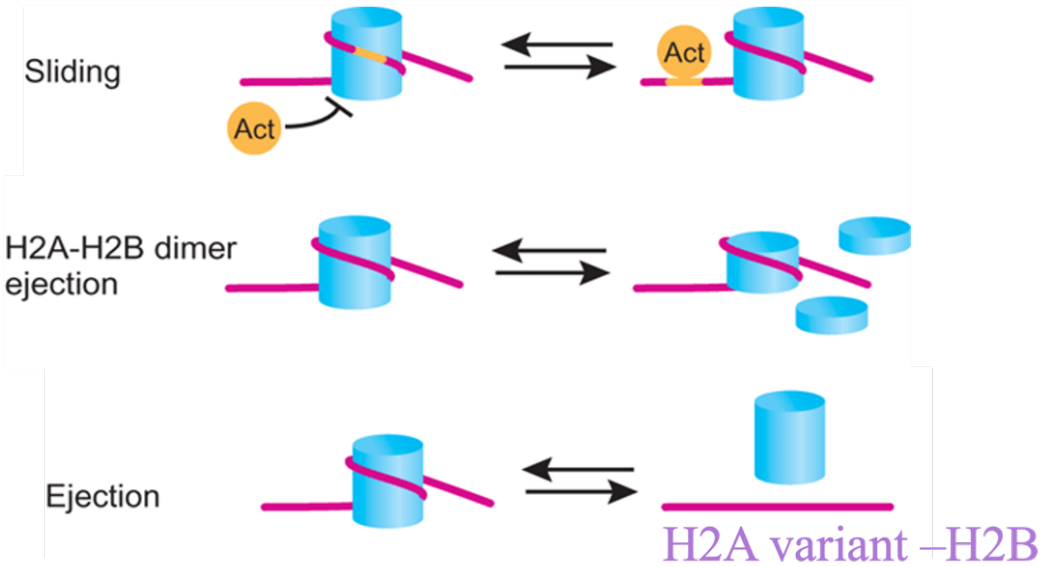


Figure 1.7: ATP-dependent chromatin remodeler mechanism. ATP-dependent remodelling complexes facilitate the opening of nucleosomes' DNA as they can slide, eject or rearrange nucleosomes by evicting H2A-H2B dimers, depending on the complex and the target site. The SWR1 complex is

distinctive in its capacity to effectively substitute H2A-H2B dimers with dimers containing a histone H2A variant (Htz1 or H2A.Z). “Act" refers to an activator that has a specific location on the DNA where it can bind. This figure was created using BioRender.

There are several families of ATP-dependent chromatin remodelling complexes, each one playing a distinct role in chromatin regulation. One such complex is the SWI/SNF complex, involved in chromatin opening and gene activation (Cairns *et al.*, 1996). This complex facilitates gene activation by disrupting histone-DNA interactions. SWI/SNF has been associated with tumour suppression in humans because it has been shown that mutations in its subunits are associated with various cancers (Clapier and Cairns, 2009). Another chromatin remodelling complex is the ISWI complex. This complex is associated with chromatin compaction and gene repression (Corona and Tamkun, 2004).

It has been found to regulate nucleosome spacing, which ensures the proper organization of chromatin into transcriptionally silent regions.

CHD (Chromodomain Helicase DNA-binding) complexes are yet another well-known remodelling complex which are shown to influence chromatin dynamics by regulating transcription and DNA repair (Fig. 1.7).

These have been shown to play key roles in development and differentiation (Björklund and Gustafsson, 2005). There other types of chromatin remodelling such as the INO80 and SWR complexes. These are found to be involved in histone exchange and the incorporation of histone variants, which in turn can influence chromatin stability and transcriptional activity (Clapier and Cairns, 2009). Chromatin remodelling is often highly interrelated to histone post-translational modifications (PTMs) via the histone code hypothesis, whereby the histone PTMs serve as regulatory marks which recruit remodelling complexes to specific genomic loci (Zhang and Reinberg, 2001).

1.5.2 Chromatin and Transcription

Chromatin in *Saccharomyces cerevisiae*, as in higher eukaryotes, serves a dual purpose by preserving genome integrity while also dynamically regulating gene expression. Transcription in *S. cerevisiae* is carried out by RNA polymerase II and associated transcription factors, which must access DNA sequences within nucleosome arrays. As stated post-translational modifications of histones, including acetylation, methylation, phosphorylation, and ubiquitination, act as marks that regulate transcriptional activity in yeast (Li *et al.*, 2007). Additionally, ATP-dependent chromatin remodelling complexes, such as SWI/SNF, ISW1, and RSC, reposition or remove nucleosomes to reveal promoter and enhancer regions, thereby enabling efficient transcription.

The interplay between chromatin organization and transcription in yeast serves as a powerful model for understanding fundamental epigenetic mechanisms also at work in human cells. Because of its genetic tractability, *S. cerevisiae* has been widely used to uncover the roles of histone modifications, nucleosome positioning, and transcriptional regulation. Importantly, many chromatin-associated processes identified in yeast are conserved in higher eukaryotes, including humans.

Disruption of these mechanisms has been implicated in diseases such as cancer and developmental disorders, emphasizing the importance of yeast as a model for dissecting chromatin-transcription regulation (Li *et al.*, 2007).

1.6 Transcriptional Control in Yeast

Transcription is a process in which DNA is transcribed into RNA, and this process is closely regulated by chromatin structure which controls accessibility to the DNA by the transcriptional machinery (Struhl and Segal, 2013).

In eukaryotic cells, the regulation of transcription is done so that the correct gene can be activated or silenced in response to the correct environmental or cellular cue.

1.6.1 Gene Promoters in Yeast

Promoters are DNA sequences that provide a binding site for the transcription machinery. The yeast promoters have their characteristic features that enable productive transcription by this

complex. Many of the yeast promoters contain TATA boxes, which are important for the precise initiation of transcription. They also contain upstream activator sequences (UASs), which assist in the recruitment of the transcription factors. However, most of those yeast promoters, are devoid of complex enhancer regions compared to higher eukaryotes, thus requiring only proximal elements for driving the process of transcriptional control. This allows rapid responses to changes in environmental conditions (Fig. 1.8).

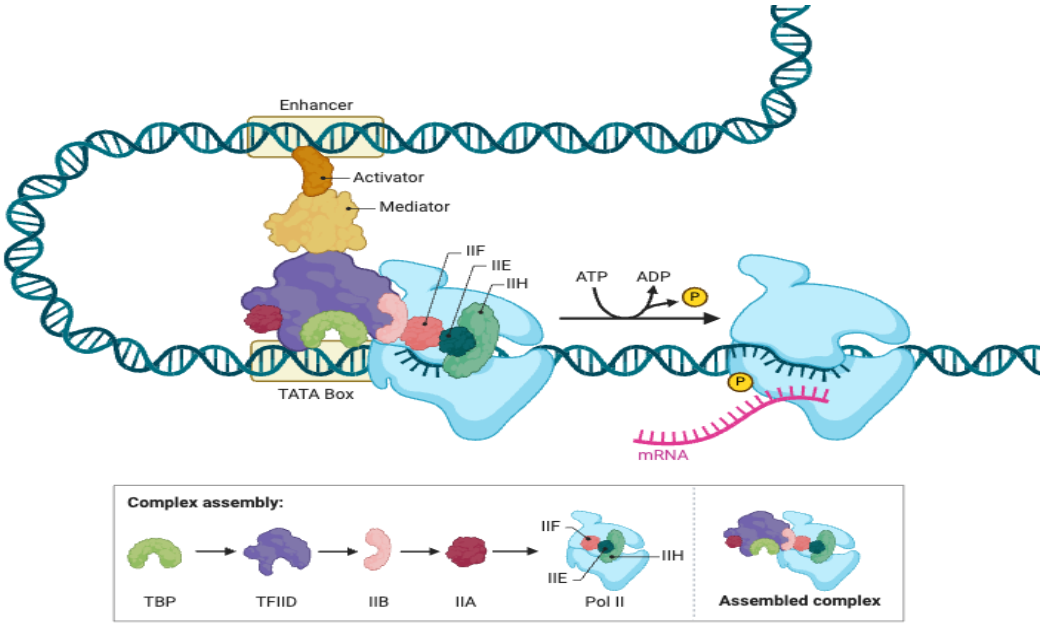


Figure 1.8: Eukaryotic Gene Regulation: Transcriptional and Initiation. A depiction of the pre-initiation complex (PIC) structure reveals the positioning of RNA polymerase II (Pol II) along with general transcription factors (GTFs) such as TFIIA, TFIIB (C-terminal domain), the TBP subunit of TFIID, TFIIE, and TFIIK subunits Ssl2 (helicase module) and TFIIK (kinase module) at a TATA box within a gene promoter. The TATA box spans positions from -63 to -56 upstream of the transcription start site (TSS), while the dashed box indicates the transcription bubble formed upon initial promoter melting. This figure was created using BioRender.

1.6.2 Initiation, Elongation, Termination of transcription

i. Initiation of Transcription

The process of initiating transcription in yeast requires the gathering of numerous transcription factors along with RNA polymerase II on the promoter sites. The PIC (pre-initiation complex) is formed when part of TFIID, TATA-binding protein, or TBP can bind to the TATA box and provide a platform for other transcription factors and RNA polymerase II binding (Buratowski *et al.*, 1989). The Mediator complex and chromatin remodelling proteins stabilize the PIC. The process of PIC becomes more proficient by removing the histones to open the promoter regions to enable the process of transcription to occur.

Following the assembly of PIC, RNA polymerase II initiates a short RNA strand that is then stabilized and allows transition to elongation to commence.

ii. Elongation

Transcription elongation is the synthesis of the RNA transcript whereby the nucleotides are incorporated sequentially, catalysed by RNA polymerase II for protein encoding genes (Brivanlou and Darnell Jr, 2002). In order to stabilize RNA polymerase II on the DNA template to ensure proper and efficient transcription, other factors such as the Spt4/5 complex are required (Hartzog, 2003). Chromatin architecture also plays an important role in elongation. Nucleosomes are removed in front of the advancing RNA polymerase, and are reassembled behind the RNA polymerase II by the action of chaperones such as the FACT complex (Orphanides *et al.*, 1998). Additionally, the phosphorylation of the CTD of RNA polymerase II facilitates the recruitment of RNA processing enzymes, allowing mRNA to be co-transcriptionally modified (Phatnani and Greenleaf, 2006).

iii. Termination

Termination of transcription in yeast is a highly coordinated process with several mechanisms to ensure the correct completion of RNA synthesis and release of RNA polymerase II from the DNA (Kim *et al.*, 2004). Predominantly, termination involves two pathways, namely, the Nrd1-dependent pathway and the Rat1-dependent pathway. In the Nrd1-dependent pathway, the complex of Nrd1-Nab3-Sen1 influences cleavage and hence termination through its

specific binding within the RNA (Steinmetz *et al.*, 2001). In contrast, the Rat1-dependent pathway degrades the RNA transcript by the action of Rat1 exonuclease and thereby releases the RNA polymerase II complex from the DNA template (Kim *et al.*, 2004).

Termination is thus an important process with regard to recycling the transcription machinery for maintaining the correct gene expression pattern (Porrua and Libri, 2015).

1.7 Mediator Complex

The Mediator complex is a crucial multi-subunit assembly that facilitates the interaction between transcription factors and RNA polymerase II. The Mediator complex plays a very important role in regulating transcription (Conaway and Conaway, 2011). Especially at constitutive and inducible promoters in yeast, it has been demonstrated that the mediator facilitates an interaction between transcription factors and RNA polymerase II, resulting in the assembly of the pre-initiation complex (Björklund and Gustafsson, 2005).

Owing to its modular architecture mediator can interact with various chromatin remodels, thereby securing the transcription machinery for efficient and productive transcription initiation and elongation (Malik and Roeder, 2005).

Through its tail, head, and kinase subunits, Mediator couples transcriptional responses to environmental changes that ensure the strict regulation of transcriptional activation according to cellular need (Allen and Taatjes, 2015).

1.8 The role of histone H2B ubiquitylation and histone H3 methylation in transcription

1.8.1 Histone H2B monoubiquitylation

The monoubiquitylation of histone H2B is a post-translational modification which involves the addition of a single ubiquitin molecule on histone H2B at lysine 123 in yeast and K120 in humans. Being a highly conserved process, H2B monoubiquitylation (H2Bub) is essential for a range of cellular processes, particularly transcription elongation. It is important to understand the molecular mechanisms underlying H2Bub, its regulatory enzymes, and its functional consequences on chromatin dynamics (Fig. 1.9).

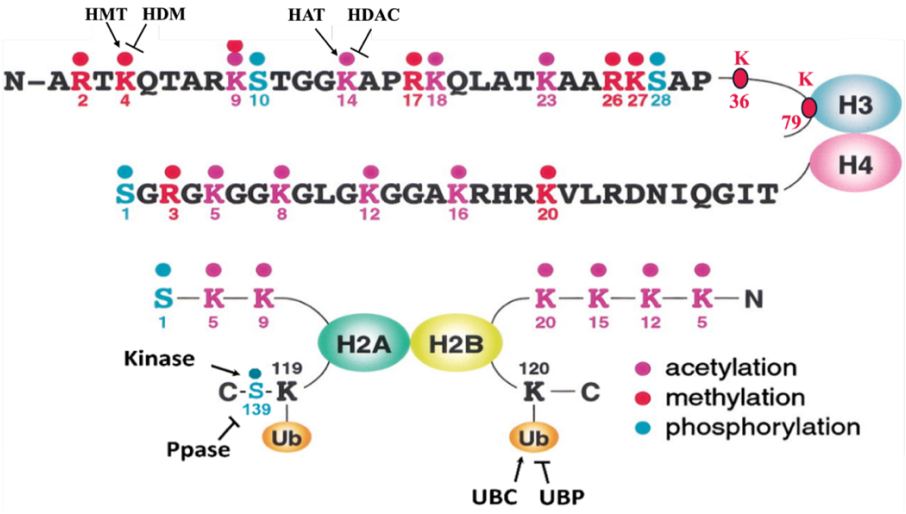


Figure 1.9: Schematic showing regulation of histone post-translational modifications. The modifications shown include acetylation (purple), methylation (red), phosphorylation (green), and ubiquitination (orange). Most of these PTMs are dynamic; there is machinery such as histone acetyltransferases (HATs), methyltransferases (HMTs), and ubiquitin conjugating enzymes (UBCs) to add these marks. Other enzymes can remove them, such as histone demethylases (HDMs), histone deacetylases (HDACs), phosphatases (Phases) and ubiquitin proteases (UBPs). This figure was uploaded by (Zhang and Reinberg, 2001).

1.8.2 Mechanism of H2B Ubiquitylation

The ubiquitylation of H2B is a multi-step process which involves a coordinated series of enzymatic activities, such as ubiquitin ligases and conjugating enzymes. E2 ubiquitin-conjugating enzyme Rad6 and the E3 ubiquitin ligase Bre1 are the key players in this process. These ligases together mediate the monoubiquitylation of H2B at lysine 123 (K123) in yeast or (K120) in humans.

The ubiquitin is first activated by Rad6 via formation of a thioester bond between ubiquitin and its active site cysteine residue. At the beginning of this process, the activation of ubiquitin by an E1 ubiquitin-activating enzyme happens. The activated ubiquitin then transfers the ubiquitin to Rad6, the E2 enzyme. The transfer of ubiquitin from Rad6 to the target lysine residue on H2B is then facilitated by Rad6, in collaboration with the E3 ligase Bre1. Bre1 recognizes H2B

and promotes its ubiquitylation, completing the catalytic cycle. The process of H2Bub is tightly coupled with transcription elongation. RNA polymerase II during the early stages of elongation interacts with Rad6 and Bre1. This interaction thereby facilitates the modification of H2B as transcription proceeds. The chromatin structure is believed to be loosened by this event through altered histone-histone and histone-DNA interactions, which help in the efficient progression of RNA polymerase II along the gene body. As a consequence, H2Bub promotes the elongation phase of transcription by modulating nucleosome dynamics and chromatin accessibility.

1.8.3 Role of H2Bub in transcription elongation:

Research has revealed a role for H2Bub in yeast as functioning to enable the nucleosome dynamics to occur during transcription elongation (Fleming *et al.*, 2008). Rad6 and Bre1 have been shown to associate with the elongating form of RNA polymerase II via the PAF complex (Fig. 1.10). When Pol II encounters a nucleosome the data suggests that H2B in that nucleosome is ubiquitylated via the action of the tethered Rad6 and Bre1 proteins and the nucleosome is evicted to allow passage of Pol II. This eviction step was shown to be independent of H2Bub. However, the authors revealed that H2Bub was essential for reassembly of the evicted nucleosome in the wake of the elongating Pol II. Subsequent de-ubiquitylation by the ubiquitin proteases also tethered to elongating Pol II via PAF, then remove the PTM and the system is re-set.

Furthermore, the authors showed that H2Bub cooperated with the histone chaperone Spt16 (a subunit of the FACT complex) to bring about the nucleosome reassembly. Mutation in either H2Bub or Spt16 resulted in loss of histone s during active gene transcription and increased levels of cryptic internal initiation events occurring within gene coding regions which titrated Pol II away from the correct start site to ultimately lower gene transcription levels.

Thus, although H2Bub is associated with actively transcribed genes, this highly dynamic PTM arguable plays a role in repression of transcription via its role in ensuring nucleosome reassembly during the elongation process which maintains the integrity of the chromatin fibre.

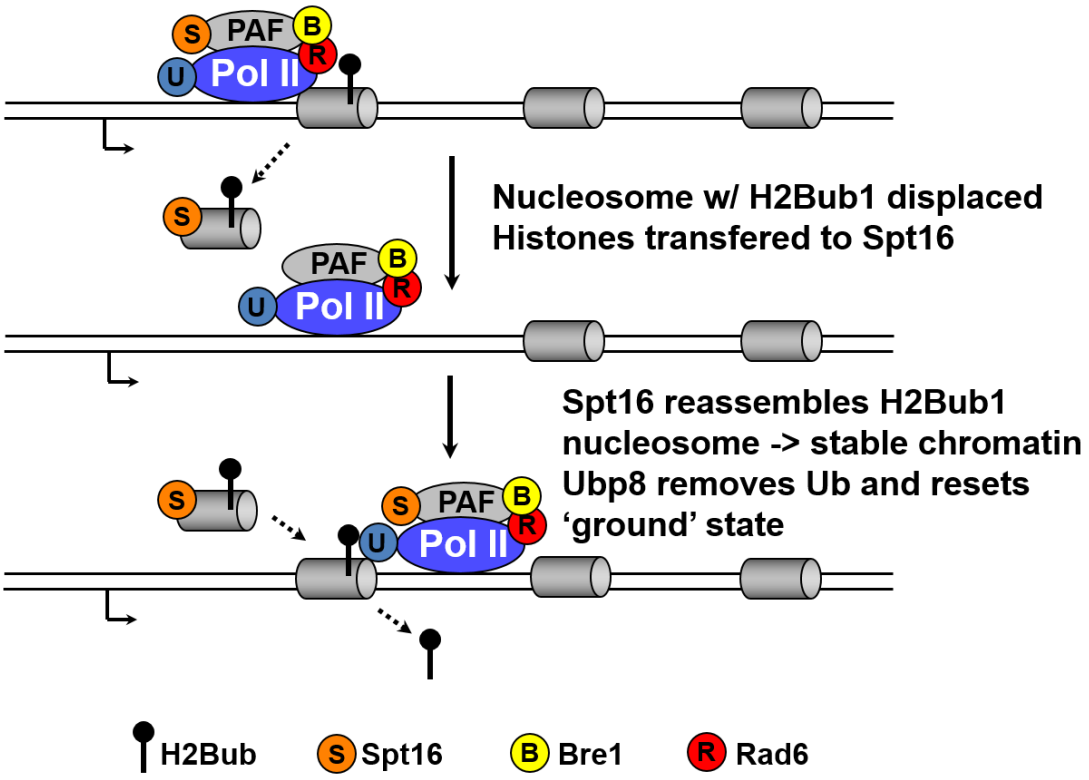


Figure 1.10: Role of H2Bub during transcription elongation. Rad6 (R), Bre1 (B) and Spt16 (S) all travel with the elongating form of RNA Pol II, in an association mediated by PAF. Upon encountering a nucleosome, H2B is ubiquitylated and the nucleosome is evicted and bound by Spt16. After passage of Pol II, Spt16 and H2bub are required for reassembly of the evicted nucleosome. The ubiquitin protease (Ubp8), which also travels with Pol II, then removes the ubiquitin from the reinstated H2B (Fleming et al., 2008).

1.9 Histone methylation in yeast

In yeast, only the lysine (K) residues 4, 36, and 79 of histone H3 can be methylated. Methyltransferases can attach up to three methyl groups to a single lysine residue, resulting in mono-, di-, or tri-methylation patterns .

Set1, which is part of an eight-protein complex called COMPASS, adds a methyl group to lysine 4 of histone H3. H3K4 methylation shows a progressive variation in levels across most active genes. Tri-methylation is concentrated near the promoter region, di-methylation is located at the 5' end of the gene, and mono-methylation is more abundant further downstream. The degree of

methylation is determined by the length of interaction between the Set1 methyltransferase complex and the nucleosome (Carozza mj et al., Cell, 2005).

Set2 methylates lysine 36 (H3K36) of histone H3 and is enriched at the 3' region of active ORFs. Dot1 (Disruptor of telomeric silencing) adds methyl groups to the H3K79 residue and was initially discovered as a factor involved in the silencing of yeast telomeres. However, H3K79me also plays a role in transcription, progression through the cell cycle, and the cell response to DNA damage (Fleming et al., 2008).

1.9.1 The role of H3 lysine 36 methylation during transcription

H3 lysine 36 methylation has been shown to be required for deacetylation of gene coding regions during transcription elongation to prevent aberrant internal transcription events from occurring (Fig. 1.11) (Carozza mj et al., Cell, 2005). Specifically, deposition of H3K36me on gene coding 3' regions by SET2 enables recruitment of the histone deacetylase, Rpd3p via a chromodomain in Rpd3p. The subsequent deacetylation of the chromatin after transcription erases the transcription coupled acetylation to maintain a repressive chromatin structure which inhibits internal transcription events. Thus, similar to the role of H2Bub during transcription elongation, this PTM, although associated with active transcription actually has a repressive effect to maintain chromatin integrity during transcription.

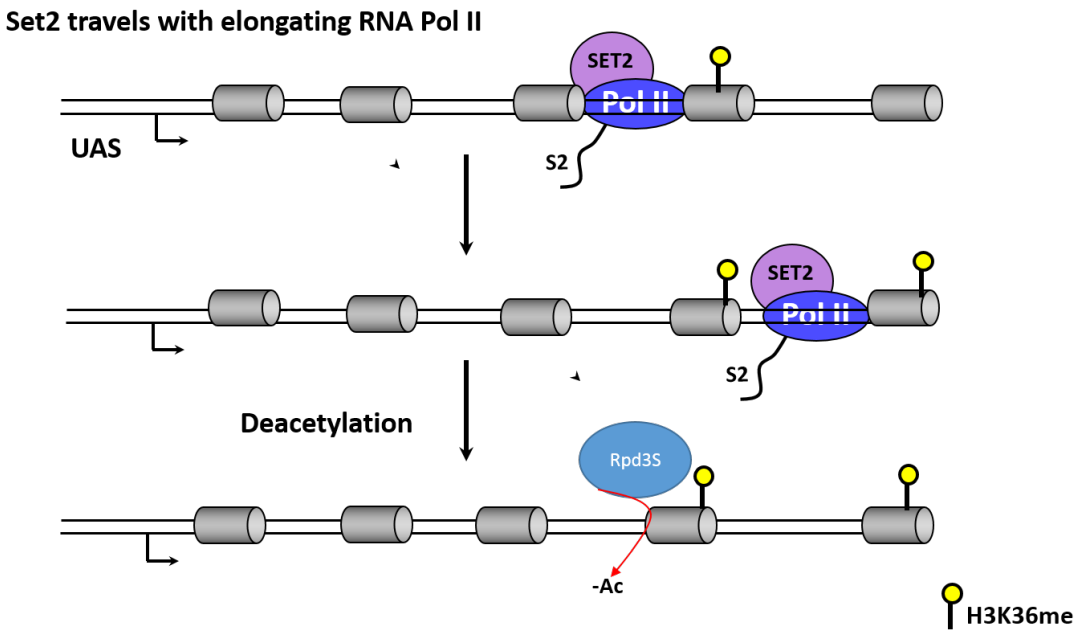


Figure 1.11: Role of H3K36me during transcription elongation. Set2 travels with the elongating form of RNA Pol II phosphorylated on its carboxy-terminal domain (CTD) at serine 2. This results in H3K36me being deposited at the 3' end of genes. Recognition of the H3K36me mark by the histone deacetylase, Rpd3p, results in histone deacetylation and restoration of repressive chromatin after Pol II has passed (Fleming et al., 2008).

1.10 The PAF Complex as a Multifunctional Regulator of RNA Polymerase II Transcription

A highly conserved multi-subunit protein complex, RNA polymerase II-associated factor 1 (PAF) is an essential element in regulating gene transcription and in the deposition of H2Bub. It was first identified in yeast and has been as an important regulator of RNA Polymerase II (Pol II) transcription (Shi et al., 1996). PAF consists of several core subunits, such as Paf1, Cdc73, Rtf1, Ctr9, and Leo1, contributing towards the complex nature of its regulatory functions (Jaehning, 2010). The PAF complex plays a critical role that bridges the relationship between transcription elongation, modification of chromatin, and RNA processing, coordinating a number of events in gene expression. This regulation is crucial for cellular homeostasis, and aberrant expression of functional PAF complex has been implicated in a wide array of diseases, including cancers and developmental disorders (Francette et al., 2021).

1.10.1 PAF Regulation through Interaction with Pol II Elongation Machinery and Promoter-Associated Transcription Factors

Through interaction with the machinery involved in elongation by Pol II and promoter-associated transcription factors, the PAF complex regulates transcription. Thus, PAF connects the events of initiation and elongation of transcription to the downstream processing of RNA. Elongation factors like DSIF (DRB Sensitivity-Inducing Factor) and Spt5, which stabilize the elongation phase of Pol II, are involved in such an interaction. The association with Pol II is further consolidated by specific transcription factors, including c-Myc, which activate transcriptional elongation on target genes, thus aiding the recruitment of PAF to the actively transcribing genes (Petrenko and Struhl, 2021).

It has been shown that PAF ensures efficient transcriptional elongation and the stability of the transcription machinery during the elongation phase by associating with Pol II at chromatin-bound sites on actively transcribing genes. By doing so, the PAF complex functions much like a scaffolding unit, coordinating the actions of multiple elongation factors and transcriptional regulators, including FACT (facilitates chromatin transcription complex), which promotes transcription through nucleosome-dense regions of chromatin (Chu *et al.*, 2013). The interaction of the PAF complex with Pol II is also subject to regulation by the phosphorylation of the C-terminal domain, the largest Pol II subunit crucial event during the elongation phase. The CTD Ser2 and Ser5 sites can get phosphorylated, enabling Pol II to cycle through different phases of transcription and thus associate with different regulatory proteins, such as the PAF complex (Hintermair *et al.*, 2012). Because of this dynamic association with phosphorylated CTD, the PAF complex integrates the multiple stages of transcription and couples initiation and elongation of transcription with RNA processing and chromatin modification (Jaehning, 2010).

1.10.2 The PAF Complex's Role in H2B Monoubiquitylation

Promoting histone H2B monoubiquitylation is one of the hallmark functions of the PAF complex in regulating transcription mainly through its subunit, Rtf. Rtf facilitates the recruitment of the Rad6/Bre1 complex to Pol II during the active transcription of genes.

In the absence of the PAF complex, the levels of H2B monoubiquitylation drastically go down, giving rise to downstream chromatin modification and transcription elongation defects. Moreover, the involvement of Rtf1 in H2B monoubiquitylation underlines its crucial role in maintaining a transcriptionally active chromatin structure because this modification serves as one of the signals that open chromatin supports Pol II elongation**.**

In addition to stimulating the H2B monoubiquitylation, the PAF complex also interacts with the SET1/MLL complex responsible for methylation of another activating histone modification-H3K4-and is associated with active transcription. Thus, H2B monoubiquitylation coupled with H3K4 methylation nucleates a chromatin environment favourable for transcription elongation and enables the progress of Pol II without hindrance along gene bodies. This environment not only allows for efficient transcription but also provides a platform for recruiting other transcriptional coactivators and chromatin remodelers, further indicating that the PAF complex is a key mediator in transcriptional regulation.

1.11 Yeast Stationary Phase

Three defined phases comprise the life cycle of yeast, namely exponential growth, diauxie, and the stationary phase (Fig. 1.12). During the stationary phase, growth and cell replication eventually halt due to the total depletion of nutrients, accumulation of waste products, and environmental stressors (Allen *et al.*, 2006).

Physiological and metabolic changes take place during the stationary phase of growth that enable yeast cells to survive under conditions that are not favourable. These changes include altered gene expression, metabolism, and cell morphology.

Studies have shown that starved yeast cells follow different cellular paths, giving rise to two subpopulations within the culture; Quiescent and non-quiescent cell populations. These populations exhibit distinct physiological states, gene expression profiles, and responses to a range of environmental stresses, which profoundly affect cellular longevity and resilience (Werner-Washburne *et al.*, 2012) (Fig. 1.12).

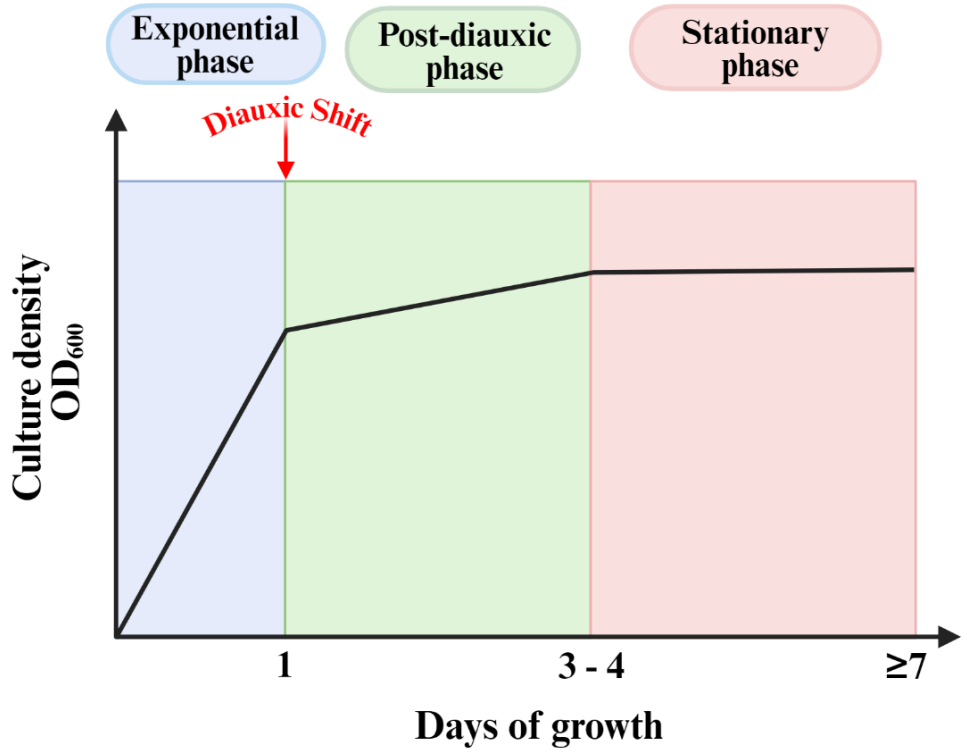


Figure 1.12: The transition to the stationary phase involves distinct growth phases. Initially, during the logarithmic phase characterized by rapid growth (depicted in light blue), yeast cells metabolize glucose through fermentation. Upon depletion of glucose, a global reprogramming event called the diauxic shift occurs, marking a shift to slower growth as yeast cells utilize fermentation byproducts via respiration (shown in light green). Eventually, when all carbon sources in the media are depleted, cells arrest in the cell cycle, entering true stationary phase (illustrated in light pink). Entry into the stationary phase typically occurs after 4 to 7 days of growth. This figure was created using BioRender.

1.11.1 Distinct Cell Populations: Quiescent (Q) and Non-Quiescent (NQ)

Isolation of these distinct populations of Q and NQ cells formed in stationary-phase yeast via density gradient centrifugation has enabled the study of these two populations (Fig. 1. 13). Quiescent cells are defined by their entry into a dormant state, akin to G0, where metabolic activity is low, transcription and translation are markedly reduced, the cell size is reduced, and they exhibit a higher resistance to environmental stressors. Such Q cells therefore exhibit greater survival under the unfavourable conditions of nutritional deprivation, but retain the ability to re-enter the cell cycle when nutrients become available (Werner-Washburne *et al.*, 2012).

Most importantly, it was discovered that the Q cell population comprised the young daughter cells within the population. NQ cells, on the other hand, are comprised of the older mother cells which ultimately undergo apoptosis. Thus, during SP the older mother cells commit suicide in an altruistic act to remove themselves from competing with the younger, fitter Q cells of the population, for when nutrients become available and the Q cells can re-enter the cell cycle.

1.11.2 Implications of Studying Q and NQ Cells

Insights from quiescent yeast cells can aid in understanding stem cell biology, as many stem cells also enter quiescent states during inactivity (Allen *et al.*, 2006). Research into stem cell maintenance, differentiation, and ageing in higher organisms can benefit from understanding the mechanisms that govern quiescence in yeast. Furthermore, these populations offer a unique opportunity to explore cellular resilience and adaptability. The initiation of growth under favourable conditions can be examined using these cells, contributing to the overall dynamics of yeast populations during fluctuating environmental conditions. In biotechnology, where yeast is used for fermentation, bio-production, and metabolic engineering, these cells can be studied for their roles (Werner-Washburne *et al.*, 1993, 2011) (Fig. 1.13).

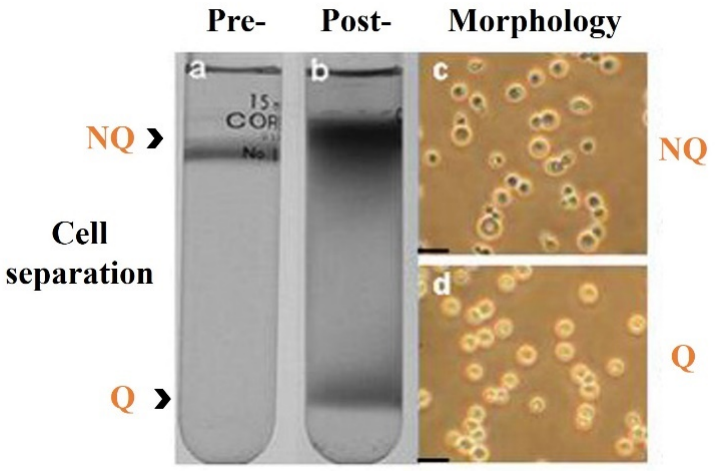


Figure 1.13: Diagram depicting the quiescent (Q) and non-quiescent (NQ) cell populations formed during Stationary phase. Percoll density gradient centrifugation to separate (Q) and (NQ) cell populations from stationary phase cultures. Cells are shown pre- and post-centrifugation. Cell morphology is shown of the separated (Q) and (NQ) cells isolated after the density gradient centrifugation. This figure was adapted from (Allen *et al.*, 2006).

1.12 Chromatin Remodelling During the Stationary Phase in Yeast

During quiescence, chromatin remodelling may play a key role in establishing the cellular adaptation process and / or in maintain Q cell integrity once formed. It has been shown that increased chromatin compaction, which limits transcriptional activity and reduces exposure to genotoxic stress, is exhibited by quiescent cells (De Virgilio, 2012). Histone deacetylation and chromatin condensing complexes also help in mediating this compaction (McKnight *et al.*, 2015). H2Bub is also removed from Q cell chromatin at diauxie. In addition to this, H2A.Z (histone variants) are incorporated during the stationary phase which alters nucleosome stability and might facilitate rapid transcriptional reactivation of Q cell growth upon return to favourable conditions (Gasch *et al.*, 2000).

Intriguingly, many histone PTMs associated with active transcription, such as H3K36 methylation, are maintained in Q cells despite the almost complete shut down in transcription in these cells (Young *et al.*, 2017). Furthermore, it was shown that mutants deficient for H3K36me and H2Bub lost viability during stationary phase.

Therefore, the aim of this thesis was to investigate the role of H3K36me and H2Bub during Q cell formation. Specifically, these histone modifications were hypothesized to establish a repressive yet dynamic chromatin landscape that enables quiescent cells to survive prolonged stress while retaining the capacity to efficiently re-enter the cell cycle when environmental conditions improve.

1.13 The Aim of This Research

This study aims to clarify the functional importance of histone modifications H2B mono-ubiquitination (H2Bub) and H3K36 methylation (H3K36me) during the yeast stationary phase (SP) and the transition to quiescence. By analysing mutants lacking H2Bub (*htb-K123R*) and H3K36me (*hht-K36A*), we will determine how the loss of H2Bub and the retention of H3K36me influence the formation of quiescent (Q) and non-quiescent (NQ) cells, their survival, and their re-entry into the cell cycle. Specifically, we will test whether H3K36me retention has an active regulatory role or simply reflects transcriptional shutdown, and whether the loss of H2Bub affects Q cell development and maintenance.

Through phenotypic and transcriptomic comparisons with wild-type cells, this work aims to clarify the roles of these PTMs in chromatin remodelling, transcriptional regulation, and long-term cell survival during SP.

1.14 The specific objectives:

This study aims to investigate the roles of H2B monoubiquitination (H2Bub) and H3K36 methylation (H3K36me) in regulating the development, maintenance, and exit of quiescent (Q) cells formed during the yeast stationary phase (SP).

Firstly, we will examine how deleting H2Bub and H3K36me3 influence the formation and differentiation of Q and NQ cells by comparing H2Bub and H3K36me-deficient mutant cels morphology and survival with that of wild-type at various SP time points.

Secondly, we will assess the role of these PTMs in maintaining Q cells in a dormant state through transcriptome profiling of wild-type and mutant Q cells, aiming to identify differentially expressed genes and pathways, particularly in metabolism, stress response, and cell cycle regulation. This will clarify how H3K36me3 retention and H2Bub loss in wild-type support Q cell identity and function.

Finally, Exit from quiescence will be evaluated by examining whether growth is resumed by wild-type and mutant Q cells after nutrient supplementation. Overall, this research will provide mechanistic insights into how these histone PTMs regulate chromatin and contribute to the survival strategies of yeast during SP.

By clarifying how eukaryotic cells control chromatin structure and transcription under stress conditions, this work will offer deeper insights into chromatin-based regulatory mechanisms that are conserved across organisms. Additionally, the findings have broader implications for biomedical research, contributing to a deeper understanding of ageing, cancer biology, and cellular stress responses.

Chapter 2

Materials & Methods

2.1 Chemicals, reagents and growth media

2.1.1 Chemicals and reagents

Chemicals and reagents for this study were obtained from a variety of sources, which are mentioned throughout in parentheses

2.1.2 Growth media

Materials used for the preparation of growth media were sourced from Formedium. Before use, all media were sterilized by autoclaving at 120°C for 20min. Solutions unsuitable for

autoclaving were sterilized by filtration through 0.22 µm Acrodisc Filters (Millipore) or, for larger volumes, through Stericup Filters (Millipore). Growth media were routinely made in double-distilled water and allowed to cool to 55°C before being supplemented as required.

2.1.3 Yeast extract, peptone, dextrose broth and media

Saccharomyces cerevisiae (*S. cerevisiae*) strains were routinely cultured in glucose-based, nutrient-rich yeast extract peptone dextrose (YEPD) medium (1% (w/v) yeast extract, 2% (w/v) Bacto peptone, 2% (w/v) dextrose) supplied by Formedium. YEPD was supplemented with adenine hydrochloride (40 µg/ml; Sigma) and ampicillin (50 µg/ml; Fisher Bioreagents) for long-term stationary phase cultures (>24 hours). Throughout this study, YEPD agar plates were used for culturing strains, reviving strains from freezer stocks, colony counting, and initial growth of transformants.

2.2 Yeast strains

The budding yeast *Saccharomyces cerevisiae* strain S288c is the standard laboratory reference strain and was the first eukaryote to have its genome completely sequenced (Goffeau *et al.*, 1996). To study histone function, a derivative strain known as JHY205 was generated, in which all four core histone loci are deleted and cell viability is maintained through plasmid-borne histone genes (Han, 1987; Hansen *et al.*, 2011). This system enables the introduction of specific histone mutations, and in this study, wild-type and mutant histone strains (*H2B-K123R, H3-K36A*) were used to assess the roles of histone modifications in chromatin regulation.
The name, genotype, and source of each strain are listed in (Table 2.1). Yeast strains were maintained as permanent stocks in 18 % (v/v) glycerol in YEPD broth and stored at -80°C.

2.2.1 Yeast culture conditions

Cells were cultivated in yeast extract peptone (YEP) broth, which was composed of 1% (w/v) yeast extract, 2% (w/v) peptone, and 2% (w/v) dextrose (glucose [D]) and YEPD agar (all for

medium) was used for growth. The cells were grown at 30°C with a shaking incubator (220 r.p.m), unless otherwise specified. Overnight starter cultures were created by inoculating 10 ml of YEPD with a single yeast colony. The next day, this culture was used to inoculate 50 ml of sterile medium in a 250 ml flask. The culture was allowed to grow until the desired (OD_{600nm}) was reached, which was determined by a spectrophotometer. A volume of this starter culture was sub-inoculated into a greater volume of YPD broth and grown under the same conditions until the log phase (Exp) was attained (Optical density (OD_{600nm}) between 0.5 - 0.6 nm on the spectrophotometer). Cell numbers were counted using a haemocytometer. The experiment showed the presence of diauxic (Dix) shift and stationary phase day 7 (SP- D7) specific quiescent cells Q. Glucose levels were monitored using Diastix's (Bayer).

The strains containing autotrophic markers were cultured in a synthetic complete (SC) medium. The SC medium was made by combining 0.19% yeast nitrogen base, 0.059% complete supplement medium, and 0.5% $[NH_4]_2SO_4$. In the case of solid media, 2% agar was added to the solution, which was then autoclaved. Glucose was later added to the medium to achieve a final concentration of 2%. Finally, amino acids were included or excluded based on the requirement, which is the carbon source (2% Glucose).

S. cerevisiae strains were in the (FY-406) background and were obtained from the gene deletion library (Table 2.1).

Strain	Genotype	Source	comment
FY-406 (wt)	*FY406 WT MATa (hta1-htb1)Δ::LEU2, (hta2-htb2)Δ::TRP1, his3Δ200 leu2Δ1 ura3-52 trp1Δ63*	This study	Background strain for deletion mutants used in this study

	lys2-128Δ <pZS146 HTA1-FLAG-HTB1-HIS3>		
YSF-201 (*htb-K123RΔ*)	*S288C (JHY205 quad histone deletion) + pRS315 HTA1-Flag-htb1-K123R, HHT1-HHF1*	This study	Background strain for *htb-K123RΔ*
YSF-202 (*hht-K36AΔ*)	*S288C (JHY205 quad histone deletion) + pRS315 HTA1-Flag-HTB1, hht1-K36A-HHF1*	This study	Background strain for *hht-K36AΔ*
YSF-203 (*K123R-K36AΔ*)	*S288C (JHY205 quad histone deletion) + pRS315 HTA1-Flag-htb1-K123R, hht1-K36A-HHF1*	This study	Background strain for *K36A-K123RΔ*
YSF-200 (wt)	*S288C (JHY205 quad histone deletion) + pRS315 HTA1-Flag-HTB1, HHT1-HHF1*	This study	Background strain for deletion mutants used in this study

Table 2.2: Yeast strains used in this research

2.3 Growth Curve and Final Cell Density

The YPD liquid medium was used to cultivate cells, and a Thermo-Spectronic (Genesys 10UV) was employed to measure ($OD600_{nm}$). Measurements were taken every 2 hours by mixing a 90 µl sample with 10 µl of H2O. Final cell density was determined after 24 and 48 hours of growth in YPD using a haemocytometer.

2.4 Microscope images of the yeast cells (Cell morphology)

Yeast cells were grown in YPD at 30°C overnight to the mid-log (Exp) and stationary phases day 7 (SP-D7). Then, the cells were washed with sterile distilled water H_2O, and 10 µl was spotted onto a glass slide.

They were viewed using a Leica DM500 microscope at x100 magnification with an oil immersion lens. Photographs were taken using Leica Application Suite (LAS) software to capture the images, which were enlarged using Microsoft PowerPoint.

2.5 Growth 'Spot' Tests

Cultures were grown to the mid-exponential stage (Exp) and the stationary phase on day 7 (SP-D7), and equal cell densities ($1x10^7$ cells/ ml) were re-suspended in YEP, the normalized to measure ($OD_{600\ nm}$ 0.5 - 0.6) and CFU counts. The cultures were spotted in 10-fold serial dilutions, and 3.5 µl of each sample was placed on appropriate agar plates and allowed to grow at 30°C for 3 days, unless otherwise stated. Cell sensitivity to cell wall-damaging agents was verified by spot tests on YPD media containing the indicated concentrations of caffeine. The cultures were grown at different temperatures, 15°C, 30°C, 37°C, and 40°C, to verify sensitivity to temperature. Sensitivity to osmotic and oxidative stress was verified by spot tests on YPD media containing different concentrations of hydrogen peroxide (H_2O_2) and sodium chloride (NaCl). The cultures were grown at a non-fermentable carbon source, Acetic Acid. The cultures were grown at Cantamythen, Sorbitol, Formamide and Lithium chloride.

2.6 Fractionation of stationary phase cultures

2.6.1 Preparation of Percoll density gradient

As described in (Allen *et al.*, 2006), fractionation of stationary phase cultures on day 7 (SP-d7) has been performed with minor modifications. To prepare a solution with a final NaCl concentration of 167 mM, Percoll (GE Healthcare) was diluted 9:1 (v/v) with 1.5 M NaCl. To create density gradients, 15 ml of glass Cortex tubes were filled with 10 ml of Percoll solution and centrifuged in a Sorvall centrifuge using an SS-34 rotor (10,500 r.p.m for 15 min, 20°C). The density gradients were prepared in advance and stored at 4°C until required for up to 24 hours (Fig. 2.2).

2.6.2 Density gradient separation of yeast cultures

To fractionate the cultures, Centrifuge 6.5 ml of cells at 1500 r.p.m for 5 minutes and remove the supernatant. Next, resuspended the cell pellets in 650 µl of Tris buffer (50 mM Tris-Cl, pH 7.5) and carefully layered pre-made gradients, overlaid drop-by-drop with the entire 650 µl of resuspended cells. The gradients were centrifuged at 2000 r.p.m for 60 minutes at 20°C, resulting in two distinct bands. Then, collected the upper fraction (non-quiescent cells, NQ) by gently pipetting some of the band (< 50 % per gradient) from two gradients to a 15 ml centrifuge tube. The cells were washed once in 5x volume Tris buffer and pelleted by centrifugation at 3000 r.p.m for 5 minutes at 18°C.

The number of cells recovered was measured by spectrophotometry, and 10 OD_{600nm} unit samples were removed for protein extraction, which we washed in 1 ml of 20% trichloroacetic acid (TCA) and stored at -80°C until required (Section 2.7.1). The lower fraction (quiescent, Q) was collected and washed in 5x volume Tris buffer and pelleted by centrifugation at 1500 r.p.m for 3 minutes at 18°C. The pellet was resuspended in 350 µl Tris buffer, loaded onto another gradient, and centrifuged as before to purify the lower band. After centrifugation, the lower band was harvested and washed it in a 5x volume Tris buffer. Then resuspended the cell pellet was resuspended in 10 ml of Tris buffer, and the optical density of the purified cells was measured (Fig. 2.2). 10 OD_{600nm} unit samples were taken for protein (Section 2.7.1) and RNA (Section 2.8.1)

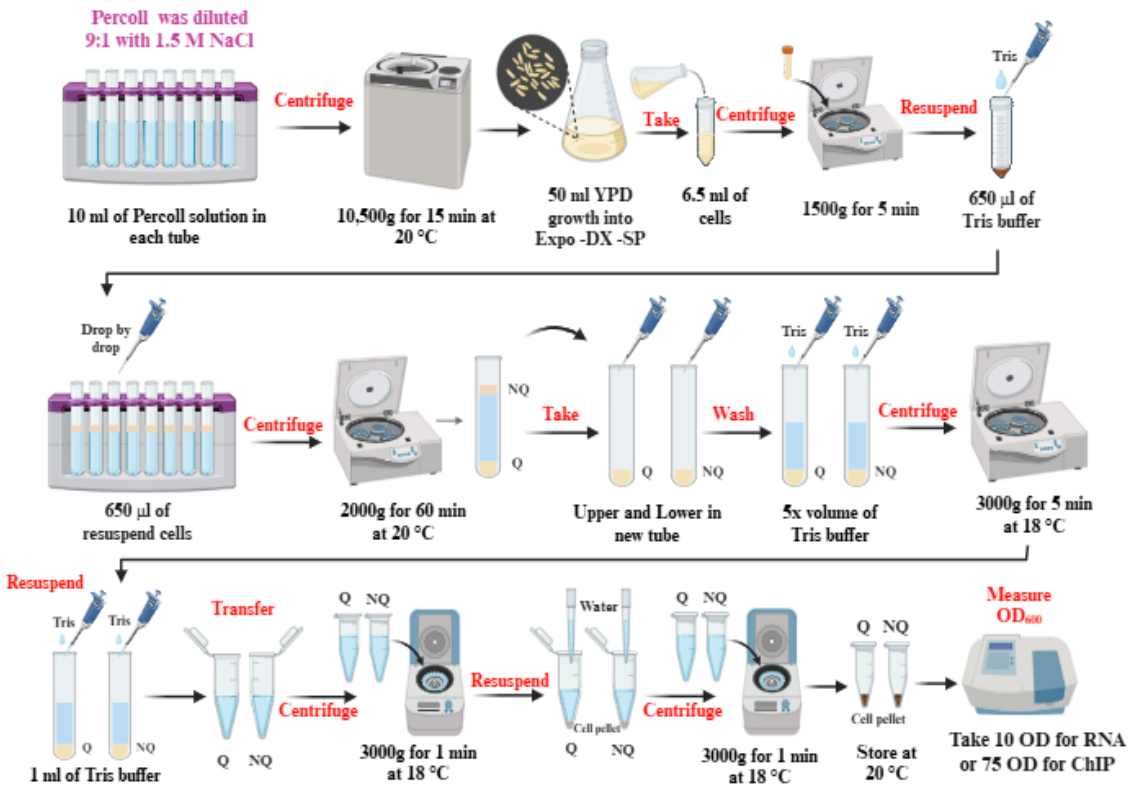


Figure 2.1: Schematic of fractionation of stationary phase cultures. This figure was created using BioRender.

2.7 Western blot analysis

2.7.1 Protein Extraction

The 20% TCA Protocol (Szymanski and Kerscher, 2013) was adapted to extract protein. Cells were grown overnight in a 50 ml culture to mid-log phase (Exp) ($OD_{600\ nm}$ 0.5 - 0.6), the diauxic shift (Dix), and stationary phase day 7 (SP–D7), specific quiescent cell (Q) (Section 2.7.1). A volume equivalent to (10 $OD_{600\ nm}$ units) was removed and centrifuged at 1500 r.p.m for 5 minutes. After removing the supernatant, the cell pellet was resuspended in 1 ml of 20% trichloroacetic acid (TCA) and transferred to a 1.5 ml microcentrifuge tube. It was then centrifuged at 13,200 r.p.m for 1 minute, and the supernatant was removed. The pellet was re-suspended in 250 µl 20% TCA, and ~500µl of glass beads (400 – 600 µm) were added. The samples were vortexed for 30 seconds using a high-speed benchtop homogenizer and kept on

ice for 1 minute, repeated thrice. The cell lysate was transferred to a 1.5 ml microcentrifuge tube.

The glass beads were washed using 500 µl 5% TCA, and the wash was added to the cell lysate and kept on ice for 3 minutes. The cell lysate was centrifuged at 13,200 r.p.m for 1 minute, and the supernatant was discarded. The pellet was resuspended in 300µl 1x Laemmli (0.1% 2-mercaptoethanol, 10% glycerol, 2% SDS & 63 mM unbuffered Tris-Cl) and incubated at 95°C for 5 minutes. After centrifuging for 1 minute at 13,200 r.p.m, the supernatant was transferred to a new 1.5 ml microcentrifuge tube and stored at -20°C (Fig. 2.3).

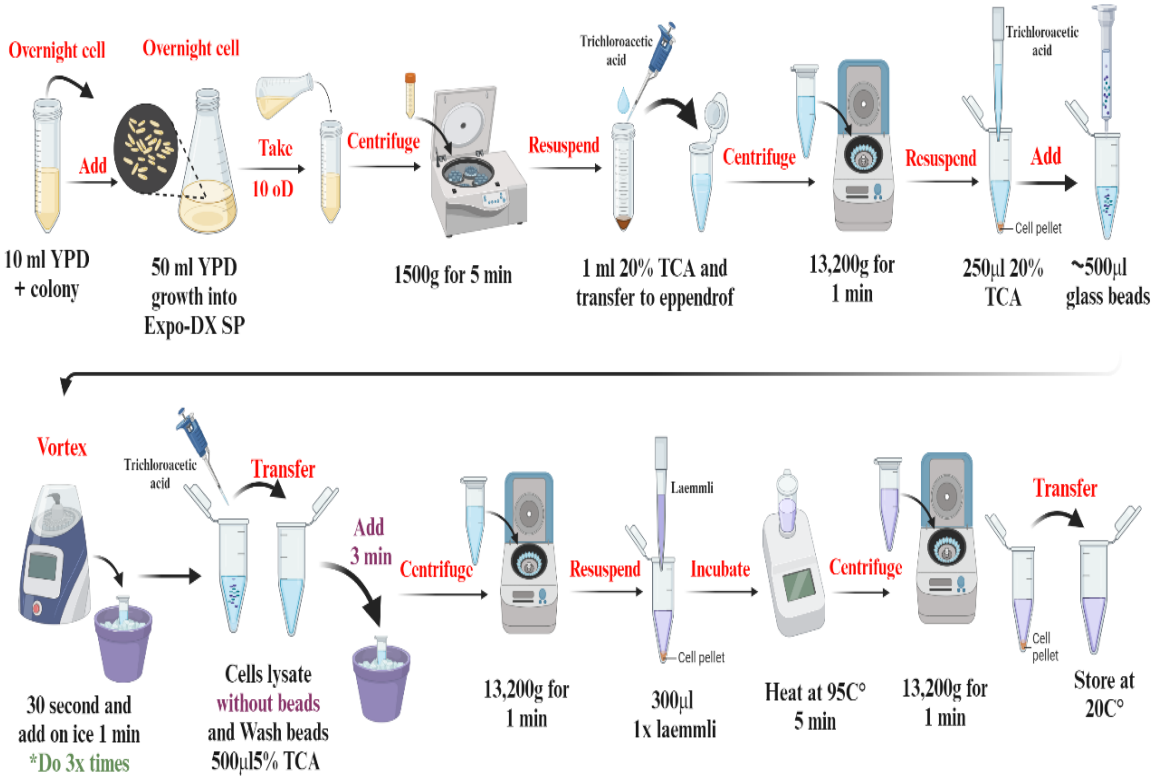


Figure 2.2: Schematic of Protein Extraction. This figure was created using BioRender.

2.7.2 Bradford Assay

Followed the instructions provided by Sigma to conduct a Bradford assay. Prepared Bovine Serum Albumin (BSA) standards, ranging from 1 to 10 µg/ml, and diluted protein samples in H_2O. Next, added the Bradford Reagent {Sigma} and measured the absorbance ($A_{595\ nm}$) with a spectrophotometer. By comparing the absorbance values to a standard curve, we were able to

calculate the protein concentration accurately. To ensure consistency, adjusted the protein sample concentrations to 2 mg/ml using 1x Laemmli buffer and stored them at -20°C. This method allowed to establishment of a reliable protein quantification system for research.

2.7.3 SDS-Polyacrylamide gel electrophoresis (SDS-PAGE)

2.7.3.1 Preparation of protein samples for SDS-PAGE

Cells (10 OD600 units) were grown overnight in a 50 ml culture to mid-log phase (Exp), ($OD_{600\ nm}$ 0.5-0.6), the diauxic shift (Dix), and stationary phase day 7 (SP – D7), specific quiescent cell (Q) (Section 2.7.1), centrifuged at 1500 r.p.m for 5 minutes.

Pellets were washed in 1 ml 20% (w/v) trichloroacetic acid (TCA) and frozen at -80°C until required. Pellets were thawed on ice and resuspended in 250 µl 20% TCA. ~500 µl of glass beads (400 – 600 µm) acid-washed beads (Sigma) were added (≈ 0.6 g), and cells were lysed using a vortex for 30 seconds using a high-speed benchtop homogenizer and kept on ice for 1 minute, repeated thrice a multi-head adaptor (Vortex Genie 2 with a Turbomix adapter).

Supernatants were transferred to fresh microcentrifuge tubes. Beads were further washed with 500 µl 5% (TCA), and supernatants were combined in a microcentrifuge tube. Lysates were centrifuged (13,200 r.p.m, 1 min, 4°C), and the supernatant was removed. Pellets were resuspended in 300 µl 1 x Laemmli Buffer (63 mM Tris HCl, 10% (v/v) glycerol, 2% (w/v) SDS, 0.0025% (w/v) Bromophenol Blue, at a final pH 6.8) and heated to 95°C for 5 min. Following brief vigorous mixing, samples were centrifuged as above, and the supernatant was transferred to a fresh micro-centrifuge tube. Protein concentration was determined using the Quick Start™ BGG Standard Set (Bio-Rad) as per manufacturer's instructions. 2 mg/ml stocks were made by dilution in 1 x Laemmli Buffer and 25 µl aliquots were frozen at -80°C until required (Fig. 2.3).

2.7.3.2 Preparation and running of SDS-PAGE

To prepare for protein examination, it is important first to clean the glass plates. Depending on the specific protein being analysed, 10 ml of either 10% or 15% (v/v) acrylamide-resolving gel solution should be made per gel. Assemble 1 mm-thick plates and clamp them tightly, then pour

the gel solution between the plates until it's 1cm below the comb top when inserted. Immediately overlay the gel with 1 ml of isopropanol to allow for polymerization, and let it set for 20 minutes. Remove the isopropanol layer and prepare 10 ml of 5% (v/v) acrylamide stacking gel to be layered on top of the resolving gel. Immerse plastic combs containing 10 wells into the stacking gel and allow the gels to set before using them for SDS-PAGE. See the recipes below for details on the resolving and stacking gels:

15 % resolving gel (5 ml): 2.3 ml H_2O, 2.5 ml 1.5 M Tris-HCl (pH 8.8), 5 ml 30% acrylamide, 100 µl 10 % (w/v) SDS, 100 µl 10 % (w/v) ammonium persulfate (APS), 4µl TEMED.

10 % resolving gel (5 ml): 3.8 ml H_2O, 2.6 ml 1.5 M Tris-HCl (pH 8.8), 3.4 ml 30% acrylamide, 100 µl 10 % (w/v) SDS, 100 µl 10 % (w/v) ammonium persulfate (APS), 2 µl TEMED.

Stacking gel (5 ml): 6.4 ml H_2O, 1.65 ml 1 M Tris-HCl (pH 6.8), 1.65 ml 30% acrylamide, 100µl 10 % (w/v) SDS, 100µl 10 % (w/v) ammonium persulfate (APS), 10µl TEMED.

For precise protein analysis, it is highly recommended to heat the protein for 5 minutes at 95°C before loading 40 µg into each well. Additionally, to include the EZ-Run™ Prestained *Rec* Protein Ladder (Fisher) was loaded as a size reference sample. The gels should be run for 3 hours at 100V in running buffer (25 mM Tris, 190 mM glycine, 0.1% w/v SDS) to ensure optimal results (Fig. 2.4).

2.7.4 Western Blot

In this study, the western blotting protocol was adapted from Current Protocols in Molecular Biology (Gallagher *et al.*, 2011). To transfer the protein to a polyvinylidene fluoride (PVDF) 0.45 µM membrane (Immobilon-P) (Millipore), a transfer buffer consisting of (25 mM Tris, 190 mM glycine, and 20% (v/v) methanol) was used. The transfer process was carried out at 300 mA for 90 minutes using (Bio-Rad) equipment (Mini trans-blot 153BR) surrounded by ice. Before use, the PVDF membrane was activated by soaking in 100% methanol for 20 seconds, followed by water for 2 minutes. Additionally, two sponges and four pieces of blotting paper were soaked in a transfer buffer. Transfer of protein was performed at 300 mA for 40 minutes (proteins 10 – 80 kDa) or 90 minutes (proteins >80 kDa) at 4°C on Ice.

2.7.4.1 Detection of protein antigens

After transfer, the membrane was incubated in 20 ml of blocking buffer at room temperature for 1 hour to prevent non-specific binding of the primary antibody, were then diluted appropriately in 20 ml of blocking solution with the membrane. The primary antibody was then added and incubated overnight at 4 °C to allow for specific binding to the target protein.

The next day, the membrane was washed four times for 5 minutes in TBST (Tris-buffered saline, 0.05% Tween 20 (v/v)) (TBST, Sigma) to remove any unbound primary antibody.

The secondary antibody (HRP) conjugated (GE Healthcare) was then added and incubated and diluted 1:10,000 in 20 ml of blocking buffer at room temperature for 90 minutes or 2 hours to bind to the primary antibody. The membrane was washed once for 10 minutes in TBST and three times for 10 minutes in Tris Buffer Saline (TBS, Sigma) to remove any unbound secondary antibodies. Finally, the bound antigens were visualized using image Image-Quant LAS4000 imager after preparing the enhanced chemiluminescent (ECL). Western blotting substrate (Pierce) according to the manufacturer's instructions (Fig. 2.4).

Notes: In proteins (H3K79m^3 and H3H79m^2) used similar steps were used above, except the step for washes in all use TBS (Tris-buffered saline, 0.1% Tween 20).

The (table 2.2) below provides information on the antibodies used in the western blot analysis, including their dilution in the blocking buffer:

Marvel blocking buffer: 5 % (w/v) Marvel non-fat dry milk in TBS with 0.05 % Tween 20 (v/v).

BSA blocking buffer: 5 % bovine serum albumin (Sigma) (w/v) in TBS with 0.1 % Tween 20 (v/v).

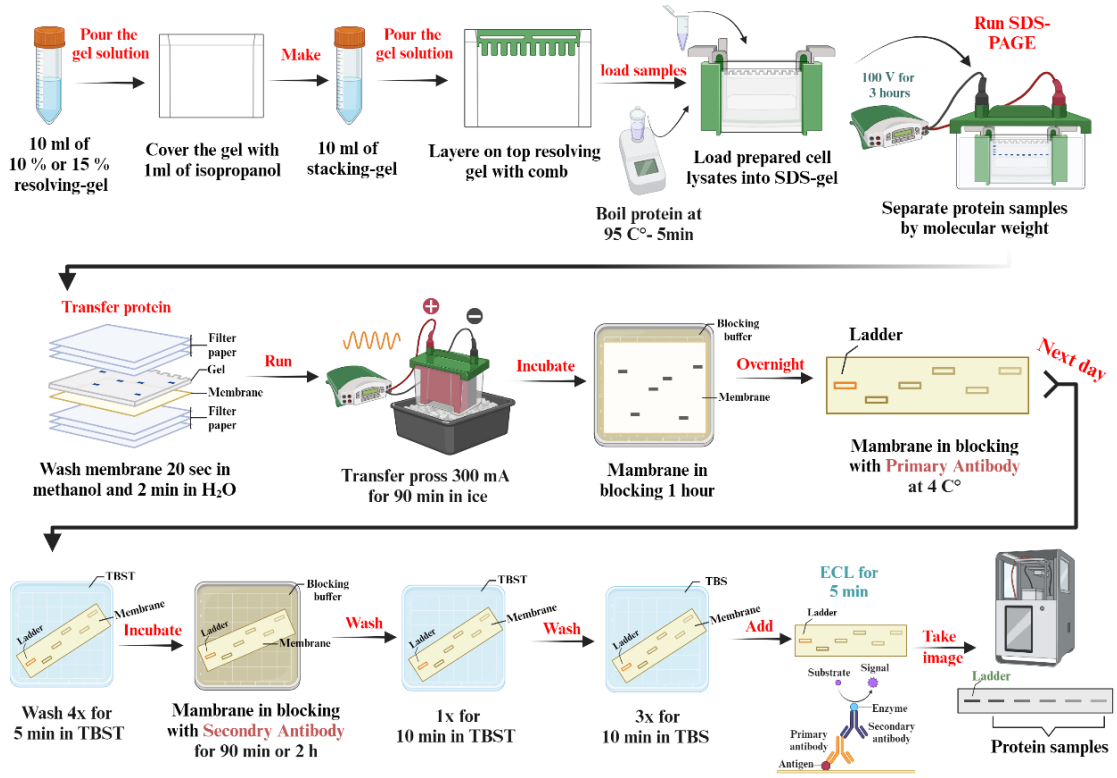


Figure 2.3: Schematic of SDS-Polyacrylamide gel and western blot. This figure was created using BioRender.

Proteins	Concentration	Species	Source	Blocking buffer
β-actin	1:3000	Mouse	Abcam (8224)	5% Milk/TBST
Pol II	1:500	Mouse	Santa Cruz (Sc-56767)	5% Milk/TBST
Pol II-ser2	1:2000	Rabbit	Abcam (5095)	5% Milk/TBST
Pol II-ser5	1:1000	Rabbit	Active motif (39750)	5% Milk/TBST
Hho1	1:1000	Rabbit	Abcam (71833)	5% Milk/TBST
Gcn5	1:500	Rabbit	Santa Cruz (Sc-9078)	5% Milk/TBST
Rpd3	1:500	Got	Santa Cruz (Sc-6655)	5% Milk/TBST
H3	1:5000	Rabbit	Active motif (39163)	5% Milk/TBST
H4	1:1000	Rabbit	Abcam (7311)	5% Milk/TBST

H2A	1:3000	Rabbit	Active motif (39236)	5% Milk/TBST
H2B	1:2500	Rabbit	Active motif (39239)	5% Milk/TBST
H3K14ac	1:5000	Rabbit	Millipore (07-353)	5% Milk/TBST
H4ac^4	1:6000	Rabbit	Millipore (06-866)	5% Milk/TBST
H3K4me^3	1:3000	Rabbit	Active motif (39-159)	5% Milk/TBST
H3K9ac	1:5000	Rabbit	Millipore (07-352)	5% Milk/TBST
H4K16ac	1:2500	Rabbit	Millipore (07-329)	5% Milk/TBST
H3K56ac	1:2000	Rabbit	Millipore (07-677)	5% Milk/TBST
H3K36me^3	1:3000	Rabbit	Abcam (9050)	5% BSA/TBST
H3K79me^2	1:3000	Rabbit	Millipore (04-835)	5% BSATBST
H3K79me^3	1:10,000	Rabbit	Abcam (2621)	5% Milk/TBST
H2A.Z / HtZ1	1:1000	Rabbit	Active motif (39648)	5% Milk/TBST
H4S10-phosphor	1:5000	Rabbit	Active motif (39253)	5% Milk/TBST

Table 2.2: Antibodies used in western immunoblotting.

2.8 Isolation of RNA

The hot-phenol method was used to isolate total RNA with some modifications. Cell was harvested (10 OD units).

2.8.1 RNA Extraction

RNA was extracted using the hot-phenol method adapted from Current Protocols (Collart and Oliviero, 1993). First, 50 ml cultures were grown to the mid-exponential growth (Exp) (OD_{600nm} 0.5 - 0.6 nm) phase of the diauxic shift (Dix), and the stationary phase on day 7 (SP -D7),

specific quiescent cell (Q). A 50 ml sample was centrifuged for 5 minutes at 1500 r.p.m. The pellet was re-suspended in 1 ml of sterile water and transferred to a 1.5 ml tube. The cells were then pelleted by centrifugation. At this point, the cell pellets were either stored at -80°C or RNA was immediately extracted. The cell pellet was resuspended in 400 µl TES (10 mM Tris-Cl, pH 7.5, 10 mM EDTA, pH 8, 0.5% w/v SDS) and 400 µl saturated phenol to extract RNA. This was incubated at 65°C heat block for 1 hr with occasional vertexing for 10-15 seconds. The sample was then placed on ice for 5 minutes and centrifuged for 5 minutes at 13,500 r.p.m. The upper layer was transferred to a new 1.5 ml tube, and 400 µl of saturated phenol was added. The sample was vortexed, kept on ice for 5 minutes, and then centrifuged for 5 minutes at 14,600 r.p.m. The upper aqueous layer was transferred to a new 1.5 ml tube, and 400 µl of chloroform was added, followed by centrifugation for 5 min at 14,600 r.p.m.

2.8.1.1 Ethanol Precipitation

The upper aqueous layer was transferred to a new 1.5 ml tube, and 40 µl of sodium acetate (4M, pH 5.3) was added, followed by 1 ml of ice-cold 100% (v/v) Ethanol. This was kept at -20°C for one hour and then centrifuged for 10 minutes at 14,600 r.p.m at 4°C. The pellet was then washed with ice-cold 70% (v/v) Ethanol and centrifuged for 5 minutes at 14,600 r.p.m at 4°C. Finally, the pellet was completely dried and then resuspended in 50-90 µl of nuclease-free water. The RNA concentration was quantified utilizing a Nano-drop ND-100 spectrophotometer (Thermo-Scientific), with measurements taken at an absorbance wavelength of (A_{260nm}) (Fig. 2.5).

2.8.1.2 Determination of nucleic acid concentration

The concentration of RNA in solution was measured using a Nanodrop ND-100 spectrophotometer (Thermo Scientific). RNA concentration was measured at an absorbance wavelength of (A_{260nm}). At this wavelength, A260nm = 1 corresponds to a concentration of 35 µg/ml of RNA. The Nanodrop simultaneously measures the purity of RNA solutions by measuring absorbance at (A_{260nm}). For pure, uncontaminated RNA, the ratio of (A_{260nm}) to

(A_{280nm}) is ≈ 2. These values were checked during all measurements to ensure the purity of nucleic acid solutions.

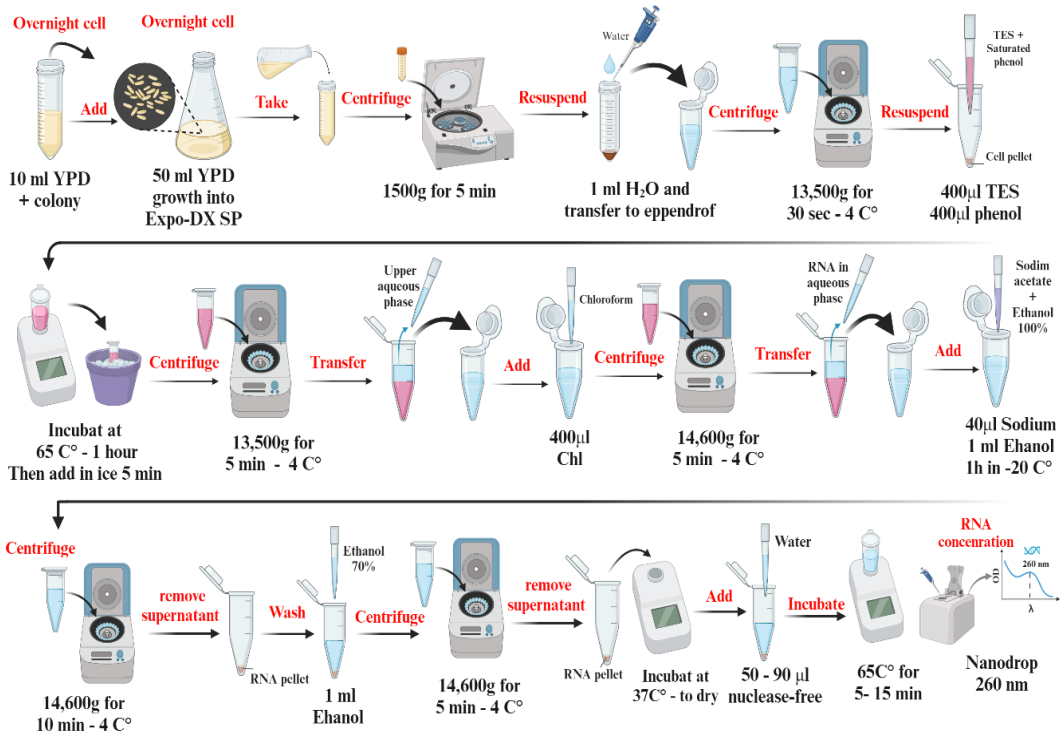


Figure 2.4: Schematic of RNA extraction. This figure was created using BioRender.

2.8.2 RNA-Seq

To perform RNA-Seq, the total RNA was extracted as per the standard protocol. Next, DNase treatment and purification of the extracted RNA were carried out using the {RNeasy Minelute Clean-up Kit from Qiagen}, following the manufacturer's guidelines. The quality of the RNA was assessed using the (2100 Bioanalyzer system) before sequencing, which is illustrated in (Fig. 2.6).

The sequencing process involved three major steps: rRNA depletion, cDNA library preparation, and sequencing on the Illumina Platform. For analysing differential gene expression (DGE) for each RNA-Seq dataset, it was carried out using the pipeline analysis (DESeq2 Bioconductor) package in (Fig. 2.6). This package normalised the raw count reads using the median of ratios method for each sample. It calculated the fold change from these normalised counts and

determined the Log2 of this number using the formula Log2 (Group2 mean normalised counts / Group 1 mean normalised counts). The RNA-Seq data were presented visually using (J-Browse 2 2.4.2), which was prepared by (Dr Karsten Hokamp, Trinity College Dublin, Ireland). Following RNA-Seq, the R^2 (square) regression coefficient (Quality control) analysis was performed on the data. It recognises the percentage of variation of the dependent variable and indicates that the data were of good quality.

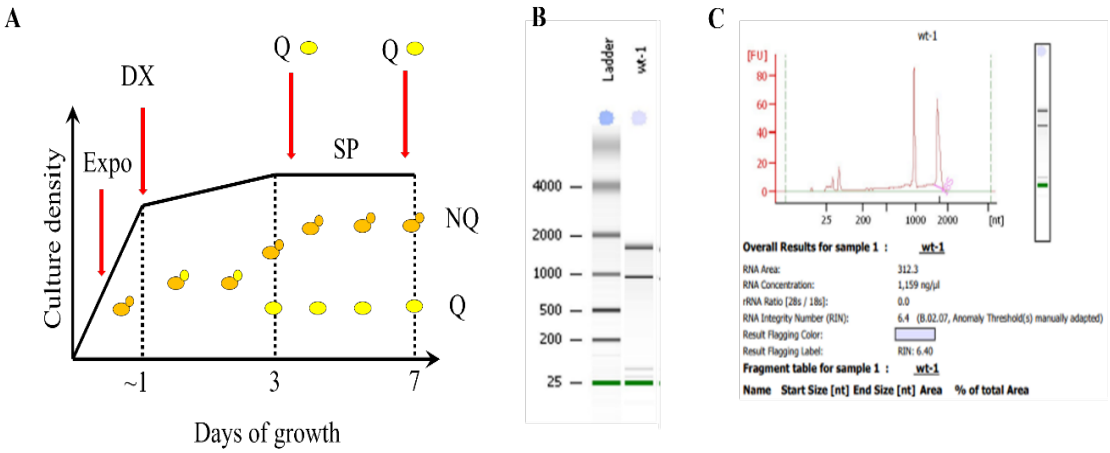


Figure 2.5: RNA sample preparation for RNA-Seq analysis. (A) Schematic to show times of RNA extraction at the exponential phase (Exp), at the diauxic shift (Dix), and in purified day 7 lower (Q) cells. (B) 1% Agarose formaldehyde gel showing the 28S and 18S rRNA bands from total RNA prepared from the representative wild-type sample (exponential phase), indicated. (C) Chromatogram of representative exponential wild-type sample showing RNA integrity (RIN) using RNA nano bioanalyzer 2100.

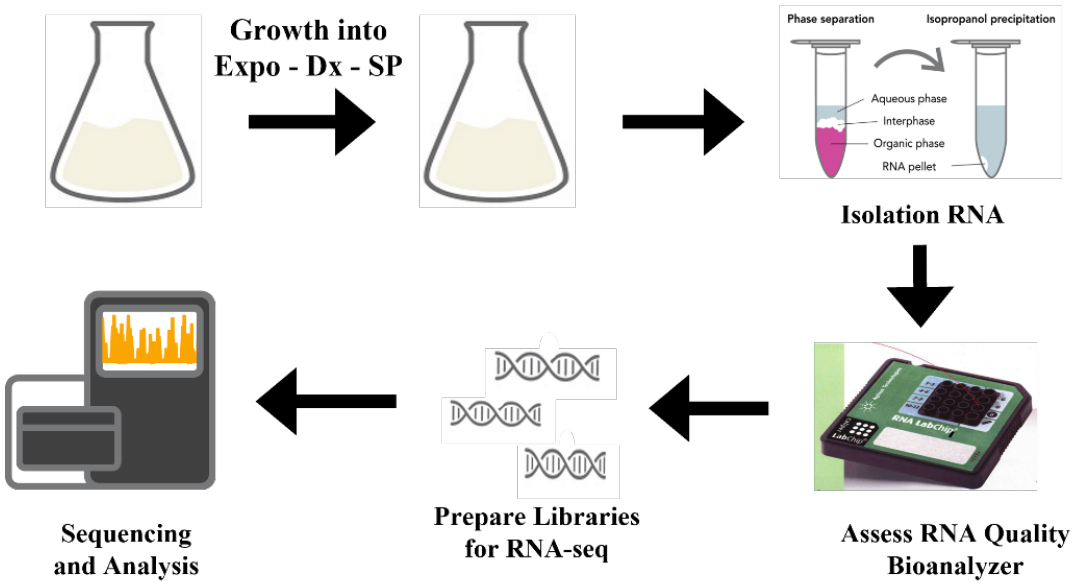


Figure 2.6: Schematic showing the main steps in RNA-Sequencing. Yeast cells were grown to mid-log phase (Exp) at the diauxic shift (DS), and RNA was isolated from purified day 7 lower (Q) cells and total RNA, then treated with DNase and purified before sequencing. The RNA sequencing involved removing ribosomal RNA (rRNA), fragmenting the RNA, and preparing cDNA, which was then sequenced. The bioinformatics analysis included mapping the reads to a reference genome, followed by differential gene expression (DGE) analysis. Figure adapted from (Carsten Kröger & Ali Bakit, 2023).

2.9 Statistical analysis

Statistical analysis was conducted using (GraphPad Prism 11). To determine the statistical significance of the results, either a T-test or a Two-way ANOVA was employed as appropriate. For multiple comparisons, a Tukey's multiple comparison test was utilized if there was no significant difference (p-value < 0.05) in the standard deviations of the groups, which was assessed by a Brown-Forsythe test. In cases where there was a significant difference in standard deviations (Xu *et al.*, 2024), a Games-Howells test was conducted for multiple comparisons. Results were considered statistically significant if the p-value was less than 0.05. (Funrich software) was utilized to generate all Venn diagrams, while (ClusterProfiler and Annotation hub) was employed to produce all Gene Ontology annotation and Enrichment analyses (Morgan and Shepherd, 2017), and the figure was plotted by ggplot2 (Wickham, 2016).

Chapter 3

Characterisation of mutants deficient for histone H2B monoubiqitylation and H3 lysine 36 methylation

3.1 Introduction

The regulation of processes such as transcription, replication, and DNA damage repair are governed by histone post-translational modifications (PTMs) such as acetylation, methylation, phosphorylation, and ubiquitination (Zhang *et al.*, 2015). They offer a dynamic system for cells to regulate cell function according to environmental and developmental cues (Kouzarides, 2007). Histone H2B mono-ubiquitination at lysine 123 (H2Bub) in yeast, equivalent to lysine 120 in mammals, has emerged as an important modification influencing chromatin structure and function during transcription elongation (Fleming *et al.*, 2008).

H2Bub1 has been shown to facilitate transcription elongation by assisting in restoring nucleosomes, and by maintaining the downstream histone H3 methylation. Indeed, histone H3 lysine 4 tri-methylation (H3K4me3), which is associated with active transcription, and histone H3 lysine 79 di- and tri-methylation (H3K79me2 and 3), involved in transcription elongation and DNA damage repair, are both dependent upon H2Bub (Sun and Allis, 2002; Kim *et al.*, 2005). Thus, these inter-dependent modifications highlight the complicated "crosstalk" between histone PTMs which enables a coordinated cellular response through the integration of chromatin activities. Although extensive research has been conducted on these PTMs during active transcription, the contributions of H2Bub and histone methylation to cell function particularly under different growth conditions and stress environments, are not yet fully understood.

In this chapter, a detailed analysis of the phenotypic and molecular characteristics of yeast mutants bearing specific substitutions at key residues in histone H2B and histone H3 methylation, which prevent H2B ubiquitylation and histone H3 lysine-36 methylation respectively, is conducted. To explore the functional relevance of H2Bub and H3K36me, the *htb-K123R*Δ, *hht-K36A*Δ, and the double mutant *K123R-K36A*Δ, were therefore designed.

In the *htb-K123R*Δ mutant, lysine (K) 123 is replaced with arginine (R); this maintains the positive charge while preventing ubiquitination. In the *hht-K36A*Δ mutant, lysine 36 is replaced

with alanine (A) which cannot be methylated. The use of a double mutant containing both H2B and H3 substitutions (*K123R-K36AΔ),* allows investigation of the consequence of the loss of both modifications upon cell function to be studied. These mutants therefore allow us to dissect the contributions of H2B and H3K36me to chromatin and stress adaptation, with a particular focus on events in stationary phase cells, which have not been well studied.

In this chapter, a systematic analysis of mutants under various physiological and stress conditions was conducted to understand the roles of these histone modifications. The study begins with an analysis of growth in glucose-containing liquid (YPD) media to establish baseline phenotypic differences. The viability of cells was then examined as they enter and remain in the stationary phase (SP), a period during which reorganisation of cell events occurs for survival over long-term periods (Allen *et al.,* 2006).

In the second part of this chapter, the phenotypic responses of mutants to various types of environmental stresses, including temperature shifts, oxidative and osmotic stresses, DNA-damaging agents, and fermentable and non-fermentable carbon sources, were analysed. The overall goal here was to identify unique sensitivities or adaptation mechanisms related to each mutant.

Finally, in the third section, the abundance of RNA Pol II, polymerase associated factor (PAF), the core histones, and various histone modifications pertinent to transcription were measured in wt and the histone mutants during exponential phase and during stationary phase to get insight into the transcriptional and histone modification landscape of wild-type and the mutants as these cells enter into stationary phase. This section ends with an analysis in the exponentially growing and SP strains of major histone acetyltransferases (HATs), histone deacetylases (HDACs) and the histone variant, Htz1p.

Taken together, this chapter interrelates the phenotypic observations with underlying molecular mechanisms to try to gain insight into understanding the contribution of H2Bub and H3K36me to cell function during growth into SP.

3.2 Results

3.2.1 Confirmation of wild-type, *htb-K123R*Δ, *hht-K36A*Δ, and *K123R-K36A*Δ strains

Prior to starting the study, the strains were confirmed by Western blot analysis (Fig. 3.1). In order to confirm the H2Bub-deficient strains, we first tried an antibody against H2Bub. However, the western blot results obtained were unreliable (data not shown). This led us to use antibodies against H3K4me3 and H3K79me3 instead (Fig. 3.1A, B) respectively. These antibodies were chosen as H2Bub has been shown to be required for the deposition of both of these modifications (Briggs *et al.*, 2001; Schulze *et al.*, 2009).

Thus, we could use the presence and absence of these methylation marks as a proxy for the presence and absence of H2Bub.

To validate the presence or absence of H3K36 methylation, we used an anti-H3K36me3 antibody (Fig. 3.1C).

The western blot analysis revealed H3K4me3 and H3K79me3 to be present in wild-type cells and the *hht-K36A*Δ mutant. However, both H3K4me3 and H3K79me3 were absent in the H2Bub-deficient strains, *htb-K123R*Δ and *K36A-K123R*Δ (Fig. 3.1 A, B). The western blot results obtained using the anti-H3K36me antibody showed that H3K36me3 was present in wild-type and *htb-K123R*Δ mutants, albeit at reduced levels in this mutant, but was absent in the H3K36me-deficient mutants, *hht-K36A* and *K123R-K36A*Δ (Fig. 3.1C). Together, the results confirmed the strains used in this study were correct.

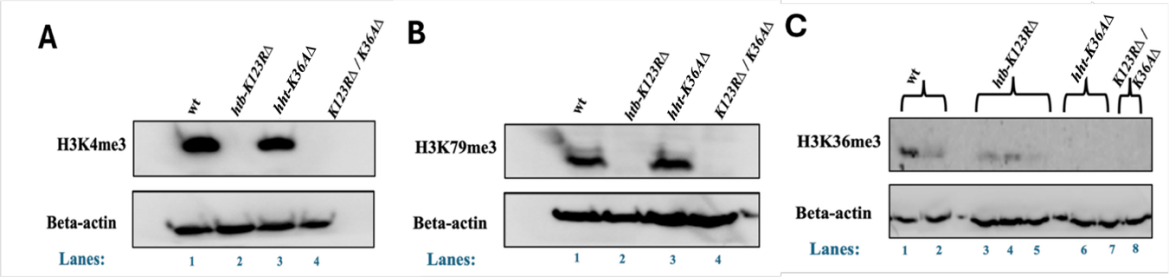


Figure 3.1: Western blot analysis to confirm the strains used in this study. The protein lysates were isolated from cells in the exponential phase. Antibodies specific for **(A)** H3K4me3, **(B)** H3K79me3, and **(C)** H3K36me3 were used in immunoblotting in wild-type, *htb-K123R*Δ, *hht-K36A*Δ, and *K36A-K123R*Δ strains, as indicated. Equal loading of protein lysate was confirmed by actin immunoblot. All

bands were of the expected sizes. In **(C)**, duplicate and triplicate samples were loaded, except for *K123R-K36A*Δ double mutant lysates, as shown. Representative images of western blots performed in triplicate are shown.

3.2.2 Section 1: Phenotypic characterisation of wild-type and mutants during growth into stationary phase.

3.2.2.1 Single and double mutants deficient for H2Bub and H3K36me show distinct phenotypes

It has been shown that histone modifications such as H2Bub and H3K36 methylation play critical roles in transcription regulation, chromatin structure, and DNA repair (Briggs *et al.*, 2001; Sun and Allis, 2002).

To further explore the functional roles of these modifications in yeast, the phenotypes and various characteristics of the *htb-K123R*Δ*, hht-K36A*Δ*,* and *K123R-K36A*Δ deletion mutants were investigated.

3.2.2.2 Analysis of growth in liquid media containing glucose

Cell cycle progression and metabolism in yeast are known to be influenced by histone modifications (Weiner *et al.*, 2012; Fuchs *et al.*, 2014). The wild-type and mutant strains were therefore individually inoculated into liquid culture containing glucose (YPD), and their growth monitored, to understand whether the deletion mutants exhibited any defects in cell proliferation. The analysis of growth was carried out by monitoring optical density (OD_{600nm}) increase over time which showed that no significant defects were observed in mutants when compared to wild-type cells (Fig. 3.2.A). However, calculation of the doubling times of each strain revealed that the *hht-K36A*Δ single mutant has a significantly longer doubling time than wild-type (Fig. 3.2.B). Interestingly, the *K123R-K36A*Δ double mutant did not display this elongated doubling time. This suggests that the H3-K36me single mutant is impaired for growth in YPD, and that the additional loss of H2Bub suppresses this growth defect. Thus, in terms of growth, H3K36me and H2Bub are having antagonistic effects.

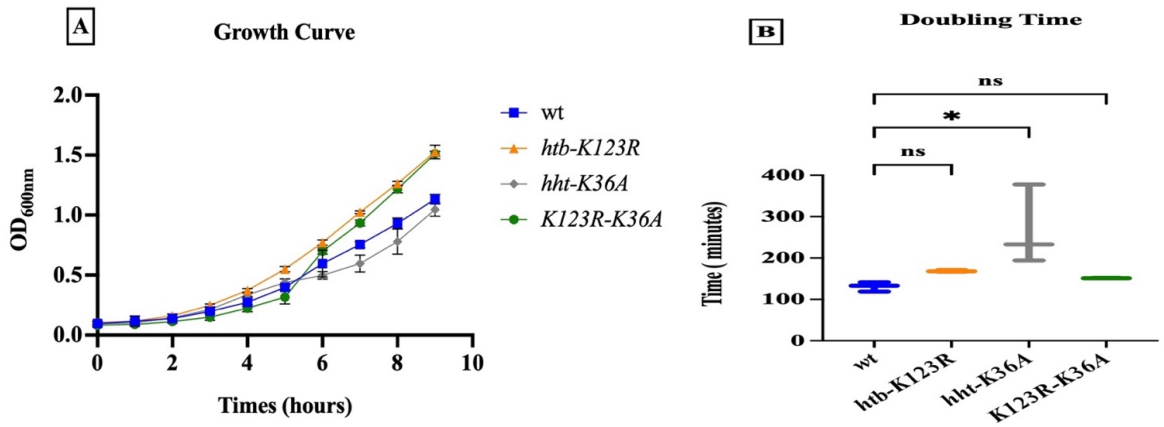


Figure 3.2: Growth Analysis of Mutant and Wild-Type Strains: (A) Growth curves of wild-type and mutant strains (*htb-K123R*Δ*, hht-K36A*Δ*,* and *K123R-K36A*Δ*)* in glucose-containing media (YPD). Strains were grown at 30°C, and OD_{600nm} was measured at specific time points. Data represent the average of three independent experiments, with error bars indicating standard deviation (SD). **(B)** Doubling time analysis of wild-type and mutant strains (*htb-K123R*Δ*, hht-K36A*Δ*,* and *K123R-K36A*Δ). The doubling time was calculated based on (OD_{600nm}) measurements over time. Statistical significance was determined using a two-tailed Student's T-test ($p < 0.05$).

3.2.2.3 Analysis of cell density during entry into stationary phase

Subsequently, growth of wild-type and mutant strains for 24 hours was performed to evaluate the effect of glucose depletion on cell growth, and final cell densities were determined (Fig. 3.3). Cell density was measured by plating out for cell colonies to give colony forming units per ml, expressed as a % relative to wild-type (set at 100%). The results showed that only the double mutant achieved a significantly lower cell density compared to wild-type following 24 hours growth. This suggests that, although the doubling time measured for the *hht-K36A*Δ single mutant was longer than wild-type (see Fig. 3.2B), this mutant did grow to wild-type cell density levels following 24 hours of growth. It was only the double mutant that showed a deficiency to achieve wild-type cell density levels after glucose exhaustion.

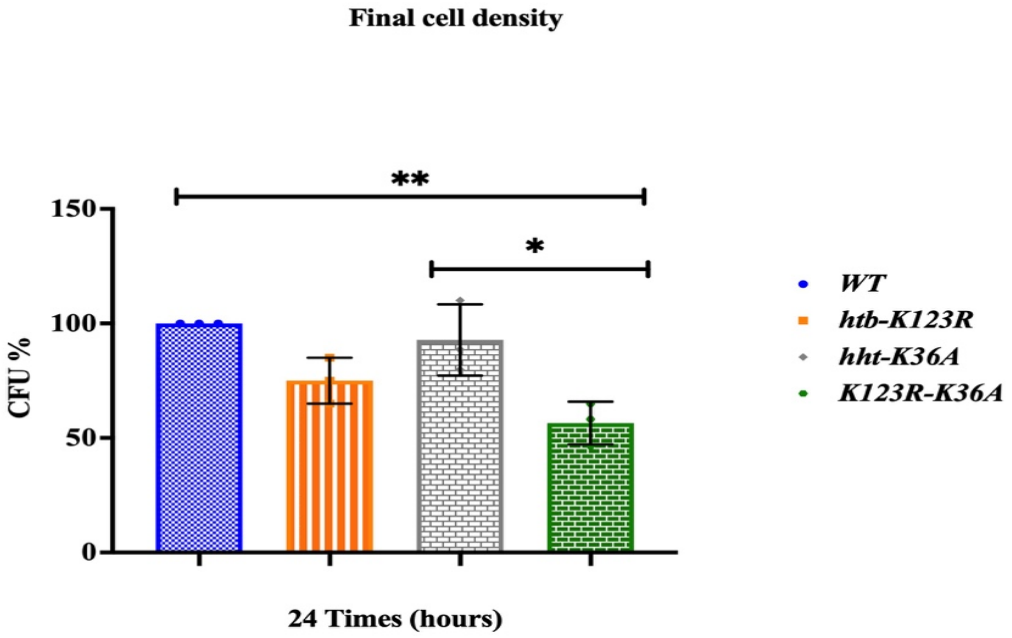


Figure 3.3: Analysis of cell density after 24h growth in YPD. Error bars represent the standard error of triplicate biologically independent experiments' mean (SEM). Standard significance using Two-way ANOVA analysis (* p = 0.05, ** p = 0.01, *** p =0.005).

3.2.2.4 Measuring Glucose Depletion in Yeast Growth

Next, growth versus glucose uptake was analysed to determine whether any of the mutants showed altered levels of glucose uptake and / or distinct times of glucose depletion.

Any discrepancy in glucose utilisation rates could explain the longer doubling time of the *hht-K36A*Δ single mutant (Fig. 3.2) or the reduced cell density achieved by the *K123R-K36A*Δ double mutant after 24 hours of growth (Fig. 3.3).

As a means to investigate these dynamics, we monitored cell growth and glucose consumption over time by tracking (OD_{600nm}) and measuring glucose concentrations in the growth medium.

wild-type cells exhibited a typical growth curve, with rapid glucose depletion occurring within the first 6 hours, whilst complete glucose exhaustion occurred at 10 hours.

The *htb-K123R*Δ mutant showed a growth and glucose consumption pattern like wild-type cells, indicating that H2B-*K123R* ubiquitination has a minimal impact on overall metabolic regulation. The results for the *hht-K36A*Δ single and the *K123R-K36A*Δ double mutant were also similar to wild-type growth and glucose uptake levels (Fig. 3.4).

The results obtained from this experiment indicate that none of the mutants displayed a significant glucose uptake defect.

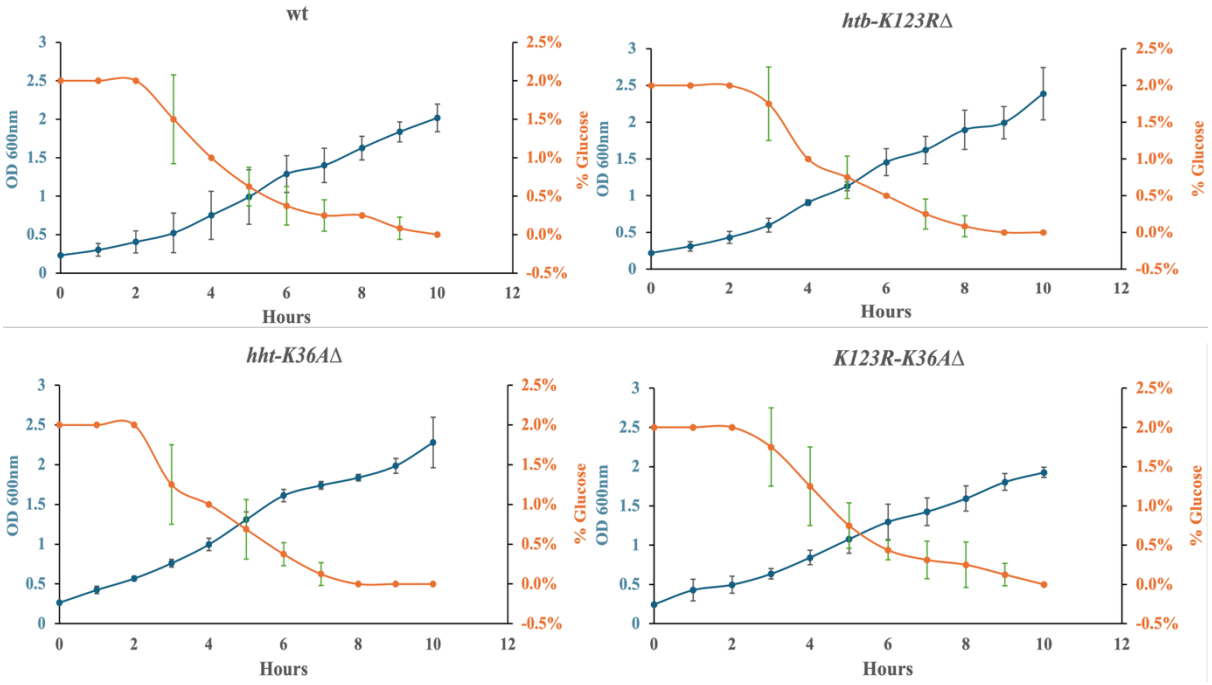


Figure 3.4: Growth and Glucose Consumption Among wild-type and Mutant Strains. Figure showing the growth dynamics (**OD_{600nm}, green line**) and glucose consumption (**percentage of glucose remaining, purple line**) over time for the yeast strains indicated grown in YPD medium at 30°C. The experiment was performed in triplicate and error bars represent SD.

3.2.2.5 Analysis of cell viability during the stationary phase

Cell viability was monitored over 7 days by measuring colony-forming units (CFUs) in wild-type and mutant strains to assess the impact of histone mutations on long-term cell survival (Fig. 3.5). Overall, although there was some variation in cell viability over the time period assessed, no significant difference could be detected in any of the mutants, at any of the times assayed, compared to that seen in wild-type.

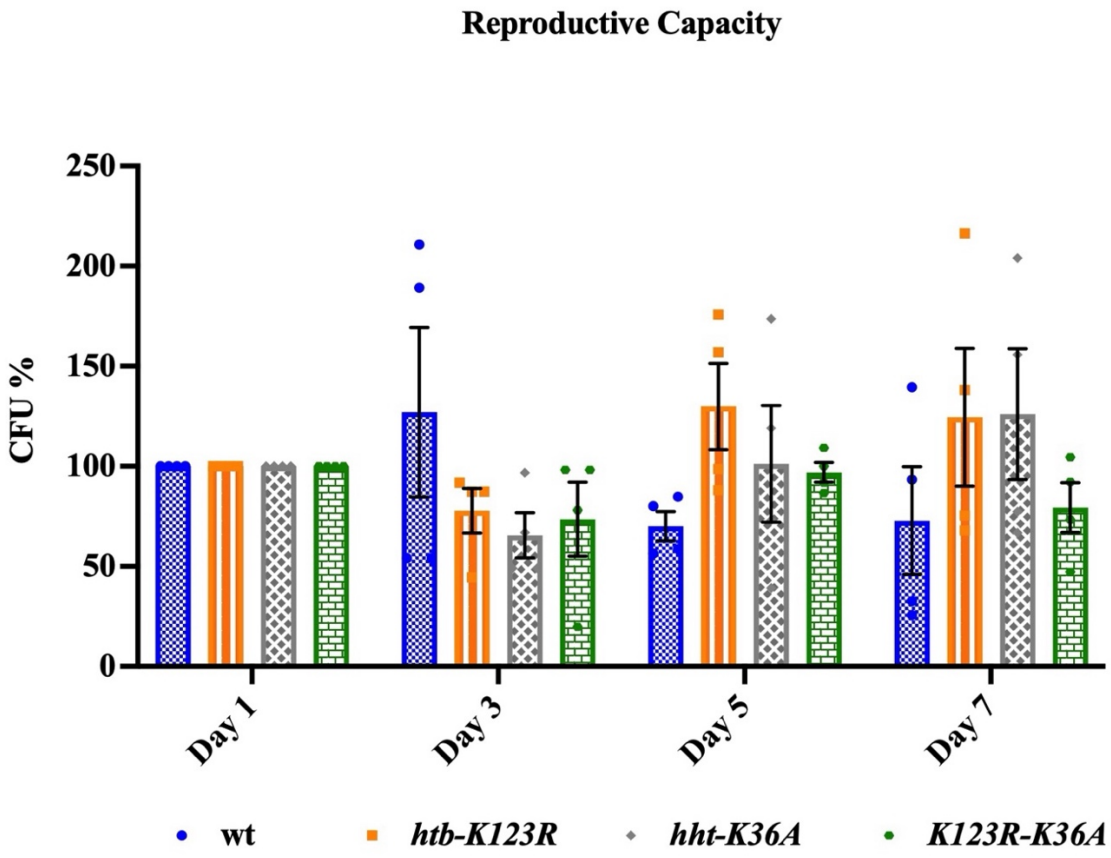


Figure 3.5: Analysis of cell viability in wild-type, *htb-K123R*Δ, *hht-K36A*Δ, and *K123R-K36A*Δ mutant strains over 7 days in YPD medium. Viability was assessed by measuring colony-forming unit (CFU) capacity at days 1, 3, 5, and 7 and expressed as a % of the values achieved in each strain at day 1 (set to 100%). Error bars represent the standard error of the mean (SEM) from five biologically independent experiments. CFU values for each strain were normalized to day 1 counts (set as 100%).

3.2.2.6 Analysing *htb-K123R*Δ,*hht-K36A*Δ and *K123R-K36A*Δ mutant cell morphology

Next, the cell morphology of each mutant strain was investigated in comparison with the wild-type. Overall, the mutants had similar cell morphologies as wild-type in exponential phase and in day 7 stationary phase cultures. However, the *K36A-K123R*Δ double mutant did appear to

have reproducibly larger cells in exponential phase compared to wild-type and the other mutants (Fig. 3.6).

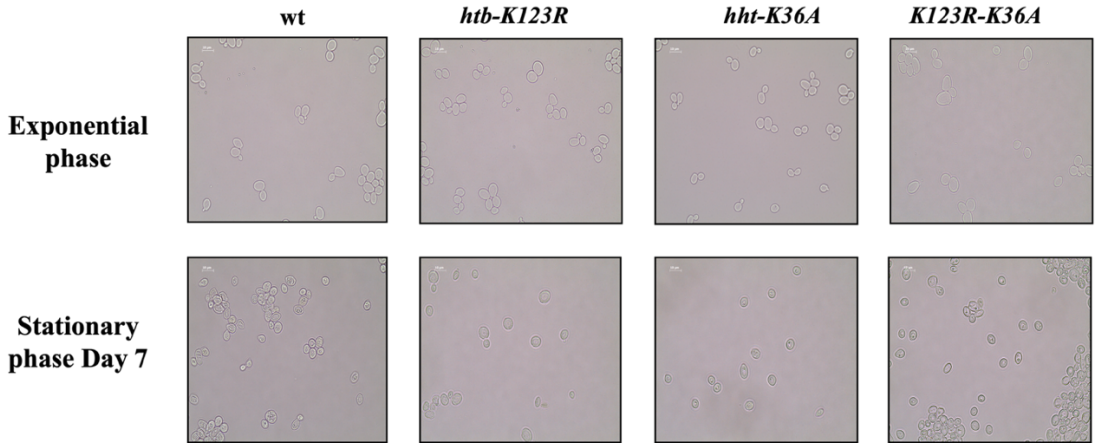


Figure 3.6: Cell images of wild-type, *htb-K123R*Δ, *hht-K36A*Δ and *K123R-K36A*Δ mutant cells. The different mutant strains shown were grown in YPD until the times indicated, were diluted to the same cell density, and were then examined under a microscope. Microscopy was conducted under a 100x immersion magnification of the oil. The white scale bar is set at 10μm.

3.2.3 Section 2: Testing for phenotypes in exponential and stationary phase cells by challenging cells in various 'spot tests'

To rapidly and easily assess the widest range of possible potential phenotypic differences between wild-type and mutant strains (*htb-K123R*Δ*, hht-K36A*Δ *and K123R-K36A*Δ*).*

A series of 'spot tests' was conducted. Cells from both the exponential phase (Exp) and day-7 stationary phase (Day 7 -SP) cultures were normalised to the same cell density, serially diluted, and spotted onto plates containing various carbon sources, stressors, or genotoxic agents and under specific growth conditions. This high throughput method allows for quick screening of potential phenotypes in exponential and stationary phase cells, providing insights into the roles of the histone PTMs and whether these roles are specific to the stationary phase (SP), or not.

This is a widely used approach for rapid phenotype detection and stress response profiling in yeast (Orphanides *et al.*, 1998) and allowed us to compare growth patterns between strains and across physiological states.

3.2.3.1 Analysis of temperature sensitivity.

Spot assays were performed on YPD plates incubated at 15°C, 30°C, 37°C, and 42°C to investigate the effect of histone mutations on thermal stress adaptation. When exponential phase cells were tested, there was no difference observed in any of the mutants compared to wild-type at any of the temperatures tested (Fig. 3.7 Exp).

When the experiment was performed on SP cells, the data suggested that the *hht-K36A*Δ single mutant showed an increased sensitivity to growth at 42°C. The *K123R-K36A*Δ double mutant also showed an increase in sensitivity at this temperature, but the impairment was not as strong as that seen in the *hht-K36A*Δ single mutant. These findings suggest a growth phase- and mutation-dependent impairment in thermal adaptation with the *htb-K123R*Δ mutation partially rescuing the defect seen in the SP cells incubated at 42°C in the *hht-K36A*Δ mutant (Fig. 3.7).

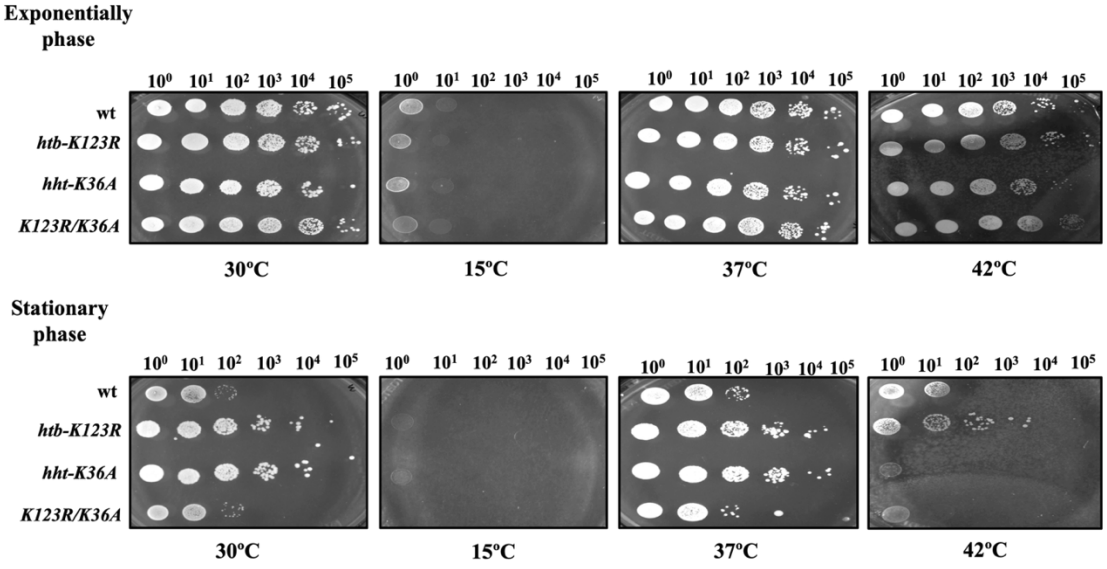


Figure 3.7: Temperature sensitivity growth tests of exponentially growth (Exp) and stationary phase (SP) growing cultures on plates. Cells of the strains indicated were serially diluted, spotted onto

YPD plates, and the plates incubated at the indicated temperatures. The images were taken after three days of growth.

3.2.3.2 Analysis of the ability to grow on different carbon sources

To look for possible metabolic adaptability differences, the growth of exponential and stationary phase wild-type and mutant cells on YEP agar containing the different carbon sources, raffinose, sucrose, galactose, ethanol, and glycerol was performed. Overall, no differences in growth of any of the mutants was evident on the different carbon sources compared to wild-type, whether from exponentially growing, or inactive SP cells (Fig. 3.8).

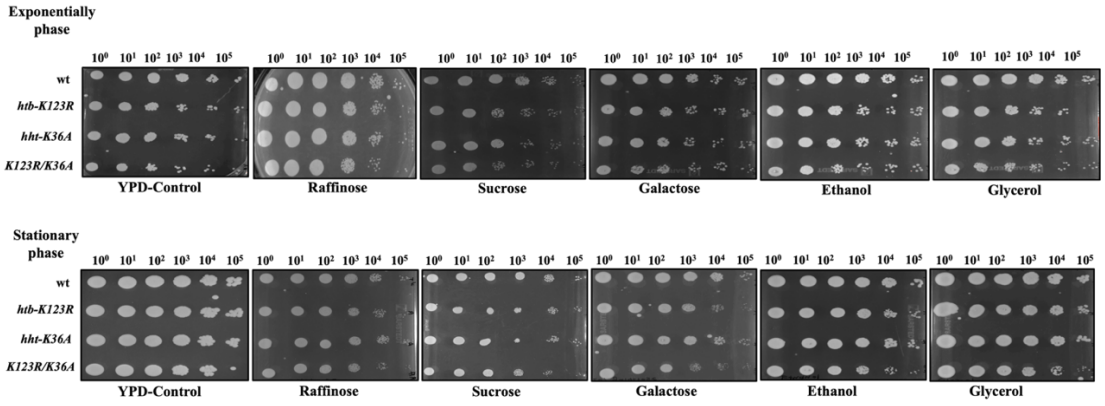
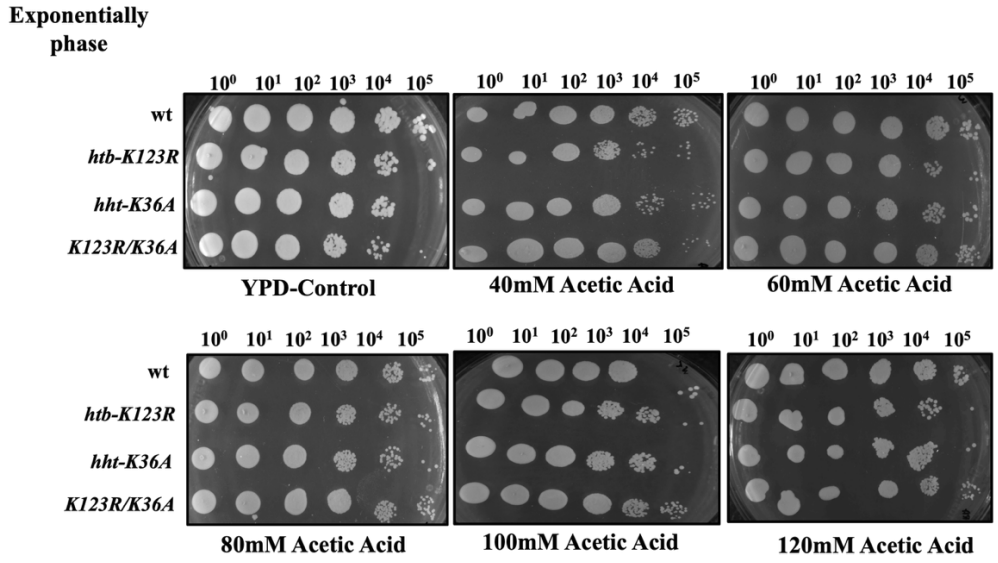


Figure 3.8: Growth tests of exponentially growing (Exp) and stationary phase (SP) cultures on plates with different carbon sources. YPD: control plates. Cells were grown on plates containing the different carbon sources as indicated. The strain incubated was plated as a 10-fold serial dilution starting from 1×10^7 cells/ml. The plates were spotted onto YP-Raffinose (YP-Raff 2%), YP-Sucrose (YP-Suc 2%), YP-Galactose (YP-Gal 2%), YP-Glycerol (YP-Glyc 2%) and YP-Ethanol (YP-Etha 2%). 5µl of culture was spotted on YPD plates and photographed following 48 hours of growth at 30 ºC.

3.2.3.3 Analysis of growth on a non-fermentable carbon source

In exponential growth (Exp) and stationary phase (SP), the strains were tested for growth on the non-fermentable carbon source, Acetic Acid. Similar to what was seen for the results of growth on ethanol containing plates, none of the mutants, whether exponentially growing, or from SP, showed any difference in growth compared to wild-type. (Fig. 3.9).



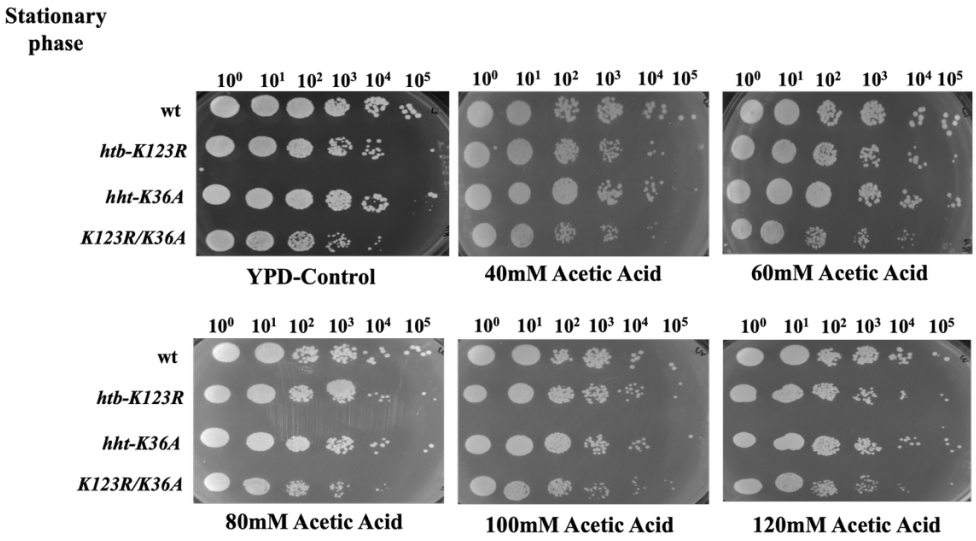


Figure 3.9: Serial ten-fold dilution growth tests on a non-fermentable carbon source (Acetic acid) of exponentially growing (Exp) and stationary phase (SP) cultures. YPD: control plates. 5µl of culture was spotted onto each plate and photographed following 48 hours of growth at 30℃.

3.2.3.4 Analysis of responses to DNA damage caused by camptothecin.

Yeast cells were first challenged with Camptothecin (CPT), a topoisomerase I inhibitor that induces double-strand breaks, to assess the effect of histone mutations on the DNA damage response. Spot tests were conducted using YEPD plates containing 10 µg/mL Camptothecin (CPT).

During exponential and stationary phase growth, the mutants showed no difference in sensitivity to camptothecin compared to wild-type cells, as growth in each test plate was similar to that seen in the exponential and SP control YPD plates (Fig. 3.10).

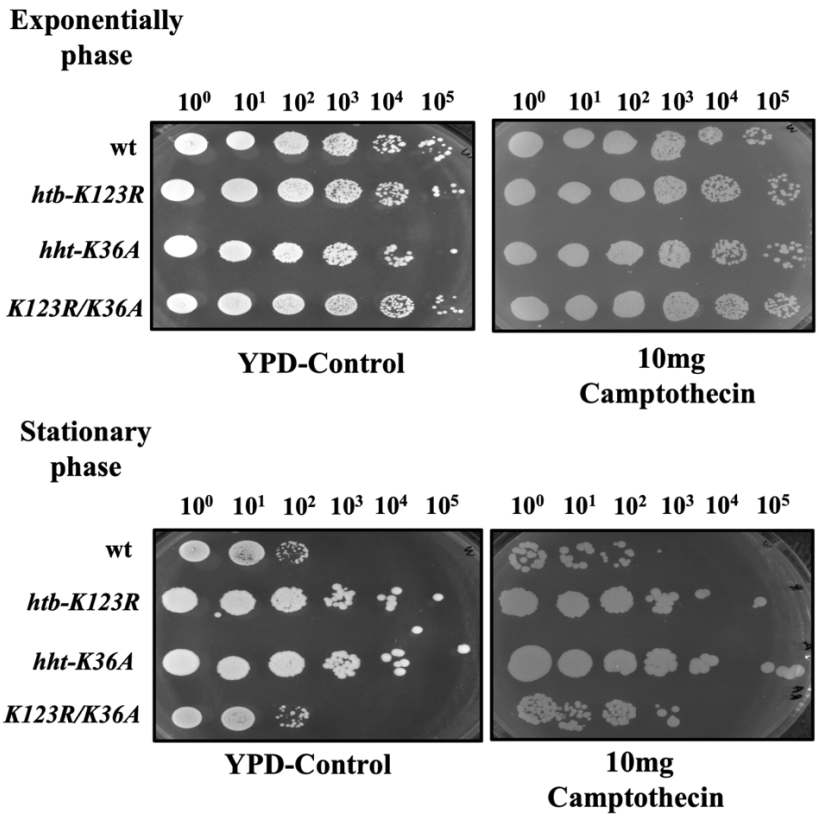


Figure 3.10: Testing response to DNA damage of exponential (Exp) and stationary phase (SP) cells. Cells were serially diluted, spotted onto YPD plates with and without 10 mg Camptothecin. The images were taken after three days of growth at 30°C.

3.2.3.5 Analysis of the growth response to the DNA-damaging agent, methyl methane sulfonate

Next, The growth of exponential (Exp) and stationary phase (SP; day 7) wild-type and mutant strains was subsequently assessed after exposure to methyl methane sulfonate (MMS). The DNA alkylating agent that inhibits replication, causing DNA fragmentation. Overall, the mutant cells from exponential and stationary phase cultures showed no significant differences in sensitivity to MMS compared to wild-type cells, as growth in each test plate, for all strains, was similar to that seen in the exponential and SP control YPD plates. However, it is possible that

the SP double mutant cells showed a slight sensitivity to MMS when plated at 0.06-0.12 %. (Fig. 3.11).

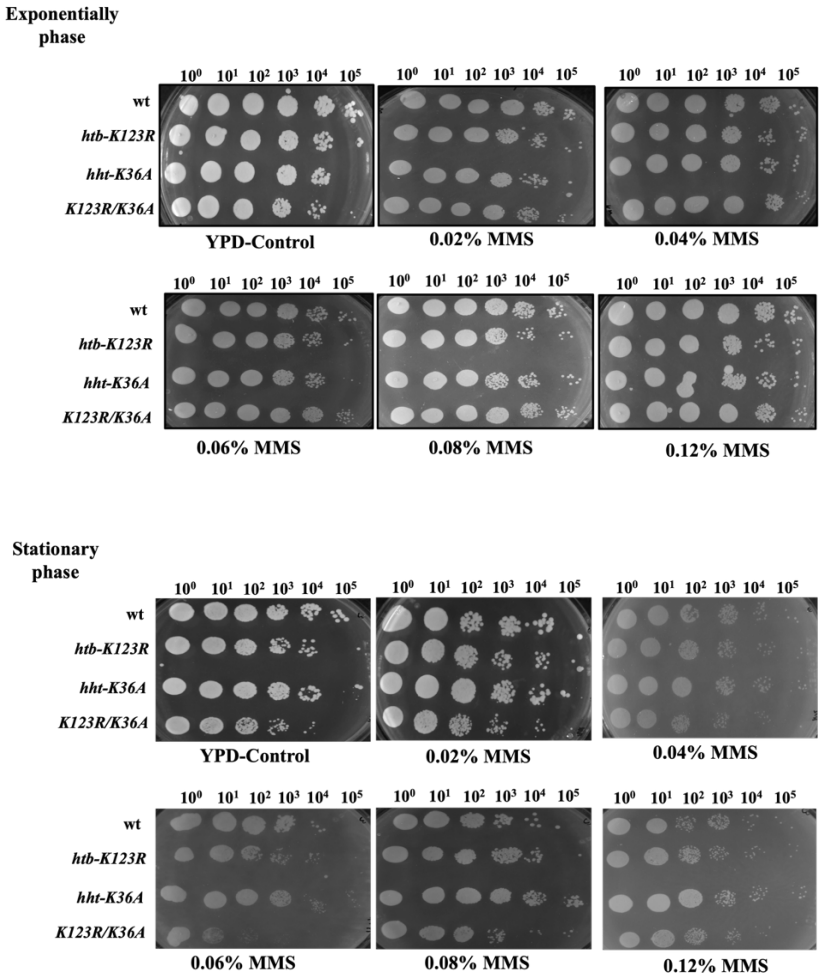


Figure 3.11: Serial ten-fold dilution growth tests of exponentially growing (Exp) and stationary phase (SP) cultures on plates containing the DNA damaging reagent, MMS. YPD: control plates. 5µl of culture was spotted on YPD plates with and without MMS and photographed following 48 hours of growth at 30ºC.

3.2.3.6 Analysis of the growth response to DNA-damaging agent, hydroxy urea

To further assess DNA damage responses, the mutant strains were tested for sensitivity to hydroxyurea (HU) following growth in exponential phase (Exp) and during stationary phase (SP-Day-7), which inhibits ribonucleotide reductase, thereby depleting dNTP pools which stalls DNA replication to cause fork collapse and induce eventual DNA double strand breaks. When

the exponential phase cells were challenged with HU, the single *htb-K123R*Δ and *K123R-K36A*Δ mutants were found to be slightly sensitive to hydroxyurea (HU), whereas growth was nearly abolished at 200 mM in the double mutant *K123R-K36A*Δ.

When the SP cells were exposed to HU, all of the mutants were potentially more resistant to this drug than wild-type. However, the differences in growth on the YPD control plates due to initial unequal cell number normalisation prior to dilution, make this a preliminary 'potential' result.

These potentially opposing results of the exponential phase and stationary phase SP cell responses to this drug are intriguing and are supported by studies linking histone modifications to replication fork stability (Silcocks, 2022) (Fig. 3.12).

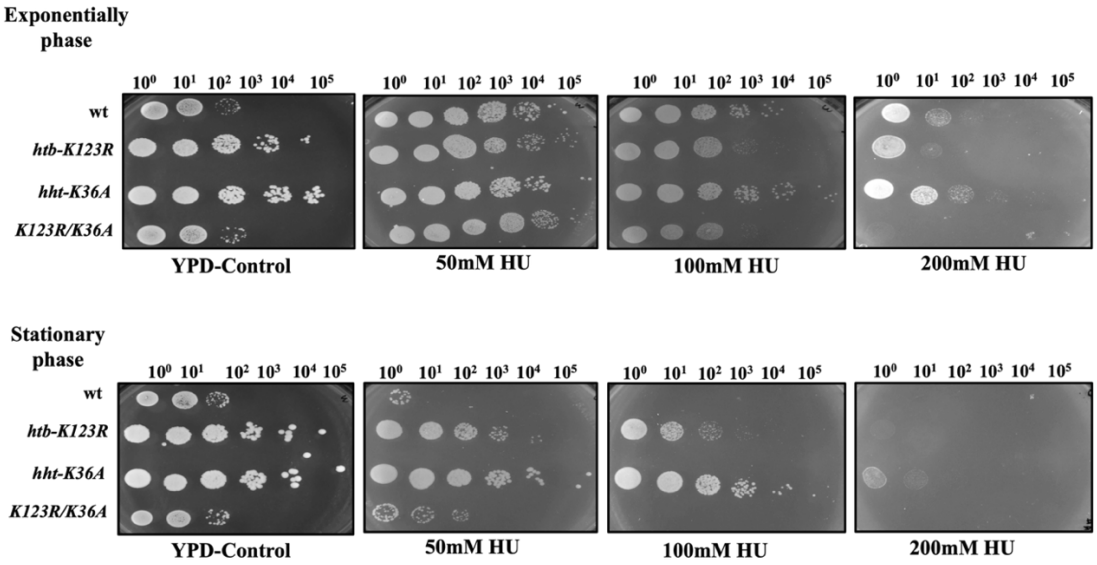


Figure 3.12: Serial ten-fold dilution growth tests to DNA-damaging reagent Hydroxyurea (HU) of exponentially growth (Exp) and stationary phase (SP) cultures. On plates with the indicated compounds or exposures YPD: control plates. Cells were grown in cultures with known DNA-damaging agents, hydroxyurea (HU). 5µl of culture was spotted on YPD plates and photographed following 48 hours of growth at 30ºC.

3.2.3.7 Analysis of sensitivity to caffeine

To assess cell wall stress resistance, Caffeine is known to induce cell wall stress in yeast by activating the cell wall integrity (CWI) pathway, primarily mediated by the Mpk1p/Slt2p MAP kinase cascade (Kuranda *et al.*, 2006). Therefore, growth in the presence of caffeine was assessed as an indirect measure of cell wall stability and the ability of cells to respond to cell wall damage.

To determine whether disruption of key histone modifications affects cell wall stress responses, mutant strains were exposed to caffeine. No differences in caffeine sensitivity were observed in any of the mutants compared to wild-type when cells were harvested from exponential phase cultures. However, when stationary phase (SP) cells were treated with caffeine, increased sensitivity to this drug was observed in the *htb-K123R*Δ and *hht-K36A*Δ single mutants. These results indicate that chromatin integrity contributes to cell wall stress resistance, particularly during quiescence, and support a functional link between chromatin state and the CWI pathway (Fig. 3.13).

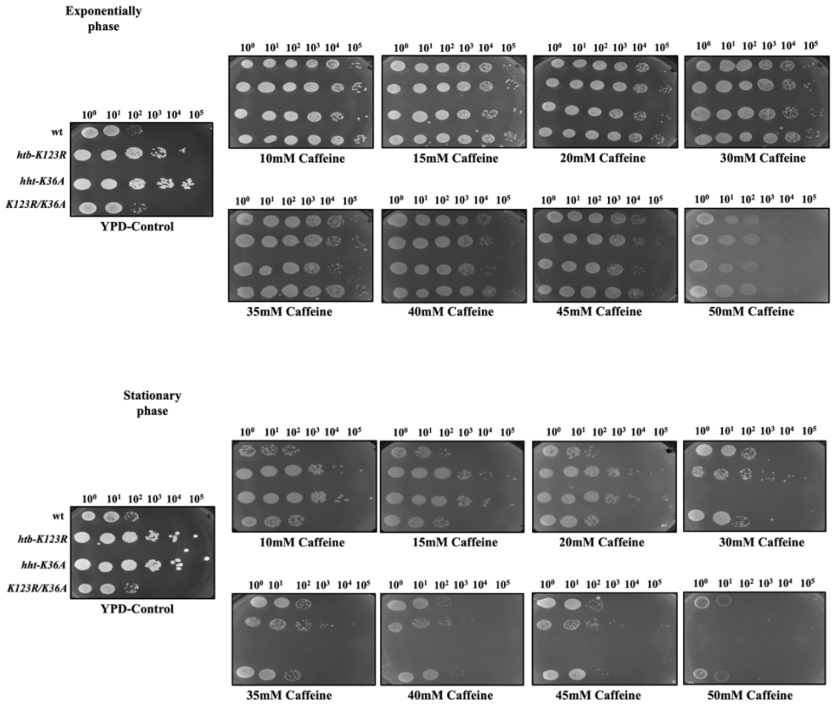


Figure 3.13: Testing cell sensitivity to the Caffeine of exponentially growth (Exp) and stationary phase (SP) cultures, the strains incubated were plated as 10-fold serial dilution starting from 1×107

cells/ml. The plates were spotted onto YP-Caffeine (YP-Caff 2%). 5µl of culture was spotted on YPD plates and photographed following 48 hours of growth at 30℃.

3.2.3.8 Analysis of sensitivity to oxidative stress

Next, cells were examined for possible differences in sensitivity to oxidative stress by exposure to hydrogen peroxide (H_2O_2). A heightened oxidative stress sensitivity was only observed in the double mutant aligning with diminished antioxidant defences in these mutant cells (Singh *et al.*, 2021). However, when the SP mutant cells were tested, all mutants behaved like wild-type, SP cells and did not show any differences in sensitivity to this reagent (Fig. 3.14).

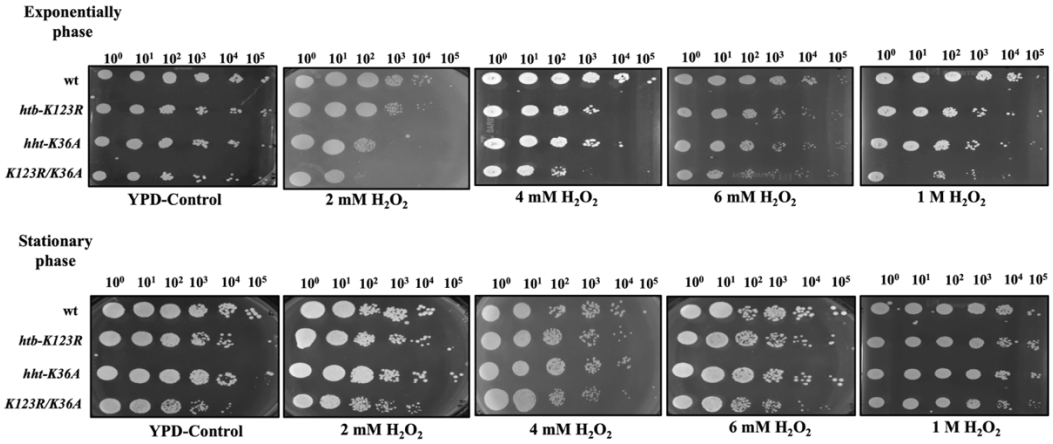
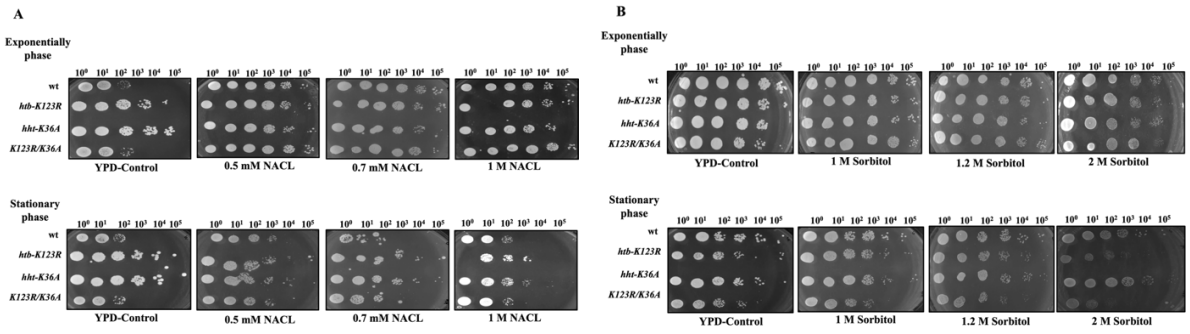


Figure 3.14: Testing cell sensitivity to osmotic and oxidative stress of exponentially growth (Exp) and stationary phase (SP) cultures. on plates with the indicated compounds or exposures. Cells were grown on plates containing Hydrogen Peroxide (H2O2) to test for sensitivity to oxidative stress, respectively. 5µl of culture was spotted on YPD plates and photographed following 48 hours of growth at 30 ºC.

3.2.3.9 Analysis of sensitivity to Osmotic and Ionic Stress Response

To assess osmotic and ionic stress sensitivity, exponential (Exp) and stationary phase (SP; day 7) cells were tested for growth under high salt concentrations. Specifically, sodium chloride (NaCl) and sorbitol were used to evaluate osmotic stress tolerance, while lithium chloride (LiCl) was used to test ionic stress tolerance (Fig. 3.15). Neither exponential (Exp) nor stationary phase (SP) mutant strains showed any difference in sensitivity to NaCl compared to wild-type at any concentration tested (Fig. 3.15.A). However, SP grown *htb-K123R*Δ and *K123R-K36A*Δ mutants did show reduced growth in the presence of high concentrations (2M) of Sorbitol (Fig. 3.15.B, SP).

When cells were plated onto LiCl plates, the exponential *htb-K123R*Δ and *hht-K36A*Δ single mutants showed poor growth on the 200 mM plates. However, when the SP cells were challenged on the LiCl plates, the *htb-K123R*Δ and the *K123R-K36A*Δ double mutants showed the poorest growth (Fig. 3.15.C).



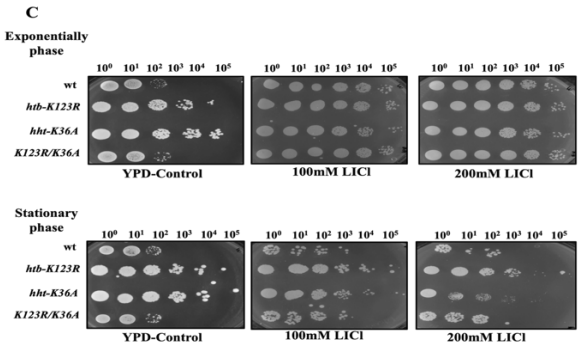


Figure 3.15: Testing cell sensitivity to osmotic and Ionic stress of exponentially growth (Exp) and stationary phase (SP) cultures. on plates with the indicated compounds or exposures. Cells were grown on plates containing **(A)** Sodium Chloride (NaCl), **(B)** Sorbitol and **(C)** Lithium Chloride (LiCl) to test for sensitivity to osmotic stress and ionic stress, respectively. 5µl of culture was spotted on YPD plates and photographed following 48 hours of growth at 30 ºC.

3.2.3.10 Analysis of sensitivity to Chemical Stress

As a final stress test, cells were exposed to chemical stress by growth in the presence of formamide. However, the mutants exhibited no differences in sensitivity to chemical (Formamide) stress compared to wild-type, regardless of whether exponential (Exp) or stationary phase (SP) cells were exposed. (Fig. 3.16).

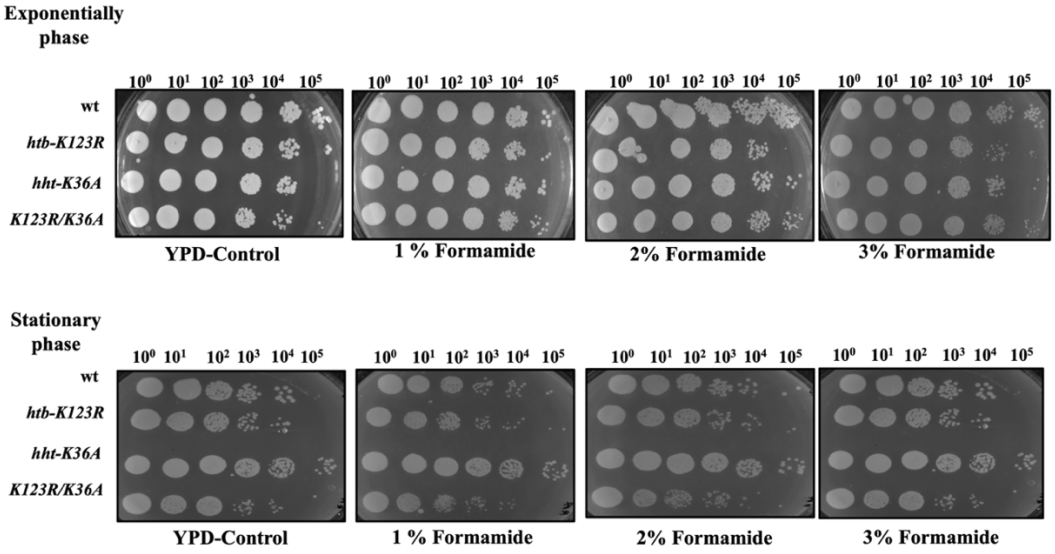


Figure 3.16: Testing cell sensitivity to Chemical stress (formamide) of exponentially growth (Exp) and stationary phase (SP) culture. on plates with the indicated compounds or exposures. Cells were grown on plates containing formamide to test for sensitivity to chemical stress. 5µl of culture was spotted on YPD plates and photographed following 48 hours of growth at 30 ºC.

3.2.4 Section 3: Investigating the transcriptional and chromatin landscape in wild-type and mutants during growth into stationary phase:

The key aim of this project is to determine if there are any global transcription changes in SP mutant cells deficient for H2Bub and H3K36me. In the next series of experiments, the levels of RNA Polymerase II were determined in exponential phase and SP in wild-type and mutant cells, as this enzyme is central to mRNA transcription in yeast (Nechaev and Adelman, 2011). The aim was to examine if there were any differences in the levels of RNA Pol II abundance in the mutants which might be relevant to the results of the subsequent RNA-Seq analysis.

RNA Pol II activity is tightly regulated through post-translational modifications such as phosphorylation of the carboxy-terminal domain (CTD) of its largest subunit, Rpb1(Corden, 2013). Consisting of repeating heptapeptide sequences (YSPTSPS), this CTD undergoes phosphorylation at serine-2 (Ser2-P) and serine-5 (Ser5-P). These modifications are essential for transcriptional elongation and termination respectively and can therefore be used to determine whether Pol II is active or not (Buratowski, 2009; Harlen and Churchman, 2017).

This is particularly relevant to quiescent cells, where evidence suggests that although RNA Pol II is present, it is not in its active form (Young *et al.*, 2017).

Because the chromatin modifications such as H2Bub1 and H3K36me3 can influence transcriptional regulation, we hypothesized that mutations *htb-K123R*Δ and *hht-K36A*Δ*,* as well as the double mutant *K123R-K36A*Δ would alter the transcription status, and thus the phosphorylation levels of RNAP II during the SP might reflect any alteration. For example, increased levels of RNAP II or of phosphorylated RNAP II in mutant cells during SP could be expected if these histone modifications serve a repressive function upon transcription, and vice-versa.

3.2.4.1 Investigating RNA Pol II levels in unseparated mutant cells during SP.

We first examined total RNAP II levels in wild-type and mutant yeast strains at mid-log phase exponential growth (Exp) and at day 7 of stationary phase (SP), using an antibody that recognizes both active and inactive forms of the enzyme (Fig. 3.17, Pol II).

In wild-type cells, it was observed that RNAP II remains at a constant level across all growth phases, which corroborates previous findings showing non-significant changes in RNAP II abundance throughout the growth cycle regardless of changes in global transcription (Komarnitsky *et al.*, 2000). In *htb-K123R*Δ and *hht-K36A*Δ mutants, like wild-type, a constant RNAP II profile was observed across all growth phases, suggesting that loss of H2B ubiquitination or loss of H3K36 methylation does not significantly impact RNAP II stability in SP. However, there was a reduced signal for RNAP II in the day 7 double mutant cells

suggesting the absence of both H2Bub and H3K36me causes a decrease in Pol II abundance in SP cells.

The Ser2-P and Ser5-P modified forms of active RNAP II were next analysed in wild-type and the mutant strains during exponential phase and in SP cells (Fig. 3.17). Consistent with previous research, in wild-type cells, Ser2-P and Ser5-P levels were high during exponential growth, where transcription is active, but dropped significantly by day 7 in stationary phase (SP) cells, where transcription levels are reduced (Young *et al.*, 2017; Zeng, 2025).

In the *htb-K123R*Δ*, hht-K36A*Δ and *K123R-K36A*Δ mutants, the levels of Pol II Ser2-P and Ser5-P in both exponential phase and SP cells were similar to those seen in wild-type. This suggests that H2B ubiquitination and H3K36 methylation on their own do not drastically impact global RNAP II activity during exponential phase or in SP cells. However, considering that the Pol II levels were reduced in the double mutant SP cells, the data suggests that there would be relatively higher levels of both active forms of Pol II in these cells. This would suggest that in the double mutant, even though there is less Pol II than that seen in wild-type SP cells, the Pol II that is there is abnormally active.

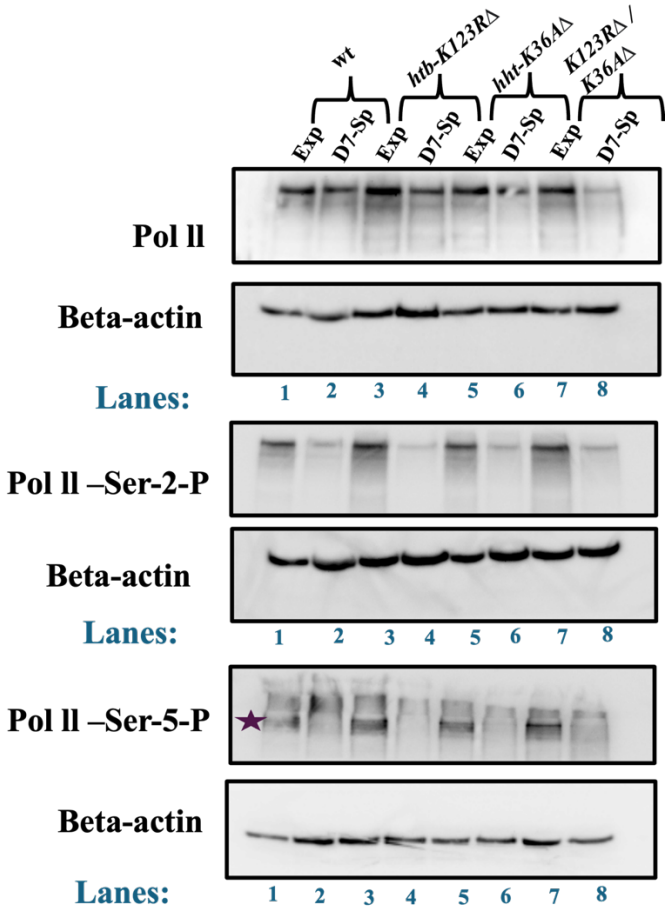


Figure 3.17: RNAP II CTD phosphorylation levels in wild-type and mutant yeast strains across different growth phases. Total RNA polymerase II (Pol II) and its phosphorylated forms (Ser2-P and Ser5-P) (* indicated to lower band size for 1,3,5 and 7 respectively), were analysed in wild-type, *htb-K123R*Δ (H2B ubiquitination-deficient mutant), *hht-K36A*Δ (H3K36 methylation-deficient mutant), and *K123R-K36A*Δ yeast strains during exponential growth (Exp) and stationary phase (SP, day 7). β-actin was used as a loading control to ensure equal protein loading and normalization of RNA polymerase II (Pol II) levels across different yeast strains and growth phases.

3.2.4.2 Regulation of PAF1 Complex During Growth into SP

The levels of Paf1p, a key subunit of the PAF1 complex, were next examined in the histone mutants during the transition from exponential growth (Exp) to stationary phase (SP) (Fig.

3.18). PAF1 interacts with RNA polymerase II and plays a critical role in transcription elongation, co-transcriptional histone modifications, and mRNA processing.

PAF1 also aids in coordinating the recruitment of chromatin modifiers such as Set2p, Rad6p and Bre1p, linking transcription to histone methylation and ubiquitination (Squazzo *et al.*, 2002; Krogan *et al.*, 2003).

Western blot analysis of PAF1p levels in wild-type cells revealed a band in wild-type, which was absent in the day 7 SP cells. Thus, in wild-type, Paf1p, and presumably the PAF complex itself, is abundant in actively growing and actively transcribing cells, but is reduced significantly such that it is undetectable in the inactive SP cells where transcription levels are low (Fig. 3.18).

All of the single mutants showed a similar profile to that seen in wt. However, in the double mutant, there was more Paf1p detected in the day 7 SP cells than there was in the exponentially growing cells Thus, the absence of both H2Bub and H3K36me correlate with higher levels than wild-type of Paf1p in SP.

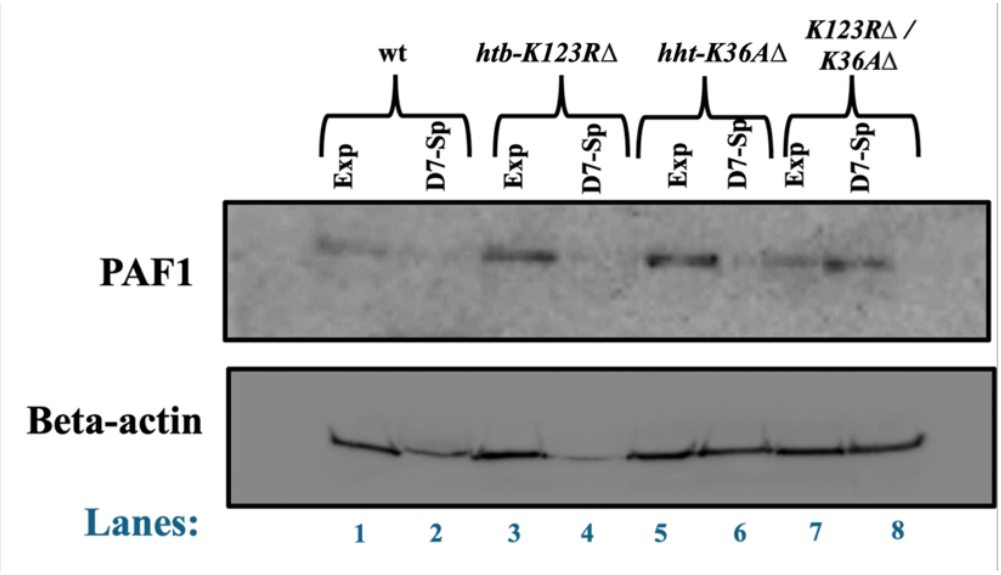


Figure 3.18: Western blot analysis of PAF1 protein levels in wild-type and *htb-K123R*Δ, *hht-K36A*Δ and *K123R-K36A*Δ mutant strains during exponential growth (Exp) and after 7 days in stationary phase (SP). Cells grow during exponential growth (Exp) and stationary phase (SP) in wild-type and *htb-K123R*Δ, *hht-K36A*Δ and *K123R-K36A*Δ mutant strains. Whole-cell lysates were prepared and probed with antibodies specific to PAF1 and were analysed in wild-type, *htb-K123R*Δ (H2B ubiquitination-

deficient mutant), *hht-K36A*Δ (H3K36 methylation-deficient mutant), and *K123R-K36A*Δ yeast strains during exponential growth (Exp) and stationary phase (SP, day 7). β-actin was used as a loading control to ensure equal protein loading and normalization of PAF1levels across different yeast strains and growth phases.

3.2.4.3 Analysing Core Histone Levels as Cells Grow into Stationary Phase (SP)

The levels of core histone proteins in both wild-type and mutant strains were next examined to gain insight into chromatin structure during the transition into stationary phase (SP). Chromatin organization and gene regulation, particularly during cellular quiescence (Q) and metabolic shifts, have been known to be impacted by the changes in histone protein abundance (Bagchi, 2016; Hauer and Gasser, 2017; Claude, 2022). Western blot analysis using antibodies specific to histones H3, H4, H2A, and H2B was performed using lysates prepared from cells harvested at mid-logarithmic exponential phase (Exp) and after 7 days in stationary phase (SP).

In wild-type cells, the H2A and H2B levels remained relatively stable between the exponential phase (Exp) and stationary phases (SP), consistent with prior studies that reported tight homeostatic control of histone expression and degradation during cell cycle arrest or quiescence (Q) (Bagchi, 2016; Hauer and Gasser, 2017). Levels of H2A and H2B similar to wild-type were also seen in all mutant strains during exponential growth and in SP (Fig. 3.19.A). Thus, levels of H2A and H2B are unaffected by the absence of either or both H2Bub and H3K36me.

In wild-type cells, high histone H3 could be seen in exponential phase cells whilst levels in SP cells was significantly lower. A similar pattern of H3 abundance to that seen in wild-type was evident in the exponential phase and stationary phase *htb-K123R*Δ and *hht-K36A*Δ single mutant cells. However, in the double mutant, although H3 levels in exponential phase cells were similar to that seen in wild-type, there was a higher level of H3 in the double mutant SP cells compared to wild-type (Figure. 3.19.B).

Similar to the result for H3, histone H4 levels in wild-type cells were high in the exponential phase (Exp) and reduced during the stationary phase (SP). The H4 level profiles in all of the mutants in both exponential phase and SP cells was similar to that seen in wild-type. Thus, core histone levels are unaffected by the absence of H2Bub and H3K36me except when both modifications were absent, H3 levels remained higher than wild-type in SP cells.

These findings demonstrate the dynamic regulation of core histone protein levels during growth arrest and suggest that both H2Bub and H3K36me are important in maintaining histone H3 stoichiometry during SP.

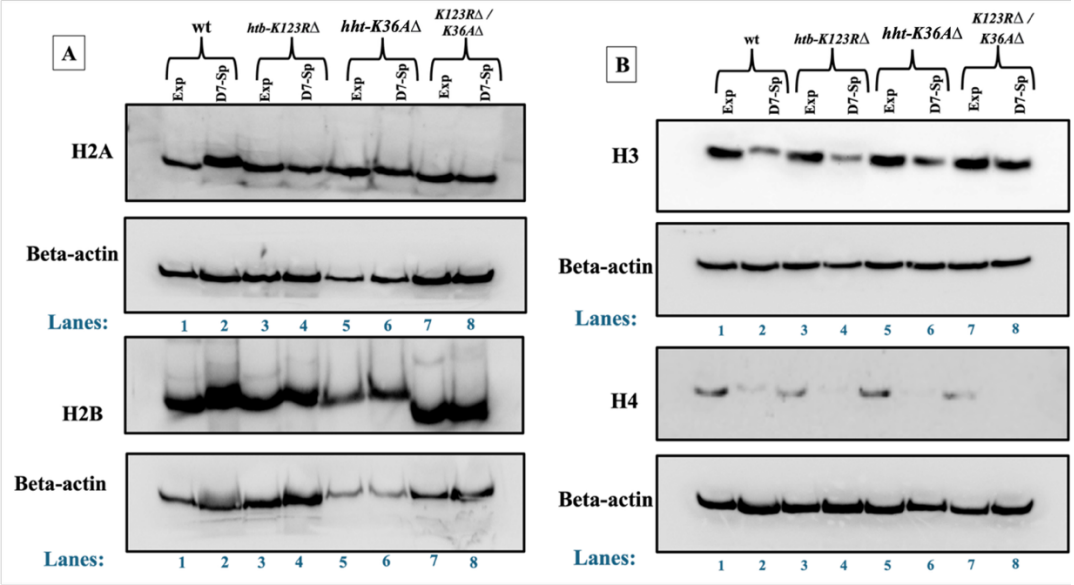


Figure 3.19: Western blot analysis of core histone protein levels Cells Grow during exponential growth (Exp) and stationary phase (SP) in wild-type and *htb-K123R*Δ*, hht-K36A*Δ and *K123R-K36A*Δ mutant strains. Whole-cell lysates were prepared and probed with antibodies specific to histones H2A, H2B (A), and H3, H4 (B) were analysed in wild-type, *htb-K123R*Δ (H2B ubiquitination-deficient mutant), *hht-K36A*Δ (H3K36 methylation-deficient mutant), and *K123R-K36A*Δ yeast strains during exponential growth (Exp) and stationary phase (SP, day 7). β-actin was used as a loading control to ensure equal protein loading and normalization of H2A, H2B (A), and H3, H4 (B) levels across different yeast strains and growth phases.

3.2.4.4 Analysis of Hho1p Abundance During Stationary Phase (SP)

The abundance of Hho1p, a high-mobility group B (HMGB) protein, was examined to further understand chromatin structural dynamics during the transition to stationary phase since Hho1p is implicated in chromatin compaction and transcriptional repression during SP (Smith, 2020). Hho1p has also been shown to bind both rDNA and non-rDNA loci, thus promoting ribosomal

protein gene transcription, particularly under growth-favourable conditions (Schäfer et al., 2008; Lawrence, 2019).

Hho1p has been shown to be loosely associated with both rDNA and non-rDNA loci under growth-favourable conditions, thereby promoting ribosomal protein gene transcription (Schäfer *et al.*, 2008; Lawrence, 2019).

In contrast, during nutrient depletion or stationary phase, Hho1p protein abundance remains stable but its chromatin association increases, functioning primarily in genome-wide chromatin compaction rather than global transcriptional repression (Schäfer *et al.*, 2008; Lawrence, 2019). Together, these findings highlight a context-dependent dual role for Hho1p, acting as a transcriptional facilitator in actively growing cells while serving as a structural factor that safeguards chromatin integrity and organization under stress conditions.

To explore whether similar regulation occurs in our mutant strains during stationary phase (SP), we performed western blot analysis on lysates collected from both wild-type, *htb-K123R*Δ*, hht-K36A*Δ and *K123R-K36A*Δ mutant cells during exponential growth (Exp) and after 7 days in stationary phase (SP) (Fig. 3.20). Our goal was to determine whether the *htb-K123R*Δ*, hht-K36A*Δ and *K123R-K36A*Δ mutant strains affected Hho1p regulation. Changes in Hho1p levels could be linked to altered chromatin compaction which might affect transcription.

In wild type cells Hho1p levels were high during exponential growth (Exp) and significantly decreased during stationary phase (SP), consistent with a previous study of Hho1p downregulation during nutrient depletion and global transcription repression (Fig. 3.20). A similar result was seen in all of the mutant strains.

However, all the mutant strains whether *htb-K123R*Δ*, hht-K36A*Δ and *K123R-K36A*Δ during exponential growth (Exp) showed elevated Hho1p levels compared to wild-type. These findings suggest that H2B ubiquitination and H3K36 methylation act to negatively impact Hho1p abundance during SP in wild-type cells.

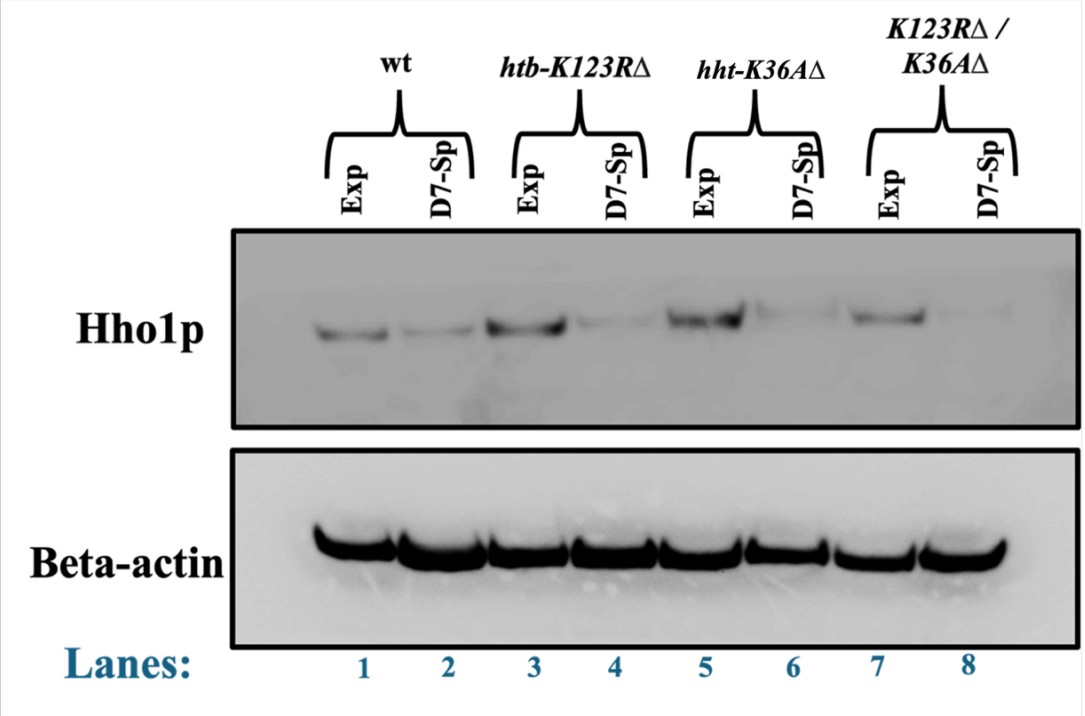


Figure 3.20: Western blot analysis of Hho1p protein levels. Cells grow during exponential growth (Exp) and stationary phase (SP) in wild-type and *htb-K123R*Δ*, hht-K36A*Δ and *K123R-K36A*Δ mutant strains. Cell lysates were probed with an antibody specific to Hho1p. were analysed in wild-type, *htb-K123R*Δ (H2B ubiquitination-deficient mutant), *hht-K36A*Δ (H3K36 methylation-deficient mutant), and *K123R-K36A*Δ yeast strains during exponential growth (Exp) and stationary phase (SP, day 7). β-actin was used as a loading control to ensure equal protein loading and normalization of Hho1p levels across different yeast strains and growth phase.

3.2.4.5 Histone acetylation levels during exponential growth and stationary phase in wild-type and histone modification-deficient yeast mutants.

Histone acetylation is a dynamic modification that regulates chromatin structure and transcription during growth phase transitions. In *S. cerevisiae*, global acetylation levels decrease during the stationary phase (SP), correlating with transcriptional repression and chromatin compaction (Young *et al.*, 2017; Chou *et al.*, 2023). To investigate how histone modifications change during growth into SP, we analyzed acetylation marks (H3K14ac, H3K9ac, H4ac4, H3K56ac, and H4K16ac) in wild-type and mutant strains (*htb-K123RΔ, hht-K36AΔ*, and *K123R-K36AΔ*) during exponential growth (Exp) and in day 7 stationary phase (SP) cells.

3.2.4.6 Analysis of H3K4ac4, H3K14ac and H3K9ac levels

In wild-type cells, the levels of both H3K14 and H4ac4 were high in exponential phase cells and low in SP cells, consistent with the high and low levels of transcription in these cells, respectively (Fig. 3.21). However, in all of the histone modification mutants, levels of these PTMs were much higher than wild-type levels in exponential phase cells. Furthermore, the levels of H4ac4 and H3K14ac were significantly higher in the double mutant SP cells compared to the levels in the wild-type SP cells.

When we tested H3K9ac abundance, the levels in wild-type were again high in exponential phase and low in SP. The *hht-K36A*Δ single and the *K123R-K36A*Δ double mutant also showed a similar profile of this PTM as was seen in wild-type. However, in the *htb-K123R*Δ single mutant, although levels in exponential phase were the same as wild-type, there was significantly more H3K9ac levels in the *htb-K123R*Δ single mutant SP cells compared to those in wild-type.

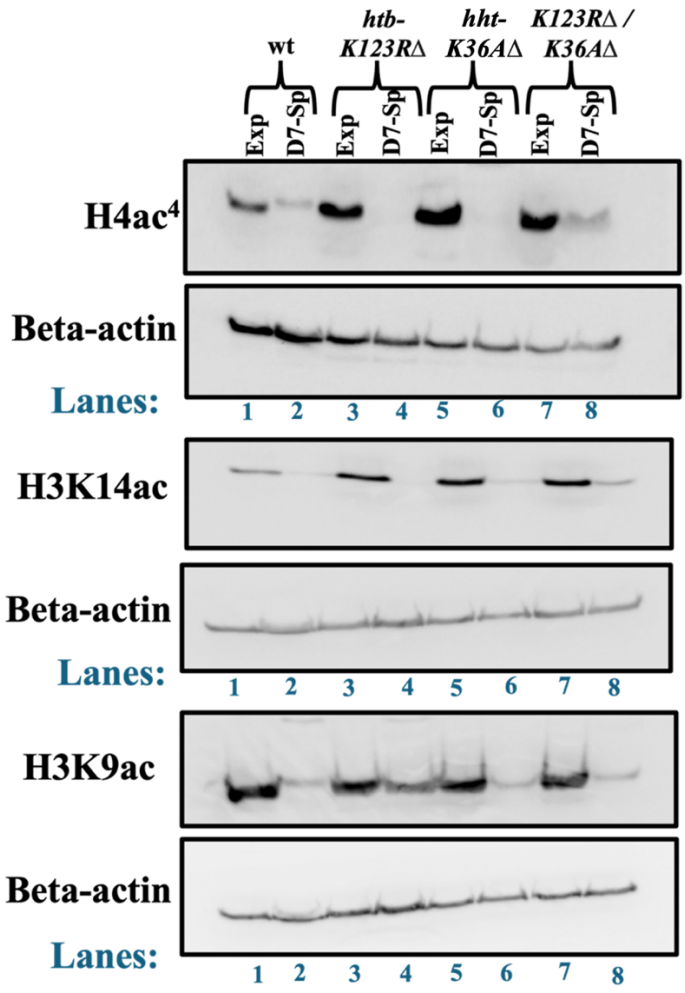


Figure 3.21: Western blot analysis of histone acetylation during exponential growth and stationary phase (SP) in wild-type, *htb-K123R*Δ, *hht-K36A*Δ and *K123R-K36A* mutant strains. Blots were probed using antibodies specific for H3K14ac, H3K9ac and tetra-acetylated H4 (H4ac4). Were analysed in wild-type, *htb-K123R*Δ (H2B ubiquitination-deficient mutant), *hht-K36A*Δ (H3K36 methylation-deficient mutant), and *K123R-K36A*Δ yeast strains during exponential growth (Exp) and stationary phase (SP, day 7). β-actin was used as a loading control to ensure equal protein loading and normalization of H3K14ac, H3K9ac and tetra-acetylated H4 (H4ac4) levels across different yeast strains and growth phases.

3.2.4.7 Analysis of H4K16 and H3K56 acetylation levels:

H3K56ac and H4K16 acetylation levels were next analysed. Histone H3K56ac is associated with newly deposited histone following DNA replication, whilst H4K16ac is associated with silencing at telomeres, at least when deacetylated (Aricthota *et al.*, 2022).

In wild-type cells, H4K16ac levels were high during stationary phase (SP) but significantly reduced in the exponential growth (Exp). An opposite profile to wild-type for H4K16ac was seen in the H3K36A single and *K123R-K36A*Δ double mutants. Thus, the H2Bub and H3K36me PTMs are negatively influencing this modification in wild-typeexponential phase cells.

Similar to the other histone acetylation marks tested, H3K56ac levels were high in wild-type exponential phase cells and low in wild-type SP cells (Fig. 3.22). A similar profile to wild-type was seen in the exponential and SP, *htb-K123R*Δ and *K123R-K36A*Δ mutants. However, there was a dramatic increase in H3K56ac levels in the exponentially growing *hht-K36A*Δ single mutant compared to wild-type suggesting a role for H3K36me in negatively influencing the levels of this acetylation mark in actively growing wild-type cells.

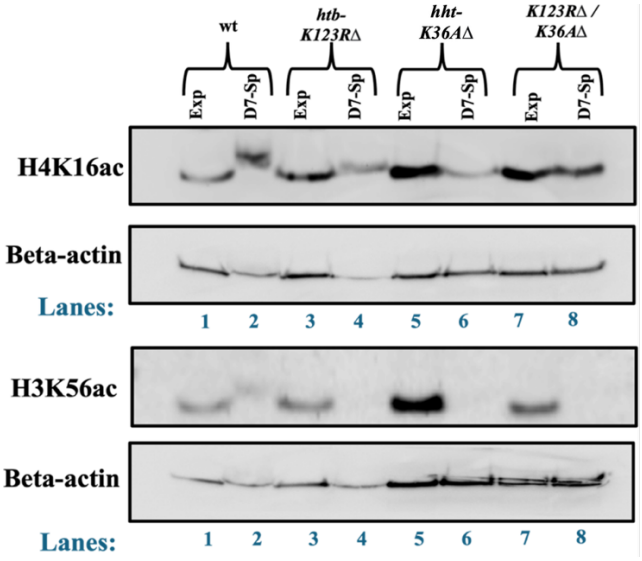


Figure 3.22: Western blot analysis of histone acetylation during exponential growth (Exp) and stationary phase (SP) in wild-type, *htb-K123R*Δ, *hht-K36A*Δ and *K123R-K36A* mutant strains. Blots

were probed using antibodies specific for H3K16ac and H3K56ac. were analysed in wild-type, *htb-K123R*Δ (H2B ubiquitination-deficient mutant), *hht-K36A*Δ (H3K36 methylation-deficient mutant), and *K123R-K36A*Δ yeast strains during exponential growth (Exp) and stationary phase (SP, day 7). β-actin was used as a loading control to ensure equal protein loading and normalization of H3K16ac and H3K56ac levels across different yeast strains and growth phases.

3.2.4.8 Examining the regulators of histone acetylation as cells enter SP

The opposing actions of histone acetyltransferases (HATs) and histone deacetylases (HDACs) control the dynamic regulation of histone acetylation. A more relaxed chromatin structure conducive to transcription is promoted by histone acetyltransferases (HATs), such as Gcn5p, which add acetyl groups to histones H3 at lysins 9 and 14, and H4 (Zhang *et al.*, 1998; Clements *et al.*, 2003). This it does as the catalytic subunit of the SAGA complex (Koutelou *et al.*, 2010; Liu *et al.*, 2019). Western blot analysis was therefore conducted using a Gcn5p-specific antibody to investigate whether the changes in H3K14ac and H3K9ac levels observed correlated with any changes in Gcn5p levels.

The results revealed that Gcn5p was readily detectable, and equally highly abundant, in wild-type and all mutant exponential phase and SP cells. Thus, distinct from the dramatic changes in histone acetylation levels observed in exponential and SP cells, Gcn5p levels remain constant throughout growth into SP.

Rpd3p levels, a major histone deacetylase (HDAC) implicated in transcriptional repression, were next checked (Keogh *et al.*, 2005), since the decrease in histone acetylation levels in SP cells could be achieved through increased abundance and activity of this enzyme (Fig. 3.23). Similar to what was seen for Gcn5p, Rpd3p levels remained unchanged in wild-type and all mutant cells throughout all stages tested. This observation suggests that histone acetylation reduction during entry into the stationary phase (SP) is not due to altered Rpd3p or Gcn5p abundance. Taken together, these data suggest a complicated interplay is occurring between H2Bub and H3K36me and some acetylation sites which can be apparent in both exponential phase and SP. However, the data suggests that this interplay between H3K36me, H2Bub and histone acetylation is not occurring at the levels of the HATs and HDACs required for adding and removing the acetyl marks.

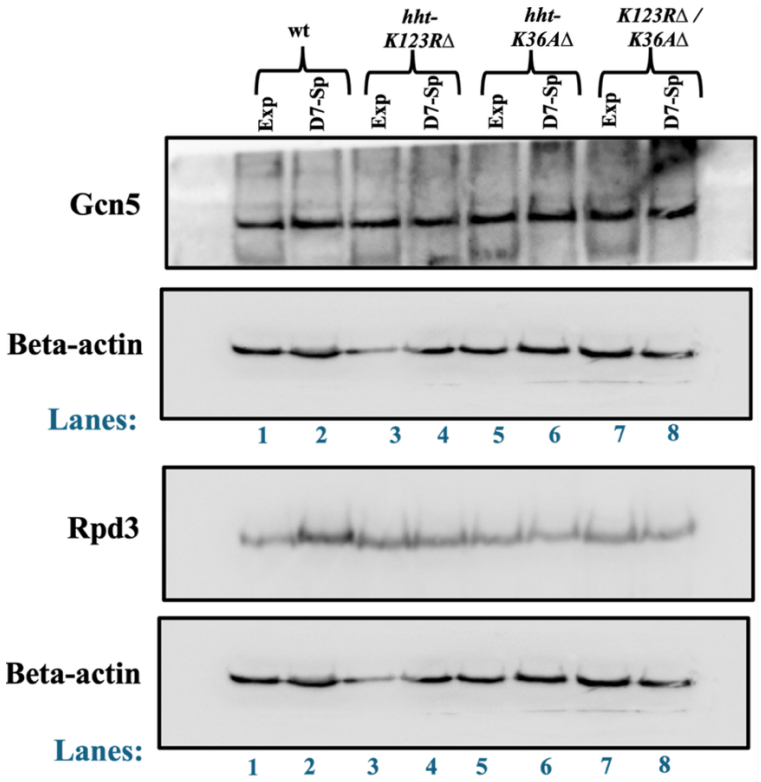


Figure 3.23: Western blot analysis of Gcn5p and Rpd3p protein levels. Cells grow during exponential growth (Exp) and stationary phase (SP) in wild-type and *htb-K123R*Δ, *hht-K36A*Δ and *K123R-K36A*Δ mutant strains. Blots were probed using antibodies specific for Gcn5p and Rpd3p. were analysed in wild-type, *htb-K123R*Δ (H2B ubiquitination-deficient mutant), *hht-K36A*Δ (H3K36 methylation-deficient mutant), and *K123R-K36A*Δ yeast strains during exponential growth (Exp) and stationary phase (SP, day 7). β-actin was used as a loading control to ensure equal protein loading and normalization of Gcn5p and Rpd3p levels across different yeast strains and growth phases.

3.2.4.9 Histone H4 serine 10-phosphate Expression Dynamics during entry into SP. To assess the potential impact of H2Bub and H3K36me on stress during growth into stationary phase (SP), we analysed the abundance of histone H4 Serine 10 phosphate (H4Ser10-P). H4Ser10-P is a histone modification involved in DNA damage repair, protection from which is a key function to aid in the survival of SP cells.

H4Ser10-P levels were therefore measured in exponential phase and SP cells of wild-type, *htb-K123RΔ*, *hht-K36AΔ*, and *K123R-K36AΔ* mutant strains. The results revealed high H4Ser10-P

levels in wild-type exponential and SP cells, although the band in the wild-type SP cells was higher than that seen in exponential phase.

However, although a band of equal intensity could be seen in all of the mutant exponential phase cells, no band was visible in any of the mutant SP cells. This suggests that H4ser10-P is absent from mutant SP cells indicating a role for H2Bub and H3K36me in potentially promoting DNA damage repair pathways in wild-type SP cells.

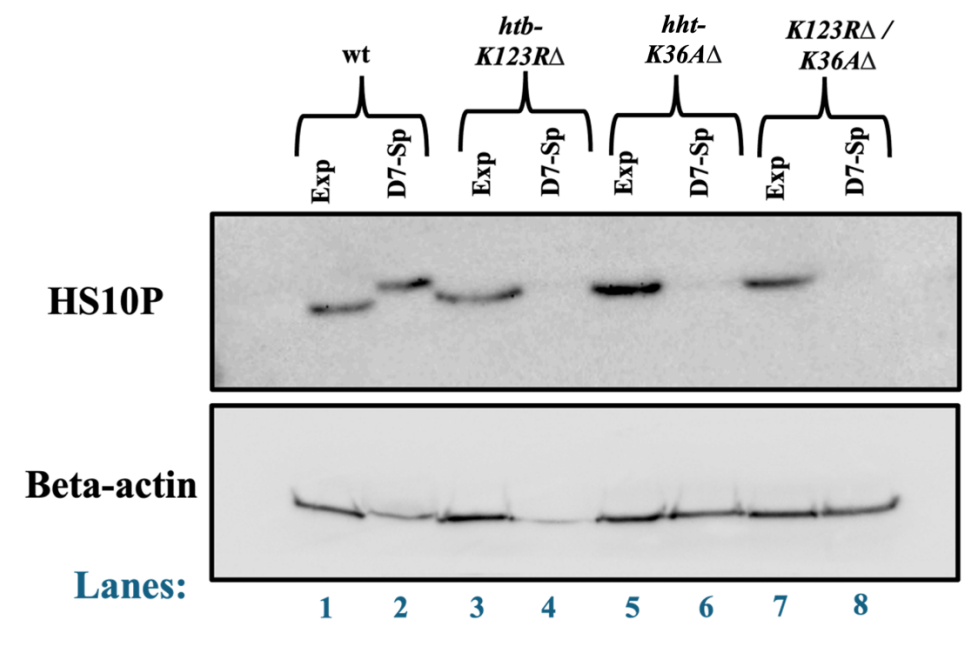


Figure 3.24: Western blot analysis of HS10P protein levels. Cells grow during exponential growth (Exp) and stationary phase (SP) in wild-type and *htb-K123R*Δ, *hht-K36A*Δ and *K123R-K36A*Δ mutant strains. Whole-cell lysates were prepared and probed with antibodies specific to HS10P were analysed in wild-type, *htb-K123R*Δ (H2B ubiquitination-deficient mutant), *hht-K36A*Δ (H3K36 methylation-deficient mutant), and *K123R-K36A*Δ yeast strains during exponential growth (Exp) and stationary phase (SP, day 7). β-actin was used as a loading control to ensure equal protein loading and normalization of HS10P levels across different yeast strains and growth phases.

3.2.4.10 Regulation of the Histone Variant H2A.Z (Htz1p) Levels in exponential and SP cells

In addition to the four canonical core histones H2A, H2B, H3, and H4, *S. cerevisiae* encodes histone variants that can substitute for their core counterparts and perform specialized functions (Redon *et al.*, 2002). H2A.Z, also referred to as (Htz1) in yeast, is one of such variants of H2A. Cse4p on the other hand acts as a specialized H3 variant found at centromeres (Fink, 2007; Halley *et al.*, 2010). Htz1p is known to be incorporated into promoter-associated nucleosomes and plays a role in transcriptional regulation by promoting chromatin accessibility and gene responsiveness under fluctuating environmental conditions. Htz1p-containing nucleosomes are generally less stable than those with canonical H2A thereby rendering chromatin in which they are incorporated more dynamic and responsive to regulatory signals (Wan *et al.*, 2009). This property of Htz1p has been thought to promote more rapid gene activation under fluctuating environmental conditions (Keogh *et al.*, 2005; Millar *et al.*, 2006).

Based on this, we hypothesized that Htz1p levels might increase during the stationary phase (SP) to poise cells for a quick re-entry into active growth when conditions improve. In support of this hypothesis, Western blot analysis was performed on wild-type cells did suggest that there were higher levels in SP cells than those in exponential phase cells, consistent with chromatin being poised for reactivation following SP exit. However, although Htz1p levels in all of the mutant exponential phase cells was similar to that seen in wild-type, the higher levels seen in the wild-type SP cells, were not evident in any of the mutants. Thus, this suggests that H2Bub and H3K36me might be required for Htz1p deposition in wild-type SP cells to potentially poise the wild-type SP cells for rapid exit from SP when appropriate conditions arise.

This is consistent with a previous study that indicates H2A.Z occupancy can remain stable under nutrient-limited conditions (Zhang *et al.*, 2005).

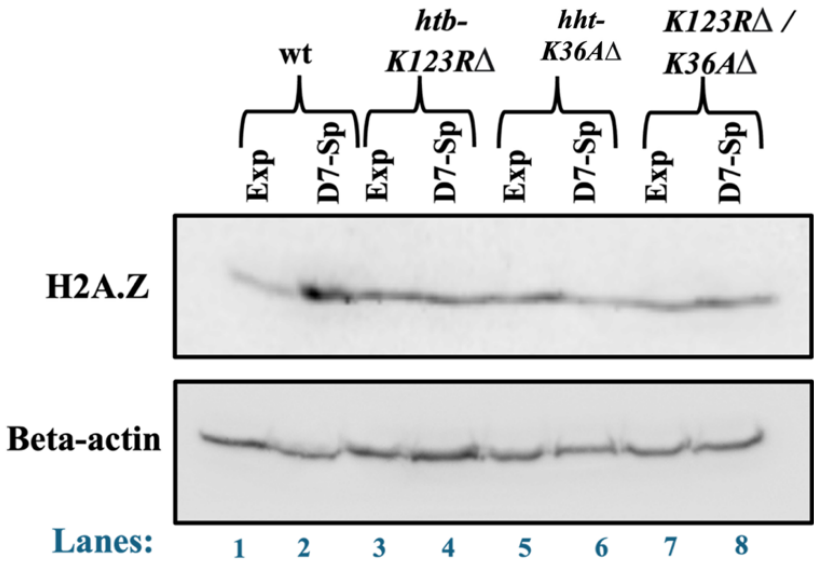


Figure 3.25: Western blot analysis of H2A.Z (Htz1p) levels. Cells grow during exponential growth (Exp) and stationary phase (SP) in wild-type and *htb-K123R*Δ, *hht-K36A*Δ and *K123R-K36A*Δ mutant strains. Whole-cell lysates were prepared and probed with antibodies specific to histones Htz1p. were analysed in wild-type, *htb-K123R*Δ (H2B ubiquitination-deficient mutant), *hht-K36A*Δ (H3K36 methylation-deficient mutant), and *K123R-K36A*Δ yeast strains during exponential growth (Exp) and stationary phase (SP, day 7). β-actin was used as a loading control to ensure equal protein loading and normalization of H2A.Z (Htz1p) levels across different yeast strains and growth phases.

3.3 Summary of main findings

- A significant growth delay was observed in *hht-K36A*Δ as indicated by doubling time analysis, while *K123R-K36A*Δ showed a non-significant increase.
- The double mutant attained lower cell densities in SP than wild-type, indicating impaired proliferation and biomass accumulation.
- No significant differences in CFU counts were observed between wild-type and mutant strains over 7 days in stationary phase.
- Heightened sensitivity to thermal, oxidative, osmotic, and genotoxic stress, particularly in stationary phase was displayed by the *K123R-K36A*Δ mutant strain. Stress responses varied by growth phase, with to caffeine, MMS, sorbitol, and LiCl showing the most effects. Carbon source utilization remained unaffected.

- Pol II levels were reduced in *K123R-K36A*Δ mutant SP cells whilst the levels of its active forms (Ser2-P and Ser5-P) remained unchanged, suggesting that the limited Pol II present in the double mutant cells is abnormally active.
- Core histone levels remain stable across phases in all strains, except for H3, which is abnormally elevated in stationary phase double mutants indicating disrupted H3 regulation when both modifications are absent.
- During exponential phase the elevated Hho1p levels in all mutants indicates that these modifications may play a role in regulating Hho1p abundance under nutrient-rich, transcriptionally active conditions.
- Expected patterns of high H3K14ac, H4ac4 and H3K9ac during exponential growth (active transcription), and low levels during SP (transcriptional repression) were observed in wild-type.
- All mutant strains showed elevated H3K14ac and H4ac4 in exponential phase, indicating that loss of H2Bub and/or H3K36me leads to hyperacetylation during active growth.
- A failure to repress transcription-associated acetylation during quiescence can be assumed in the double mutant since this mutant's SP cells retained high levels of H3K14ac and H4ac4 compared to wild-type.
- In SP, the *htb-K123R*Δ single mutant shows abnormally high H3K9ac levels, suggesting that H2Bub specifically influences repression of H3K9ac during this phase.
- A broader chromatin disruption may be reflected from mis-regulation of H4K16ac in mutants as it appears to be regulated independently of H2Bub and H3K36me.
- Elevated levels of H3K56ac in the *hht-K36A*Δ mutant points towards a repressive role for H3K36 methylation in modulating acetylation during active growth.
- Expected patterns of high of PAF1p was observed during Exp (active transcription), and low levels during SP (transcriptional repression) of wild-type and mutant cells.
- Elevated PAF1p levels in mutants during exponential growth indicates that H2Bub and/or H3K36me loss may enhance PAF1p abundance under transcriptionally active conditions.
- Gcn5p and Rpd3p remained unchanged across wild-type and mutants during all growth phases indicating that interplay between H3K36me, H2Bub and histone acetylation is not occurring at the levels of the HATs and HDACs required for adding and removing the acetyl marks.

- In all the mutants during SP complete loss of H4Ser10-P was seen, implying that H2Bub and H3K36me are required for this modification under stress or nutrient-depleted conditions.
- Htz1p (H2A.Z) levels increase in wild-type cells during SP suggests a chromatin state primed for reactivation.

3.4 Discussion

In the current study, a systematic investigation on the phenotypic and molecular effects of specific lysine substitutions in histone H2B at residues K123 and K36 was performed. The results offered an insight into the role of histone marks in influencing cellular adaptation, stress responses, and overall physiology. Our study reveals that H2B-K123 ubiquitination and H3K36 methylation critically regulate growth, stress responses, and chromatin dynamics. Below, we contextualize these results with prior work and propose mechanistic models.

H3K36 methylation and H2B mono-ubiquitination have been shown to influence yeast growth and metabolism (Weiner *et al.*, 2012; Fuchs *et al.*, 2014). Current study showed *hht-K36A* mutant has a longer doubling time than wild-type, indicating a growth defect. Interestingly this defect was not seen in the *K123R-K36A*Δ double mutant. These results imply towards the antagonistic roles for H3K36me and H2Bub in regulating proliferation.

The *hht-K36A*Δ mutant reaches wild-type cell density after 24 hours despite its slower growth rate. Double mutant on the other hand does not, suggesting compounded defect in adapting to glucose depletion. These observations were concomitant to prior studies that have shown to link histone modifications to efficient transcription and chromatin organization, both required for optimal growth (Li *et al.*, 2007; Chou *et al.*, 2023).

No significant differences in colony-forming capacity were observed over seven days across all strains, including wild-type and mutants. This result suggests that these histone marks are not necessary for viability under stationary condition. This finding aligns with study which showed that in the absence of these modifications cell survival during nutrient depletion or quiescence is not affected (Gray *et al.*, 2004). This suggests that while these marks are important for growth and metabolic adaptation, however they may not be necessary for viability in stationary phase which is characterised by reduced transcriptional activity.

The heightened sensitivity, particularly by the *K123R-K36A*Δ double mutant, was demonstrated under various stress conditions. A marked impairment in thermal resilience of SP cells of *hht-K36A*Δ and *K123R-K36A*Δ double mutant at elevated temperature was revealed by thermal stress assays, which was consistent with previous studies highlighting the role of histone modifications in chromatin remodelling during thermal stress (Petty *et al.*, 2016; Negesse, 2024).

During both Exp and SP there was no increased sensitivity to DNA damage agents CPT and MMS in the histone mutants indicating that H3K36 methylation and H2B ubiquitination do not contribute to the canonical DNA damage response pathways. This is consistent with previous findings where the role of these modifications in transcriptional regulation rather than direct DNA repair mechanisms has been shown (Carrozza *et al.*, 2005; McDaniel *et al.*, 2017; Bilokapic and Halic, 2019).

All mutants exhibit increased sensitivity to oxidative stress during exponential phase, indicating impaired antioxidant defences. This result was consistent with the reduced antioxidant defences associated with disrupted histone modifications (Cencioni *et al.*, 2013). In contrast, stationary phase (SP) mutants displayed no sensitivity, suggesting that stress response mechanisms in non-dividing cells may compensate for the mutation.

All mutant strains in current study showed no significant growth defects on various alternative carbon sources, suggesting that these marks are not essential for broad metabolic adaptability. In the double mutant a slight growth impairment on sucrose may be indicative of subtle transcriptional dysregulation, aligning with previous study linking histone crosstalk to carbon source utilization (Howe, 2012). Furthermore, the unseparated and clumped cellular morphology seen in mutant strains indicates towards the disruptions in cell cycle regulation. This was consistent with findings from studies on histone modifications' role in maintaining cellular structure (Karkowska-Kuleta and Kozik, 2015).

The functional interplay between H2B K123 ubiquitination and H3 methylation marks, such as H3K4me3 and H3K79me2 and 3 was also confirmed in this study. The importance of H2Bub in maintaining the epigenetic landscape was highlighted through the disruption of these marks in mutants. These findings also confirm the concept of "histone crosstalk," which focuses on modifications on one histone influence others to coordinate chromatin-dependent processes

(Sun and Allis, 2002). This interplay is supporting the observed phenotypic differences, particularly the impaired stress responses and reduced viability in the stationary phase (SP).

Our findings reinforce the notion that histone modifications play a pivotal role in maintaining chromatin integrity and facilitating cellular adaptation to replication stress. The pronounced sensitivity of the H2B lysine double mutant *K123R-K36Δ* to (HU, 200 mM) during exponential (Exp) growth highlights the functional importance of these residues in stabilizing replication forks under conditions of DNA synthesis stress.

This observation aligns with earlier reports demonstrating increased stress sensitivity in histone mutants (Kaabache *et al.*, 1995; Kari *et al.*, 2022), and supports a broader model in which specific histone modifications contribute to the preservation of genome stability. Moreover, our results are consistent with prior work linking histone modifications to replication fork maintenance and DNA damage tolerance pathways (Sun and Allis, 2002). Together, these findings suggest that H2B lysine residues are not merely structural components of chromatin but actively participate in regulating replication dynamics and genome integrity during stress, potentially through interactions with replication and repair factors.

No significant differences in glucose consumption among wild-type and histone mutant strains were observed, suggesting that H3K36 methylation and H2B ubiquitination do not have direct impact on glucose uptake. This was consistent to previous findings that these modifications primarily regulate transcriptional fidelity and stress responses rather than core metabolic processes (Cullen and Sprague Jr, 2000; Cheng *et al.*, 2018; Polanco, 2019). The growth defects observed in mutants are therefore unlikely to stem from altered glucose utilization.

Total RNA Polymerase II (Pol II) levels remained stable across growth phases in wild-type and single histone mutants. This observation was consistent with previous study that Pol II abundance remains unchanged by transcriptional activity shifts (Komarnitsky *et al.*, 2000). However, the reduced Pol II signal in SP double mutant cells suggests a synergistic role for these modifications in maintaining Pol II stability under nutrient-limited conditions.

An expected pattern in wild-type cells high during exponential growth and diminished in SP was followed by phosphorylation of the Pol II C-terminal domain (CTD) at Ser2 and Ser5,

aligning with established transcriptional downregulation during quiescence (Baxter and Diffley, 2008; Harlen and Churchman, 2017; Isern *et al.*, 2025; Zeng, 2025). Although single mutants mirrored wild-type phosphorylation dynamics. In the double mutant during SP disproportionately high Ser2-P and Ser5-P relative to total Pol II was seen indicating that the remaining Pol II in these cells is hyperphosphorylated and potentially aberrantly active. Therefore, a combined loss of H2Bub and H3K36me seems to disrupts normal transcriptional repression during SP.

In wild-type cells, elevated levels of H3K14ac, H3K9ac, H4ac4, and H3K56ac during exponential growth and their reduction in SP is in line with transcriptional activity patterns, consistent with research connecting acetylation to active chromatin states (Millar *et al.*, 2006).

Interestingly mutants exhibited hyperacetylation of H3K14ac and H4ac4 in exponential phase. However, in *K123R-K36A*Δ double mutant elevated levels persisted in SP. These results suggest that loss of H2B ubiquitination and H3K36 methylation disrupts normal acetylation turnover, potentially impairing transcriptional repression during quiescence (Venkatesh *et al.*, 2012; Venkatesh and Workman, 2015). H3K9ac levels remained largely unchanged in the *hht-K36A*Δ and *K123R-K36A*Δ double mutants but were significantly elevated in SP in the *htb-K123R*Δ single mutant, indicating a specific role for H2Bub in regulating H3K9 acetylation during transcriptional downregulation (Henry *et al.*, 2003). An inverse pattern for H4K16ac levels in mutants compared to wild-type, with reduced levels in SP and increased levels in exponential phase was seen which suggests that H2Bub and H3K36me indirectly modulate telomeric silencing-associated acetylation (Clapier and Cairns, 2009).

A dramatic increase in H3K56ac in the *hht-K36A*Δ mutant during exponential growth implicates H3K36 methylation in suppressing replication-coupled acetylation. This observation was consistent with its role in chromatin compaction and transcriptional fidelity (Venkatesh and Workman, 2015). Altogether an interplay between histone methylation and ubiquitination in shaping acetylation landscapes and transcriptional states across cellular phases is revealed by these results.

Gcn5p and Rpd3p protein levels remained constant in wild-type and mutant strains despite marked changes in histone acetylation across growth phases. This supports previous study that that showed Gcn5p (as part of the SAGA complex) acetylates H3K9 and H3K14 without major

change in expression (Koutelou *et al.*, 2010; Liu *et al.*, 2019). On the Similar note, Rpd3p-mediated deacetylation is known to regulate transcriptional repression which is not dependent on its protein level (Carrozza *et al.*, 2005). These results suggest that the interplay between H2Bub, H3K36me, and histone acetylation occurs downstream of HAT and HDAC abundance, likely through modulation of enzyme activity or chromatin accessibility.

In wild-type and single mutant strains core histone levels remained largely stable across growth phases which was consistent with previous studies of tight histone homeostasis during quiescence (Hauer and Gasser, 2017; Bonitto *et al.*, 2021; Zeng, 2025). However, elevated H3 levels in SP double mutants suggest disruption of chromatin remodelling during growth arrest due to combined loss of H2Bub and H3K36me. This supports the role of histone PTMs in regulating chromatin structure and transcriptional silencing during metabolic transitions (Roy *et al.*, 2020).

During stationary phase across all strains Hho1p abundance decreased this was consistent with prior studies linking nutrient depletion to reduced HMGB protein levels and chromatin relaxation (Schäfer *et al.*, 2008). During exponential growth elevated Hho1p in mutant strains was observed which suggests that H2Bub and H3K36me may influence chromatin accessibility under nutrient-rich conditions. In SP there was the lack of differential Hho1p regulation which implies that these histone modifications do not govern Hho1p-mediated chromatin compaction during growth arrest. This aligned with finding that Hho1p downregulation is primarily stress-driven (Lawrence, 2019).

Htz1p levels increased in wild-type SP cells, consistent with its role in promoting chromatin accessibility and transcriptional responsiveness under stress (Keogh *et al.*, 2005; Millar *et al.*, 2006; Wan *et al.*, 2009). This suggests that elevated H2A.Z may prime chromatin for rapid reactivation upon exit from quiescence. In contrast, mutant strains deficient in H2Bub and H3K36me failed to show this SP-specific increase, indicating that these histone modifications may facilitate Htz1p deposition during growth arrest. These findings align with prior evidence that H2A.Z incorporation is regulated by chromatin context and post-translational modifications (Zhang *et al.*, 2005).

Paf1p levels are markedly reduced in wild-type cells upon entry into SP which was consistent with the transcriptional downregulation characteristic of this phase. This decline suggests that

PAF1C quantity is tightly linked to transcriptional activity. Interestingly mutants (*htb-K123R*Δ*,* *hht-K36A*Δ*,* and *K123R-K36A*Δ) exhibited elevated Paf1p levels during exponential growth compared to wild-type, despite showing similar depletion in SP. These findings suggest that H2B ubiquitination and H3K36 methylation do not directly regulate PAF1C stability during SP however, may influence its expression/ recruitment during exponential phase. Given that PAF1C facilitates Set2-mediated H3K36 methylation and Rad6/Bre1-dependent H2B ubiquitination (Wood *et al.*, 2003; Li *et al.*, 2024), the upregulation of Paf1p in these mutants may reflect a compensatory response to disrupted chromatin signalling.

Our results show that wild-type cells maintain high levels of H4Ser10-P during both exponential growth and SP, with increased signal intensity in SP, suggesting enhanced chromatin remodelling or DNA repair activity during nutrient limitation. On the contrary, all mutant strains exhibited complete loss of H4Ser10-P in SP, despite normal levels during exponential phase.

This indicates that H2B ubiquitination and H3K36 methylation are required for H4Ser10 phosphorylation during SP, potentially by facilitating recruitment of kinases or chromatin accessibility necessary for DNA repair signalling (Serrano-Quílez *et al.*, 2020; Ryu, 2024). These findings suggest a functional interplay between histone crosstalk and stress-induced chromatin responses, where loss of H2Bub and H3K36me disrupts protective phosphorylation events critical for SP survival.

In summary, a systematic dissection of the phenotypic and molecular consequences of lysine substitutions at H2B-K123 and H3-K36 is provided in this study. An intricate interplay is revealed between histone ubiquitination and methylation in regulating chromatin-dependent processes. The critical roles of H2Bub and H3K36me in modulating yeast growth, stress responses, transcriptional dynamics, and chromatin architecture are highlighted by the results. Main findings showed that while these modifications are dispensable for viability under stationary conditions. These modifications are essential for optimal proliferation, stress adaptation, and transcriptional repression during quiescence. The differential phenotypes of single and double mutants revealed the antagonistic relationship between H2Bub and H3K36me in regulating growth and metabolic adaptation. Additionally, aberrant acetylation patterns, impaired replication stress tolerance, and altered chromatin remodelling was resultant of the disruption of histone crosstalk particularly during nutrient limitation. Importantly, the loss of

H4Ser10 phosphorylation in stationary phase mutants indicates towards a mechanistic link between histone modifications and DNA repair signalling, suggesting that H2Bub and H3K36me facilitate protective chromatin responses under stress. The changes observed in histone variant incorporation, transcriptional machinery, and chromatin regulators further support a model in which PTMs orchestrate a coordinated response to environmental cues. Taken together, current study strengthens the concept of histone crosstalk as a central regulator of cellular physiology and chromatin integrity. This study also offers a new insight into how transcriptional landscapes and stress resilience are shaped by specific histone marks. This study can be utilized for future investigations into the dynamic regulation of chromatin states and their implications for cellular adaptation and genome stability.

Chapter 4

Analysis of wild-type, *htb-K123R*Δ, *hht-K36A*Δ, and *K123R-K36A*Δ mutants during growth into stationary phase

4.1 Introduction

Living organisms frequently encounter various forms of stress, with starvation being one of the most common. To survive prolonged periods of nutrient scarcity, organisms must detect and adapt to these conditions. For instance, *Saccharomyces cerevisiae* responds to nutrient limitation by ceasing growth and entering a non-proliferative state known as the stationary phase (SP).

When cultivated in glucose-rich media, *S. cerevisiae* undergoes distinct growth phases. Initially, it exhibits rapid logarithmic growth fuelled by fermentation. Upon glucose depletion, the cell cycle arrests, triggering global reprogramming events that enable a slower growth phase. During this phase, fermentation by-products serve as secondary carbon sources through respiration, a transition termed the diauxic shift (Dix). Once all carbon sources are exhausted, the cells enter the true stationary phase, where growth and proliferation halt (Werner-Washburne *et al.*, 1993; Herman, 2002).

Earlier assumptions suggested that all cells in SP cultures were quiescent, or non-proliferative, but recent studies have revealed heterogeneity within these populations. Specifically, SP cultures consist of two distinct cell types: quiescent (Q) and non-quiescent (NQ) cells (Allen *et al.*, 2006). The Q population comprises young daughter cells that remain viable for extended periods, while the NQ population primarily consists of older mother cells that undergo apoptosis or necrosis. These populations exhibit differing physical and behavioural traits, including variations in stress resistance and thermotolerance. Notably, Q cells can re-enter the cell cycle upon nutrient replenishment (Allen *et al.*, 2006).

Histone modifications play a pivotal role in chromatin structure and gene regulation. These modifications can influence gene expression by altering recruitment of other transcription factors to genes, thereby impacting the cell's ability to adapt to stress. Studies have demonstrated that methylation and ubiquitylation of histones, such as methylation at H3K36 and ubiquitylation at H2BK123, are critical for chromatin remodelling during these transitions (Klosinska *et al.*, 2011; McKnight *et al.*, 2015).

It has been shown that some histone markers of active transcription, such as histone H3 lysine methylation (H3K36me) are retained in Q cells, despite the general shut down in transcription in these cells (Young *et al.*, 2017; Bonitto *et al.*, 2021).

Conversely, histone H2B monoubiquitylation (H2Bub), although also a mark associated with active transcription, is lost at SP and is absent in Q cells (Young *et al.*, 2017). However, the role of the retention or loss of such histone modifications in quiescence remains unclear. Investigating specific histone mutations such as H2Bub and H3K36me can provide insights into how chromatin modifications influence cellular adaptation and survival during SP.

In the current study, the growth and separation of wild-type and mutant strains *htb-K123R*Δ*,* *hht-K36A*Δ*,* and *K123R-K36A*Δ under SP conditions were analysed. In order to distinguish between Q and NQ cell populations and assess their morphological differences across different time points, Q cells were separated according to density by Percoll-gradient centrifugation. We then examined how the Q and NQ ratios, as well as cell morphology and viability, were affected by the histone modifications. These studies should contribute to a deeper understanding of chromatin-dependent regulation of quiescence.

4.2 Results

4.2.1 Percoll-gradient centrifugation to separate quiescent (Q) and non-quiescent (NQ) cells

To fractionate Q and NQ cell populations, Percoll gradient centrifugation was performed. This technique separates cells based on their buoyant density: Q cells, being denser, migrate to the lower fraction, while the less dense NQ cells remain in the upper fraction (Allen *et al.*, 2006).

Wild-type and mutant strains *htb-K123R*Δ*,* *hht-K36A*Δ*,* and *K123R-K36A*Δ were cultured for 7 and 14 days to promote deep cell growth into SP. An equal number of cells from each culture was loaded onto separate Percoll gradients and centrifuged. After centrifugation, in wild-type and *K123R-K36A*Δ strains, two distinct bands were observed at both day 7 and 14: an upper NQ band and a lower Q band (Fig. 4.1, Fig. 4.2). In contrast, *htb-K123R*Δ and *hht-K36A*Δ mutants showed a higher proportion of cells in the lower fraction compared to the upper NQ fraction, indicating a shift towards quiescent Q.

These results suggest that by day 7 and day 14 of SP, the development of Q and NQ cells in *htb-K123R*Δ and *hht-K36A*Δ mutants turn from the typical pattern observed in wild-type, with a greater formation of Q cells in the single mutants.

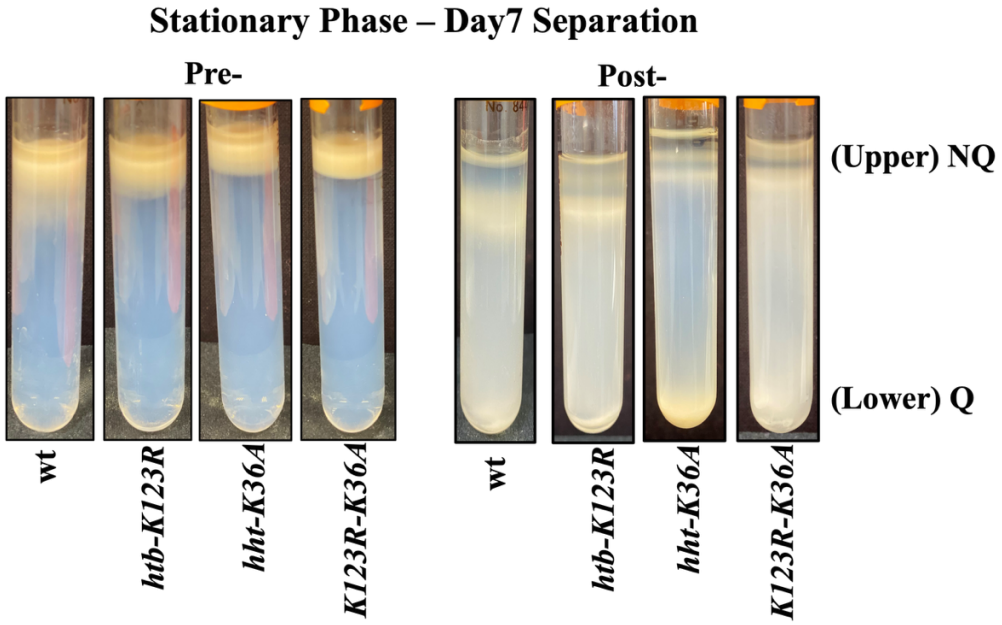


Figure 4.1: Separation of Day 7 cultures into quiescent Q and non-quiescent cell NQ populations. Images of day 7 wild-type, *htb-K123R*Δ*, hht-K36A*Δ*,* and *K123R-K36A*Δ mutant cells before (pre-) and after (post-) centrifugation of Percoll density gradients loaded with cells harvested from 6.5 ml of day 7 cultures.

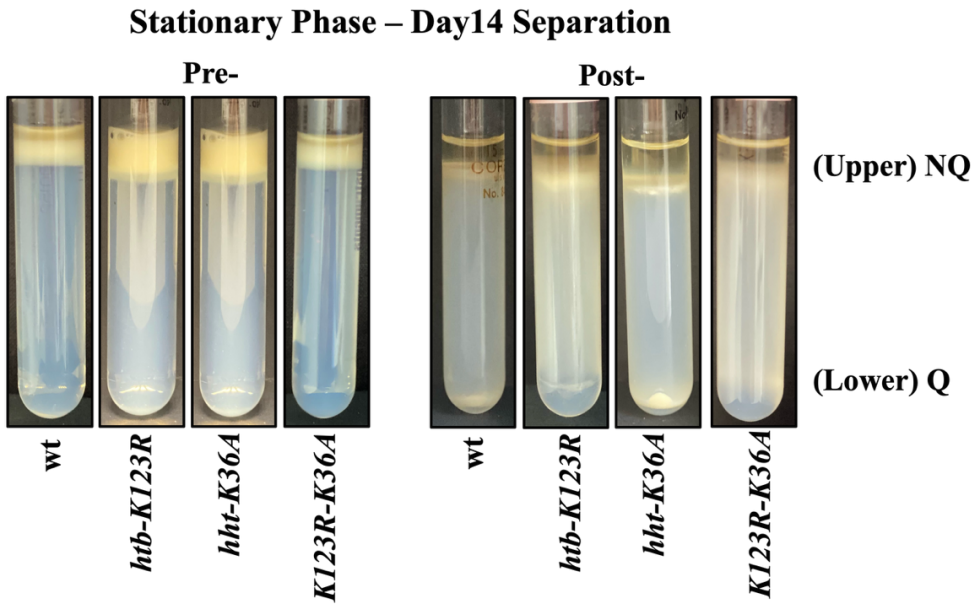


Figure 4.2: Separation of Day 14 cultures into quiescent Q and non-quiescent cell NQ populations. Images of day 14 wild-type, *htb-K123R*Δ*, hht-K36A*Δ*,* and *K123R-K36A*Δ mutant cells before (pre-) and after (post-) centrifugation of Percoll density gradients loaded with cells harvested from 6.5 ml of day 14 cultures.

4.2.2 Exponential phase wild-type and mutants did not form two cell populations

As a control, we performed the Percoll density gradient separation on exponentially growing cells of each strain. We found no distinct Q and NQ cell populations in wild-type and mutant strains *htb-K123R*Δ*, hht-K36A*Δ*,* and *K123R-K36A*Δ during the exponential phase (Exp) (Fig. 4.3). This finding indicates that the separation of SP cultures into Q and NQ populations is limited only to stationary phase conditions indicating that metabolic and transcriptional changes required for Q and NQ separation are triggered upon entry into the stationary phase SP (Laporte *et al.*, 2017).

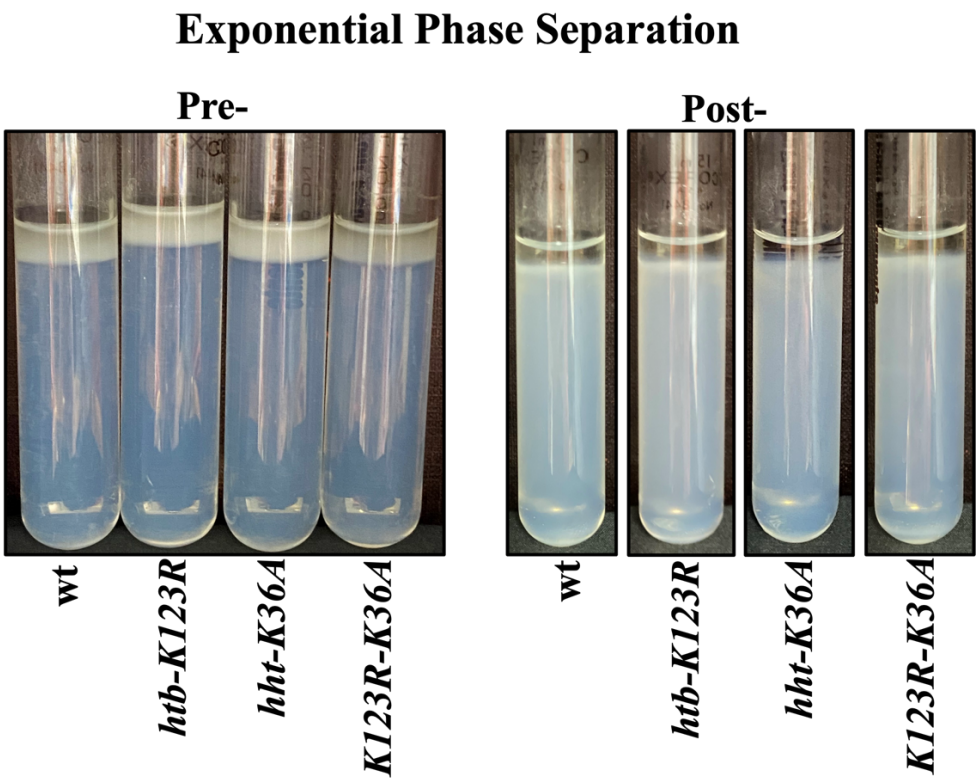


Figure 4.3: Exponential phase cells do not form two populations following Percoll-gradient centrifugation. Images of exponential (Exp) **wild-type, *htb-K123R*Δ, *hht-K36A*Δ, and *K123R-K36A*Δ** cells before (pre-) and after (post-) centrifugation of Percoll density gradients loaded with equal cell numbers.

4.2.3 The gradients were fractionated to isolate the two populations

To quantify how the histone mutations affect cell separation, the separated cell populations were fractionated after centrifugation, and the number of cells in the upper NQ band and lower Q bands were counted (Fig. 4.4). Following counting of the cells in the two separated populations, the wild-type strain formed nearly equal numbers of cells in the upper NQ and lower Q fractions (Fig.4.4. A). In contrast, *htb-K123R*Δ and *hht-K36A*Δ mutants yielded a larger proportion of Q

lower cells than upper NQ cells (Fig. 4.4.A). The *K123R-K36A*Δ double mutant resembled wild-type, with a more balanced distribution between Q and NQ fractions (Fig. 4.4.A).

Cell viability in the separated cell fractions was next examined by plating for colony-forming units (CFU), and the CFU values were compared to the total number of cells counted previously to determine the % value of survival (Fig. 4.4.B). This confirmed that wild-type cultures contained ~50% viable cells in the Q fraction and only ~10% in the NQ fraction, consistent with the expected loss of viability in NQ cells. In the *htb-K123R*Δ and *hht-K36A*Δ mutants, NQ cell viability was almost 2-fold higher than in wild-type (Fig. 4.4.C). This suggests that the *htb-K123R* and *hht-K36A*Δ single mutant strains have enhanced survival in the upper NQ cell population. Interestingly, in the double mutant *K123R-K36A*Δ, NQ cell viability surpassed even that of the single mutants, indicating the highest level of viability retention in the upper NQ fraction.

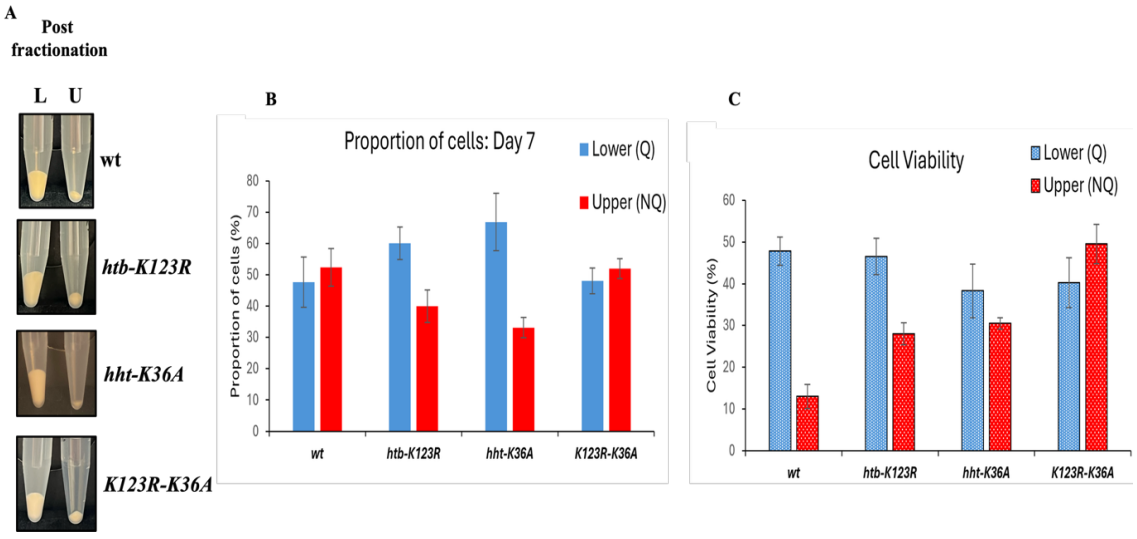


Figure 4.4: The gradients were fractionated to isolate the two populations. (A) Cells were harvested from the fractionated gradients. **(B)** The total numbers of cells in the upper (NQ) and lower (Q) fractions were quantified using hemocytometer counts and were expressed as a proportion (%) of the total cell count. **(C)** The % of viable cells from both fractions in wild-type, *htb-K123R*Δ, *hht-K36A*Δ, and *K123R-K36A*Δ, were determined by plating out for colony forming units and viability was

shown as a % of the total number of cells counted in each fraction. (**A-B-C**). The data shown is from between 4 – 5 biological replicates. Error bars show standard deviation of the mean (SEM).

Repeating the experiment with (Day 14) cultures yielded similar trends, reinforcing the conclusion that these histone mutations influenced both the formation and viability of NQ cells during SP (Fig. 4.5).

Together, these data suggest that H2Bub and H3K36me are required for correct formation of Q and NQ populations such that in the absence of either H2Bub or H3K36me, more Q cells and less NQ cells are formed compared to wild-type . However, this aberrant cell development is rescued when both modifications are absent.

The data also suggest that H2Bub and H3K36me are having pro-apoptotic functions in the upper mother cell fraction, such that in the absence of these modifications, more cells survive in the upper cell fraction compared to wild-type . Importantly, the data also suggest that both H2Bub and H3K36me are acting together in their pro-apoptotic activity since the increase in NQ viability in the double mutant is greater than that seen in either single mutant.

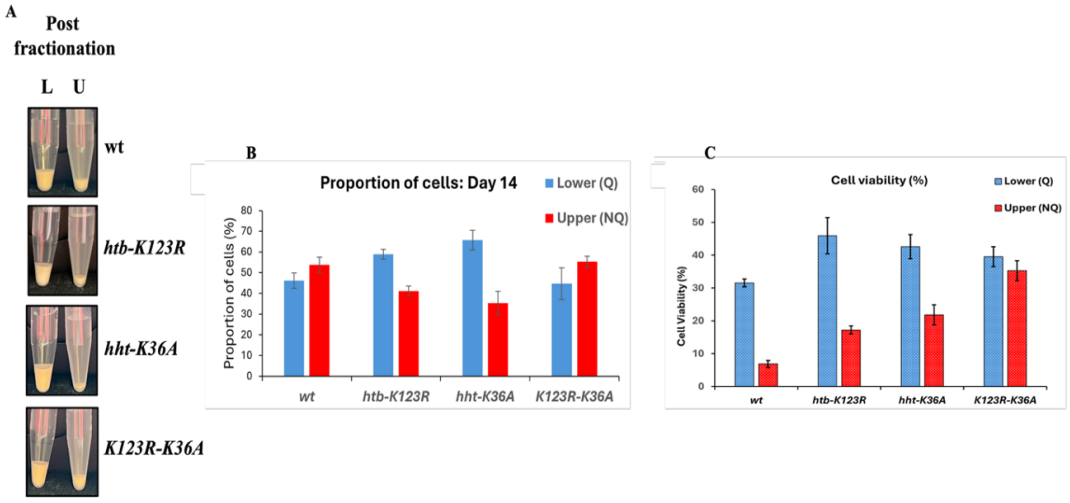


Figure 4.5: The gradients were fractionated to isolate the two populations. Cells were harvested from the fractionated gradients; **(A)** Total cell counts for the upper fraction NQ and lower fraction Q were calculated using a hemacytometer. **(B)** The total numbers of cells in the upper (NQ) and lower (Q) fractions were quantified using hemocytometer counts and were expressed as a proportion (%) of the total cell count. **(C)** The % of viable cells from both fractions in wild-type, *htb-K123R*Δ, *hht-K36A*Δ,

and *K123R-K36A*Δ,were determined by plating out for colony forming units and viability was shown as a % of the total number of cells counted in each fraction. (A-B-C). The data shown is representative of the experiment performed in triplicate. The data shown is from between 4 – 5 biological replicates. Error bars show standard deviation of the mean (SEM).

4.2.4 Cell morphology of unseparated, Q cell and NQ cells in *htb-K123R*Δ*, hht-K36A*Δ, and *K123R-K36A*Δ strains during SP

To investigate how histone modifications affect cell morphology during the stationary phase, microscopy was performed on exponential (Exp), quiescent (Q), and non-quiescent (NQ) cells in wild-type and mutant strains *htb-K123R*Δ*, hht-K36A*Δ, and *K123R-K36A*Δ.

During the exponential phase, microscopy analysis revealed distinct morphological trends across strains and populations (Figs. 4.6, 4.7). During the exponential phase (Exp), all strains, including mutants, exhibited the uniform, rounded morphology typical of proliferating yeast, confirming that histone mutations do not disrupt overall cell architecture during active growth. However, subtle differences were observed when comparing the wild-type to the mutants: while wild-type cells displayed consistently regular and rounded shapes, *htb-K123R*Δ cells appeared slightly irregular, and *K123R-K36A*Δ cells showed mild elongation, suggesting that these mutations may cause minor morphological perturbations despite maintaining the general yeast growth-phase phenotype.

In the Q cell population, microscopy analysis of quiescent (Q) cells isolated via Percoll gradient centrifugation at Days 7 and 14 revealed distinct morphological differences between wild-type and histone mutant cells. wild-type Q cells maintained the classic small, round, and unbudded morphology typical of quiescent yeast at both time points. In comparison, *htb-K123R*Δ Q cells largely resembled wild-type but displayed mild irregularities in shape, while *hht-K36A*Δ Q cells frequently appeared elongated, suggesting a partial disruption of quiescence-associated structural organization. The *K123R-K36A*Δ double mutant exhibited a combination of these phenotypes, with both elongation and irregularity, indicating an additive effect of the mutations. By Day 14, these deviations became more pronounced in the mutants, particularly in the *K123R-K36A*Δ double mutant, which showed increased morphological abnormalities compared to the

uniform wild-type Q population. Despite these differences, all mutants largely retained the unbudded, spherical structure characteristic of Q cells, though with varying degrees of distortion.

In the NQ cell fraction, microscopy analysis of non-quiescent (NQ) cells revealed clear morphological differences between wild-type and histone mutants. wild-type NQ cells consistently exhibited the expected large, budded morphology typical of ageing or stressed mother cells. In contrast, *htb-K123R*Δ NQ cells showed severe surface distortions and irregular shapes, while *hht-K36A*Δ mutants developed pronounced filamentous elongation, a phenotype never seen in wild-type. The *K123R-K36A*Δ double mutant displayed the most severe defects, combining both irregular shapes and elongation, often appearing fragmented or abnormally enlarged. These morphological abnormalities worsened progressively by Day 14 (Figs. 4.6, 4.7). The findings suggest that while wild-type NQ cells maintain characteristic ageing-associated morphology, histone mutations disrupt cellular integrity, with the double mutant showing synergistic defects that worsen over time.

The distinct morphological differences observed in both Q and NQ cell populations strongly support the role of histone modifications in regulating nuclear and cellular architecture during the stationary phase (SP). The mutants' aberrant phenotypes, particularly the irregular shapes in *htb-K123R*Δ and elongation in *hht-K36A*Δ Q cells, along with the severe distortions in NQ populations, suggest that these histone mutations disrupt chromatin organisation linked to quiescence establishment and ageing.

These findings align with established models in which chromatin remodelling directly influences cellular morphology during quiescence (Swygert et al., 2019), further demonstrating that proper histone function is essential for maintaining structural integrity in both dormant and ageing yeast populations. The progressive worsening of mutant phenotypes over time, particularly in the double mutant, underscores the cumulative impact of these epigenetic perturbations on cell fate.

Notably, *htb-K123R*Δ mutants exhibited irregular cell shapes in the Day 14 NQ population, indicating impaired maintenance of normal cellular architecture in ageing cells. In contrast, *hht-*

*K36A*Δ mutants showed significant cell elongation mainly in the Day 14 Q fraction, suggesting potential defects in cell wall integrity or cytoskeletal organisation during quiescence. The *K123R-K36A*Δ double mutant displayed a combination of both phenotypes, irregular and elongated cells, particularly in the Day 14 NQ population, implying that these histone modifications may act additively or synergistically to disrupt cell morphology during the stationary phase (SP). These findings reinforce the critical role of histone H3 K36 and H2B K123R in maintaining proper cellular structure under both quiescent and non-quiescent conditions.

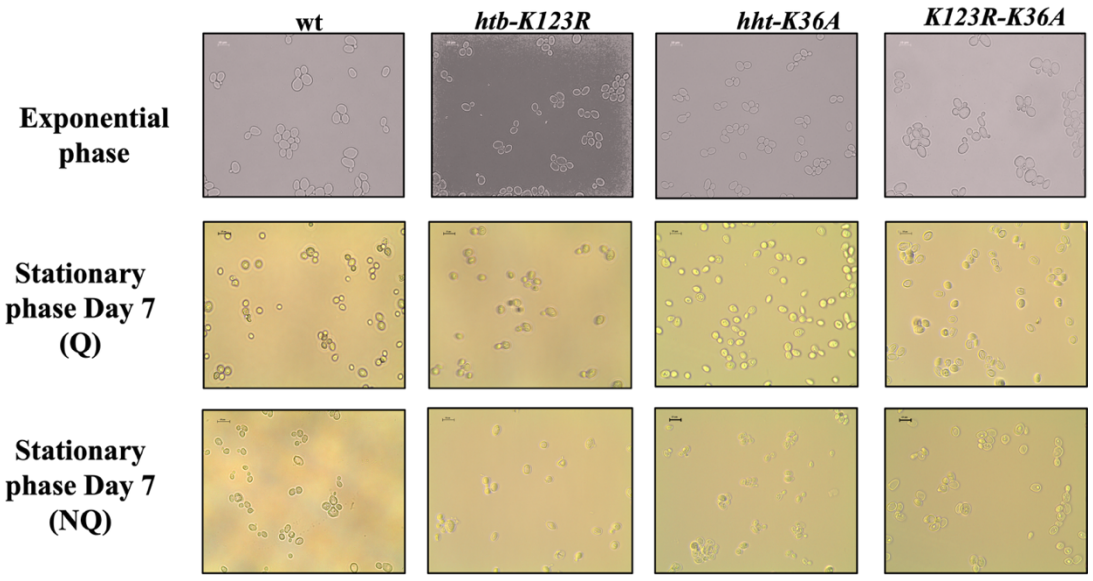


Figure 4.6: Day 7, Q, and NQ cell morphology in wild-type, *htb-K123R*Δ, *hht-K36A*Δ and *K123R-K36A*Δ mutants strains. Day 7 wild-type, *htb-K123R*Δ, *hht-K36A*Δ *and K123R-K36A*Δ grown day 7, (Q), and (NQ) cells were examined from growing culture under the microscope. Microscopy was conducted under a 100x immersion magnification of the oil. The white scale bar is 10µm.

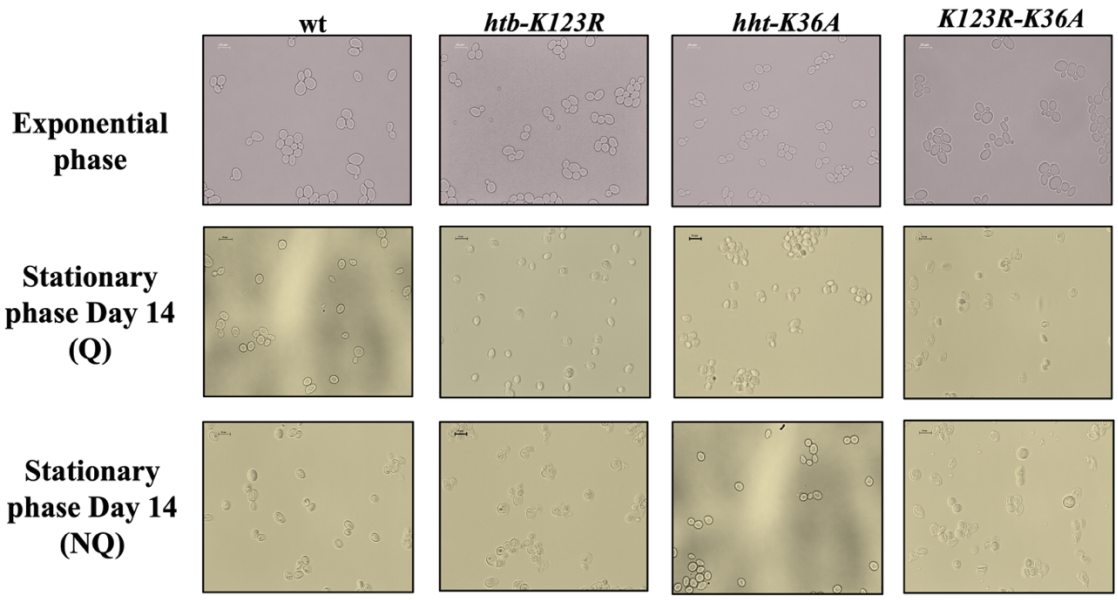


Figure 4.7: Day 14, Q, and NQ cell morphology in wild-type, *htb-K123R*Δ, *hht-K36A*Δ and *K123R-K36A*Δ mutants strains. Day 14 wild-type, *htb-K123R*Δ, *hht-K36A*Δ *and K123R-K36A*Δ grown day 14, (Q), and (NQ) cells were examined from growing culture under the microscope. Microscopy was conducted under a 100x immersion magnification of the oil. The white scale bar is 10μm.

4.3 Summary of Main Findings

- The *htb-K123R*Δ and *hht-K36A*Δ single mutants formed more Q cells and less NQ cells compared to wild-type .
- The *htb-K123R*Δ and *hht-K36A*Δ single mutants showed increased viability in the NQ populations compared to wild-type .
- The *K123R-K36A*Δ double mutant shows the greatest increase in viability of the NQ population compared to the single mutants and wild-type .
- The *K123R-K36A*Δ shows the greatest morphological differences within the Q and NQ populations.

4.3.1 *htb-K123R*Δ Mutant

- This mutant produced less NQ cells compared to the wild-type strain.
- These NQ cells showed greater viability than wild-type NQ cells.
- Additionally, the *htb-K123R*Δ Q cells showed abnormal cell morphology.

4.3.2 *hht-K36A*Δ Mutant

- This mutant produced less NQ cells compared to the wild-type strain.
- These NQ cells showed greater viability than wild-type NQ cells.
- *hht-K36A*Δ mutant Q cells exhibited elongated cell morphology.

4.3.3 *K123R-K36A*Δ Double Mutant

- *K123R-K36A*Δ strains formed Q and NQ cell populations in proportions similar to wild-type
- However, the double mutant NQ cells showed the greatest loss in viability compared to wild-type and either of the single mutants
- The double mutant exhibited mixed cell morphologies, characterized by both irregular and elongated cell shapes.

4.4 Discussion

This study highlights the significant role of histone modifications in regulating yeast cell fate during the stationary phase SP, particularly in differentiating quiescent Q and non-quiescent NQ cells. The observed lack of Q and NQ separation during the exponential Exp phase suggests that these phenotypic divergences are specific to SP adaptation, where cells undergo profound changes to survive nutrient limitation.

We successfully utilized Percoll density gradient centrifugation to distinguish between Q lower band and NQ upper band cell populations in yeast cultures during SP. In wild-type Day 7 cultures, NQ cells were predominantly large and budded with approximately ~50% viability, while Q cells were typically small, unbudded, and maintained about ~45% viability. This distinct separation served as a crucial reference for assessing phenotypes in mutant strains.

Mutant strains displayed altered Q and NQ ratios along with distinct cell morphologies, highlighting that chromatin structure, regulated by histone modifications, significantly influences the shift between cellular states. The *htb-K123R*Δ and *hht-K36A*Δ mutations, for

example, caused irregular Q cell morphologies not present in wild-type. The double mutant's combined morphological defects suggest synergistic roles for H2BK123ub and H3K36me in maintaining cell structure during SP. These results indicate that modifications H2BK123 and H3K36 have distinct roles in regulating cell state changes.

Most strikingly, both *htb-K123R*Δ and *hht-K36A*Δ single mutants produced fewer NQ cells than the wild type. However, these NQ cells displayed increased viability, suggesting that these histone marks promote correct NQ cell formation and survival, possibly by promoting apoptosis under nutrient stress. Furthermore, the increase in viability in the NQ cell populations was even greater in the double mutant suggesting H2Bub and H3K36me may function together in promoting the required apoptosis that occurs in wild-type during SP.

Our findings demonstrate that H2BK123ub *htb-K123R*Δ and H3K36me *hht-K36A*Δ play non-redundant roles in SP adaptation: loss of H2BK123ub htb-K123RΔ causes severe surface distortions in NQ cells, implicating H2Bub in maintaining cell wall integrity during stress. Additionally, loss of H3K36me *hht-K36A*Δ triggers elongation, akin to cytoskeletal dysregulation (Swygert et al., 2019). The double mutant's hybrid phenotype suggests these marks operate on distinct pathways.

Conversely, morphological defects in mutants are observed that correlate with viability shifts; for example, elongated *hht-K36A*Δ NQ cells show progressive death, while *K123R-K36A*Δ fragmented cells unexpectedly survive (Fig. 4.5L), indicating possible compensatory mechanisms. The retention of wild-type like Q cell morphology in mutants, despite NQ defects, underscores quiescence as a conserved survival_strategy. Conversely, NQ-specific anomalies highlight chromatin-dependent stress responses in ageing cells (Baek & Kim, 2017).

In contrast, the *K123R-K36A*Δ double mutant displayed a unique and important hybrid phenotype. Initially, its ability to form Q cells was impaired at Day 7, with low viability; however, these Q cells subsequently recovered. Simultaneously, the NQ cell population in this double mutant displayed a consistent increase in viability over time, sharply contrasting with the decline observed in wild-type and single mutant patterns. This suggests that the double mutation disrupts apoptotic regulation, favoring the survival of both cell types and implying a potential interaction between the H2BK123 and H3K36 modifications. This observation is

consistent with findings that mono-ubiquitylation of H2B (H2Bub) is induced by carbohydrates and reduced during glucose starvation, conditions typical of the stationary phase.

These results are consistent with previous research that emphasizes histone modifications as vital regulators of quiescence entry and maintenance (McKnight et al., 2015). For instance, H3K36 methylation aids in chromatin compaction and transcriptional silencing during quiescence (Weiner et al., 2015), while H2BK123R acetylation affects chromatin accessibility and gene expression during stress responses (Wang et al., 2019). Our findings support these observations, showing that changes at these specific histone residues notably impact Q and NQ cell ratios and their morphology. Additionally, in normal yeast cells, histone modifications such as H3K36me and H2Bub regulate various genomic and transcriptomic processes, including DNA replication and repair. However, during SP nutrient stress, cells lacking these marks exhibit increased sensitivity to glucose depletion.

Altogether, the data support a model in which *htb-K123R*Δ*, hht-K36A*Δ*,* and *K123R-K36A*Δ play distinct yet complementary roles in promoting survival during the stationary phase SP. The *htb-K123R*Δ and *hht-K36A*Δ mutants appear to promote correct NQ and Q cell formation but fail to ensure loss in NQ viability, possibly due to disrupted pro-apoptotic mechanisms. Furthermore, the increase in NQ viability is even greater in the *K123R-K36A*Δ double mutant, suggesting a synergistic relationship between these marks in normally promoting NQ cell death. This dual regulation may balance survival strategies during nutrient depletion by clearing metabolically active but vulnerable NQ cells and preserving dormant Q cells. This synergistic regulation likely reflects a conserved evolutionary strategy that enhances the correct Q cell population survival in nutrient-deprived environments, offering critical insights into how microbial cells adapt to stress and maintain viability over extended periods (Herman, 2002).

Understanding quiescence Q in yeast is critical, as quiescent cells Q are key contributors to chronic fungal infections. Insights from this study may shed light on how pathogenic fungi persist in host tissues and could lead to new antifungal therapies targeting dormant cell populations. Identifying histone post-translational modifications PTMs like H3K36me3 and H2Bub as regulators of quiescence Q opens possibilities for targeted interventions. Modifying these PTMs or their associated enzymes could influence cellular quiescence Q in yeast and other

organisms, offering new therapeutic opportunities for conditions linked to dormant cell states (Baek and Kim, 2017).

While these results are promising, further validation is essential. Future studies should focus on confirming the purity of the separated cell populations, assessing the expression of apoptosis-related markers, and characterizing the signaling pathways involved.

Investigating genome-wide transcriptional changes and chromatin remodeling events in these mutants, along with studies on chromatin-associated proteins and their interactions with histone modifications, will provide deeper insights into the mechanistic pathways through which these histone modifications regulate quiescence and govern the transition between proliferative and quiescent states in response to environmental challenges (Young *et al.*, 2017).

Chapter 5

Analysis of global transcription during development of cellular quiescence in *htb-K123RΔ*, *hht-K36AΔ*, and *K123R-K36AΔ* mutants

5.1 Introduction

RNA sequencing (RNA-Seq) is a technology that allows comprehensive analysis of the transcriptome, the complete set of RNA transcripts produced by the genome at any given time. Critical insights into gene expression, alternative splicing, and other aspects of RNA biology can be obtained using this methodology. In the current chapter, the application of RNA-Seq to examine the transcriptional regulation facilitated by histone modifications H3K36me3 and H2Bub during the exponential phase (Exp), diauxic shift (Dix), and quiescent state (SP-D7-Q) was explored.

We harvested cultured yeast cells at different stages: exponential phase (Exp) (actively growing), diauxic shift (Dix) (transition point at glucose depletion), and purified day-7

quiescent (SP-D7-Q) cells in order to elucidate the roles of H3K36me3 and H2Bub in transcription during cell development. The Percoll density gradient centrifugation protocol (Allen *et al.*, 2006) was utilized to obtain purified day 7 quiescent cell samples. The aim was to perform RNA-Seq analysis and identify the genes regulated by H2Bub and H3K36me3 during these key growth phases by comparing the global transcriptome data from the various mutant strains and wild-type (Fig. 5.1).

The comprehensive analysis of upregulated and downregulated genes in mutant strains compared to the wild-type will be described and discussed, providing insight on the functional consequences of these histone modifications during growth into SP and development of the quiescent cell population formed therein.

This should help in advancing our knowledge of transcriptional regulation in yeast and also pave the path for future research into the broader effects of histone modifications in cellular development and gene expression.

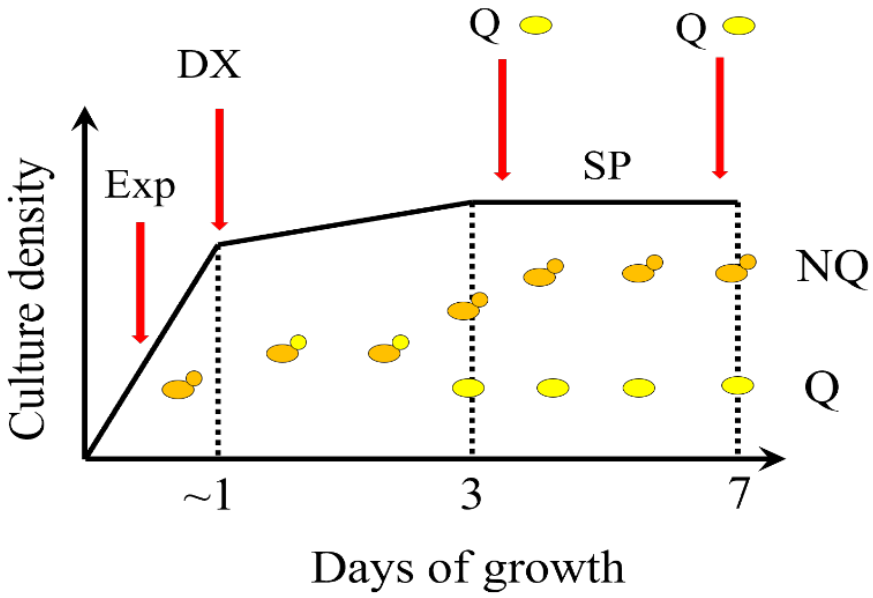
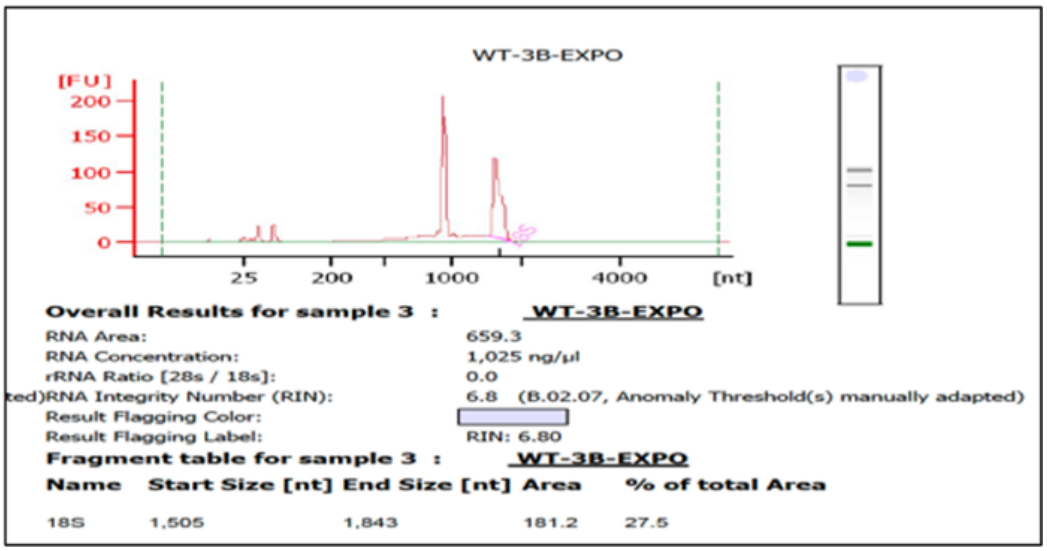


Figure 5.1: The diagram illustrates the timing of RNA isolation during the exponential phase (Exp), at the Diauxic shift (Dix), and in purified day 7 quiescent (Q) cells for wild-type and all mutant strains.

5.2 Results

5.2.1 RNA Quality Assessment

RNA was prepared from each strain at each time point from biological triplicate cultures. To ensure the integrity and quality of the RNA extracted from the exponentially growing wild-type, *htb-K123R*Δ*, hht-K36A*Δ, and *K123R-K36A*Δ mutant strains we employed the Agilent 2100 Bioanalyzer for detailed analysis of all replicates. The results demonstrated the high quality of RNA from each biological replicate was suitable for subsequent RNA-Seq analysis, except for the *htb-K123R*Δ Day 7 Q cell samples, which only yielded duplicate RNA samples of suitable quality. Indeed, chromatograms obtained from the Agilent 2100 Bioanalyzer, illustrated all the samples had an RNA Integrity Number (RIN) values of above 6.5. High RNA integrity across all samples was indicated by the RIN values, supporting their suitability for RNA-Seq analysis (Fig. 5.2). Three biological replicates were included for each experimental condition, ensuring robustness and reproducibility and enabling reliable estimation of biological variability and increased statistical power for downstream differential expression analysis.

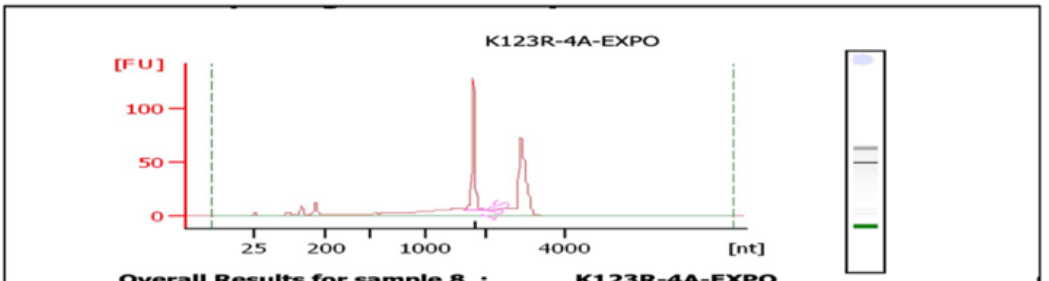


Overall Results for sample 3 : WT-3B-EXPO

RNA Area:	659.3
RNA Concentration:	1,025 ng/µl
rRNA Ratio [28s / 18s]:	0.0
RNA Integrity Number (RIN):	6.8 (B.02.07, Anomaly Threshold(s) manually adapted)
Result Flagging Color:	
Result Flagging Label:	RIN: 6.80

Fragment table for sample 3 : WT-3B-EXPO

Name	Start Size [nt]	End Size [nt]	Area	% of total Area
18S	1,505	1,843	181.2	27.5

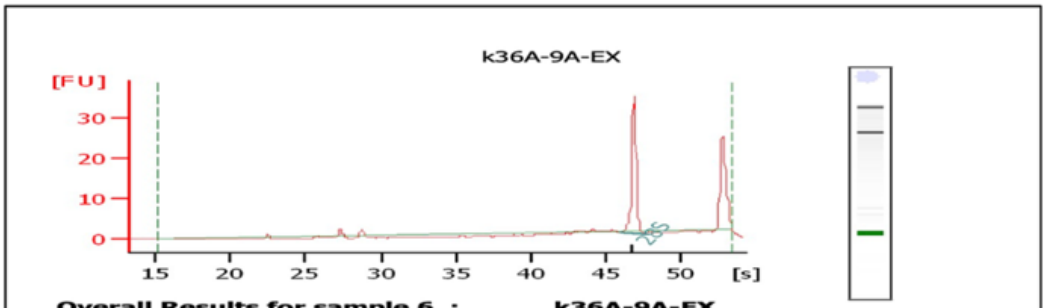


Overall Results for sample 8 : K123R-4A-EXPO

RNA Area:	401.9
RNA Concentration:	625 ng/µl
rRNA Ratio [28s / 18s]:	0.0
RNA Integrity Number (RIN):	6.8 (B.02.07, Anomaly Threshold(s) manually adapted)
Result Flagging Color:	
Result Flagging Label:	RIN: 6.80

Fragment table for sample 8 : K123R-4A-EXPO

Name	Start Size [nt]	End Size [nt]	Area	% of total Area
18S	1,658	2,090	94.3	23.5



Overall Results for sample 6 : k36A-9A-EX

RNA Area:	50.3
RNA Concentration:	159 ng/µl
rRNA Ratio [28s / 18s]:	0.0
RNA Integrity Number (RIN):	7.4 (B.02.07, Anomaly Threshold(s) manually adapte
Result Flagging Color:	
Result Flagging Label:	RIN: 7.40

Fragment table for sample 6 : k36A-9A-EX

Name	Start Size [nt]	End Size [nt]	Area	% of total Area
28S	1,706	1,971	26.1	51.8

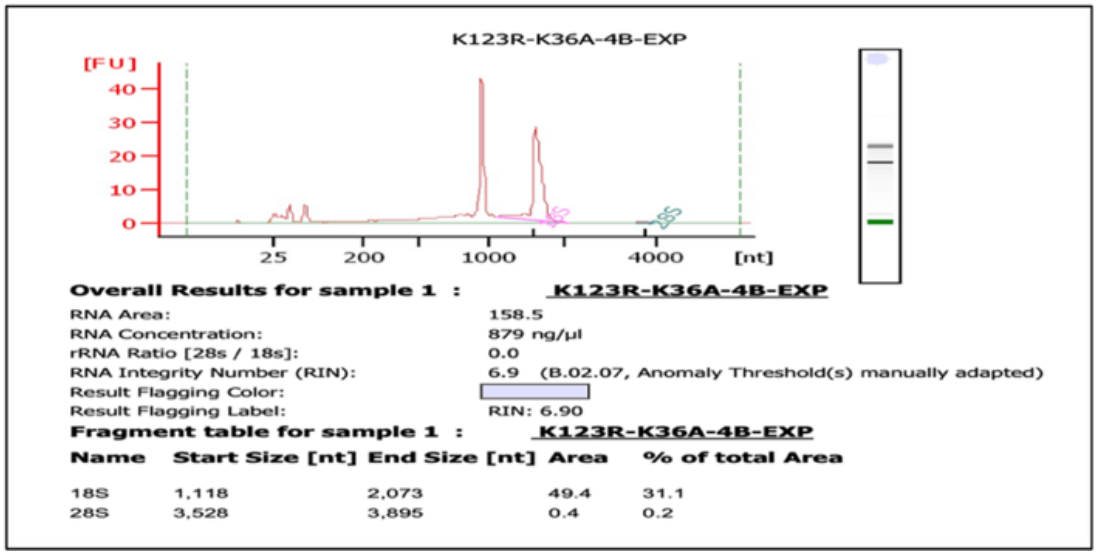


Figure 5.2: Assessment of RNA Quality from Yeast Strains During Exponential Phase: 1% agarose formaldehyde gel electrophoresis showing total RNA extracted from wild-type and mutant yeast strains during the exponential phase (Exp). The ladder ranges from 25 kb to 4,000 kb. Distinct bands representing 28S and 18S rRNA indicate high-quality RNA with minimal degradation. Multiple images are chromatograms from the Agilent 2100 Bioanalyzer depicting examples showing RNA integrity of wild-type (wt-3B-Exp), *htb-K123R*Δ (*htb-K123R*-4A-Exp), *hht-K36A*Δ (*hht-K36A*-9A-Exp), and *K123R-K36A*Δ (*K123R-K36A*-4B-Exp) yeast strains during the exponential phase.

5.2.2 Principal Component Analysis (PCA) of RNA-Seq Data

In order to assess the variability and quality of RNA-Seq data across different yeast strains and growth phases, principal component analysis (PCA) was performed. This visualization into the sample distribution based on gene expression profiles, assists in the identification of outliers and ensuring consistency across biological replicates. clustering. Differential gene expression analysis was conducted using the DESeq2 pipeline. Raw count data were normalized to account for differences in sequencing depth, and gene-wise dispersion was estimated. Statistical testing was performed using a negative binomial model, with p-values adjusted for multiple testing using false discovery rate (FDR) correction. Data quality and sample relationships were assessed using principal component analysis (PCA) and sample-to-sample correlation heatmaps.

As revealed from the PCA plot of RNA-Seq data from wild-type, *htb-K123RΔ, hhtK36A*Δ, and *K123R-K36A*Δ yeast strains during the exponential phase (Exp) the first principal component (PC1) and the second principal component (PC2) explain ~70% and ~20% of the total variance, respectively. The plot showed a clear separation between the different strains, indicative of distinctive transcriptional profiles associated with each histone modification. The reproducibility of the RNA-Seq data was confirmed by the clustering of biological replicates within each strain group (Fig. 5.2).

Similarly, the PCA plot for RNA-Seq data from the same strains during the diauxic shift phase revealed PC1 and PC2 accounting for ~65% and ~25% of the total variance, respectively. Comparable to the exponential phase, distinctive clustering of the different strains is observed, indicating towards the unique gene expression changes associated with the diauxic shift (Dix). The data's consistency was further supported by the tight clustering of biological replicates within each strain group (Fig. 5.2).

From the wild-type and mutant strains in the quiescent (Q-D7-SP) state the PCA analysis showed PC1 and PC2 accounting for ~60% and ~30% of the variance, respectively. The PCA plot discloses a more marked separation between the wild-type and mutant strains in the quiescent state (Q-D7-SP) when compared to the other growth phases suggesting a significant transcriptional reprogramming influenced by histone modifications during cellular quiescence (Fig. 5.2). The consistent clustering of replicates reinforces the robustness of the RNA-Seq data (Fig. 5.3).

The clear separation of samples by strain and phase suggest distinct transcriptional landscapes directed by histone modifications H3K36me3 and H2Bub in yeast cells occurs indicating the significance of these modifications in regulating gene expression dynamics during cell growth and development.

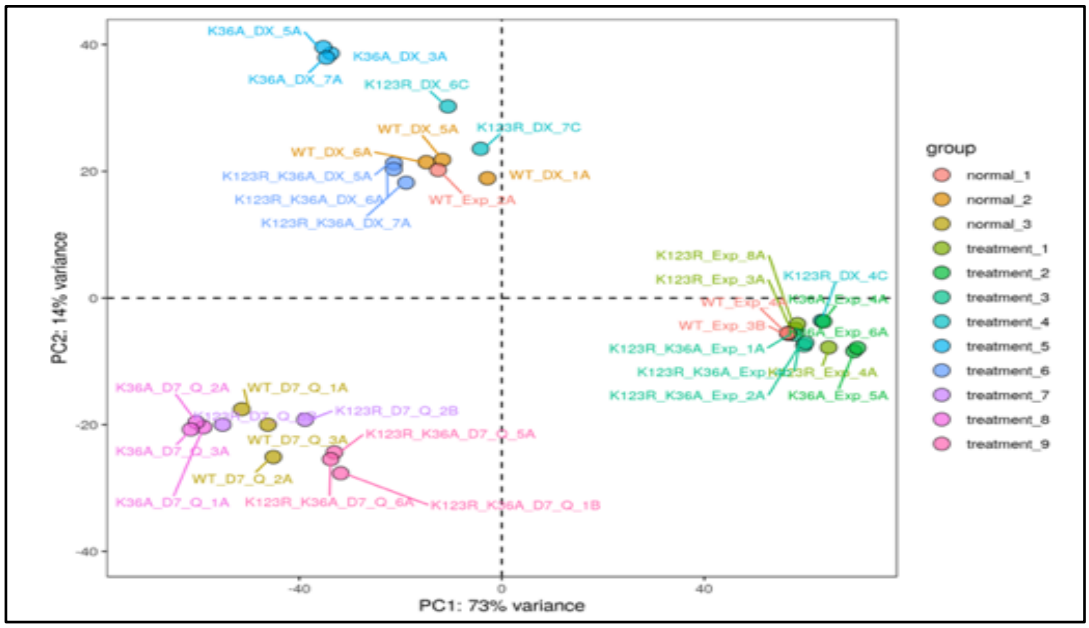


Figure 5.3: Principal Component Analysis (PCA) of RNA-Seq data from wild-type and mutant yeast strains across the different growth phases: Exponential Phase PCA plot for wild-type, *htb-K123R*Δ, *hht-K36A*Δ, and *K123R-K36A*Δ strains. PCA plot for the same strains during diauxic shift. PCA plot for wild-type and mutants in quiescence (Q- D7- SP). Plot shows pronounced separation between strains and growth phase highlighting potential transcriptional reprogramming by H2Bub and H3K36me.

5.2.3 Heatmap Analysis

The top 1000 variable genes were selected to compute the variance between genes and samples after transformation of the counts into logarithmic scale. Distinct gene expression patterns across the different conditions in the different strains was demonstrated by the heatmap that clearly clustered the samples. The reproducibility and consistency of the biological replicates was highlighted by well clustered samples into their respective groups.

The robustness of the clustering was further supported by the Euclidean distance dendrogram, indicating significant differences in gene expression profiles among the various experimental conditions (Fig. 5.4). However, the data suggests that the wild-type exponential phase sample (wt-Exp-2A) was harvested too late during exponential phase since the heat map for this sample more resembles the wild-type diauxic shift sample profiles.

Furthermore, *htb-K123R*Δ sample, *K123R*-Dix-4C, looked to have been harvested prior to the diauxic shift since its heat map profile looked more like the exponential *htb-K123R*Δ sample profiles.

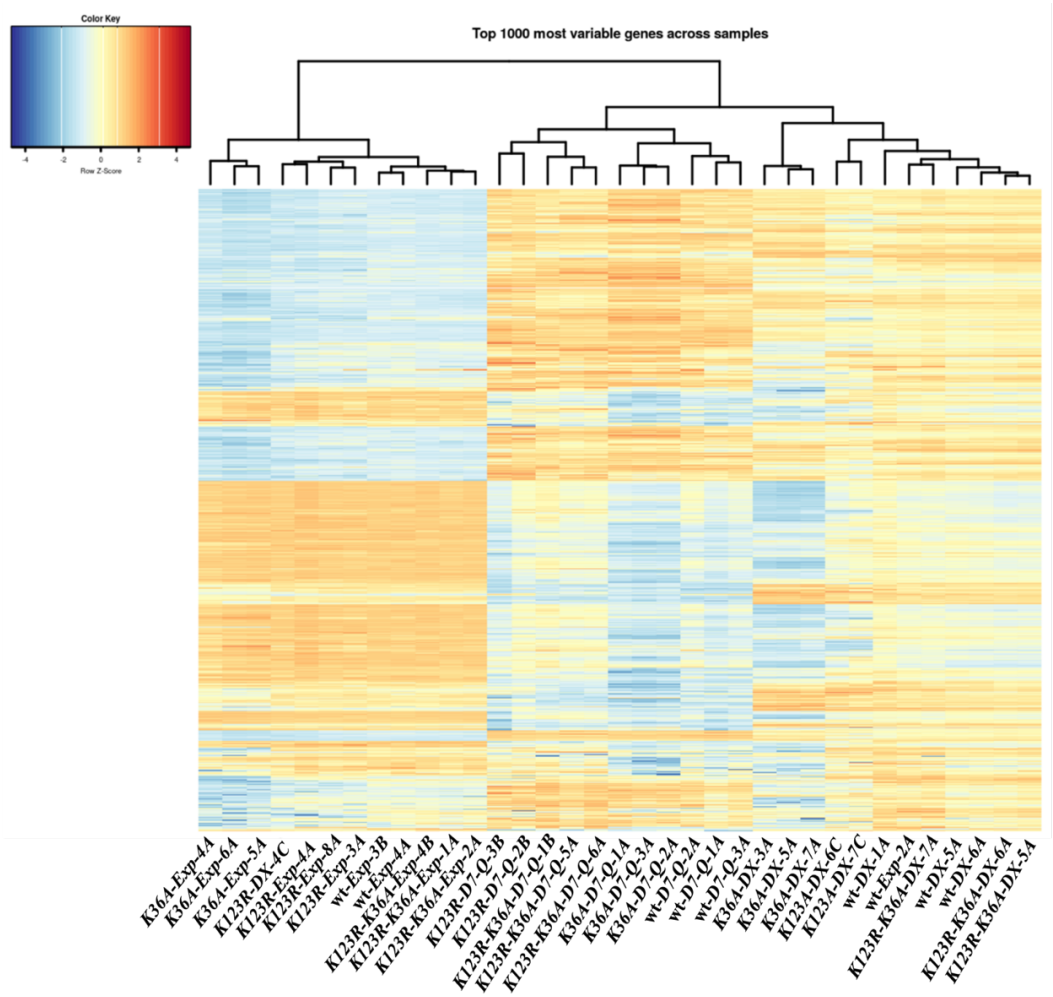


Figure 5.4: Heatmap of Gene Expression Profiles Across Different Experimental Conditions: The heatmap displays the normalized read counts of RNA-Seq data from various samples, transformed to a logarithmic scale. The top 1000 variable genes were selected based on variance to generate this heatmap. Each row represents a gene, and each column represents a sample. The colour scale ranges from blue (low expression) to red (high expression), indicating the relative expression levels of genes. Samples are clustered using Euclidean distance, with dendrograms illustrating the hierarchical relationships between samples based on their gene expression profiles.

5.2.4 R-squared (R^2) Regression Analysis

In order to assess the consistency of RNA-Seq data across biological replicates the R^2 regression analysis was performed as a quality control measure. The R^2 values were calculated for the exponential phase (Exp), diauxic shift (Dix), and quiescent day 7 (Q-D7-SP) samples. High R^2 values, indicative of high reproducibility, were observed for most datasets, with the exception of the wild-type exponential phase (Exp) replicate 1 (wt-Exp-2A) and the *htb-K123R*Δ diauxic shift (Dix) replicate 1 (*K123R*-Dix-4C) samples, which yielded lower R^2 values in the comparisons, consistent with the heat map results described earlier. These data sets were subsequently excluded from further analyses to ensure that only high-quality and reliable data were used for downstream analyses, reinforcing the robustness of the experimental results (Fig. 5.5).

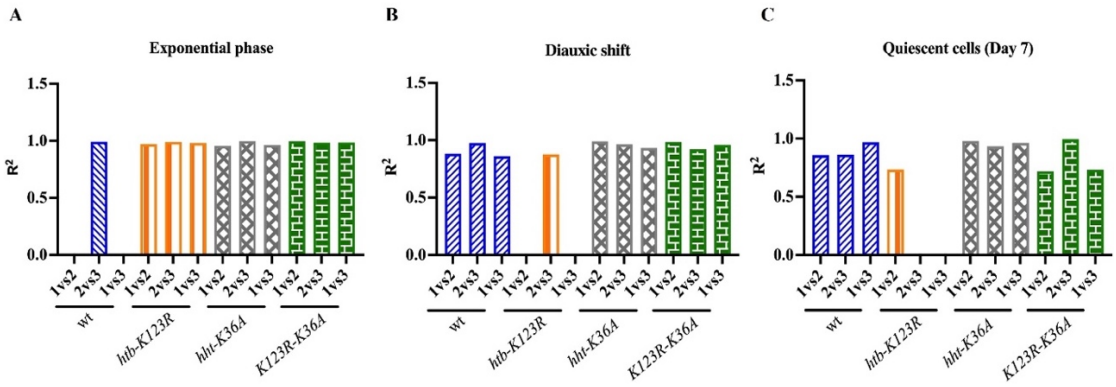


Figure 5.5: R^2 Regression Analysis of RNA-Seq Data: The R^2 regression analysis evaluates the reproducibility of RNA-Seq data across biological replicates in three phases: **(A)** Exponential (Exp), **(B)** Diauxic shift (Dix), and **(C)** Quiescent day 7 (Q -D7- SP). Each bar shows the R^2 value for a replicate, with higher values indicating greater reproducibility. Outliers, wild-type, (Exp) replicate 1 and *htb-K123R*Δ (Dix) replicate 1, displayed lower R^2 values and were excluded from further analysis. Overall, high R^2 values confirm the reliability and consistency of the RNA-Seq data.

5.3 Gene Expression Changes in the Exponential Phase

The gene expression changes in the exponential phase (Exp) of wild-type versus mutant strains *htb-K123R*Δ*, hht-K36A*Δ*,* and *K123R-K36A*Δ was determined via analysis of RNA-Seq data.

Using a threshold of Log2 fold change ≥ 1 and an adjusted p-value ≤ 0.01 the significantly up and downregulated genes in each mutant compared to wild-type were identified (Table. 5.1).

In the *htb-K123R*Δ mutant a total of 379 genes were significantly upregulated in this strain (Log2 fold change ≥ 1 and adjusted p-value of ≤ 0.01) suggesting that H2Bub normally acts to repress these genes. The highest number (482) of upregulated genes was exhibited by the *hht-K36A*Δ mutant indicating a key role played by H3K36me in repressing gene expression during the exponential phase (Exp).

A much smaller number of upregulated genes, only (163) were displayed by the *K123R-K36*Δ A double mutant, which lacks both H2Bub and H3K36me. This lower number suggests a possible compensatory interaction between the two modifications, which may alleviate the depressive effects seen in the single mutants.

Conversely, the *htb-K123R*Δ mutant had (64) downregulated genes, the *hht-K36A*Δ mutant showed (324) downregulated genes, and the *K123R-K36A*Δ double mutant exhibited only (13) downregulated genes. These results suggest a complex regulatory role of the mutations, particularly in *hht-K36A*Δ, which had the most substantial impact on downregulating gene expression. However, yet again, loss of both H2Bub and H3K36me together had less of an effect on gene activation than loss of either modification on its own.

Exponential Phase	Upregulated	Downregulated	Total No. of Gene
***htb-K123R*Δ**	**379**	**64**	**443**
***hht-K36A*Δ**	**482**	**324**	**806**
***K123R-K36A*Δ**	**163**	**13**	**176**

Table 5.1: Differential Gene Expression in Mutant Strains During the Exponential Phase: Table showing the number of significantly upregulated and downregulated genes in *htb-K123R*Δ, *hht-K36A*Δ, and *K123R-K36A*Δ mutant strains compared to the wild-type strain during the exponential phase (Exp). Genes with Log2 fold change ≥ 1 and an adjusted p-value ≤ 0.01 were considered significant. The bar chart shows 379 upregulated and 64 downregulated genes for *htb-K123R*Δ, 482 upregulated and 324

downregulated genes for *hht-K36A*Δ, and 163 upregulated and 13 downregulated genes for the double mutant *K123R-K36A*Δ.

5.3.1 Levels of upregulation in Mutant Strains During Exponential Phase

Comparison of the extent of the upregulation of gene transcription in each mutant versus wild-type during exponential phase revealed that, on average, the extent of upregulation of the genes in the H3K36A mutant was higher than that in the *htb-K123R*Δ single and the double mutant (Fig. 5.6). Thus, H3K36me not only represses the most genes during exponential phase, this PTM also shows the strongest negative influence upon the genes it normally down regulates.

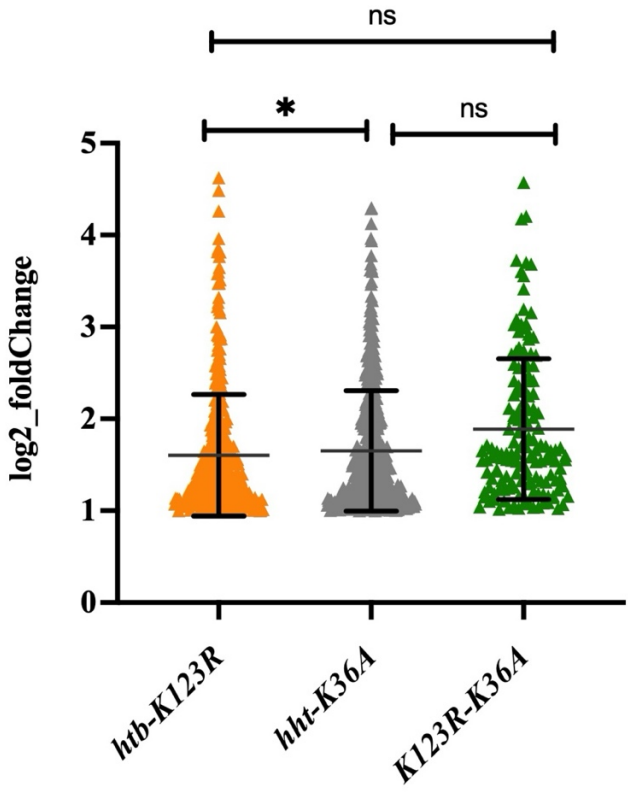


Figure 5.6: Total Genes Significantly Upregulated in Each Mutant Compared to Wild-Type During Exponential Phase. The bar chart shows the number of significantly upregulated genes (Log2 fold change ≥ 1, adjusted p-value ≤ 0.01) in the *htb-K123R*Δ, *hht-K36A*Δ, and *K123R-K36A*Δ mutant strains compared to the wild-type during the exponential phase (Exp). The *htb-K123R*Δ mutant had 379 upregulated genes, the *hht-K36A*Δ mutant had 482 upregulated genes, and the *K123R-K36A*Δ double

mutant had 150 upregulated genes. The graph also indicates the mean and standard deviation. Significance using Two way ANOVA analysis (* p = 0.05, ** p = 0.01, **** p = <0.0001).

5.4 Gene Ontology (GO) Analysis of *htb-K123R*Δ Upregulated Genes

A significant enrichment in several molecular functions and biological processes was revealed by GO analysis of upregulated genes in the *htb-K123R*Δ mutant strain (Table 5.2 and Fig. 5.7).

In the cellular components category, the GO term enriched was peroxisomal matrix with (31 genes such as C*TA1, POX1, TES1, GPX1* and *LPX1)* indicating a significant role in the compartmentalization and metabolism of fatty acids and reactive oxygen species within the cell.

In the biological process category significant enrichment in several key processes were observed.

The response to xenobiotic stimulus, with (6 genes *DDI3, BDS1, POT1, DDI2, PDR18,* and *PDR15)* highlights the cell's mechanisms for detoxifying and adapting to foreign substances. Fermentation, represented by (9 genes *DAK2, CSF1, PDC5, ACS1, NDE2, ADH4, ADH2, GUT2 and THI21)* underscores its role in anaerobic energy production, crucial for cells in low-oxygen environments. Iron ion transport, with (37 genes such as *FRE6, FRE1, FIT1*, and *PET9*) emphasizes the importance of maintaining iron homeostasis, essential for various cellular functions including respiration and DNA synthesis. Cell adhesion, with (28 genes such as *FIG2, HSP12, FLO9* and *FLO1)* points to its critical role in maintaining tissue integrity and facilitating cell communication. Lastly, the tricarboxylic acid cycle, with (14 genes such as *CIT2, SDH2, IDP2 and KGD2)*, underscores its central role in aerobic energy production and metabolic integration. In the molecular functions category significant enrichment in several key activities was seen. Primary active transmembrane transporter activity, with (18 genes such as *QCR6, COX8, ENA1, CCC2)* highlights its role in moving solutes across membranes against their concentration gradient using energy, critical for maintaining cellular homeostasis. Nucleobase transmembrane transporter activity included (7 genes such as *THI7, FUR4, THI72, DAL4)*, highlights its importance in the transport of nucleobases, essential for nucleotide synthesis and DNA and RNA metabolism. Solute: monoatomic cation symporter activity included (20 genes

such as *ALR2, YFL040W, QCR6 ,SPO75*) implies its role in the co-transport of cations along with solutes, vital for nutrient uptake and ion balance.

The broad category of transmembrane transporter activity included (120 genes such as *AGP1, ADY2, GIT1* and *ALR2),* and highlights the critical function of transporting various molecules across cellular membranes, essential for nutrient uptake, waste excretion, and signal transduction.

Category	Function	Number of Genes	Example Genes
GO Molecular Functions	Primary active transmembrane transporter activity	18	*QCR6, COX8, ENA1, CCC2*
	Nucleobase transmembrane transporter activity	7	*THI7, FUR4, THI72, DAL4*
	Solute: monoatomic cation symporter activity	20	*ALR2, YFL040W, QCR6, SPO75*
	Transmembrane transporter activity	120	*AGP1, ADY2, GIT1, ALR2*
GO Biological Processes	Response to xenobiotic stimulus	6	*DDI3, BDS1, POT1, DDI2, PDR18, PDR15*
	Fermentation	9	*DAK2, CSF1, PDC5, ACS1, NDE2, ADH4, ADH2, GUT2, THI21*
	Iron ion transport	37	*FRE6, FRE1, FIT1, PET9*
	Cell adhesion	28	*FIG2, HSP12, FLO9, FLO1*

	Tricarboxylic acid cycle	14	*CIT2, SDH2, IDP2, KGD2*
GO Cellular Components	Peroxisomal matrix	31	*CTA1, POX1, TES1, GPX1, LPX1*

Table 5.2: List of genes commonly up-regulated during Exponential Phase in *htb-K123R*Δ compared to wild-type.

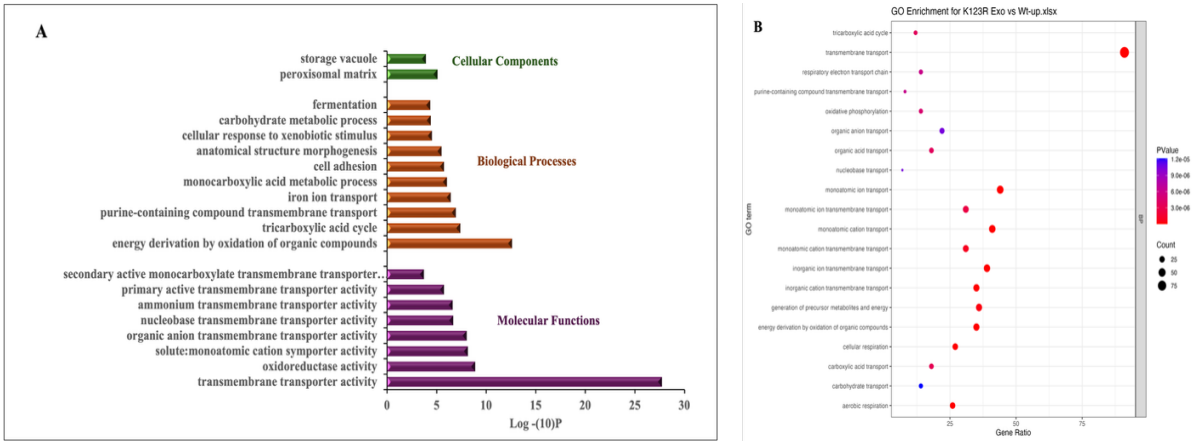


Figure 5.7: Gene Ontology (GO) analysis of upregulated genes in the *htb-K123R*Δ mutant strain. **"(A)** Bar chart (left); **(B)** Plot (right)." The bar graph shows the most significantly enriched molecular functions and biological processes among the upregulated genes, including transmembrane transporter activity, oxidoreductase activity, and energy derivation by oxidation of organic compounds. The enrichment levels are indicated by the corresponding Log2 fold change values.

5.4.1 Gene Ontology (GO) Analysis of *hht-K36A*Δ Upregulated Genes

In the *hht-K36A*Δ mutant strain (Table 5.3 and Fig. 5.8), there was significant enrichment of GO terms in the cellular components category which included (23 genes involved with peroxisomes such as *AGX1, MGT1, PEX19, PEX5)*. In the biological process category significant enrichment in several key processes were found such as the pyridoxine biosynthetic process with (18 genes, including *SNZ3, SNO1, SNZ1, SNZ2)*, which highlights this PTMs crucial role in the synthesis of vitamin B6, essential for numerous enzymatic reactions.

Upregulated genes were also enriched in the oligosaccharide metabolic process (11 genes *MAL32, AMS1, IMA4, IMA2)*, and the hexose catabolic process (4 genes *GAL10, GAL1, AMS1, YNR071C)*, highlighting the importance of H3K36me in regulating carbohydrate metabolism in energy production and storage. Genes enriched in homologous chromosome pairing at meiosis (14 genes, *RED1, ZIP1, ZIP2, AMA1*), underlines its role in ensuring accurate genetic recombination and stability during cell division and its role in the response to extracellular stimulus (26 genes, *ADY2, GAT1, GAL3, REG1*), shows this PTM plays a role in the cell's mechanisms for adapting to environmental changes.

There were (99) upregulated genes involved in small molecule catabolic process (99 genes including *DAK2,JLP1,PUT1,GDH2)*, emphasizing H3K36me's role in regulating metabolic pathways important for maintaining cellular function and homeostasis. In the molecular functions category significant enrichment in several key activities were observed.

Carnitine O-acetyltransferase activity (10 genes, *YAT1,CAT2,YAT2,ATG15*), highlights its role in the metabolism of fatty acids and energy production. Water transmembrane transporter activity, represented by (4 genes, *AQY3,YLL053C,AQY2,AQY1)*, underlines its importance in maintaining cellular hydration and osmotic balance. Ammonium transmembrane transporter activity (12 genes, *ADY2,MEP1,MEP2,ATO2*), points towards its role in nitrogen metabolism and waste removal. The broad category of transmembrane transporter activity (100 genes, *AGP1,ADY2,GIT1,AGP3*), emphasizes the critical function of transporting various molecules across cellular membranes, essential for nutrient uptake, waste excretion, and signal transduction. Lastly, oxidoreductase activity (57 genes, *HBN1,ADH7,QCR6,JLP1*), indicates its significant role in redox reactions, crucial for cellular respiration and detoxification processes.

Thus, H3K36me plays a broad role in downregulating genes during exponential phase required for important cell functions and metabolism.

Category	Function	Number of Genes	Example Genes
GO Molecular Functions	Carnitine O-acetyltransferase activity	10	*YAT1, CAT2, YAT2, ATG15*
	Water transmembrane transporter activity	4	*AQY3, YLL053C, AQY2, AQY1*
	Ammonium transmembrane transporter activity	12	*ADY2, MEP1, MEP2, ATO2*
	Transmembrane transporter activity	100	*AGP1, ADY2, GIT1, AGP3*
	Oxidoreductase activity	57	*HBN1, ADH7, QCR6, JLP1*
GO Biological Processes	Pyridoxine biosynthetic process	18	*SNZ3, SNO1, SNZ1, SNZ2*
	Oligosaccharide metabolic process	11	*MAL32, AMS1, IMA4, IMA2*
	Hexose catabolic process	4	*GAL10, GAL1, AMS1, YNR071C*
	Homologous chromosome pairing at meiosis	14	*RED1, ZIP1, ZIP2, AMA1*

	Response to extracellular stimulus	26	*ADY2, GAT1, GAL3, REG1*
	Carboxylic acid transport	25	*AGP1, ADY2, AGP3, SEO1*
	Alditol metabolic process	11	*DAK2, SOR2, SOR1, GCY1*
	Organic hydroxy compound metabolic process	42	*DAK2, SOR2, DLD1, SOR1*
	Energy derivation by oxidation of organic compounds	58	*DAK2, IGD1, QCR6, SDH2*
	Cellular aldehyde metabolic process	18	*SNZ3, IDP2, NQM1, AAD10*
	Small molecule catabolic process	99	*DAK2, JLP1, PUT1, GDH2*
GO Cellular Components	Peroxisomes	23	*AGX1, MGT1, PEX19, PEX5*

Table 5.3: List of genes commonly up-regulated during Exponential Phase in *hht-K36A*Δ compared to wild-type.

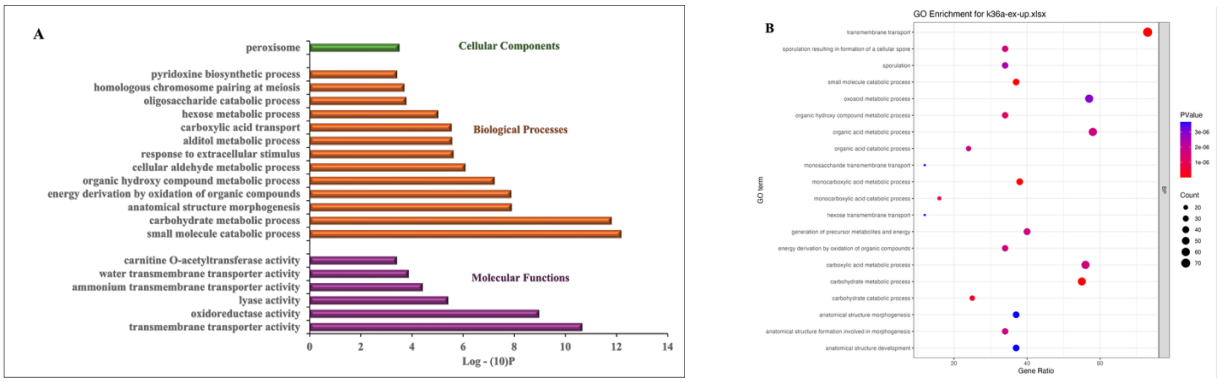


Figure 5.8: Gene Ontology (GO) analysis of upregulated genes in the *hht-K36A*Δ mutant strain. **"(A)** Bar chart (left); **(B)** Plot (right)**."** The bar graph displays the top enriched molecular functions and biological processes, such as lyase activity, water transmembrane transporter activity, and small molecule catabolic process. The enrichment is measured by Log2 fold change values, reflecting the degree of upregulation in these functional categories.

5.4.2 Gene Ontology (GO) Analysis of *K123R-K36A*Δ Upregulated Genes

In the *K123R-K36A*Δ double mutant strain (Table 5.4 and Fig. 5.9), significant GO terms of the upregulated genes were enriched in the cellular components category such as those involved in the respiratory chain complex (16 genes including *QCR6,SDH2,COX12,SDH4*) indicating an important repressive role for H3K36me and H2Bub in mitochondrial function and energy production through oxidative phosphorylation. Furthermore, there were upregulated genes enriched involved in the tricarboxylic acid cycle (12 genes, including *SDH2,IDP2,KGD2,SDH4*), the glyoxylate by-pass (8 genes, including *IDP2,MLS1,IDP3,ICL1*), the carboxylic acid metabolic process (7 genes including *PUT1,GDH3,GDH2,KGD2*), and energy derivation by oxidation of organic compounds (86 genes, including *IGD1,QCR6,SDH2,COX12*), indicating a significant role of both PTMs upon repressing oxidative phosphorylation and energy metabolism.

These PTMs also were both involved in repressing genes involved in the response to extracellular stimulus (16 genes, including *ADY2,GAT1,ATG8,EDS1*), and ammonium transmembrane transport (12 genes, including *ADY2,MEP2,ATO2,MEP3*), indicating these PTMs both function to negatively influence nitrogen metabolism and waste removal.

Category	Function	Number of Genes	Example Genes
GO Molecular Functions	Secondary active transmembrane transporter activity	10	*UGA4, SNF3, STL1, SFC1*
	Organic cation transmembrane transporter activity	6	*UGA4, CRC1, DUR3, GAP1*
	Carnitine O-acetyltransferase activity	8	*YAT1, CAT2, YAT2, CRC1*
	Carboxylic acid transmembrane transport	8	*SFC1, DIP5, ODC1, CRC1*
	Ammonium transmembrane transport	12	*ADY2, MEP2, ATO2, MEP3*
GO Biological Processes	Response to oxygen-containing compound	6	*SNF3, CTA1, YKL107W, SIP18*

	Gluconeogenesis	7	*FBP1, PYC1, PCK1, SOR2*
	Carbohydrate metabolic process	20	*IGD1, IDP2, FBP1, SOR2*
	2-oxoglutarate metabolic process	10	*GDH2, KGD2, KGD1, PUT1*
	Response to extracellular stimulus	16	*ADY2, GAT1, ATG8, EDS1*
	Carboxylic acid metabolic process	7	*PUT1, GDH3, GDH2, KGD2*
	Glyoxylate cycle	8	*IDP2, MLS1, IDP3, ICL1*
	Small molecule catabolic process	13	*AGX1, PUT1, IDP2, FBP1*
	Tricarboxylic acid cycle	12	*SDH2, IDP2, KGD2, SDH4*
	Energy derivation by oxidation of organic compounds	86	*IGD1, QCR6, SDH2, COX12*
GO Cellular Components	Respiratory chain complex	16	*QCR6, SDH2, COX12, SDH4*

Table 5.4: List of genes commonly up-regulated during Exponential Phase in *K123R-K36A*Δ compared to wild-type.

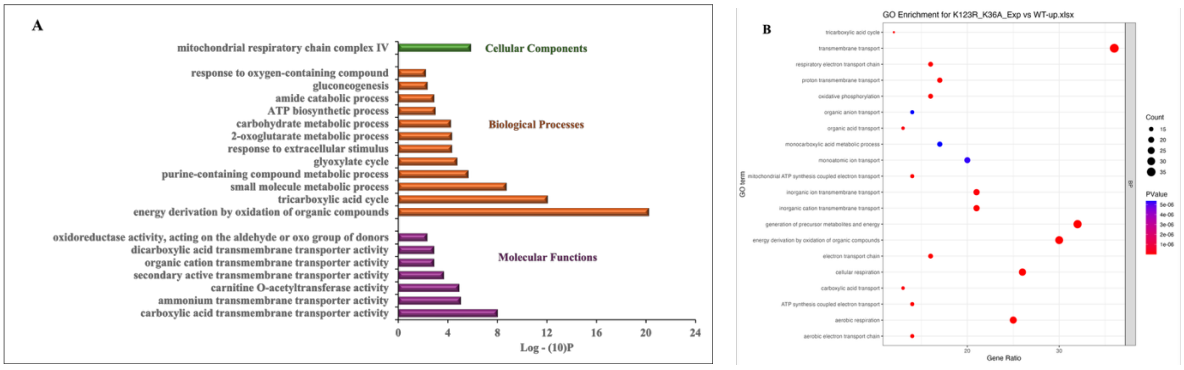


Figure 5.9: Gene Ontology (GO) analysis of upregulated genes in the combined *K123R-K36A*Δ mutant strain. **"(A)** Bar chart (left); **(B)** Plot (right)**."** The bar graph presents the most significantly enriched molecular functions and biological processes, including carboxylic acid transmembrane

transporter activity, ammonium transmembrane transporter activity, and energy derivation by oxidation of organic compounds. The graph highlights the upregulation levels with corresponding Log2 fold change values.

5.4.3 Venn Diagram to show unique and shared upregulated genes in exponentially growing H2Bub and H3K36me-deficient mutants

To visualize any overlap of upregulated genes among the three mutant strains a Venn diagram was constructed (Fig. 5.10). The results revealed that the H3K36me mutant showed the greatest number of uniquely upregulated genes (254) compared to the 181 and 21 genes uniquely upregulated in the *htb-K123R*Δ and *K123R-K36A*Δ double mutants, respectively. Surprisingly, there was only an overlap of 94 genes that were upregulated in all three mutants compared to wild-type.

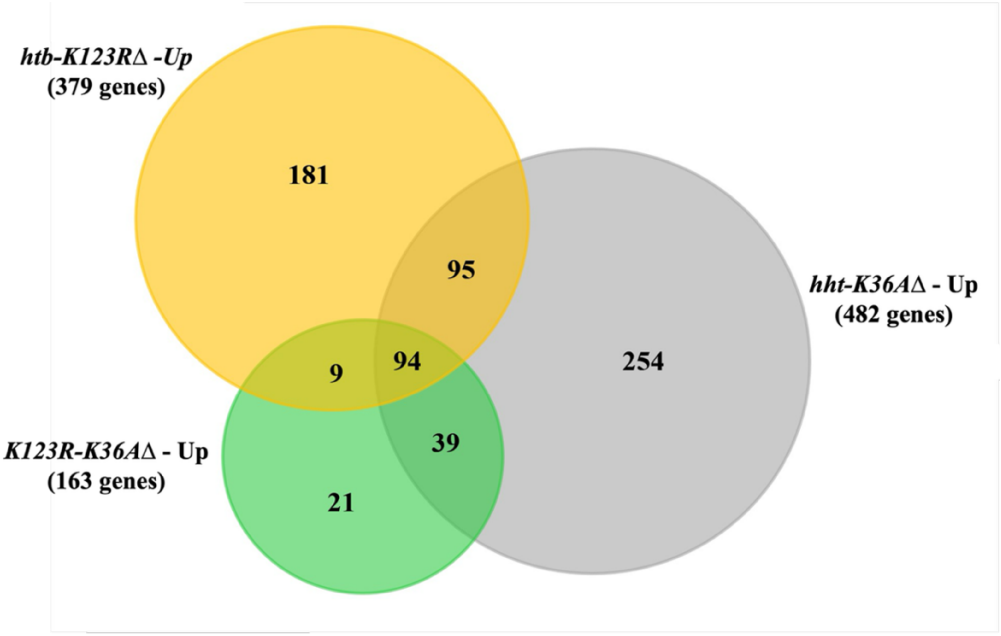


Figure 5.10: Venn diagram illustrating the overlap and uniqueness of upregulated genes among the three mutant strains compared to the wild-type. The diagram quantifies the number of genes that are uniquely upregulated in each mutant *htb-K123R*Δ, *hht-K36A*Δ, and the combined *K123R-K36A*Δ and those that are commonly upregulated across all mutants, showcasing the shared and distinct genetic responses to the mutations.

5.4.4 Analysis of Gene Downregulation in Mutant Strains in exponential phase

The genes significantly downregulated in each mutant strain *htb-K123R*Δ*, hht-K36A*Δ*,* and the double mutant *K123R-K36A*Δ compared to the wild-type during exponential growth, were next analysed (Table 5.1). These genes represent those genes in wild-type that would be subject to activation by H2bub and H3K36me. The data showed that the H3K36me-deficient mutant

showed the most downregulated genes (324) which was significantly greater in number compared to the 64 and 13 genes downregulated in the *htb-K123R*Δ and *K123R-K36A*Δ double mutant, respectively.

Analysis of the average levels of down regulation of the genes in the different strains revealed that the 13 genes downregulated in the double mutant showed, on average, the greatest decrease in transcription levels compared to wild-type (Fig. 5.11).

These data show that the absence of H3K36me has the greatest impact upon activation of the number of genes during exponential phase and that this effect is suppressed by the additional mutation of H2Bub. However, the greatest impact upon the extent of gene activation is shown in the double mutant. This suggests a complicated interplay between H3K36me and H2Bub is required to maintain the correct number and levels of gene activation during exponential growth.

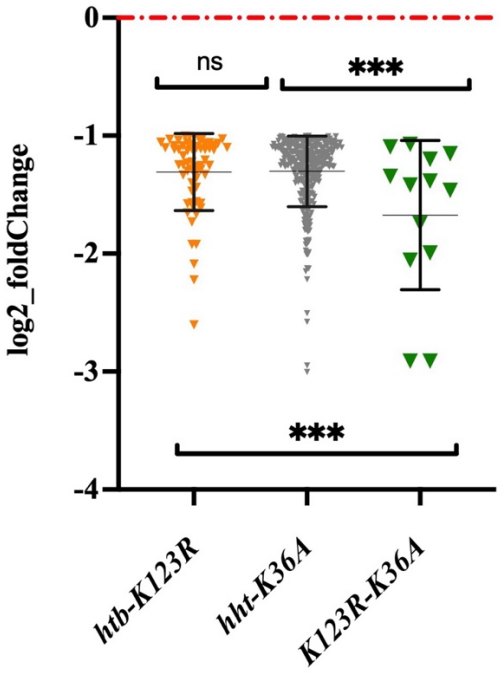


Figure 5.11: Total genes significantly downregulated in each mutant compared to wild-type. Significant differences were observed among *htb-K123R*Δ, *hht-K36A*Δ, and *K123R-K36A*Δ (P-Value

provided in the original document). The graph also indicates the mean and standard deviation. Significance using Two way ANOVA analysis (* p = 0.05, ** p = 0.01, **** p = <0.0001).

5.4.5 Gene ontology analysis of genes downregulated in different mutants during exponential phase

The gene ontology of the genes down regulated in the mutants compared to wild-type during exponential phase, were next analysed. The *htb-K123RΔ* mutant during exponential phase (Exp) exhibits significant downregulation in several gene ontology (GO) terms (Table 5.5 and Fig. 5.12). In the cellular components category the GO term enriched was mitochondrial intermembrane (3 genes, *RIB4, CYC7, HMF1*) indicating a significant role for H2Bub in regulating transcription related to mitochondrial function and the processes involved in energy production and cellular respiration. In the biological process category enrichments of GO terms in the K123R mutant included Protein localization to the nucleus, with (3 genes; *BTN2,OPI10,CUR1*), highlighting the mechanisms by which proteins are transported into the nucleus, essential for regulating gene expression and cellular function and translational initiation (3 genes; *HCR1,RPL24B,TMA20*), indicating an important role for H2Bub in promoting the key stages of protein synthesis.

The organophosphate biosynthetic process was also enriched for GO terms (19 genes including *URA4,ADE8,BNA1,OPI10*) which indicates a substantial involvement of H2Bub in the synthesis of organophosphate compounds, which are vital for energy transfer and signalling. The aromatic amino acid metabolic process was also enriched (6 genes including *DTD1,ARO4,BNA1,SRY1*), pointing towards H2Bub importance in the metabolism of essential amino acids like phenylalanine, tyrosine, and tryptophan. Lastly, (5 genes) involved in protein localization to the plasma membrane were downregulated in the K123R mutant (*FHN1,SFH5,PDR17,OPI10,ERG12*), highlighting a role for H2Bub in the processes that ensure proteins are correctly positioned at the cell membrane which are crucial for cell signalling and interaction with the environment (Fig. 5.12).

Category	Function	Number of Genes	Example Genes
GO Biological Processes	Protein localization to the nucleus	3	*BTN2, OPI10, CUR1*

	Translational initiation	3	*HCR1, RPL24B, TMA20*
	Organophosphate biosynthetic process	19	*URA4, ADE8, BNA1, OPI10*
	Aromatic amino acid metabolic process	6	*DTD1, ARO4, BNA1, SRY1*
	Protein localization to the plasma membrane	5	*FHN1, SFH5, PDR17, OPI10, ERG12*
GO Cellular Components	Mitochondrial intermembrane	3	*RIB4, CYC7, HMF1*

Table 5.5: List of genes commonly down-regulated during Exponential Phase in *htb-K123R*Δ compared to wild-type.

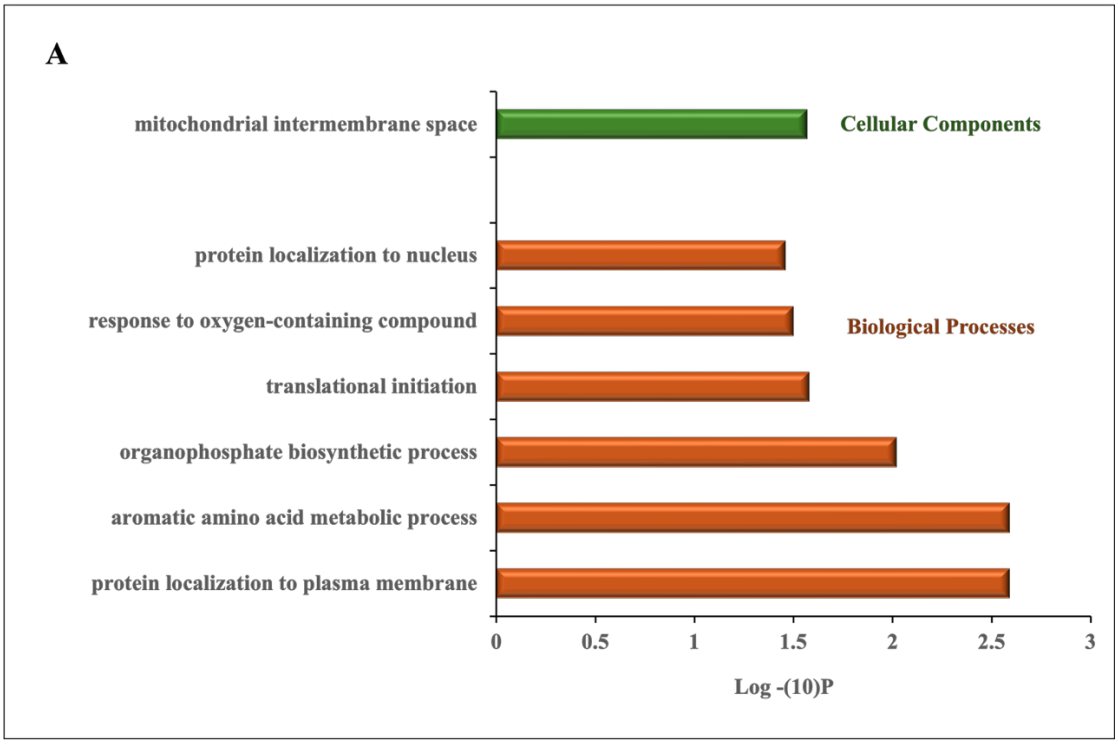


Figure 5.12: Gene ontology terms for downregulated genes in *htb-K123R*Δ. "(A) Bar chart.**"** The terms are associated with various biological processes, with significant Log10(P) values indicating the extent of downregulation.

In the *hht-K36A*Δ mutant, during exponential phase (Exp) there was downregulation of a broad range of genes involved in metabolic and biosynthetic processes, reflecting significant disruptions in cellular function in this mutant (Table 5.6 and Fig. 5.13). The GO analysis of down regulated genes in *hht-K36A*Δ mutant, during exponential phase revealed several key GO term enrichments including 25 genes involved in the cytosolic large ribosomal subunit (including *RPL2A,RPP0,RPP1A,RPL4B*), 60 ribosomal assembly genes, and 19 tRNA (guanine) methyltransferase genes (including *TRM8,TRM7,TRM11,TRM112*) which points to a central role for H3K36me in the process of translating mRNA into proteins.

There were also 51 genes downregulated in the *hht-K36A*Δ mutant involved in the plasma membrane emphasizing a significant function in maintaining cellular integrity, facilitating communication, and regulating the transport of substances in and out of the cell. Downregulation of 38 fungal-type cell wall genes including *SSA2,CCW12,YPS1,YPS3*, indicates its importance in providing structural support and protection to the cell.

In the biological process category significant enrichment of genes in the steroid metabolic process were found to be downregulated, emphasizing H3K36me's role in the synthesis and metabolism of steroids, essential for cell signalling. There were also 67 genes downregulated involved in the purine nucleoside diphosphate metabolic process suggesting an important role for H2Bub in nucleotide metabolism, crucial for DNA and RNA synthesis.

Finally, of note, there were 57 genes involved in small molecule biosynthetic processes and 119 genes involved in small molecule metabolism.

Overall, the impact of the loss of H3K36me upon positively influencing transcription of genes in exponentially growing cells was extensive and impacted a broad range of cell functions.

Category	Function	Number of Genes	Example Genes
GO Molecular Functions	Transition metal ion transmembrane transport	11	*ZRT2, GDT1, MRS3, ATX2*
	tRNA (guanine) methyltransferase activity	19	*TRM8, TRM7, TRM11, TRM112*
	Di-phosphotransferase activity	10	*PRS4, PRS1, THI80, FOL1*
	Intramolecular oxidoreductase activity	12	*TPI1, RKI1, HIS6, MRI1*
GO Biological Processes	Spermidine metabolic process	6	*SPE4, SPE2, SPE3, HIS6*
	GDP-mannose biosynthetic process	11	*SEC53, PSA1, PMI40, ERD1*
	Spermine transport	10	*TPO1, TPO2, PTK1, TPO3*

	Cellular metabolic compound salvage	12	*URH1, MDE1, ADO1, APT1*
	S-adenosylmethionine metabolic process	5	*MDE1, MRI1, ERC1, UTR4, SAH1*
	Cellular modified amino acid metabolic process	10	*SPE4, HMT1, MIS1, SPE2*
	Steroid metabolic process	76	*YEH1, ERG3, CAB1, ERG4*
	Ribosome assembly	60	*RPS14A, PWP2, RSA4, RPS0B*
	Purine nucleoside diphosphate metabolic process	67	*PGK1, CDC19, TPI1, ADK1*
	Small molecule biosynthetic process	57	*PGK1, ELO2, PDC1, ERG3*
	Small molecule metabolic process	119	*PGK1, ELO2, SEC53, PDC1*
GO Cellular Components	Rixosome complex	4	*IPI3, IPI1, RIX1, ADK1*
	Lipid droplet	12	*YEH1, CST26, EHT1, TSC10*
	Cytosolic large ribosomal subunit	25	*RPL2A, RPP0, RPP1A, RPL4B*
	Plasma membrane	51	*PGK1, STE2, TPO1, SSA2*
	Fungal-type cell wall	38	SSA2,CCW12,YPS1,YPS3

Table 5.6: List of genes commonly down-regulated during Exponential Phase in *hht-K36A*Δ compared to wild-type.

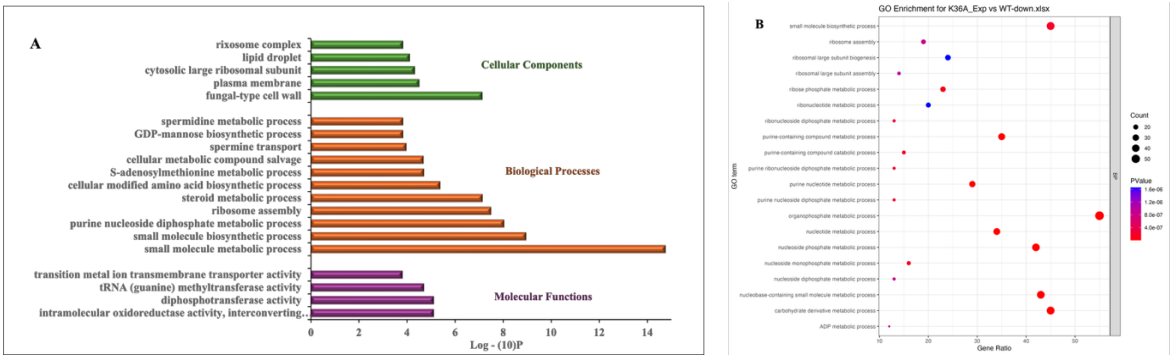


Figure 5.13: Gene ontology terms for downregulated genes in *hht-K36A*Δ. "(A) Bar chart (left); **(B)** Plot (right)." The terms cover a wide range of biological processes and molecular functions, with significant Log10(P) values.

The double mutant *K123R-K36A*Δ only downregulated 13 genes during exponential phase, 3 of which were enriched in intracellular protein transport (*BTN2,ATG41,CUR1*) (Table 5.7). This suggests that the bulk of the 324 genes downregulated in the K36A single mutant are returned to wild-type levels when H2Bub is additionally removed (Fig. 5.14). Therefore, loss of H2Bub in the H3K36A mutant largely rescues the defective transcription of those genes that were downregulated in the H3K36A mutant. This therefore suggests some sort of antagonistic interplay between H3K36me and H2Bub influences transcription during exponential phase.

Category	Function	Number of Genes	Example Genes
GO Biological Processes	Intracellular protein transport	3	*BTN2, ATG41, CUR1*

Table 5.7: List of down-regulated genes enriched for GO term indicated during Exponential Phase in *K123R-K36A*Δ compared to wild-type.

5.4.6 Venn Diagram Analysis of downregulated Genes

When the genes down-regulated during the exponential phase (Exp) in the mutant strains *htb-K123R*Δ, *hht-K36A*Δ, and *K123R-K36A*Δ, were analysed in a Venn diagram (Fig. 5.14) the results revealed that only 3 genes were commonly down-regulated in the three mutant strains. These findings highlight that each mutant had a largely distinct influence of upon activation of transcription during exponential phase.

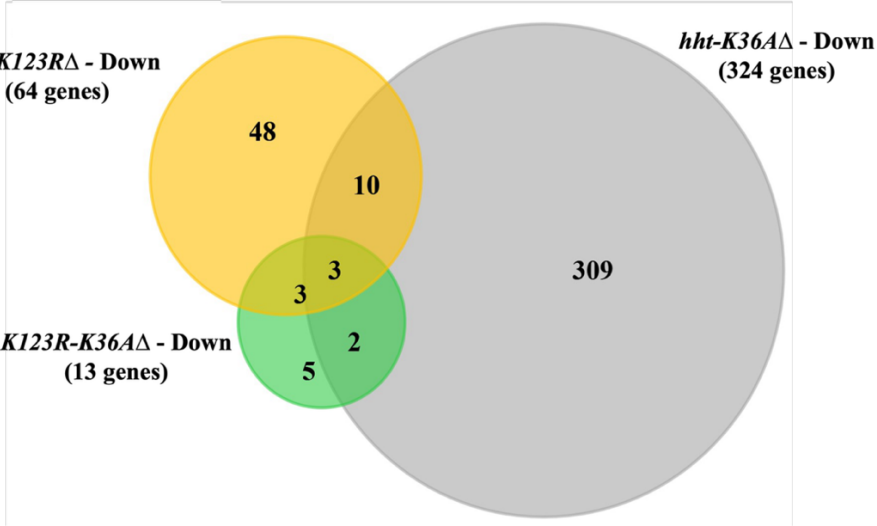


Figure 5.14: Venn diagram illustrating the overlap and uniqueness of downregulated genes among the three mutant strains compared to the wild type. The diagram quantifies the number of genes that are uniquely upregulated in each mutant *htb-K123RΔ, hht-K36A*Δ, and the combined *K123R-K36A*Δ and those that are commonly downregulated across all mutants, showcasing the shared and distinct genetic responses to the mutations.

5.5 Summary

This study utilized RNA-Seq to examine transcriptional regulation by histone modifications H3K36me3 and H2Bub in yeast cells during different growth phases: exponential phase (Exp), diauxic shift (Dix), and quiescent state (Q- D7- SP). Yeast cells were harvested at these stages, and RNA was extracted and sequenced. The study aimed to identify genes regulated by H2Bub and H3K36me3 by comparing RNA transcriptome data from mutant and wild-type strains.

The results showed high-quality RNA extraction, confirmed by Agilent 2100 Bioanalyzer and agarose formaldehyde gel electrophoresis, with RNA Integrity Number (RIN) values of around 6.80 being the cut-off for samples to be sent for sequencing.

PCA analysis initially suggested clear separation between different strains, and the different growth stages, indicating distinct transcriptional profiles and consistent clustering of biological replicates confirmed data reproducibility. Heatmap analysis also showed distinct gene expression patterns across different conditions, with clear clustering of most similar samples indicating reproducibility and consistency. However, although R^2 regression analysis indicated

high reproducibility of most of the RNA-Seq data, there were a few outliers which were excluded from further analysis.

Differential gene expression analysis of the exponentially growing cells revealed that the *htb-K123R*Δ mutant had 379 upregulated and 64 downregulated genes, the *hht-K36A*Δ mutant had 482 upregulated and 324 downregulated genes, and the *K123R-K36A*Δ double mutant had 150 upregulated and 13 downregulated genes compared to wild-type. Thus, the loss of H3K36me affects transcription of the largest cohort of genes in exponentially growing cells whilst, overall, the numbers suggest that H2Bub and H3K36me have a dominant negative effect upon transcription in exponential phase cells i.e. they are showing a predominantly repressive role upon transcription.

My analysis initially focused on the genes significantly up-regulated in mutant strains *htb-K123R*Δ*, hht-K36A*Δ, and the double mutant *K123R-K36A*Δ compared to the wild-type in exponential phase (Exp). Indeed, these up-regulated genes can be inferred to be subject to repression by the appropriate histone modification in wild-type. As previously described, the absence of H3K36me led to the greatest number of up-regulated genes, analysis of which showed that these genes were, on average, up regulated to the greatest extent compared to the other mutants. Thus, H3K36me is responsible for negatively influencing the most genes in wild-type exponential phase cells, and it does so to the greatest extent.

Most strikingly, the data shows that loss of both H2Bub and H3K36me in the double mutant results in an almost 50% rescue of the genes up regulated in either single mutant. This could be explained by the H2Bub in the H3K36A mutant, and H3K36me in the *htb-K123R*Δ mutant, actually having a positive effect upon transcription of these genes, such that when both are absent, this activating effect is abolished.

A similar potential interplay between the two modifications was revealed from the analysis of the genes down regulated in each mutant compared to wild-type. These down regulated genes can be inferred to be subject to activation by the appropriate PTM in wild-type.

Here, there were only 64 and 13 genes down regulated in the respective *htb-K123R*Δ and *K123R-K36A*Δ double mutant. However, there were 324 genes down regulated in the *hht-K36A*Δ mutant. This result suggests that the down regulation in the *hht-K36A*Δ mutant is largely

due to the presence of H2Bub now negatively influencing the bulk of the 324 genes. Additional removal of H2Bub in the *hht-K36A*Δ mutant in the *K123R-K36A*Δ double mutant, could then relieve this repression resulting in only 13 genes being down regulated in the double mutant.

However, this interpretation of the data is complicated by the fact that very few of the up and down regulated gene cohorts in any of the mutants overlap. In summary, the results have revealed a potential interplay between H2Bub and H3K36me in regulating transcription in wild-type exponential phase cells, with H3K36me showing the dominant role in regulation of transcription at this growth stage.

5.6 Gene Expression Changes at the Diauxic shift

The gene expression changes in the Diauxic shift (Dix) of wild-type and mutant strains *htb-K123R*Δ*, hht-K36A*Δ, and *K123R-K36A*Δ was determined via analysis of RNA-Seq data. Using a threshold of Log2 fold change ≥ 1 and an adjusted p-value ≤ 0.01 the significantly up and downregulated genes were identified (Table 5.8). The *htb-K123R*Δ mutant exhibited 372 upregulated genes, the *hht-K36A*Δ mutant had 513 upregulated genes, and the double mutant *K123R-K36A*Δ showed 143 upregulated genes. Examination of the genes downregulated in the mutants at Diauxie revealed that the *htb-K123R*Δ mutant had 790 downregulated genes, the *hht-K36A*Δ mutant showed 532 downregulated genes, and the *K123R-K36A*Δ double mutant exhibited 158 downregulated genes. These results showed that the mutation in *hht-K36A*Δ*,* which abolishes H3K36me, affects gene repression at diauxie the most, with the *hht-K36A*Δ mutation resulting in the highest number of upregulated genes. However, the *htb-K123R*Δ mutant effects gene activation the most at diauxie since more genes are down regulated in this mutant compared to the other mutants. Together, these results suggest distinct regulatory roles for H3K36me and H2Bub upon transcription at diauxie.

Diauxic shift	Upregulated	Downregulated	Total No. of Genes

htb-K123RΔ	**372**	**790**	**1162**
hht-K36AΔ	**513**	**532**	**1045**
K123R-K36AΔ	**143**	**158**	**301**

Table 5.8: Differential Gene Expression in Mutant Strains During the Diauxic Shift: Table showing the number of significantly upregulated and downregulated genes in *htb-K123R*Δ, *hht-K36A*Δ, and *K123R-K36A*Δ mutant strains compared to the wild-type strain during the diauxic shift. Genes with Log2 fold change ≥ 1 and an adjusted p-value ≤ 0.01 were considered significant. The bar chart shows 372 upregulated and 790 downregulated genes for *htb-K123R*Δ, 513 upregulated and 532 downregulated genes for *hht-K36A*Δ, and 143 upregulated and 158 downregulated genes for the double mutant *K123R-K36A*Δ.

5.6.1 Analysis of genes upregulated in the Mutant Strains at the Diauxic Shift

The genes that were significantly upregulated in each mutant strain, were initially focused on for analysis (Fig. 5. 15, hatched box). In the *htb-K123R*Δ mutant a total of 372 genes were significantly upregulated in this strain, suggesting that H2Bub normally acts to repress these genes. However, the highest number (513) of upregulated genes was exhibited by the *hht-K36A*Δ mutant indicating H3K36me playing the most important role in repression of gene transcription during the diauxic shift (Dix).

Most interestingly however, a much smaller number of upregulated genes, only 143, were evident in the *K123R-K36A*Δ double mutant, which lacks both H2Bub and H3K36me. This suggests a possible compensatory interaction between the two modifications upon negatively influencing transcription at diauxie, whereby loss of both modifications may alleviate the repressive effects seen in the single mutants.

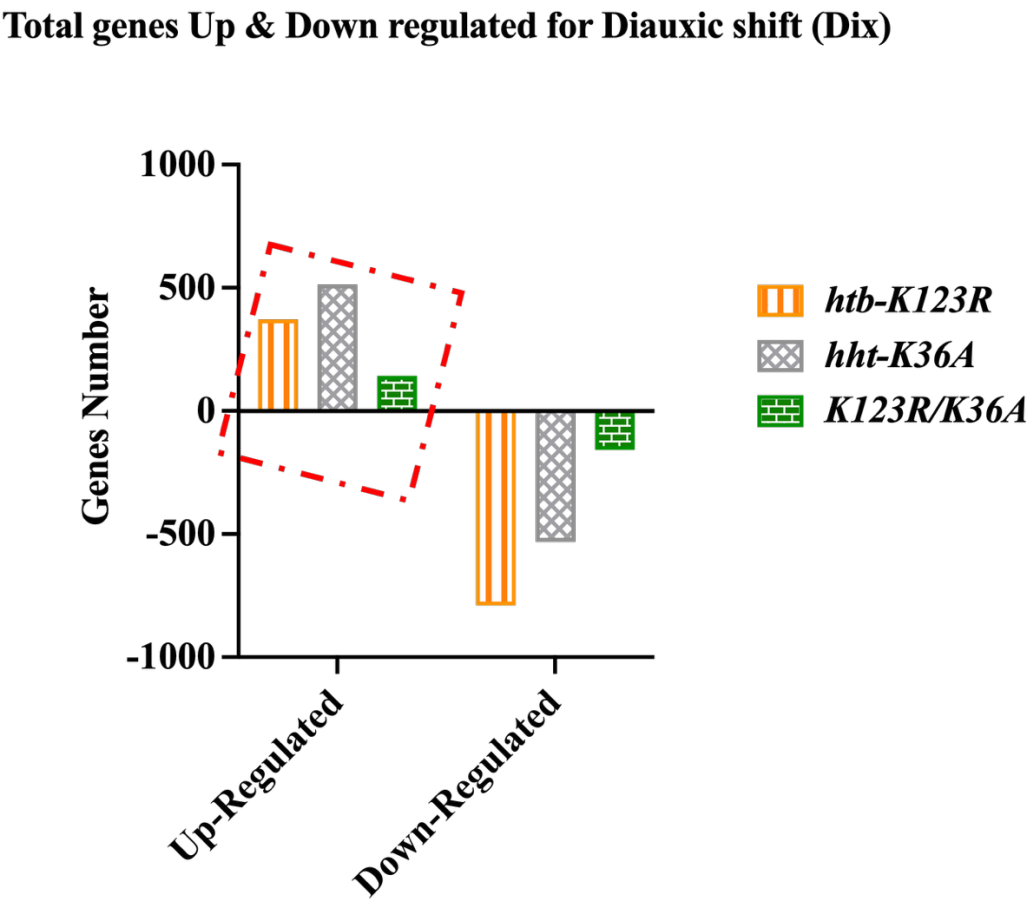


Figure 5.15: Genes showing more than a two-fold Up and Down regulated in expression in each strain compared to the wild-type during the diauxic shift.

5.6.2 Scatterplot Analysis of Upregulated Genes in different mutants in Diauxic Shift

The levels of de-repression of the genes upregulated in the mutants versus wild-type at diauxic shift, were next investigated (Fig. 5.16). The analysis showed that, on average, the genes upregulated in the *htb-K123R*Δ and *hht-K36A*Δ mutants were upregulated to the same extent. However, the average upregulation of the genes in the double mutant was significantly lower than that seen either of the single mutants. Thus, loss of either H2Bub or H3K36me has a greater effect on the levels of de-repression than the loss of both modifications together.

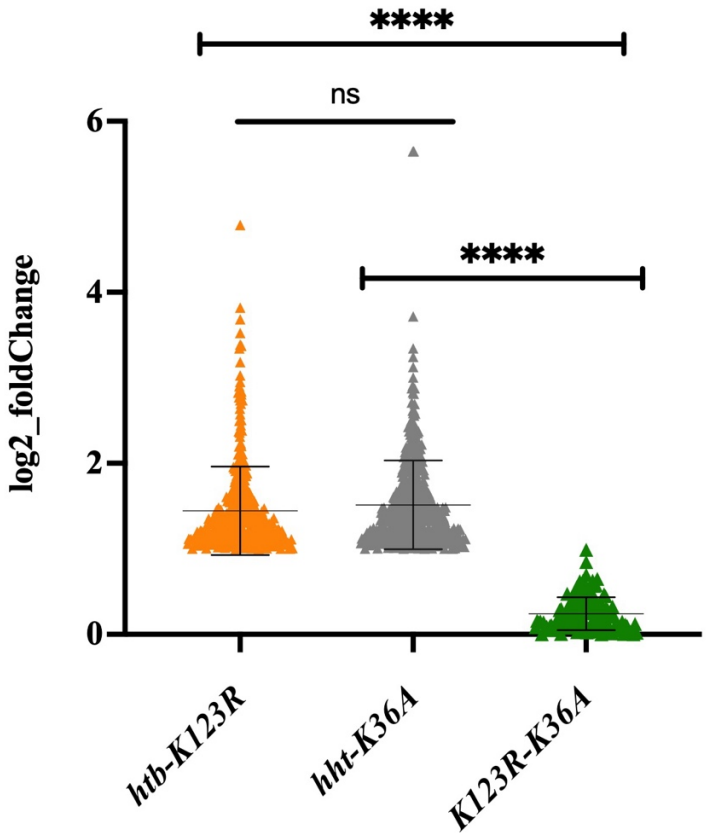


Figure 5.16: Total Genes Significantly Upregulated in Each Mutant Compared to Wild-Type During Diauxic shift. The bar chart shows the number of significantly upregulated genes (log2 fold change ≥ 1, adjusted *p*-value ≤ 0.01) in the *htb-K123R*Δ**,** *hht-K36A*Δ**,** and *K123R-K36A*Δ mutant strains compared with wild-type during the diauxic shift. The *htb-K123R*Δ mutant had 372 upregulated genes, the *hht-K36A*Δ mutant exhibited 513 upregulated genes, and the *K123R-K36A*Δ double mutant had 143 upregulated genes. The graph also indicates the mean ± standard deviation. Statistical significance was assessed using Two-way ANOVA analysis**;** no post hoc multiple comparison tests were performed (*p* = 0.05, **p* = 0.01, ***p* < 0.0001).

5.7 Gene Ontology (GO) Analysis of *htb-K123R* Upregulated Genes

Gene ontology analysis was next performed to gain insight into the 372 genes upregulated in the mutants versus wild-type at diauxic shift (Table 5.9 and Fig. 5.17). GO Analysis for the up regulated genes in the *htb-K123R*Δ mutant during the diauxic shift (Dix) revealed an enrichment of genes involved in the vacuole (45 genes, *GIT1,YFL040W, FAB1, FRE6*), checkpoint signalling (31 genes, including *RAD9,GCN2,MUS81,TEL1*), telomere capping (33 genes, including *CDC13,POL12,RIF1,SGS1*), chromatin domain organization (65 genes, such as *MSH3,GAT1,RED1,EST2*), and transmembrane transporter activity (92 genes, *includingAGP1,GIT1,ALR2,YFL040W*).

There were also genes upregulated in the K123R mutant involved in the DNA damage signalling (7 genes) and DNA double-strand break repair (11). Also of note was a considerable class of genes involved in sexual reproduction being up-regulated (85 genes, such as *BF2,BUB1,TOR2,SMC5*).

The GO analysis indicates H2Bub might be involved in regulating a heightened cellular response to the absence of glucose, particularly in processes related to cell structure, DNA repair, and reproduction. Indeed, many of the genes upregulated in the K123R mutant were involved in maintaining genomic integrity, responding to external stimuli, and preparing for reproduction. The significant upregulation in these areas highlights a role for H2Bub in regulating the cellular response to glucose depletion (Fig. 5.17).

Category	Function	Number of Genes	Example Genes
GO Biological Processes	Ascospore wall assembly	4	*RRT12, SPO75, CRR1, LDS1*
	Checkpoint signaling	31	*RAD9, GCN2, MUS81, TEL1*
	DNA damage response via regulation of cell cycle checkpoints	7	*RAD9, GCN2, MUS81, TEL1*
	Telomere capping	33	*CDC13, POL12, RIF1, SGS1*
	Double-strand break repair via homologous recombination	11	*SLX4, IRC20, PSY3, SCC2*
	Pyrimidine nucleobase transport	6	*FUR4, FCY2, FCY21, FCY22*
	Response to extracellular stimulus	22	*GAT1, TIS11, ENA1, ATO3*
	Sexual reproduction	85	*BF2, BUB1, TOR2, SMC5*
	Cell flocculation	23	*FLO9, FLO1, FLO10, FLO11*
GO Molecular Functions	Transmembrane transporter activity	92	*AGP1, GIT1, ALR2, YFL040W*
	DNA binding at promoter region (nucleolar chromatin domain)	65	*MSH3, GAT1, RED1, EST2*
	Vacuole	45	*GIT1, YFL040W, FAB1, FRE6*

GO Cellular Components	Import across plasma membrane	6	*AGP1,YFL040W,MUP1,CCH1*

Table 5.9: List of genes commonly up-regulated during diauxic shift in *htb-K123R*Δ compared to wild-type.

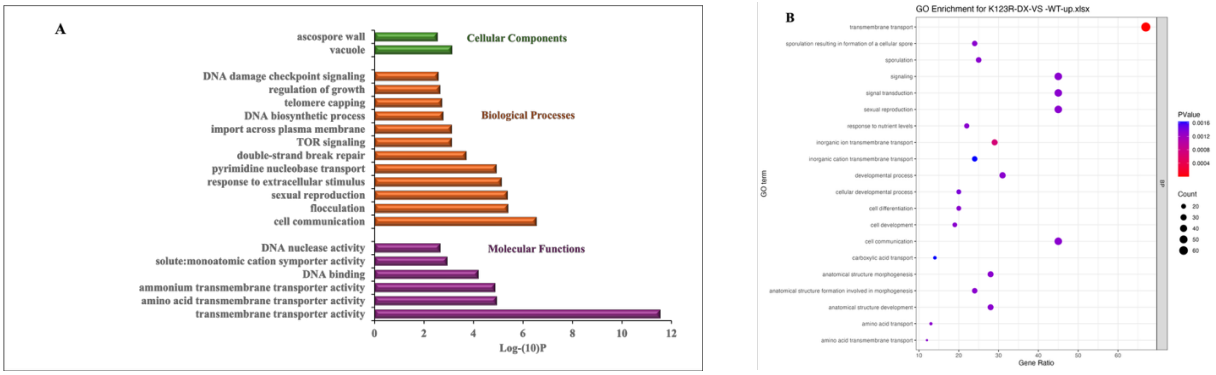


Figure 5.17: Gene Ontology (GO) analysis of upregulated genes in the *htb-K123R*Δ mutant strain. **"(A)** Bar chart (left); **(B)** Plot (right)**."** The bar graph shows the most significantly enriched molecular functions and biological processes among the upregulated genes, including transmembrane transporter activity, oxidoreductase activity, and energy derivation by oxidation of organic compounds. The enrichment levels are indicated by the corresponding Log2 fold change values.

5.7.1 Gene Ontology (GO) Analysis of *hht-K36A*Δ Upregulated Genes

In *hht-K36A*Δ mutant during the diauxic shift (Dix) the GO analysis of upregulated genes reveals significant changes in various biological processes (Table 5.10 and Fig. 5.18). Processes involved in protein synthesis were particularly enriched and included the cytosolic ribosome (195 genes, *RPS14A,RPL22B,RPL2A,RPL29*), ribosome biogenesis (168 genes, *KRR1,RPS14A,RSA4,YCR087C-A*), ribosome assembly (44 genes, *RPS14A,RSA4,RPS0B,RPL10*), ribosomal large subunit biogenesis (43 genes, *RSA4,RPL2A,RIX7,NOC3*), and ribosomal subunit export from nucleus (29 genes, *RIX7,RPS0B,GSP1,BCP1*). Related to protein synthesis, there was also enrichment of upregulated genes involved in RNA binding (38 genes, *RPL2A,RPL37A,EMG1,RPP0*), and catalytic activity acting on a tRNAs (70 genes, *FRS1,POP5,SEN34,DTD1*).

Other processes that showed significant enrichment within the upregulated gene cohort included small molecule biosynthetic process (51 genes, *CTR86,SNO3,SNZ3,THI5*) and DNA repair (18 genes, *PSY3,DPB4,POL30,DPB3*), and

These findings suggest the absence of K36me during diauxie leads primarily to an increase in activities related to ribosome biogenesis and ribosomal subunit production (Fig. 5.18).

Category	Function	Number of Genes	Example Genes
GO Biological Processes	Cytosolic ribosome	195	*RPS14A, RPL22B, RPL2A, RPL29*
	Ribosome biogenesis	168	*KRR1, RPS14A, RSA4, YCR087C-A*
	Ribosome assembly	44	*RPS14A, RSA4, RPS0B, RPL10*
	Ribosomal large subunit biogenesis	43	*RSA4, RPL2A, RIX7, NOC3*
	Ribosomal subunit export from nucleus	29	*RIX7, RPS0B, GSP1, BCP1*
	DNA synthesis involved in DNA repair	18	*PSY3, DPB4, POL30, DPB3*
	Cleavage in ITS2 between 5.8S rRNA and LSU-rRNA	4	*RPL37A, RPL37B, RPL17A, LAS1*
	Deoxyribonucleoside monophosphate biosynthetic process	17	*DUT1, CDC21, DCD1, HAM1*
	tRNA nucleoside ribose methylation process	19	*TRM3, TRM7, TRM13, RTT10*
	Regulation of translational fidelity	10	*RPL31B, DTD1, RPL31A, RPS9B*

	Small molecule biosynthetic process	51	*CTR86, SNO3, SNZ3, THI5*
	Thiamine metabolic process	36	*PET18, SNZ3, THI5, THI13*
GO Molecular Functions	Dioxygenase activity	7	*JLP1, YHB1, BNA2, YJR154W*
	RNA binding	38	*RPL2A, RPL37A, EMG1, RPP0*
	Catalytic activity acting on a tRNA	70	*FRS1, POP5, SEN34, DTD1*

Table 5.10: List of genes commonly up-regulated during diauxic shift in *hht-K36A*Δ compared to wild-type.

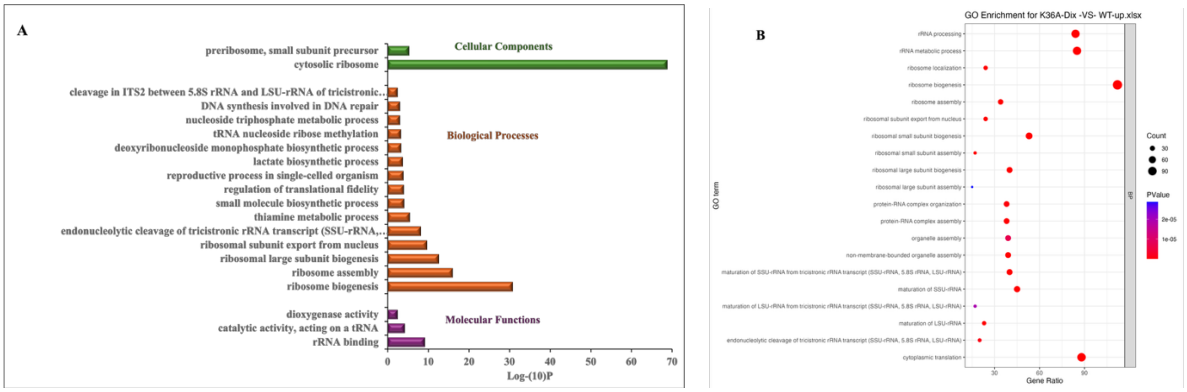


Figure 5.18: Gene Ontology (GO) analysis of upregulated genes in the *hht-K36A*Δ mutant strain. **"(A)** Bar chart (left); **(B)** Plot (right)**."** The bar graph displays the top enriched molecular functions and biological processes, such as lyase activity, water transmembrane transporter activity, and small molecule catabolic process. The enrichment is measured by Log2 fold change values, reflecting the degree of upregulation in these functional categories.

5.7.2 Gene Ontology (GO) Analysis of *K123R-K36A*Δ Upregulated Genes

The GO analysis of the 143 genes upregulated in *K123R-K36A*Δ double mutant during the Diauxic shift (Dix) reveals several key insights into the biological processes that are upregulated (Table 5.11 and Fig. 5.19).

A significant enrichment in the GO term mitochondrial inner membrane (11 genes, *ATP1,CMC2,COR1,PET9*) was seen, suggesting that the double mutant may have enhanced mitochondrial activity, which could be crucial for energy production during the Diauxic shift (Dix) when cells switch from fermentative to oxidative metabolism. Go term replication fork (19 genes, *RFA1,MCM2,HHT1,RFC5*) were also enriched indicating that the *K123R-K36A*Δ double mutation upregulates genes involved in DNA replication and repair mechanisms, suggesting this mutant might be subject to stress causing genomic instability during the Diauxic shift (Dix).

The enrichment in GO terms for carbohydrate derivative biosynthetic process (37 genes, *PMT2, ATP1, ALG3, PRS4*) suggests that the cells are likely enhancing their metabolic pathways to produce essential carbohydrate derivatives, which could be crucial for energy storage, structural component within the cell. The GO term protein retention in ER lumen (15 genes, *ERP2,ERP1,ERD2,MYO4*) enrichment suggests that the cells are likely enhancing their mechanisms for ensuring proper protein folding, assembly, and quality control before these proteins are transported to their final destinations.

The enrichment in the term cell wall chitin biosynthetic process (4 genes, *SKT5,CHS3,CHS2,MNN2*) suggests a significant role in the formation and maintenance of the cell wall structure.

The upregulation in GO term organophosphate biosynthetic process (18 genes, *ATP1,BNA4,SCS22,PRS4*) was also seen in double mutant both. This process is essential for the synthesis of key molecules like ATP, which are vital for energy transfer and cellular metabolism. The enrichment in nitrogen compound transport genes (33 genes, *MYO4,DRS2,PMT2,ERP2*) shows a higher level of upregulation indicating towards efficient nitrogen transport, which is crucial for amino acid and nucleotide synthesis, essential for cell growth and division. Several other processes, such as regulation of dephosphorylation (7 genes, *SCS22,REG2,IST2,CLN3*), mitotic cell cycle process (22 genes, *CLN3,MTW1,SPC72,KIP1*), and vacuole fusion (4 genes, *CLN3,SEC17,SEC18,CMD1*), were also upregulated in the double mutant *K123R-K36A*Δ.

These processes are important for cell cycle regulation, intracellular transport, and cellular homeostasis.

Overall, the *K123R-K36A*Δ double mutant exhibits significant enrichment of upregulated genes involved in various biological processes during the Diauxic shift (Dix). The enhanced mitochondrial activity, DNA replication and repair, and nitrogen transport suggest that this double mutant is having to adapt to the metabolic shift that occurs during this phase (Fig. 5.19).

Category	Function	Number of Genes	Example Genes
GO Cellular Components	Mitochondrial inner membrane	11	*ATP1, CMC2, COR1, PET9*
	Protein retention in ER lumen	15	*ERP2, ERP1, ERD2, MYO4*
GO Biological Processes	Replication fork	19	*RFA1, MCM2, HHT1, RFC5*
	Carbohydrate derivative biosynthetic process	37	*PMT2, ATP1, ALG3, PRS4*
	Cell wall chitin biosynthetic process	4	*SKT5, CHS3, CHS2, MNN2*

	Organophosphate biosynthetic process	18	*ATP1, BNA4, SCS22, PRS4*
	Isoprenoid metabolic process	3	*RFT1, RER2, COQ1*
	Nitrogen compound transport	33	*MYO4, DRS2, PMT2, ERP2*
	Regulation of dephosphorylation	7	*SCS22, REG2, IST2, CLN3*
	Mitotic cell cycle process	22	*CLN3, MTW1, SPC72, KIP1*
	Vacuole fusion	4	*CLN3, SEC17, SEC18, CMD1*
GO Molecular Functions	ATP-dependent activity	14	*MYO4, DRS2, SSA1, ATP1*
	Ligase activity	9	*ATP1, PET112, ILS1, URA7*

Table 5.11: List of genes commonly up-regulated during diauxic shift in *K123R-K36A*Δ compared to wild-type.

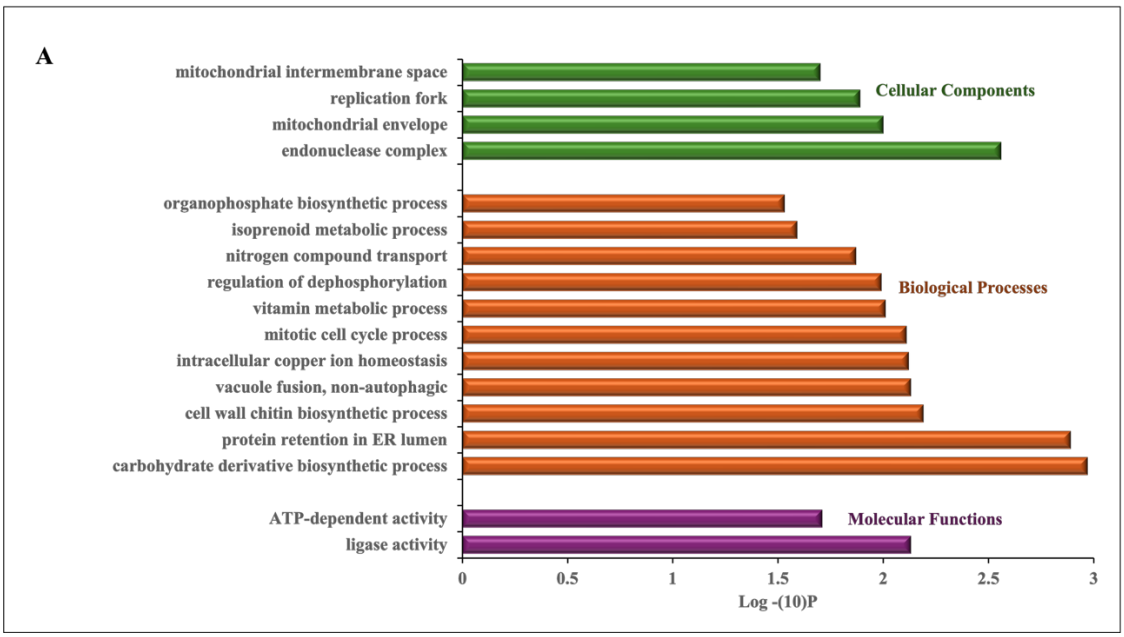


Figure 5.19: Gene Ontology (GO) analysis of upregulated genes in the combined *K123R-K36A*Δ mutant strain. **"(A)** Bar chart.**"** The bar graph presents the most significantly enriched molecular functions and biological processes, including carboxylic acid transmembrane transporter activity, ammonium transmembrane transporter activity, and energy derivation by oxidation of organic compounds. The graph highlights the upregulation levels with corresponding Log2 fold change values.

5.7.3 Venn Diagram Analysis of upregulated Genes

A Venn diagram of the genes upregulated in the three mutants versus wild-type at diauxie was constructed which revealed that the genes upregulated in each mutant were largely unique, with little overlap (Fig. 5.20). Although the unique upregulation of genes might be expected in the two single mutants versus wild-type, it would be predicted that the double mutant would overlap considerably with the genes upregulated in the two single mutants. However, this was not the case. Indeed, only 7 of the genes upregulated in the double mutant overlapped with those genes upregulated in the *htb-K123R*Δ mutant and only 19 genes in the double mutant overlapped with the K36me single mutant upregulated genes.

These findings highlight the distinct upregulation patterns among the mutant strains during the diauxic shift.

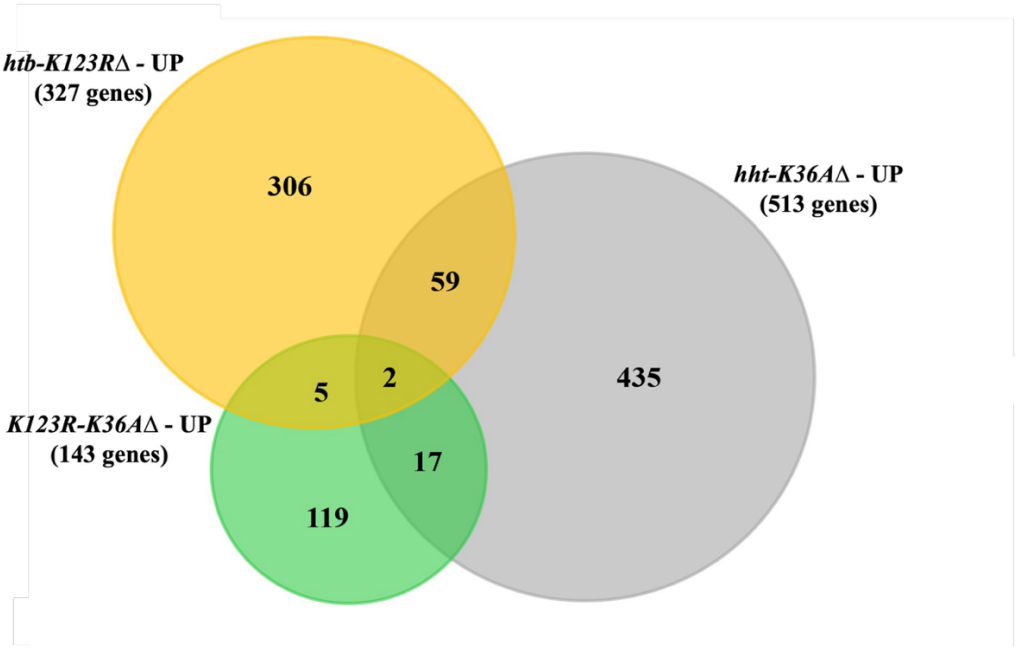


Figure 5.20: Venn diagram illustrating the overlap and uniqueness of upregulated genes among the three mutant strains compared to the wild type. The diagram quantifies the number of genes that are uniquely upregulated in each mutant *htb-K123R*Δ*, hht-K36A*Δ, and the combined *K123R-K36A*Δ and

those that are commonly upregulated across all mutants, show casing the shared and distinct genetic responses to the mutations.

5.7.4 Genes downregulated in the mutant strains during Diauxic Phase

Genes that were significantly downregulated in each mutant strain, were next analysed. These genes would represent those genes normally subject to a positive influence upon transcription by H2Bub and H3K36me. In the *htb-K123R*Δ mutant 790 genes were significantly downregulated compared to wild-type, 532 genes were down regulated in the *hht-K36A*Δ mutant, and only 158 genes were downregulated in the *K123R-K36A*Δ double mutant, which lacks both H2Bub and H3K36me (see Table 5.8).

Examination of the levels of down regulation of the genes in the different mutants showed that, on average, the genes down regulated in the two single mutants were equally down regulated compared to wild-type, and were down regulated to a greater extent than the average of the genes down-regulated in the double mutant (Fig. 5.21).

Together, the lower number of genes downregulated in the double mutant, and the fact they were down regulated to a lesser extent than those in the two single mutants, suggests a possible compensatory interaction between the two modifications, which may alleviate the activation effects seen in the single mutants.

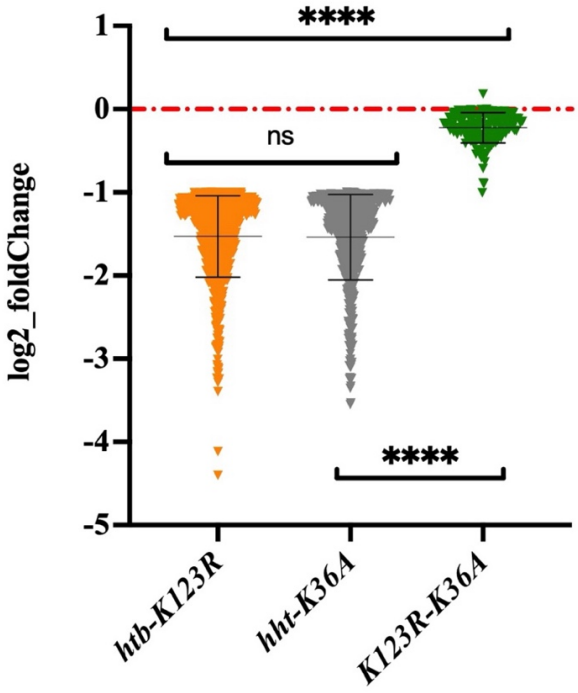


Figure 5.21: Total Genes Significantly Downregulated in Each Mutant Compared to wild-type During Diauxic shift. The bar chart shows the number of significantly downregulated genes (log2 fold change ≤ −1, adjusted *p*-value ≤ 0.01) in the *htb-K123R*Δ*,* *hht-K36A*Δ, and *K123R-K36A*Δ mutant strains compared with wild-type during the diauxic shift (Dix). The *htb-K123R*Δ mutant had 790 downregulated genes, the *hht-K36A*Δ mutant exhibited 532 downregulated genes, and the *K123R-K36A*Δ double mutant had 158 downregulated genes. The graph also represent the mean ± standard deviation. Statistical significance was assessed using Two-way ANOVA**;** no post hoc multiple comparison tests were performed ($p = 0.05$, *$p = 0.01$, ***$p < 0.0001$).

5.7.5 Gene Ontology (GO) Analysis of *htb-K123R*Δ downregulated Genes

The GO analysis of the 790 genes downregulated in the *htb-K123R*Δ mutant revealed significant enrichment in several key processes such as cytosolic ribosome (226 genes,), cytosolic small ribosomal subunit (120 genes,) and endoplasmic reticulum sub-compartment (100 genes), suggesting a potential impact on protein synthesis and transport machinery (Table 5.12 and Fig. 5.22).

In the biological process category key enrichments were in small molecule metabolic process (187 genes), carbohydrate derivative metabolic process (178 gene), and lipid biosynthetic process (68 genes).

This GO analysis result indicates significant enrichments among the downregulated genes in the *htb-K123R*Δ mutant in processes related to protein synthesis machinery and various metabolic processes (e.g., small molecule metabolism, carbohydrate derivatives, lipid biosynthesis), ribosome assembly, and other cellular functions.

These findings suggest a positive role for H2Bub in activating genes involved in metabolism and protein synthesis at diauxie.

Category	Function	Number of Genes	Example Genes
GO Cellular Components	Cytosolic ribosome	226	*RPS14A, RPL22B, RPL2A, RPL29*
	Cytosolic small ribosomal subunit	120	*RPS14A, RPS0B, RPS31, RPS28B*
	Endoplasmic reticulum sub-compartment	100	*ELO2, PER1, SED4, EMP47*
GO Biological Processes	Small molecule metabolic process	187	*APA1, POF1, GLK1, HIS4*
	Ribosome assembly	48	*RPS14A, SDO1, RPS0B, RPS31*
	Carbohydrate derivative metabolic process	178	*APA1, GLK1, PGK1, PER1*
	Glucose 6-phosphate metabolic process	14	*GLK1, HXK1, NGK1, EMI2*
	Lipid biosynthetic process	68	*ELO2, PER1, ELO3, HMG2*
	Trehalose biosynthetic process	18	*TPS2, TPS1, PGM1, UGP1*
	Very long-chain fatty acid biosynthetic process	21	*ELO2, ELO3, TSC13, IFA38*
	Ribosomal large subunit biogenesis	36	*RPL2A, RPL37A, RPP0, RPL26A*
	Ribosomal subunit export from nucleus	28	*RPS0B, RPS28B, RLI1, RPS18A*
	Regulation of translational fidelity	24	*FRS2, RPL31B, DTD1, RPL31A*
	Purine nucleoside monophosphate metabolic process	31	*ADE1, ADK1, ADE8, GUK1*
	S-adenosylmethionine cycle	19	*MDE1, SAM4, MRI1, UTR4*

	Secondary alcohol biosynthetic process	35	*HMG2, BDH1, ERG4, ERG26*
	Histidine biosynthetic process	6	*HIS4, HIS7, ADE3, HIS3, HIS6, HIS1*
GO Molecular Functions	Glycosyltransferase activity	42	*APA1, GLK1, PGK1, PER1*
	Sequence-specific mRNA binding	32	*RPS14A, RPS0B, RPS31, RPS28B*
	Glucokinase activity	10	*GLK1, HXK1, NGK1, EMI2*

Table 5.12: List of genes commonly down-regulated during diauxic shift in htb-*K123R*Δ compared to wild-type.

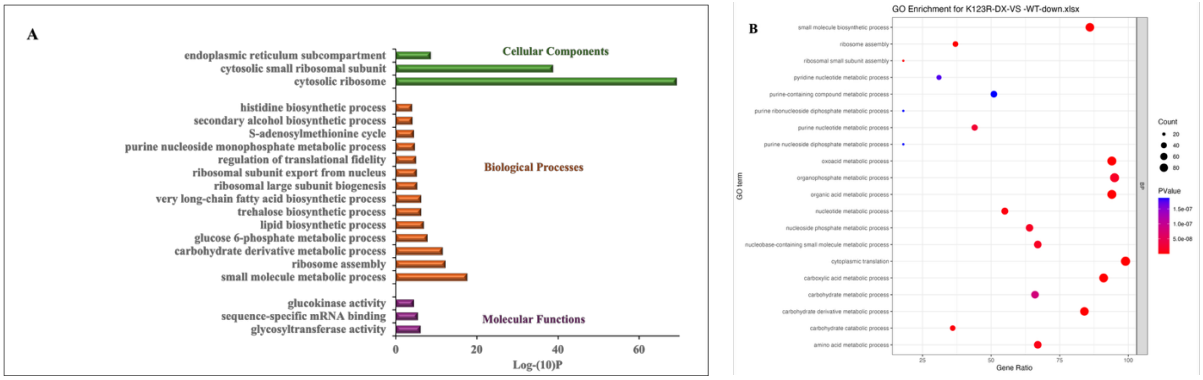


Figure 5.22: Gene Ontology (GO) analysis of downregulated genes in the *htb-K123R*Δ mutant strain. "(A) Bar chart (left); **(B)** Plot (right)**."** The bar graph in Figure illustrates the down-regulation of various biological processes and molecular functions in the *htb-K123R*Δ-(Dix)-Down Regulated condition. The x-axis represents the Log10(p) values, indicating the significance level of each process being down-regulated. The use of Log10(p) values underscores the statistical significance of these changes, providing a robust framework for understanding the molecular mechanisms affected by the mutation.

5.7.6 Gene Ontology (GO) Analysis of *hht-K36A*Δ downregulated Genes

The GO analysis of the 532 genes downregulated in the *hht-K36A*Δ mutant revealed significant enrichment in several critical GO terms including the plasma membrane (88 genes), which included 9 genes involved in the membrane raft pathway, suggesting a role for H3K36me in organizing membrane microdomains for signal transduction (Table 5.13 and Fig. 5.23). Downregulated genes were also enriched for the vacuole (76 genes), and the fungal-type cell

wall (52 genes), highlighting important roles for H3K36me in storage within the cell and for maintaining cell integrity and morphology.

In the biological process category the most prominent term was DNA integration, with 122 genes, highlighting a role for H3K36me at diauxie in genetic recombination and stability. Importantly, genes involved in carbohydrate metabolic processes (48 genes), including trehalose metabolic process (27 genes) and carbohydrate phosphorylation (20 genes), were also enriched, highlighting the importance of H3K36me in energy production and carbohydrate storage.

Genes involved in the response to external stimulus (23 genes) and response to hydrogen peroxide (30 genes) were also downregulated in the mutant, indicate a role for H3K36me in the cell's mechanisms for adapting to environmental changes and oxidative stress.

The energy reserves metabolic process (41 genes), and transition metal ion transport (20 genes, *SMF3,FTH1,PCA1,ZRT1*), were also enriched, further highlighting H3K36me's role for maintaining energy balance and metal ion homeostasis. Lastly, 16 downregulated genes involved in the fatty acid metabolic process were enriched pointing to a role for H3K36me in lipid metabolism.

Overall, the data suggested H3K36me was important for promoting transcription at diauxie for genes involved in carbohydrate metabolism and storage which are potentially important for survival of quiescent cells formed during stationary phase.

Category	Function	Number of Genes	Genes
GO Cellular Components	Plasma membrane	88	*GLK1, FUS1, YCP4, ADY2*
	Vacuole	76	*ADY2, ADP1, TPO1, SMF3*
	Ribosome	13	*YCP4, RFS1, PIL1, YGR130C*
	Fungal-type cell wall	52	*RRT12, CTS1, EXG1, DIA3*
	Cellular bud scar	9	*HSP150, PIR1, EGT2, NIS1*
	Membrane raft pathway	9	*YCP4, FMP45, TMS1, IVY1*
	Endoplasmic reticulum tubular network	4	*POM33, PER33, RTN2, YOP1*
GO Biological Processes	DNA integration	122	*YLR035C-A, YLR227W-B, YLR410W-B, YAR009C*
	Carbohydrate metabolic process	48	*GLK1, RBK1, GSY1, HXK1*
	Trehalose metabolic process	27	*HSP104, TPS2, NTH2, TPS1*
	Carbohydrate phosphorylation	20	*GLK1, RBK1, HXK1, YLR345W*

	Response to external stimulus	23	*ADY2, TIS11, DCS1, ADR1*
	Response to hydrogen peroxide	30	*HSP42, CTA1, CTT1, DDR2*
	Glucose 6-phosphate metabolic process	18	*GLK1, HXK1, NGK1, EMI2*
	Energy reserves metabolic process	41	*GLK1, GSY1, TPS1, PGM1*
	Transition metal ion transport	20	*SMF3, FTH1, PCA1, ZRT1*
	Fatty acid metabolic process	16	*ECI1, TMA17, MDH3, EHT1*
GO Molecular Functions	Acetylesterase activity	13	*EHT1, MGL2, EEB1, GPT2*
	Enzyme inhibitor activity	14	*SYP1,RFU1,SIC1,TFS1*

Table 5.13: List of genes commonly down-regulated during diauxic shift in *hht-K36A*Δ compared to wild-type.

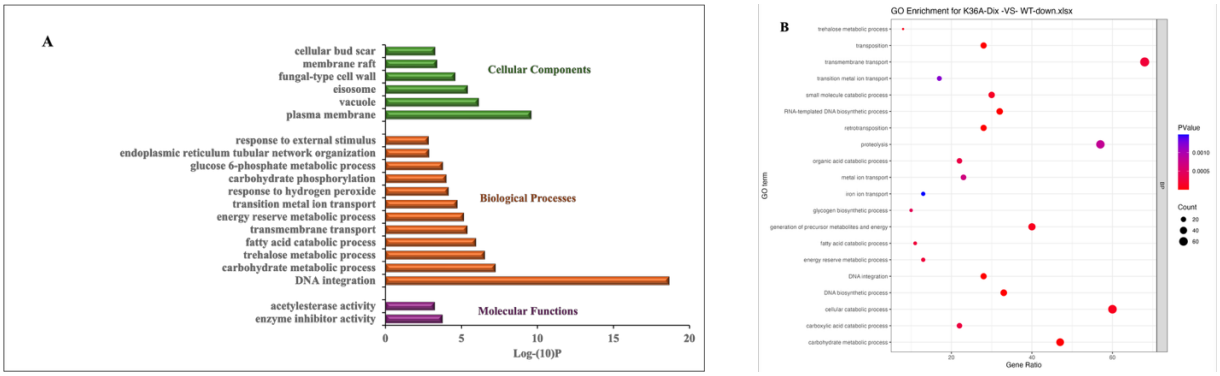


Figure 5.23: Gene Ontology (GO) analysis of downregulated genes in the *hht-K36A*Δ mutant strain. "(A) Bar chart (left); **(B)** Plot (right)**."** The bar graph displays the top enriched molecular functions and biological processes, such as lyase activity, water transmembrane transporter activity, and small molecule catabolic process. The enrichment is measured by Log2 fold change values, reflecting the degree of upregulation in these functional categories.

5.7.7 Gene Ontology (GO) Analysis of *K123R-K36A*Δ downregulated Genes

Of the 158 genes down regulated at diauxie in the *K123R-K36A*Δ double mutant, there was a mix of small groups of genes involved in diverse cellular processes such as the plasma membrane (23 genes), cellular bud neck processing, and genes involved in the regulation of exit from mitosis (13 genes), highlighting a role for both PTMs in ensuring proper cell division and cytokinesis (table 5.14 and Fig. 5.24).

Genes involved in the positive regulation of lipid metabolic process were also enriched and, although represented by only 3 genes (*OAF1,YEL1,TSC3*), highlights the importance of both H2Bub and H3K36me in maintaining lipid homeostasis and energy balance. Finally, 16 Peptidase activity genes were enriched pointing towards a role for both PTMs in protein degradation and processing, while 26 DNA binding genes, including *FUN30*, suggests the role of the two PTMs could be mediated and amplified by the downstream activation of transcription factors involved in the gene regulation and expression. (Fig. 5.24).

Category	Function	Number of Genes	Example Genes
GO Cellular Components	Plasma membrane	23	*CDC19, SNC1, LTE1, FUN26*
	Rpd3L-expanded complex	42	*FUN19, DEP1, TOD6, RXT2*
	Cellular bud neck	17	*CDC24, SNC1, TPD3, BUD14*
GO Biological Processes	Regulation of exit from mitosis	13	*CDC24, LTE1, BUD14, CDC15*
	Positive regulation of lipid metabolic process	3	*OAF1, YEL1, TSC3*
	Nucleobase-containing compound biosynthetic process	23	*CCR4, ACS1, PTA1, TFC3*
	Membrane docking	7	*SYN8, MDM10, GEM1, CNM1*

	Membrane fusion	12	*SNC1, SYN8, VPS8, BOI1*
	Galactose catabolic process via UDP-galactose	5	*GAL7, GAL10, GAL1,*
GO Molecular Functions	3'-5' exonuclease activity	3	*CCR4, YBL055C, APN2*
	Organic anion transmembrane transporter activity	6	*SEO1, FLC2, QDR3, BAP2, TAT1, YMC2*
	Peptidase activity	16	*YAR009C, YBL100W-B, MAP2, UBP13*
	Zinc ion binding	23	*BDH2, BDH1, OAF1, VPS8*
	Catalytic activity, acting on a protein	24	*FUN30, SWC3, YAR009C, YBL100W-B*
	Protein-membrane adaptor activity	3	*VPS8, RCR1, ALG14*
	DNA binding	26	*FUN30, OAF1, TFC3*
	Protein phosphatase regulator activity	17	*GIP4, TPD3, BUD14, SHP1*
	Calcium ion binding	4	*GEM1, EDE1, NTH2, YBR053C*

Table 5.14: List of genes commonly down-regulated during diauxic shift in *K123R-K36A*Δ compared to wild-type.

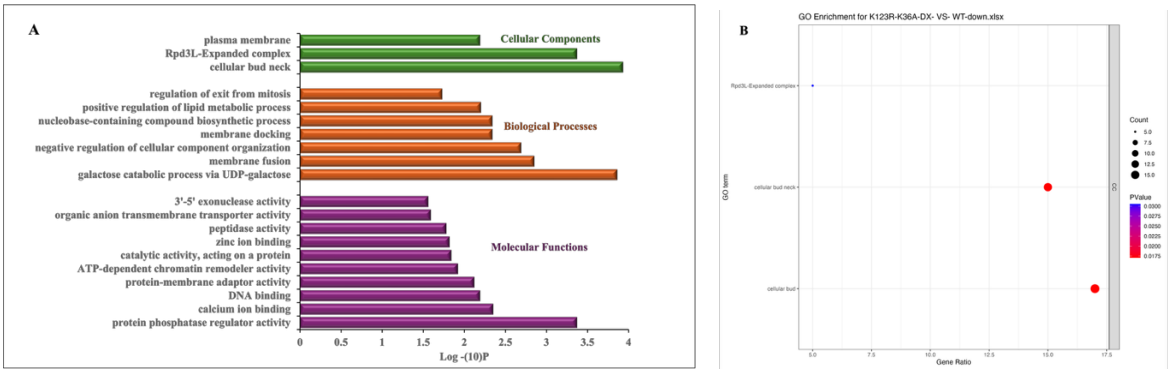


Figure 5.24: Gene Ontology (GO) analysis of downregulated genes in the *K123R-K36A*Δ mutant strain. "(A) Bar chart (left); **(B)** Plot (right)**."** The bar graph in Figure illustrates the down-regulation of various biological processes and molecular functions in the *K123R-K36A*Δ–(Dix) -Down Regulated condition. The x-axis represents the Log10(p) values, indicating the significance level of each process being down-regulated. The use of Log10(p) values underscores the statistical significance of these

changes, providing a robust framework for understanding the molecular mechanisms affected by the mutation.

5.7.8 Venn Diagram Analysis of downregulated Genes

A Venn diagram of the genes downregulated in each mutant versus wild-type was next prepared to determine the extent of overlap, which might indicate weather H2Bub and H3K36me share functions at diauxic shift , or work independently (Fig. 5.25).

As can be seen, of the 532 down regulated genes in the K36 A mutant and the 790 genes downregulated in the K123R mutant, there was an overlap of 151 genes. This suggests that most genes are influenced in an independent manner by H2Bub and H3K36me. Surprisingly, although consistent with previous findings, only 4 genes were commonly upregulated in all three mutants. Thus, loss of either H2Bub or H3K36me has a greater effect on gene activation at diauxie than loss of both modifications together. Furthermore, most of the genes downregulated in the absence of either H3K36me or H2Bub are unaffected when both PTMs are absent.

These findings highlight that although most gene regulation by each PTM is distinct, there are a small subunit of genes subject to positive regulation by both PTMs acting together. However, the data also suggests that the downregulation of transcription seen at the majority of gens in each single mutant is mediated by the negative action of the remaining histone modification. This suggests the PTMs can work antagonistically at the same genes.

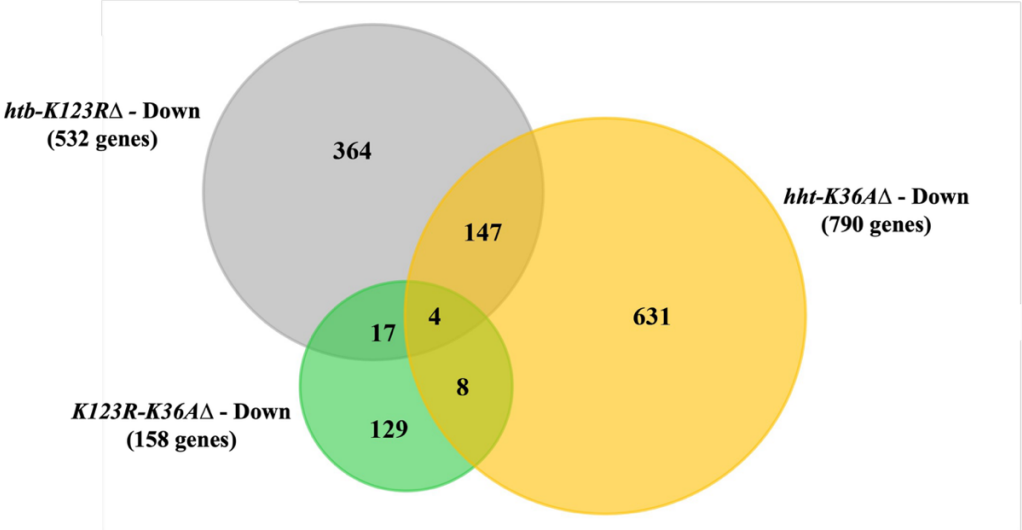


Figure 5.25: Venn diagram illustrating the overlap and uniqueness of upregulated genes among the three mutant strains compared to the wild type. The diagram quantifies the number of genes that are uniquely down regulated in each mutant *htb-K123R*Δ, *hht-K36A*Δ, and the combined *K123R-K36A*Δ and those that are commonly upregulated across all mutants, showcasing the shared and distinct genetic responses to the mutations.

5.8 Summary

Gene expression changes were analysed in wild-type and mutant strains (*htb-K123R*Δ*, hht-K36A*Δ*,* and *K123R-K36A*Δ*)* during the diauxic shift (Dix). The highest number of upregulated genes among the mutants was seen in the *hht-K36A*Δ mutant which had 513 upregulated genes. Conversely, the highest number of genes downregulated at diauxie was seen in the *htb-K123R*Δ mutant with 790 down regulated genes. This suggests that H3K36me plays the greatest role in gene repression at diauxie while H2Bub plays there greatest role in promoting gene transcription at diauxie.

GO analysis of the upregulated genes revealed distinct biological processes affected in each mutant. In the *htb-K123R*Δ mutant, significant changes were observed in processes like ascospore wall assembly, checkpoint signalling, and DNA damage response. The *hht-K36A*Δ mutant showed notable changes in ribosome biogenesis, DNA repair, and tRNA nucleoside ribose methylation. The *K123R-K36A*Δ double mutant exhibited upregulation in mitochondrial

inner membrane, replication fork processing, and nitrogen compound transport. This suggest unique roles for each PTM upon gene transcription and cell function occurs at diauxie.

The Venn diagram analysis of genes upregulated at diauxie confirmed largely unique gene expression changes among the mutants. However, most strikingly, only 2 genes were commonly upregulated in all three mutants. These findings emphasize the complex interplay between H2Bub and H3K36me for gene repression during the diauxic shift.

GO analysis of the genes down regulated in the mutants compared to wild-type, again suggested distinct roles for the PTMs in their positive influence upon transcription during diauxie. Furthermore, it was also shown that the overlap in genes down regulated in the *hht-K36A*Δ and *htb-K123R*Δ mutants was not very large, again suggesting that they act to promote gene transcription in a largely independent manner.

However, the fact that there was only a 4 gene overlap in the genes commonly down regulated in all three mutants suggests a complex interplay is occurring between H3K36me and H2Bub at diauxie such that each PTM seems to be having an opposing influence upon gene transcription when in the absence of the other modification.

5.9 Gene Expression Changes in Day-7 Quiescent Cells

The gene expression changes in purified day 7 quiescent (Q) of wild-type and mutant strains, *htb-K123R*Δ*, hht-K36A*Δ, and *K123R-K36A*Δ was determined via analysis of RNA-Seq data. Using a threshold of Log2 fold change ≥ 1 and an adjusted p-value ≤ 0.01 the significantly up- and downregulated genes were identified (Table 5.15). The *htb-K123R*Δ mutant exhibited 305 upregulated genes, the *hht-K36A*Δ mutant had 665 upregulated genes, and the double mutant *K123R-K36A*Δ showed 401 upregulated genes. These results showed that the removal of H3 K36me in the *hht-K36A*Δ mutant results in the highest number of upregulated genes, suggesting that H3K36me has the greatest repressive effect upon transcription in quiescent cells.

Conversely, when we examined the genes downregulated in each mutant, the *htb-K123R*Δ mutant had 366 downregulated genes, the *hht-K36A*Δ mutant showed 607 downregulated genes, and the *K123R-K36A*Δ double mutant exhibited 416 downregulated genes. These results again highlight that the *hht-K36A*Δ mutant shows the greatest number of

genes downregulated in the quiescent cells, suggesting H3K36me plays the greatest role upon gene activation during quiescence.

Therefore, overall, H3K36me is playing the greatest role upon regulating gene transcription in day 7 quiescent cells. However, as was seen in the RNA-Seq analysis at the other stages of growth, the aberrant up and down regulation of transcription seen in the H3K36A single mutant is somewhat suppressed when the *htb-K123R*Δ mutation is additionally present in the double mutant.

Quiescent cells Day 7	Upregulated	Downregulated	Total No. of Genes
***htb-K123R*Δ**	**305**	**366**	671
***hht-K36A*Δ**	**665**	**607**	1272
***K123R-K36A*Δ**	**401**	**416**	**767**

Table 5.15: Differential Gene Expression in Mutant Strains During the Quiescent Phase: Table showing the number of significantly upregulated and downregulated genes in *htb-K123R*Δ, *hht-K36A*Δ, and *K123R-K36A*Δ mutant strains compared to the wild-type strain during the exponential phase. Genes with Log2 fold change ≥ 1 and an adjusted p-value ≤ 0.01 were considered significant. The bar chart shows 305 upregulated and 366 downregulated genes for *htb-K123R*Δ, 635 upregulated and 607 downregulated genes for *hht-K36A*Δ, and 401 upregulated and 366 downregulated genes for the double mutant *K123R-K36A*Δ.

5.9.1 Analysis of genes upregulated in Mutant Strains During Quiescent Phase

The fold upregulation values of gene transcription occurring in each mutant versus wild-type, were next plotted to determine whether the different mutants affected the extent of de-repression of transcription compared to wild-type (Fig. 5.26). The results showed that the average fold upregulation of the 665 genes in the *hht-K36A*Δ mutant was significantly higher than the levels of upregulation of the 305 and 401 genes seen in the *htb-K123R*Δ and *K123R-K36A*Δ double

mutants, respectively. This suggest that not only does H3K36me repress the most genes in day 7 Q cells, this PTM exerts the greatest levels of repression upon genes compared to that achieved via H3K36me or H3K36me and H2bub combined.

Interestingly, the higher average upregulation of transcription seen in the *hht-K36A*Δ single mutant versus wild-type is lower compared to the average fold upregulation of transcription seen in the double mutant versus wild-type (Fig. 5.33). This suggests that loss of K36me on its own has a greater impact upon the extent of gene repression than that seen when both H2Bub and H3K36me are lost.

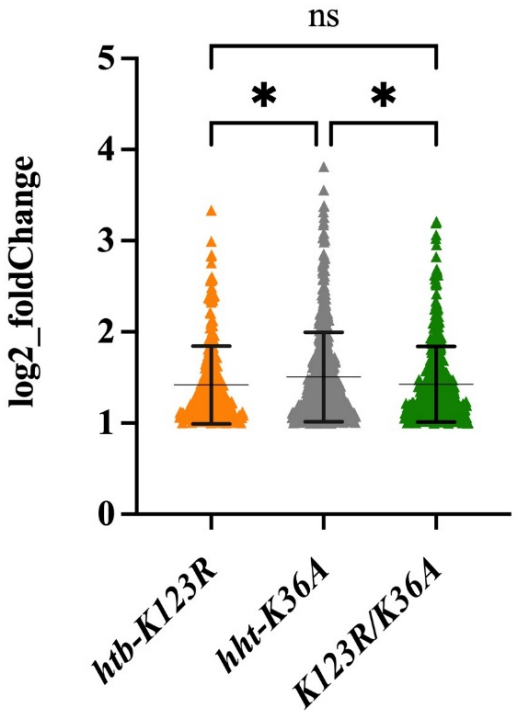


Figure 5.26: Total Genes Significantly Upregulated in Each Mutant Compared to wild-type During Quiescent Phase. The bar chart shows the number of significantly upregulated genes (Log2 fold change ≥ 1, adjusted p-value ≤ 0.01) in the *htb-K123R*Δ*, hht-K36A*Δ, and *K123R-K36A*Δ mutant strains compared to the wild-type during the quiescent phase. The *htb-K123R*Δ mutant had 372 upregulated genes, the *hht-K36A*Δ mutant had 513 upregulated genes, and the *K123R-K36A*Δ double mutant had 143 upregulated genes. (* p = 0.05, ** p = 0.01, **** p = <0.0001).

5.10 Gene Ontology (GO) Analysis of *htb-K123R*Δ Upregulated Genes

GO analysis was next used to investigate what types of genes were upregulated in the Day 7 Q cells of each mutant, providing insight into the repressive function of H2Bub and H3K36me during quiescence. The categories of upregulated genes in the *htb-K123R*Δ Q cells were enriched for those involved in mitosis, meiosis, cell division, and the cytoskeleton (Fig. 5.27A).

For example, the seven genes including *SKM1,EGT2,CBK1,* and *MYO1* are involved in septum digestion after cytokinesis (Table 5.16). 33 genes were found to be involved in Cytoskeleton organization including *GEM1,HSP42,GIN4,* and *STU1,* and 28 genes including *BUD5,RAX2,VRP1,*and *CDC9* were involved in the mitotic cell cycle. Together, this suggests an important role for H2Bub in repressing genes involved in sexual and asexual cell proliferation.

It was interesting to note that genes involved in flocculation such as *FLO9, FLO1, FLO10, FLO11* we also upregulated, suggesting H2Bub is acting to repress this stress response in Q cells.

In *htb-K123R*Δ during quiescence the upregulated cohort is enriched for programs that are ordinarily suppressed in dormant cells. This included mitosis/meiosis, cytokinesis/septum digestion, bud-site assembly, cytoskeleton organization, and flocculation. This observed pattern confirms H2Bub role in acting as a gatekeeper that restrains premature re-entry and stress-adhesion behaviours in quiescent cells.

Loss of repression of modules required for rapid morphogenesis and division readiness can be resultant of the coordinated upregulation of genes involved in septum digestion and bud-site/cytoskeletal organization (e.g., SKM1, EGT2, CBK1, MYO1). Quiescent cells in yeast are thought to remain in a balanced, low-energy state with selective capability of repair and maintenance but not of cell-cycle execution (Allen et al., 2006; De Virgilio, 2012). The observation that *htb-K123R*Δ activates these re-entry-linked modules is concomitant to reports that H2Bub supports transcriptional fidelity and prevents inappropriate activation of developmental or cell-cycle programs under restrictive conditions (Weiner et al., 2012; Braun et al., 2011). The simultaneous induction of flocculation genes (FLO1/9/10/11) shows activation of adhesion-based stress responses. Community resilience under nutrient limitation and environmental stress has been shown to be enhanced by flocculation (Verstrepen et al.,

2003; Soares, 2011). The elevation of FLO genes in *htb-K123RΔ* corroborates the findings that perturbations to histone ubiquitylation can derepress sub telomeric and stress-responsive loci (Braun et al., 2011; Weiner et al., 2015), suggesting H2Bub normally prevents cells from sticking together too tightly in deep quiescence. Taken together, these enrichments support a model in which H2Bub keeps quiescent cells into quiet-but-ready state. It suppresses high-cost transitions such as cell-cycle re-entry and adhesion, while allowing essential maintenance to proceed. This fits with other known roles of H2Bub in tuning promoter architecture, preventing cryptic transcription, and safeguarding chromatin integrity during stress and non-proliferative states (Fuchs et al., 2014; Shema et al., 2011).

The selective de-repression observed in *htb-K123RΔ,* rather than a global transcriptional surge, were similar to prior observations that loss of H2Bub induces targeted changes rather than wholesale activation (Batta et al., 2011; Weiner et al., 2012).

Category	Function	Number of Genes	Genes
GO Cellular Components	Plasma membrane	74	*BUD5, AQY3, FET5, SPO75*
	ER membrane insertion complex	9	*HSP104, SGT2, YDJ1, BST1*
	Vacuole	44	*ATG15, FET5, YFL040W, SMF3*
	Cell cortex	48	*BUD5, MMR1, VRP1, FKS1*
GO Biological Processes	Septum digestion after cytokinesis	7	*SKM1, EGT2, CBK1, MYO1*
	Protein localization to cell division site	10	*HOF1, IQG1, BSP1, MYO1*
	Cytoskeleton organization	33	*GEM1, HSP42, GIN4, STU1*
	Mitotic cell cycle	28	*BUD5, RAX2, VRP1, CDC9*

	Flocculation	28	*FLO9, FLO1, FLO10, FLO11*
GO Molecular Functions	Nucleobase transmembrane transporter activity	11	*THI7, FUR4, THI72, DAL4*
	Protein serine kinase activity	34	*RIM15, STE11, KIN3, GIN4*
	Ribonucleotide binding	81	*YFL066C, DAK2, RIM15, HSP104*

Table 5.16: List of genes up-regulated during Quiescent cells Day 7 in *htb-K123R*Δ compared to wild-type.

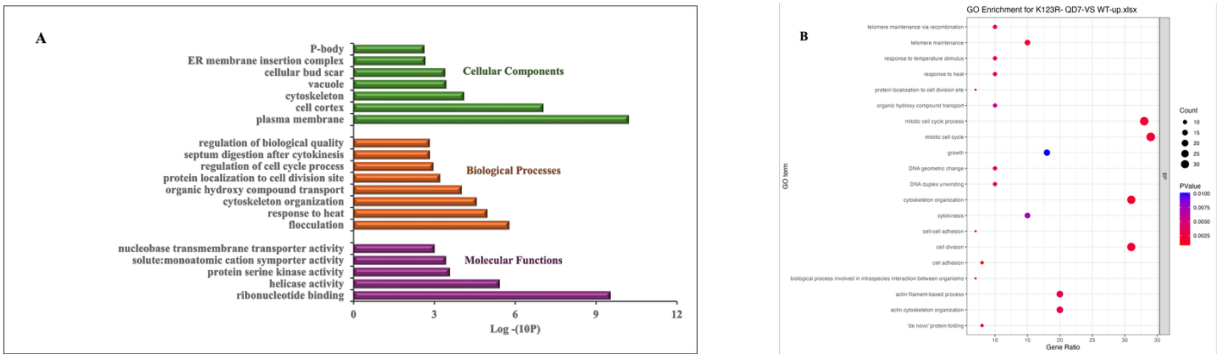


Figure 5.27: Gene Ontology (GO) analysis of upregulated genes in the *htb-K123R*Δ mutant strain. **"(A)** Bar chart (left); **(B)** Plot (right)**."** The bar graph illustrates the upregulation of various biological processes due to the *hhb-K123R*Δ mutation in (Q-D7). The x-axis represents the log (base 10) of the p-value, ranging from 0 to 12, indicating the statistical significance of the upregulation. The y-axis lists specific biological processes or molecular functions. Key upregulated processes include ER membrane insertion complex, vacuole, cell cortex, septum digestion after cytokinesis, protein localization to cell division site, cytoskeleton organization, flocculation, nucleobase transmembrane transporter activity, protein serine kinase activity, and ribonucleotide binding. The length of each bar corresponds to the degree of upregulation, with longer bars indicating more significant upregulation. This visual representation highlights the broad impact of the *htb-K123R*Δ mutation on cellular activities, providing insights into the specific processes most affected.

5.10.1 Gene Ontology (GO) Analysis of *hht-K36A*Δ Upregulated Genes

The GO analysis of upregulated genes in the *hht-K36A*Δ mutant during the quiescent phase (Q-D7) indicates significant enrichment in several cellular components which were similar to that seen in the *htb-K123R*Δ mutant (Table 5.17 and Fig. 5.28). These include the cytoskeleton (145 genes, including *BIK1,BUD3,CDC10,SYP1*), which is crucial for cell structure and movement; cellular buds (61 genes, including *BUD3,CDC10,SYP1,ACT1*), cellular bud scars (23 genes, including *BUD4,PIR1,RAX1,EGT2*), and the cytoskeleton, which are all important for cell division and growth. This suggest that, similar to H2Bub, H3K36me is repressing genes involved in cell proliferation in Q cells.

Many more genes switch on during quiescence in the *hht-K36A*Δ mutant compared to the other strains. This pattern suggests the cell is preparing to remodel and move even while resting. Genes (cytoskeleton, budding structures, actomyosin ring; for example ACT1 and CDC10) that build the cell's internal scaffolding and division machinery are elevated, even though quiescent cells usually keep these low to conserve energy (Allen et al., 2006; De Virgilio, 2012). Meanwhile, the cell's protein maintenance and repair systems become more active, which included proteasome subunits and chaperones (RPN genes, HSP104/SSA). This was consistent with the idea that losing H3K36 methylation lifts a brake that normally keeps transcription tidy and prevents unnecessary remodelling (Carrozza et al., 2005; Kaplan et al., 2003; Smolle et al., 2013).

Increase in stress-ready signals was also seen (heat and abiotic stress responses), in line with evidence that chromatin marks such as H3K36me tightly control stress programs in yeast (Weiner et al., 2012; Venkatesh et al., 2016). Together, these changes indicate that a low-energy, quiet state in quiescence is enforced by H3K36 methylation. Its loss partly releases that restraint by turning on structure-building, protein quality control, and stress preparedness ahead of growth. This may enable faster exit but at higher energy cost (Allen et al., 2006; De Virgilio, 2012; Carrozza et al., 2005; Venkatesh et al., 2016).

Category	Function	Number of Genes	Genes
GO Cellular Components	Cytoskeleton	145	*BIK1, BUD3, CDC10, SYP1*
	Cellular buds	61	*BUD3, CDC10, SYP1, ACT1*
	Cellular bud scars	23	*BUD4, PIR1, RAX1, EGT2*
	Proteasomal complex	47	*UBP6, RPN12, RPN5, RPN9*
	Cytosolic small ribosomal subunit	33	*RPS31, RPS22B, RPS29A, RPS1A*
GO Biological Processes	Cortical actin cytoskeleton organization	68	*BIK1, BUD3, CDC10, SYP1*
	Actomyosin structure organization	28	*ACT1, SHS1, CHS2, MLC1*
	Amino acid activation	56	*FRS1, NAM2, SES1, PET112*
	Protein folding	42	*HSP104, SSA2, CPR6, SSA1*

	Organelle localization	54	*BIK1, CSM1, MMM1, SED5*
	Positive regulation of organelle organization	52	*RIM1, ABP1, CDC14, SWI6*
	Response to abiotic stimulus	28	*CDC14, HSP104, SSK1, SGD1*
	Response to heat	45	*HSP104, NUP60, NUP84, HSP42*
	Regulation of cell cycle	48	*CDC39, YPI1, CDC14, SMC2*
	Microtubule polymerization or depolymerization	9	*BIK1, STU2, TUB4, SPC72*
GO Molecular Functions	Structural molecule activity	88	*CDC10, MRPL32, ACT1, TUB2*
	Structural constituent of cytoskeleton	35	*CDC10, ACT1, TUB2, TUB4*
	Protein-containing complex binding	64	*TAF2, ABP1, BLM10, UBP6*
	Phospholipid binding	28	*CDC10, PEP3, MMR1, CDC3*
	Protein-folding chaperone binding	14	*HSP104, JAC1, BTN2, ZUO1*

Table 5.17: List of genes up-regulated during Quiescent cells Day 7 in *hht-K36A*Δ compared to wild-type.

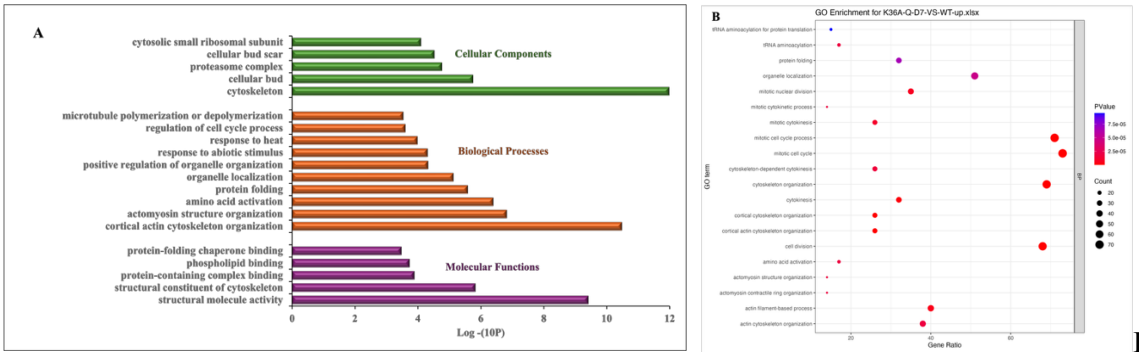


Figure 5.28: Gene Ontology (GO) analysis of upregulated genes in the *hht-K36A*Δ mutant strain. "(A) Bar chart (left); **(B)** Plot (right)**."** The bar graph illustrates the upregulation of various biological processes due to the *hht-K36A*Δ mutation in quiescent phase (Q-D7). The x-axis represents the log (base 10) of the p-value, ranging from 0 to 12, indicating the statistical significance of the upregulation. The y-axis lists specific biological processes or molecular functions. Key upregulated processes include cytosolic Small Ribosomal Subunit, Protein Folding Chaperone Binding, Response to Heat and Abiotic Stimulus,

Structural Constituent of Cytoskeleton, Microtubule Polymerization and Regulation of Cell Cycle Process. The length of each bar corresponds to the degree of upregulation, with longer bars indicating more significant upregulation. This visual representation highlights the broad impact of the *hht-K36A*Δ mutation on cellular activities, providing insights into the specific processes most affected.

5.10.2 Gene Ontology (GO) Analysis of *K123R-K36A*Δ Upregulated Genes

The GO analysis for the upregulated genes in the *K123R-K36A*Δ double mutant during the quiescent phase indicates significant enrichments in the proteasome complex (e.g *RPN11,UBP6,RPN12, and RPN5*), which are crucial for protein degradation, and in metabolism (table 5.18 and Fig. 5.29).

For example, 125 genes involved in the carboxylic acid catabolic process which is crucial for breaking down carboxylic acids were upregulated in the double mutant Q cells, while genes involved in the nucleoside bisphosphate metabolic process (21 genes,) and nucleotide metabolic process (58 genes,) which are essential for nucleotide synthesis and energy production, also required both H2Bub and H3K36me for repression. Furthermore, genes involved in the tricarboxylic acid cycle were also de-repressed in the double mutant.

Thus, these data suggest a key role for H3K36me and H2Bub, potentially acting together, is in downregulating unnecessary protein degradation and metabolism.

The genes that turn on in quiescence in the *K123R-K36A*Δ double mutant, point to a shift toward cleanup and energy production rather than building new cell structures. More proteasome components (e.g., RPN11, UBP6) and metabolism pathways were switched on. The metabolic pathways included carboxylic acid breakdown, the TCA cycle, and reactive oxygen species handling, as well as nucleotide/nucleoside phosphate metabolism.

This indicates that the cell is favouring protein quality control and central carbon metabolism to keep itself stable while resting.

Proteasome and stress-clearance programs in yeast are tightly regulated by chromatin marks, including H2B ubiquitylation and H3K36 methylation. They help tune transcription according to growth state (Carrozza et al., 2005; Weiner et al., 2012; Venkatesh et al., 2016). Cells often

rewire toward catabolism and redox balance to manage increased proteome turnover and stress by-products when both marks are lost (Smolle et al., 2013; Fuchs et al., 2014). The double mutant's focus on energy generation and cleanup implies a compensatory route that stabilizes quiescence through housekeeping rather than preparing for growth (De Virgilio, 2012; Allen et al., 2006). This was in contrast to the *hht-K36A*Δ single mutant, which broadly turns on structural and proteostasis programs. Overall, H2Bub and H3K36me normally act together to keep metabolism and protein turnover at a low, steady level in quiescence. The balance toward catabolic metabolism and proteasome activity is tilted when both marks are removed, likely helping the cell cope with stress while delaying costly rebuilding (Carrozza et al., 2005; Venkatesh et al., 2016).

Category	Function	Number of Genes	Genes
GO Cellular Components	Proteasome complex	25	*RPN11, UBP6, RPN12, RPN5*
	Proteasome core complex	11	*PRE7, SCL1, PUP2, PRE3*
	Cortical cytoskeleton	19	*LSB5, ABP1, SPA2, ARP2*
	Actomyosin contractile ring	15	*SPA2, MLC1, BUD4, CAP2*
	Ribosome	14	*YCP4, PST2, PIL1, YGR130C*

	Proteasome regulatory particle, lid subcomplex	7	*RPN11, RPN12, RPN5, RPN6*
	Glycine cleavage complex	4	*LPD1, GCV3, GCV1, GCV2*
GO Biological Processes	Carboxylic acid catabolic process	125	*CHA1, LPD1, ECI1, CAR2*
	Nucleoside bisphosphate metabolic process	21	*PCD1, ACS1, CAB5, CAB1*
	Nucleotide metabolic process	58	*PPR1, PCD1, IDP2, URA4*
	Tricarboxylic acid cycle	27	*IDP2, MDH3, LSC2, SDH9*
	Reactive oxygen species metabolic process	21	*LPD1, FBP1, CTA1, CTT1*
	Negative regulation of protein localization to the nucleolus	24	*BNS1, TEM1, CDC5, SPO12*
GO Molecular Functions	Oxidoreductase activity	52	*MXR2, YCP4, LPD1, LOT6*
	Oxidoreductase activity (acting on NAD(P)H, quinone, etc.)	9	*YCP4, LOT6, NDE2, PST2*
	Lipid binding	25	*PEP3, TFS1, MMR1, UPS1*
	Protein phosphatase regulator activity	19	*CDC48, SHP1, GIP1, REG2*
	Formate dehydrogenase (NAD+) activity	12	*FDH1, FDH2, YPL276W, IDP2*
	Polyubiquitin modification-dependent protein binding	21	*CDC48, SHP1, CUE5, DSK2*
	Oxidoreductase activity (acting on CH-NH_2 group of donors)	4	*ETR1, ZTA1, YML131W, SPS19*

Table 5.18: List of genes up-regulated during Quiescent cells Day 7 in *K123R-K36A*Δ compared to wild-type.

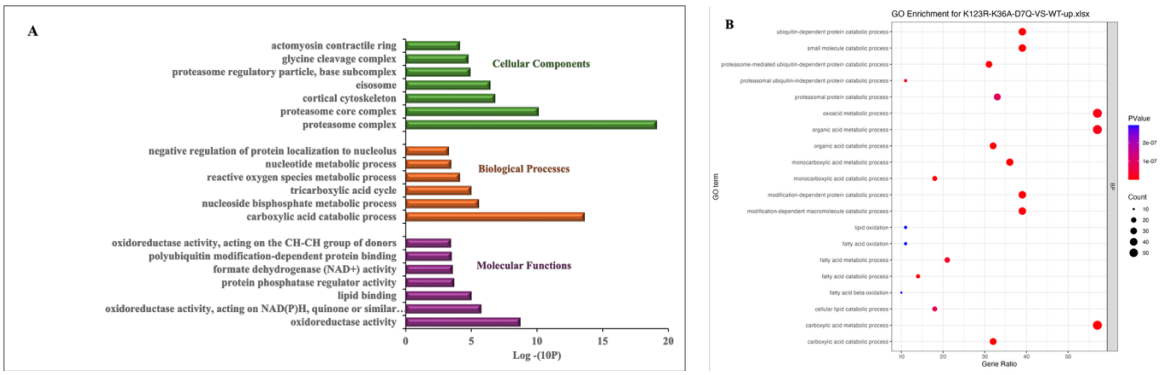


Figure 5.29: Gene Ontology (GO) analysis of upregulated genes in the combined *K123R-K36A*Δ mutant strain. "(A) Bar chart (left); **(B)** Plot (right)**."** This figure illustrates the significantly upregulated biological processes in the *K123R-K36A*Δ double mutant during quiescent phase (Q-D7). The processes are represented by bars, with the length of each bar corresponding to the -Log (P) value, indicating the level of statistical significance. The most prominently upregulated processes include the actomyosin contractile ring, glycine cleavage complex, proteasome regulatory particle (base subcomplex), ribosome, cortical cytoskeleton, and proteasome core complex. These processes are crucial for various cellular functions such as cell division, metabolism, protein degradation, membrane organization, and maintenance of cell structure. The data highlights the extensive changes in cellular structure, protein turnover, and metabolic activities in the *K123R-K36A*Δ double mutant during this growth phase.

5.10.3 Venn Diagram Analysis of upregulated Genes

A Venn diagram of the genes upregulated in each of the three mutants versus wild-type during quiescence, was next prepared (Fig. 5.30). the Venn diagram revealed that of the 401 gene upregulated in the *htb-K123R*Δ mutant, over half of these genes were only upregulated in this mutant. In the *hht-K36A*Δ mutant almost 500 of the 665 upregulated genes were unique to this mutant. Finally in the *K123R-K36A*Δ double mutant, 208 of the 305 upregulated genes were only upregulated in the absence of both H2Bub and H3K36me. Thus, the mutants showed largely unique repression of genes during quiescence.

Furthermore, although the *htb-K123R*Δ and *hht-K36A*Δ single mutants shared 149 upregulated genes, there was only an overlap of 39 genes between all three mutants. These findings highlight that distinct genes are subject to repression by H2Bub and H3K36me in Q cells and demonstrate

that the absence of both modifications has less of an impact upon gene repression in Q cells than absence of either modification on its own.

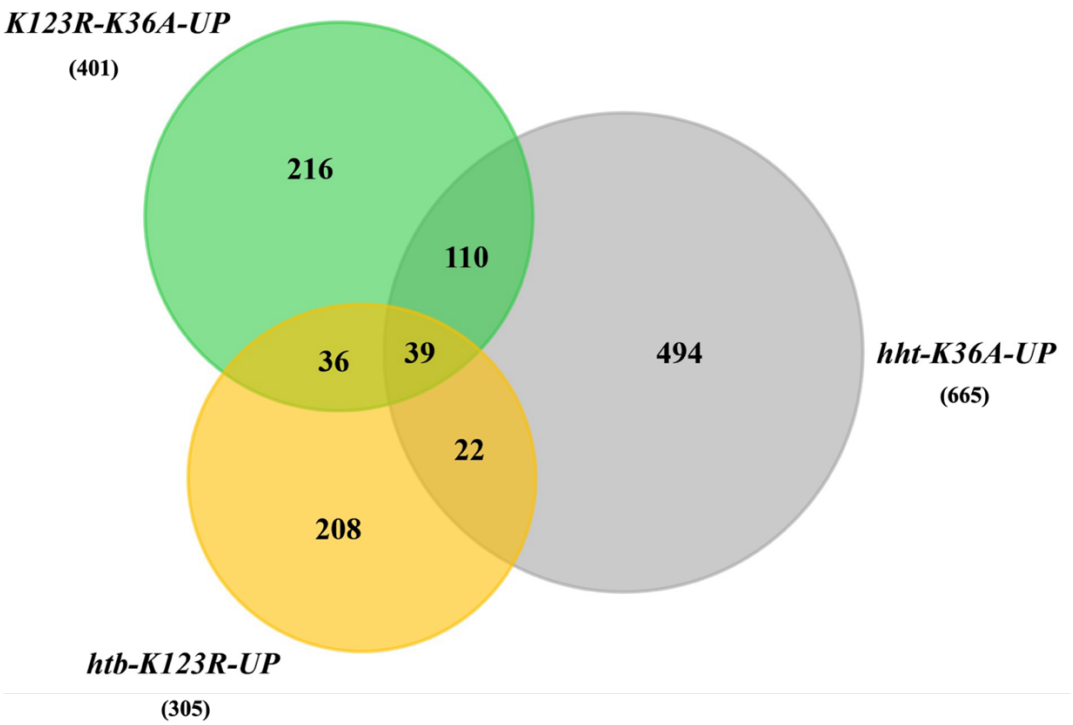


Figure 5.30: Venn diagram illustrating the overlap and uniqueness of upregulated genes among the three mutant strains compared to the wild type. The diagram quantifies the number of genes that are uniquely upregulated in each mutant *htb-K123R*Δ*,* *hht-K36A*Δ, and the combined *K123R-K36A*Δ and those that are commonly upregulated across all mutants, show casing the shared and distinct genetic responses to the mutations.

5.11 Analysis of genes downregulated in day-7 quiescent cells

The genes downregulated in the mutants versus wild-type in day 7 quiescent cells, were next analysed. As described before, 366 genes were significantly downregulated in the *htb-K123R*Δ mutant, 607 in the *hht-K36A*Δ mutants, and 416 were downregulated in the *K123R-K36A*Δ double mutant, which lacks both H2Bub and H3K36me (Table. 5. 15). These downregulated genes represent those genes normally subject to activation by the relevant modification in wild-type.

Initial analysis of the average fold decrease in transcription of the genes downregulated in each mutant revelated no significant difference suggesting the impact of H3K36me and H2Bub on positively regulating target gene transcription in Q cells, was the same for each PTM (Fig. 5. 31).

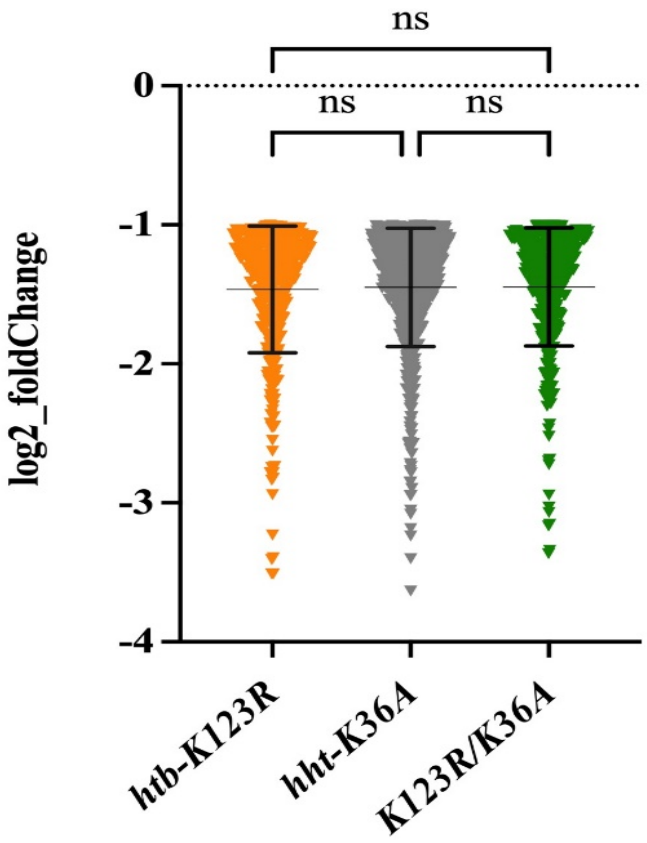


Figure 5.31: Total Genes Significantly Downregulated in Each Mutant Compared to wild-type During Quiescent Phase. The bar chart shows the number of significantly downregulated genes (Log2 fold change ≥ 1, adjusted p-value ≤ 0.01) in the *htb-K123R*Δ, *hht-K36A*Δ, and *K123R-K36A*Δ mutant strains compared to the wild-type during the (Q- D7). The *htb-K123R*Δ mutant had 366 downregulated genes, the *hht-K36A*Δ mutant had 607 downregulated genes, and the *K123R-K36A*Δ double mutant had 366 downregulated genes.

5.11.1 Gene Ontology (GO) Analysis of *htb-K123R*Δ downregulated Genes

GO analysis of the genes downregulated in the *hhb-K123R*Δ mutant during the quiescent phase (Q- D7) was dominated by a high enrichment of nucleolar genes suggesting a role for H2Bub

in promoting ribosome biogenesis. Also of note were the enrichment of 27 genes involved in centromeric chromatin condensation suggesting a role for H2Bub in promoting chromatin compaction at centromeres in Q cells (Table 5.19 and Fig. 5.32). Additionally, processes such as tubulin complex assembly (3 genes, *YKE2,GIM3,CIN2*) and phosphatidylethanolamine metabolic process (3 genes, *CKI1,UPS2,EPT1*) were downregulated , suggesting H2Bub could impact cytoskeletal dynamics and membrane lipid metabolism during quiescence.

The downregulation of genes involved in protein N-linked glycosylation (7 genes) and those involved in the positive regulation of protein ubiquitination points to a role for H2Bub in regulating protein modification and protein degradation during quiescence.

Finally, it was interesting to note that genes involved in DNA repair mechanisms were enriched, such as *RAD55*, suggesting H2Bub may be playing an active role in potential on-going DNA damage repair during quiescence.

Overall, these findings highlight a focussed role for H2Bub on some essential molecular functions, such as rRNA production and possible ribosome maintenance, chromatin condensation, and DNA damage repair, within the quiescent cell.

Many genes that go down in quiescence in the *htb-K123R*Δ mutant, are tied to the nucleolus and snoRNPs (ribosome biogenesis), centromere chromatin condensation, and DNA repair, with additional effects on cytoskeleton and membrane-related pathways. This means H2B ubiquitylation usually helps cells stay in good shape while resting. It keeps a steady level of rRNA and snoRNA production, maintains the structure of the nucleolus, keeps centromeric DNA tightly packed, and ensures the cell is ready to fix damage if needed. (Allen et al., 2006; De Virgilio, 2012). Previous research have shown that H2Bub promotes proper transcription and chromatin structure, which can be important for housekeeping functions in non-dividing states (Weiner et al., 2012; Fuchs et al., 2014). Also, research have shown that nucleolar and repair programs are sensitive to chromatin regulation (Braun et al., 2011; Shema et al., 2011). The decrease in these genes in *htb-K123R*Δ supports a model wherein loss of H2Bub reduces baseline ribosome maintenance and chromatin/repair support, potentially making quiescent cells less prepared to fix DNA damage or maintain genome organization (Allen et al., 2006; De Virgilio, 2012; Weiner et al., 2012).

Category	Function	Number of Genes	Genes
GO Cellular Components	Nucleolus	89	*LOC1, FYV7, RMP1, ACS2*
	Box H/ACA snoRNP complex	22	*SNR84, SNR82, SNR37, SNR42*
	U2 snRNP	15	*SMD3, PRP21, CUS1, SMB1*
	Condensed chromosome, centromeric region	27	*SCM3, CHL4, MCM21, DUO1*
GO Biological Processes	UDP-N-acetylglucosamine metabolic process	14	*GNA1, YMR084W, YMR085W, PCM1*
	NAD biosynthetic process	8	*BNA6, BNA1, NPT1, NRK1*
	Glutamate biosynthetic process	7	*IDH2, GDH1, IDH1, FUM1*
	Catabolite repression	4	*VPS36, NRG2, DAL80, MIG3*
	Tubulin complex assembly	3	*YKE2, GIM3, CIN2*
	Phosphatidylethanolamine metabolic process	3	*CKI1, UPS2, EPT1*
	Meiotic sister chromatid cohesion	8	*ECO1, CHL4, REC8, MCM21*
	Protein N-linked glycosylation	7	*ALG14, CAX4, MNN4, KTR2*
	Positive regulation of protein ubiquitination	3	*PEX22, AMA1, MAD2*
	Binding	3	*PEX21, RMI1, SNR30*
	Thiamine biosynthetic process	5	*THI13, THI4, THI11, PDC6, ALD6*
	Formate dehydrogenase (NAD+) activity	8	*FDH1, FDH2, YPL276W, LEU2*

GO Molecular Functions	Iron ion binding	6	*ERG3, GRX6, TRR1, OLE1*
	Double-stranded RNA binding	3	*HNT3, RNT1, LRP1*
	Oxidoreductase activity (paired donors, oxygen incorporation)	6	*ERG3, OLE1, YHB1, YJR154W*
	Mismatched DNA binding	5	*MSH4, MLH2, HNT3, RAD55, RMI1*

Table 5.19: List of genes commonly down-regulated during Quiescent cells Day 7 in htb-*K123R*Δ compared to wild-type.

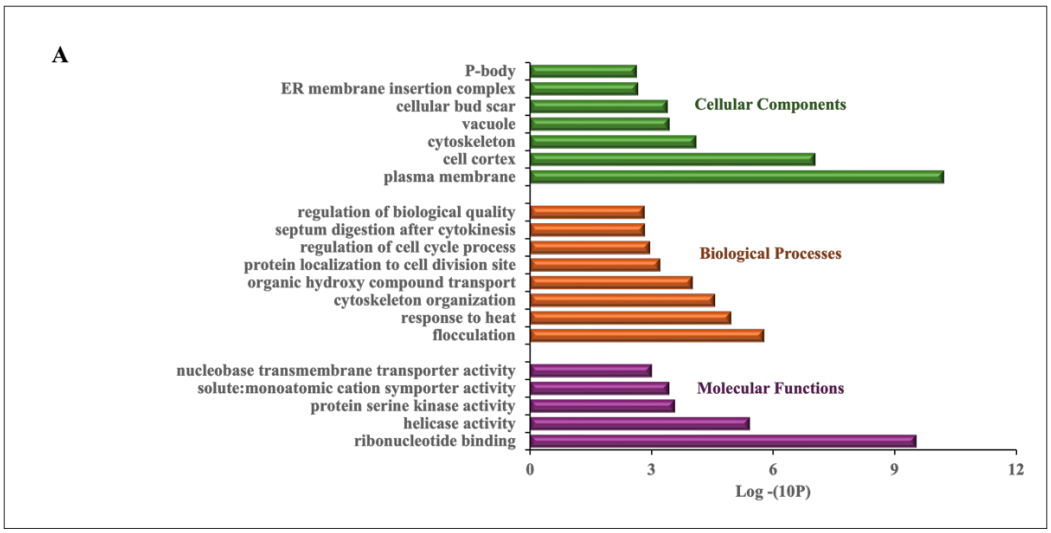


Figure 5.32: Gene Ontology (GO) analysis of downregulated genes in the *htb-K123R*Δ mutant strain. "(A) Bar chart." The figure presents the GO analysis of upregulated genes in the *htb-K123R*Δ mutant during the quiescent phase. The bar graph depicts the negative logarithm (base 10) of the p-value (Log -p (10P)) for various biological processes and molecular functions, with taller bars indicating higher significance levels. Key upregulated processes include the condensed chromosome, centromeric region, box H/ACA snoRNP complex, and thiamine biosynthetic process, positive regulation of binding, protein N-linked glycosylation, meiotic sister chromatid cohesion, and phosphatidylethanolamine metabolic process. Other notable upregulated functions are tubulin complex assembly, catabolite repression, glutamate biosynthetic process, NAD biosynthetic process, UDP-N-acetylglucosamine metabolic process, mismatched DNA binding, oxidoreductase activity acting on paired donors, double-stranded RNA binding, iron ion binding, and formate dehydrogenase (NAD+) activity.

5.11.2 Gene Ontology (GO) Analysis of *hht-K36A*Δ downregulated Genes

The GO analysis of genes downregulated in the *hht-K36A*Δ mutant during the quiescent phase (Q-D7) revealed significant alterations in various biological processes, molecular functions, and cellular components. In the cellular components category the significant go terms enriched were for genes involved in the plasma membrane (91 genes) and the vacuole (83 genes).

In the biological process category the GO terms significantly enriched were in monocarboxylic acid metabolic process (72 genes) and response to chemical stress (66 genes).

In the molecular functions category the GO terms significantly enriched were for transmembrane transporter activity (111 genes), and oxidoreductase activity (54 genes, *PDI1,TRX3,YCR102C,AAD3*),

These downregulation of transcription highlight the positive impact of H3K36me on key cellular structures such as the plasma membrane and vacuole. The analysis also highlights disruptions caused by loss of H3K36me in critical biological processes including responses to chemicals and various metabolic pathways. Overall, these findings provide insight into the role of H3K36me in Q cells and a view of the molecular and cellular disruptions which occur in the absence of this important PTM (Table 5.20 and Fig. 5.33).

In the *hht-K36A*Δ mutant, many genes that were downregulated in quiescence are related to how the cell interacts with its surroundings, plasma membrane and vacuole components, a wide range of transporters (including xenobiotic, ion, and organic anion transport), and several oxidoreductases. These systems are kept ready by quiescent cells to sense nutrients, manage ions, store and recycle materials, and handle chemical stress (Allen et al., 2006; De Virgilio, 2012). It has been shown through previous studies that H3K36 methylation supports accurate transcription across gene bodies, helps tune metabolic and stress-responsive programs thus preventing inappropriate shutdown or activation (Carrozza et al., 2005; Venkatesh et al., 2016; Weiner et al., 2012). The fact that H3K36me is needed to maintain a baseline capacity for uptake, detoxification, and ion homeostasis during dormancy, while also supporting redox balance through oxidoreductases is suggested by the coordinated decrease of membrane/vacuole and transporter genes in *hht-K36A*Δ (Carrozza et al., 2005; Weiner et al., 2012). In simple terms, without H3K36me, the cell seems worse at bringing in supplies,

handling stress, and saving up resources. At the same time, other genes show signs of being ready to reorganize inside. This mismatch could make it harder for the cell to adapt when things change (Allen et al., 2006; De Virgilio, 2012; Venkatesh et al., 2016).

Category	Function	Number of Genes	Genes
GO Cellular Components	Plasma membrane	91	*AGP1, GIT1, ALR2, FET5*
	Vacuole	83	*DFP3, GIT1, FET5,*
GO Biological Processes	Ribonucleoside diphosphate catabolic process	72	*CDC19, TPI1, PGI1, PFK1, ENO1*
	Response to oxygen-containing compound	29	*PDI1, SFA1, RGT2, SSY1*
	Generation of precursor metabolites and energy	36	*GSY1, PDC1, SHH4, CDC19*
	Cellular aldehyde metabolic process	42	*AAD3, SNO3, SNZ3, SFA1*
	Monocarboxylic acid metabolic process	72	*PDC1, TML25, CDC19, TPI1*
	Response to chemical	66	*PDI1, TRX3, YCR102C, RDS1*
	Cellular response to nutrient levels	33	*FET5, ASP3-1, ASP3-2, ASP3-3*
	Transition metal ion transport	40	*ET5, FRE8, CCC1, PET9*
	Organophosphate metabolic process	66	*SNO3, SNZ3, ICT1, GAB1*
GO Molecular Functions	Transmembrane transporter activity	111	*AGP1, GIT1, ALR2, HXT10*
	Carbohydrate binding	34	*EMP46, FLO9, FLO1, RGT2*
	Oxidoreductase activity	54	*PDI1, TRX3, YCR102C, AAD3*

	Transferase activity (alkyl or aryl groups, other than methyl)	28	*SAM1, RAM1, ARO3, SAM2*
	Organic anion transmembrane transporter activity	27	*AGP1, GIT1, SEO1, FLC2*
	Inorganic anion transmembrane transporter activity	9	*OAC1, FEX1, SYG1, ATR1*
	ABC-type xenobiotic transporter activity	14	*SNQ2, YOR1, PDR5, PDR18*
	DNA-binding transcription factor activity	43	*RDS1, PDR8, STP4, NRG1*
	Antiporter activity	12	*TPO1, NHA1, PET9, GDT1*

Table 5.20: List of genes down-regulated during Quiescent cells Day 7 in *hht-K36A*Δ compared to wild-type.

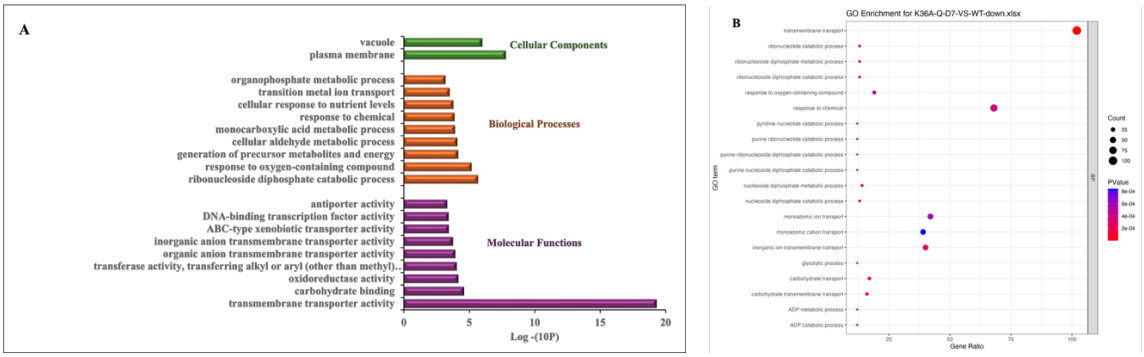


Figure 5.33: Gene Ontology (GO) analysis of downregulated genes in the *hht-K36A*Δ mutant strain. "(A) Bar chart (left); **(B)** Plot (right)**."** The bar graph illustrates the significance of various GO terms, measured as -Log10(P), with higher bars indicating more significant changes. The y-axis lists the affected biological processes, molecular functions, and cellular components, including vacuole, organic anion transmembrane transport, and DNA-binding transcription factor activity. The bars are color-coded: orange for biological processes, green for cellular components, and blue for molecular functions. This analysis highlights the broad impact of the *hht-K36A*Δ mutation on cellular metabolism and gene regulation mechanisms during quiescent phase.

5.11.3 Gene Ontology (GO) Analysis of *K123R-K36A*Δ downregulated Genes

The GO analysis of the downregulated genes in the *K123R-K36A*Δ mutant during the quiescent phase revealed significant alterations in various biological processes, molecular functions, and cellular components. In the cellular components category, the significant go terms enriched were involved in the endoplasmic reticulum (76 genes). In the biological process category the GO terms significantly enriched were involved in the small molecule biosynthetic process (66 genes). In the molecular functions category the GO terms significantly enriched were for transmembrane transporter activity (101 genes*).*

Thus, the genes downregulated in the absence of both H2Bub and H3K36me were fewer in number, and less diverse in function, than when either H3K36me or H2Bub were absent on their own. Specifically, the double mutation appears to impact the cell's transport mechanisms, as well as its ability to synthesize small molecules and manage ion homeostasis. These alterations could potentially compromise the cell's structural integrity and overall functionality, highlighting the broad and significant impact of the *K123R-K36A*Δ mutation on cellular health during the quiescent phase (Table 5.21 and Fig. 5.34).

The genes that were downregulated in the *K123R-K36A*Δ double mutant during quiescence mostly affect the cell's core infrastructure. Endoplasmic reticulum and storage vacuole functions, many classes of membrane transporters, and several small-molecule biosynthesis pathways, including glycolysis and ion homeostasis are included represents this change. These systems are kept at a steady baseline by quiescent cells to fold and traffic proteins, store and recycle materials, move nutrients and ions, and make essential metabolites when needed (Allen et al., 2006; De Virgilio, 2012). Previous research have shown that H2B ubiquitylation and H3K36 methylation help maintain accurate transcription and balanced metabolism in non-dividing states. This help in preventing inappropriate shutdown of maintenance programs (Carrozza et al., 2005; Weiner et al., 2012; Venkatesh et al., 2016). The corresponding decrease of ER, vacuole, transporter activity, and small-molecule biosynthesis in the double mutant are indicative of the fact that, without both marks, the cell reduces its supply lines and factory capacity while resting. Thus, impairing its ability to import, process, and synthesize what it needs (Carrozza et al., 2005; Fuchs et al., 2014).

Category	Function	Number of Genes	Genes
GO Cellular Components	Storage vacuole	55	*DFP3, GIT1, COS4, EMP70*
	Endoplasmic reticulum	76	*AGP1, EMC6, AQY2, ERG3*
	Side of membrane	43	*AFB1, CCW12, YPS1, YPS3*
GO Biological Processes	Small molecule biosynthetic process	66	*LEU2, PGK1, ERG3, PDC5*
	Inorganic ion homeostasis	27	*EMP70, TIS11, NHA1, FRE1*
	Ubiquitin-dependent protein catabolic process via MVB sorting pathway	17	*COS4, COS7, UBC4, COS2*
	Glycolytic process	30	*PGK1, TPI1, HXK2, TDH3*
	Sodium ion transport	8	*NHA1, ENA2, ENA1, PHO89*
	Carbohydrate derivative metabolic process	34	*PGK1, TPI1, IPT1, APT2*

	Cell wall biogenesis	15	*OSW2, LDS1, FLC2, DTR1*
GO Molecular Functions	Transmembrane transporter activity	101	*AGP1, GIT1, QCR6, YLL053C*
	Organic anion transmembrane transporter activity	24	*AGP1, GIT1, FLC2, UGA4*
	Secondary active transmembrane transporter activity	22	*NHA1, UGA4, AAC3, GDT1*
	Iron ion binding	27	*ERG3, GRX6, TRR1, OLE1*
	Inorganic molecular entity transmembrane transporter activity	35	*QCR6, YLL053C, AQY2, ZRT2*
	snoRNA binding	24	*NOP56, UTP6, UTP8, NOP58*
	Glycosyltransferase activity	15	*IPT1, APT2, GPI18, ALG14*
	Nucleobase-containing compound transmembrane transporter activity	9	*FLC2, GGC1, AAC3, VRG4*
	Oxidoreductase activity	34	*HBN1, LEU2, AAD6, QCR6*
	Water transmembrane transporter activity	6	*YLL053C, AQY2, AQY1, MEP1*

Table 5.21: List of genes down-regulated during Quiescent cells Day 7 in *K123R-K36A*Δ compared to wild-type.

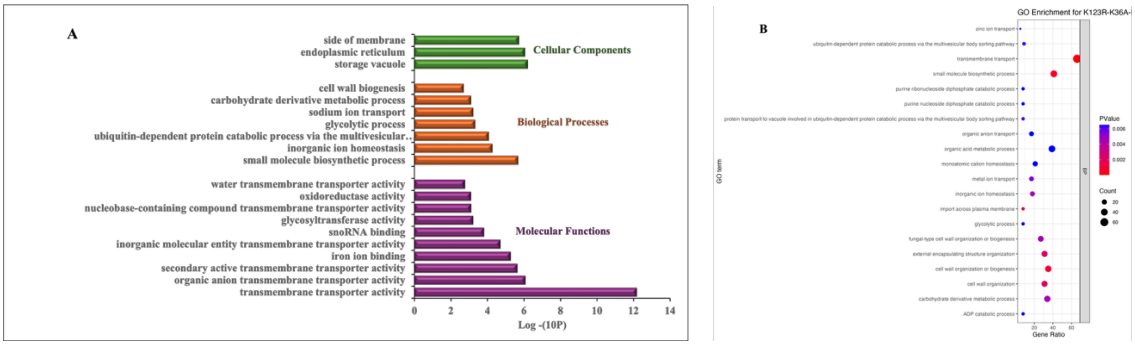


Figure 5.34: Gene Ontology (GO) analysis of downregulated genes in the *K123R-K36A*Δ mutant strain. "(A) Bar chart (left); **(B)** Plot (right)**."** The bar graph illustrates the GO analysis results, highlighting the degree of downregulation in various biological processes, cellular components, and molecular functions. The x-axis represents the -Log10(P) values, indicating the significance of downregulation, while the y-axis lists the specific GO terms. Orange bars denote biological processes,

green bars represent cellular components, and blue bars indicate molecular functions. Notable downregulated processes include siderophore metabolic process, side of membrane, storage vacuole, carbohydrate derivative biosynthetic process, and cell wall biogenesis. Significant molecular functions affected include oxidoreductase activity acting on paired donors with incorporation or reduction of molecular oxygen and iron ion binding. This analysis provides insights into the functional impacts of the *K123R-K36A*Δ mutations on cellular activities during the quiescent phase.

5.11.4 Venn Diagram Analysis of downregulated Genes

A three-way Venn diagram of the genes downregulated in each of the three mutants, was next prepared to identify any commonly downregulated genes (Fig. 5.35). The data revealed that the *htb-K123R*Δ mutant exhibited 227 uniquely down-regulated genes, *hht-K36A*Δ exhibited 445 uniquely downregulated genes, whist *K123R-K36A*Δ exhibited 168 uniquely down-regulated genes. Importantly, only 29 genes were commonly downregulated in the quiescent cells of all three mutants.

These findings highlight the predominantly distinct genes subject to activation by H2Bub and H3K36me with very few genes subject to co-regulation by both PTMs working together.

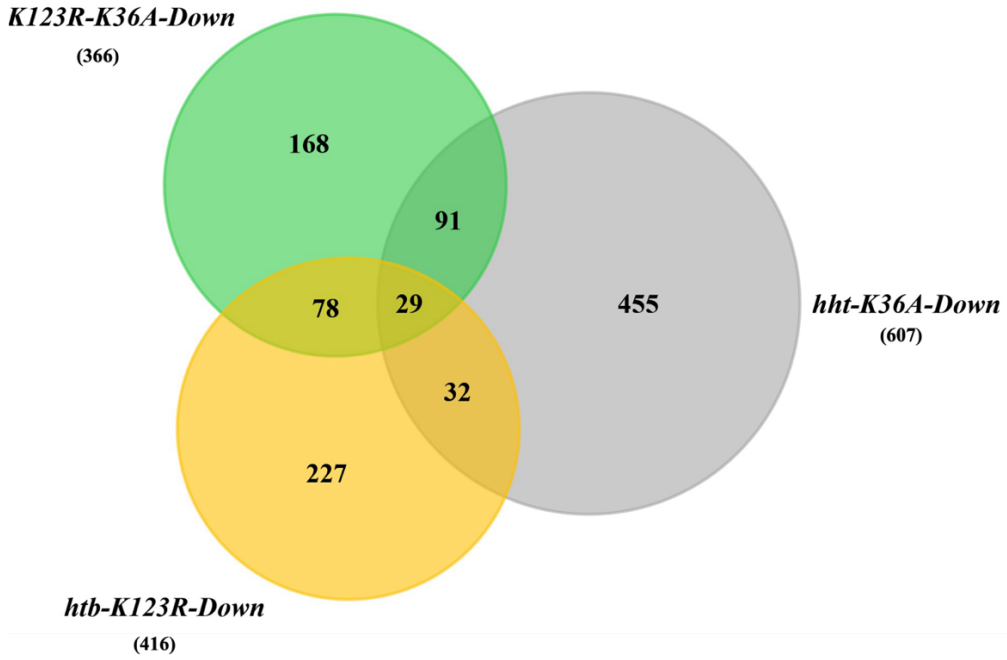


Figure 5.35: Venn diagram illustrating the overlap and uniqueness of downregulated genes among the three mutant strains compared to the wild type. The diagram quantifies the number of genes that are uniquely down regulated in each mutant *htb-K123R*Δ*, hht-K36A*Δ, and the combined *K123R-K36A*Δ and those that are commonly downregulated across all mutants, show casing the shared and distinct genetic responses to the mutations.

5.12 Summary

The study analysed gene expression changes in wild-type and mutant strains *htb-K123R*Δ*, hht-K36A*Δ*,* and *K123R-K36A*Δ during the quiescent Phase (Q- D7). The *htb-K123R*Δ mutant had 305 upregulated and 366 downregulated genes, the *hht-K36A*Δ mutant had 665 upregulated and 607 downregulated genes, and the *K123R-K36A*Δ double mutant had 401 upregulated and 366 downregulated genes. These results indicate that the modifications significantly affect gene transcription both positively and negatively in day-7 Q cells, with *hht-K36A*Δ showing the highest number of upregulated and downregulated genes suggesting the greater role for H3K36me in regulating gene transcription in these cells. Overall, the analysis also revealed minimal overlaps between the genes up and downregulated in the mutants, although some up and down regulated genes were common to all mutants, suggesting common pathways or regulatory mechanisms affected by the mutations were apparent.

Gene Ontology (GO) analysis showed significant enrichment in various cellular components and biological processes for each mutant. For instance, the *htb-K123R*Δ mutant showed enrichment in plasma membrane and cytoskeleton organization, while the *hht-K36A*Δ mutant showed enrichment in cytoskeleton and protein processing. The *K123R-K36A*Δ double mutant showed enrichment in proteasome complex and carboxylic acid catabolic process. Also of note was the fact that genes involved in DNA repair and chromatin compaction were downregulated in the *htb-K123R*Δ mutants suggesting a role for H2Bub in transcribing DNA repair mechanism-related genes in quiescent cells and contributing to potential compaction of the genome. Considering that quiescent cells are proposed to be largely dormant, this might suggest that they still retain the ability to repair DNA damage and that H2Bub is of importance in mediating this effect. Thus, these data suggest distinct roles for the PTMs in Q cells that could contribute to maintaining the integrity of these cells as they sit out of the cell cycle.

In common with what was seen from the transcription data of the mutants at the other growth stages, the double mutant showed a largely unique cohort of genes that were up and down regulated compared to what was seen in either single mutant. This again could suggest that H2Bub and H3K36me could compensate for the loss of each other such that in the absence of both modifications this compensation is lost resulting in a distinct cohort of genes being altered in their transcription.

5.13 Discussion

This study delineates how transcription across yeast growth phases, exponential, diauxic shift, and day-7 quiescence is reprogrammed by the loss of histone H2B monoubiquitylation (H2Bub; *htb-K123RΔ),* loss of histone H3K36 methylation (H3K36me; *hht-K36AΔ),* and their combined loss (*K123R-K36AΔ).* RNA integrity numbers (RIN) above 6.5 showed comprehensive quality control. Principal component analysis (PCA) showing clear separation by strain and phase. The distinct PCA separation observed in quiescent samples highlights extensive chromatin and metabolic reprogramming in stationary-phase (Gasch et al., 2000; De Virgilio, 2012). It also supports the fact that these post-translational histone marks act as phase-sensitive regulators of global gene expression. Across phases, three simple patterns emerged. First, the widest effect was seen by the loss of H3K36me which broadly de-represses genes while biosynthetic programs, especially in exponential and quiescent cells was weakened. Second, a more focused shift was seen by the loss of H2Bub, especially in the diauxic shift which showed change in transporter activity, mitochondrial/peroxisomal functions, and genome surveillance.

Third, fewer overall changes were seen in the *K123R-K36A*Δ double mutant which specifically unleashes oxidative and gluconeogenic pathways, revealing an antagonistic relationship between H2Bub and H3K36me.

It is known that H2Bub promotes RNA polymerase II elongation and modulates H3K4/H3K79 methylation via Paf1C/FACT (Sun & Allis, 2002; Pavri et al., 2006), while Set2-dependent H3K36me recruits Rpd3S to deacetylate coding regions, suppressing cryptic initiation and restraining inappropriate transcription in gene bodies (Ng et al., 2003; Keogh et al., 2005; Carrozza et al., 2005). Our results obtained by our phase-based study build on this, partly

different but overlapping programs for metabolism, transport, and biosynthesis are controlled by the two PTMs and together these PTMs buffer each other's genome-wide effects. This was consistent with complex genetic interactions seen among co-transcriptional chromatin pathways (Lenstra et al., 2011; Weiner et al., 2015).

5.13.1 Transcriptional Regulation During Exponential Phase

Upregulation: In exponential phase *hht-K36A*Δ shows the largest upregulation (482 genes), which exceeded *htb-K123R*Δ (379) and the double mutant (163). The magnitude of upregulation is greater on average in *hht-K36A*Δ than in the other strains. Gene Ontology (GO) analyses highlight enrichment for small-molecule catabolism, energy derivation by oxidation of organic compounds, transmembrane transporter activity, oxidoreductases, peroxisomal components, and ammonium transport. These results were consistent with H3K36me restricting metabolic plasticity and stress-responsive programs while preserving chromatin integrity over highly transcribed loci (Carrozza et al., 2005; Venkatesh et al., 2012).

Upregulated pathways in the *htb-K123R*Δ mutant was peroxisomal matrix, xenobiotic response, iron transport, fermentation, TCA cycle, cell adhesion/flocculation, and broad transporter classes. These upregulated pathways implicated H2Bub in dampening peroxisomal/mitochondrial metabolism and membrane transport during rapid growth.

Selective enrichment in respiratory chain components, TCA cycle, glyoxylate bypass, gluconeogenesis, carboxylic acid metabolism, and ammonium transport was seen in the *K123R-K36A*Δ double mutant, pointing to a cooperative repression by both PTMs over oxidative phosphorylation and gluconeogenic routes.

The modest overlap of upregulated genes across strains was seen in exponential phase (94 common). This indicates that H2Bub and H3K36me regulate largely distinct modules but converge on central energetic pathways, including peroxisome/mitochondria and nitrogen assimilation (DeRisi et al., 1997; Gasch et al., 2000; Conrad et al., 2014)

Downregulation: In exponential phase *hht-K36A*Δ most profound reduction in ribosome biogenesis and translation components (cytosolic large ribosomal subunits, assembly factors), tRNA methyltransferases, plasma membrane, and fungal cell wall modules, along with purine diphosphate metabolism and small-molecule biosynthesis was seen. This reduction reinforces the link between chromatin state and growth-rate–coupled biosynthetic capacity (Jorgensen et al., 2004; Venters & Pugh, 2009; Smolle et al., 2013). *htb-K123R*Δ downregulates smaller sets in exponential phase (organophosphate biosynthesis, aromatic amino acid metabolism, protein localization) along with a mitochondrial intermembrane signal, this downregulation is suggestive of selective mitochondrial impacts.

In the double mutant, only 13 genes were downregulated, and most of the 324 genes downregulated in *hht-K36A*Δ return toward wild-type when H2Bub is also removed. An antagonism is indicative of this rescue, H2Bub creates an elongation environment that makes cells rely on H3K36me for ribosomal and biosynthetic gene expression, and removing H2Bub reduces that dependency (Keogh et al., 2005; Venkatesh et al., 2012; Radman-Livaja & Rando, 2010). Venn analyses of downregulated genes show minimal overlap across strains, confirming that activation programs under H2Bub vs. H3K36me are largely distinct.

5.13.2 Transcriptional Regulation During Diauxic Shift

Upregulation: In the upregulated genes during diauxic shift, the *hht-K36A*Δ again has the largest set (513), followed by *htb-K123R*Δ (372), with the double mutant far fewer (143) and lower average magnitude. In *htb-K123R*Δ upregulated pathways included checkpoint signaling, telomere capping, DNA damage response/repair, chromatin domain organization, transporter activity, flocculation, and sexual reproduction. This is consistent with heightened genome surveillance and morphological adaptation during glucose depletion. In *hht-K36A*Δ upregulated pathways were cytosolic ribosome, ribosome biogenesis/assembly, RNA binding, and tRNA-associated catalytic functions.

This indicates that loss of H3K36me at diauxic shift drives ribosome-centric programs, possibly reflecting altered control of growth recovery and protein synthesis as cells transition metabolic states.

Downregulation: In diauxic shift the *htb-K123R*Δ downregulated cytosolic ribosome (226), small ribosomal subunit (120), endoplasmic reticulum sub-compartment (100), and multiple metabolic pathways (small molecules, carbohydrate derivatives, lipids). This implied towards a positive role for H2Bub in activating protein synthesis and core metabolism during diauxic transition. *hht-K36A*Δ in diauxic shift downregulated plasma membrane, vacuole, fungal-type cell wall, trehalose and carbohydrate processes, transition metal ion transport, hydrogen peroxide response, and fatty acid metabolism. This highlights an H3K36me role in energy storage, stress defence, and membrane/cell wall remodelling at diauxic shift. A reduced breadth for both up- and downregulated cohorts was seen in double mutant and only limited overlap with single mutants (only 7 and 19 shared upregulated genes with *htb-K123R*Δ and *hht-K36A*Δ, respectively) was seen. This observation supports a compensatory cross-talk that buffers activation/repression amplitudes while selectively disinhibiting mitochondrial inner membrane, ER retention/quality control, and cell-cycle processes.

5.13.3 Transcriptional Regulation During Quiescence

Upregulation: During quiescence the upregulated genes in *hht-K36A*Δ presented the largest cohort (665), with higher average fold-change than *htb-K123R*Δ (305) and the *K123R-K36A*Δ double mutant (401). Cytoskeleton/budding modules (cytoskeleton organization, actomyosin structures, organelle localization), flocculation, protein folding chaperones, and cell-cycle regulation were upregulated in both single mutants, indicating that H3K36me and H2Bub normally repress genes associated with cellular proliferation and structural remodelling in quiescent cells. Proteasome complex/core/regulatory particle genes and extensive metabolism (carboxylic acid catabolism, nucleotide/nucleoside bisphosphate metabolism, TCA cycle, reactive oxygen species metabolism) was enriched in double mutant suggesting that combined loss disinhibits protein turnover and oxidative metabolism in quiescence.

Downregulation: During quiescence *htb-K123R*Δ downregulated nucleolar modules (snoRNPs, U2 snRNP), centromeric chromatin condensation, tubulin assembly, glycosylation, and NAD biosynthesis. This was consistent with a positive role of H2Bub in sustaining rRNA production/ribosome biogenesis and chromosome architecture in stationary phase. In *hht-K36A*Δ downregulated pathways included plasma membrane, vacuole, monocarboxylic acid metabolism, response to chemicals/oxygen-containing compounds, and transporter/oxidoreductase functions. These down regulations again highlighted H3K36 methylation role in cellular integrity and metabolic/homeostatic control under quiescence. Fewer and less diverse functions than single mutants were seen in the double mutant, the functions were endoplasmic reticulum, storage vacuole/side of membrane, small-molecule biosynthesis, transmembrane transport, ion homeostasis, glycolysis, and cell wall biogenesis. This was consistent with broad but moderated impacts on transport and metabolic maintenance when both marks are absent. Venn analyses showed predominately unique sets across mutants, with a small common core, reinforcing distinct activation/repression targets for each PTM in quiescence.

From these data a unified model emerged suggesting that H3K36me acts as a broad constraint on metabolic plasticity and stress-responsive pathways. Oxidative/peroxisomal and nitrogen assimilation modules are repressed while ribosome biogenesis and biosynthetic capacity through gene-body chromatin integrity mediated by the Set2–Rpd3S axis are preserved (Carrozza et al., 2005; Venkatesh et al., 2012).

A transporter-heavy, mitochondrial/peroxisomal, and genome-surveillance programs is shaped by H2Bub which supports the activation of protein synthesis and core metabolism at the diauxic transition (Sun & Allis, 2002; Pavri et al., 2006). These marks together are involved in buffering genome-wide expression changes. The combined loss of these marks reduces the breadth and average magnitude of differential expression compared with single losses. However, it specifically disinhibits oxidative phosphorylation, the glyoxylate cycle, and gluconeogenesis, partially decoupling transcriptome control from glucose status (DeRisi et al., 1997; Gasch et al., 2000; Conrad et al., 2014). It was seen that H2Bub removal rescues the extensive downregulation caused by H3K36 loss for ribosomal and biosynthetic modules during

exponential growth, indicating antagonistic interactions, this imply that elongation-linked chromatin features (Paf1C/FACT and nucleosome dynamics) set the dependency thresholds for Set2–Rpd3S functions (Keogh et al., 2005; Smolle et al., 2013).

5.14 Implications

The observed phase specific and antagonistic responses suggest that chromatin post translational modifications link metabolic state to growth-phase transitions. Early upregulation of respiratory and glyoxylate pathways in exponential phase mutants indicates premature priming for respiratory metabolism, which may affect fitness under fluctuating nutrient conditions (De Virgilio, 2012; Laporte et al., 2011).

5.15 Limitations

Growth phase staging uncertainty and the lack of direct assessment of downstream effectors, including Set2, Rpd3S, RNA polymerase II elongation complexes, Paf1C, and FACT, limit mechanistic interpretation.

5.16 Future Directions

Future studies employing NET-Seq or PRO-Seq and ChIP-Seq analyses of H2Bub, H3K36me, Set2, Rpd3S, and RNA Pol II will enable finer resolution characterization of transcriptional and chromatin dynamics across growth phases. Also, a high-resolution nucleosome maps, and quantitative acetylation profiling to test whether changes in elongation kinetics and gene-body deacetylation directly generate the observed buffering and selective upregulation of respiratory/glyoxylate pathways is warranted. Complementary metabolomics and flux assays, together with growth competitions across carbon sources are needed to connect chromatin-driven transcriptome changes to functional metabolic outcomes.

5.17 Conclusion

A broad upregulation was seen due to the loss of H3K36me in mitochondrial/peroxisomal and stress/metabolic programs. A weakened ribosome and biosynthetic modules were seen due to loss of H3K36me. A selective metabolic/transporter and genome-surveillance signatures and activation of protein synthesis and core metabolism was seen by loss of H2Bub at diauxic transition.

Combined loss of both marks attenuates genome-wide differential expression yet activating oxidative and gluconeogenic pathways, revealing robust antagonistic buffering between H2Bub and H3K36me. This antagonism safeguards transcriptional homeostasis and phase-appropriate expression. These findings position the H2Bub–H3K36me axis as a central chromatin rheostat coordinating growth-phase transitions and metabolic state in budding yeast.

Chapter 6

Transcriptional Reprogramming by Histone Modification in Yeast Across Growth Transitions

6.1 Introduction

A coordinated regulation of gene expression, metabolism, and chromatin states is required in *Saccharomyces cerevisiae* for the transition from fermentative growth to respiration during the diauxic shift (Dix), and the establishment of stationary phase (SP) quiescence cells (Q) (DeRisi *et al.*, 1997; Gasch *et al.*, 2000; Brauer *et al.*, 2008; De Virgilio, 2012; Laporte *et al.*, 2017). While transcription factors and signalling pathways help in driving this metabolic shift, the role of histone PTMs in this process is not well studied.

Chromatin-based mechanisms such as histone PTMs contribute to elongation-coupled regulation of transcription (Li *et al.*, 2007; Venkatesh and Workman, 2015). Histone H2B monoubiquitination (H2Bub) at lysine 123 and histone H3 lysine 36 methylation (H3K36me) are the two pertinent marks involved in this process. Both modifications interface with RNA polymerase II elongation. These modifications remodel chromatin accessibility and engage trans histone crosstalk that channels metabolic and environmental inputs into transcriptional outcomes (Robzyk *et al.*, 2000; Ng *et al.*, 2002; Carrozza *et al.*, 2005; Keogh *et al.*, 2005; Pavri *et al.*, 2006). The Rad6/Bre1 pathway catalyses the monoubiquitination of H2B at lysine 123,

and is linked to transcriptional elongation. Nucleosome reorganization in the wake of elongating RNA Pol II is promoted by H2Bub which collaborates with elongation factors such as FACT and the Paf1 complex to ensure chromatin integrity and transcription fidelity (Robzyk *et al.*, 2000; Ng *et al.*, 2002; Pavri *et al.*, 2006). Importantly, downstream H3K4 and H3K79 methylation by COMPASS and Dot1, respectively is regulated by H2Bub. This establishes a trans histone crosstalk that tunes promoter proximal activation and early elongation checkpoints (Sun and Allis, 2002; Lee *et al.*, 2007; Weake and Workman, 2008). This methylation landscape is therefore also perturbed by disruption of H2Bub.

H2Bub levels are directly affected by metabolic inputs; H2Bub is reduced due to glucose deprivation, and glucose restoration increases it, thus providing a link between carbon source availability to elongation competence and gene activation amplitude (Lan *et al.*, 2016). Owing to these characteristics H2Bub is positioned as a candidate modulator of transcriptional reorganization during the diauxic shift and the restrained transcriptional state of quiescence cells (Q).

H3K36 methylation is enriched over coding regions of actively transcribed genes which is catalysed by the Set2 methyltransferase. This functions as a positional signal for the Rpd3S histone deacetylase complex (Carrozza *et al.*, 2005; Keogh *et al.*, 2005). The Set2–Rpd3S pathway deacetylates gene bodies during transcription, suppressing intragenic cryptic initiation, minimizing noise, and maintaining fidelity (Carrozza *et al.*, 2005; Keogh *et al.*, 2005; Venkatesh and Workman, 2015).

Accumulation of gene-body acetylation is resultant of the loss of H3K36me or Rpd3S. This leads to persistent cryptic transcription and exaggerated transcriptional responses to stimuli highlighting H3K36me role as a check on inappropriate activation and chromatin integrity during elongation (Li *et al.*, 2007; Wagner and Carpenter, 2012). As metabolic transitions in yeast require precise induction of respiratory, stress programs and repression of growth-associated pathways, global allocation rules need to be enforced by H3K36me. This prevents uncontrolled activation of anabolic processes under nutrient limitation.

A system-wide transition from glycolysis to oxidative phosphorylation, followed by downregulation of ribosome biogenesis, translation and upregulation of mitochondrial, oxidative, and stress pathways is characterised by the diauxic shift (DeRisi *et al.*, 1997; Gasch *et al.*, 2000; Brauer *et al.*, 2008; Galdieri *et al.*, 2010). On the other hand, entry into quiescence cells (Q) involves global transcriptional restraint, chromatin compaction, and maintenance of a ready translational system that, when required enables entry into the cell cycle upon nutrient replenishment (De Virgilio, 2012; McKnight *et al.*, 2015a; Laporte *et al.*, 2017). At the transcriptome level these trajectories are well described, however the questions like how elongation coupled histone modifications coordinate magnitude and fidelity of these transitions and how their disruption reorganizes transcriptional capacity across growth versus respiratory programs is unknown.

In this chapter, RNA-Seq data were analysed over the time period from log phase and into quiescent in each histone mutant, *htb-K123R*Δ*, hht-K36A*Δ, and *K123R-K36A*Δ, and in wild-type. The aim was to understand how loss of H2B ubiquitination and H3K36 methylation affects transcriptional regulation over time during metabolic transitions and entry into quiescence.

To simplify the analysis, genes commonly regulated between mutants were focused on, and their fold-change values were compared to assess whether the mutants showed stronger or weaker transcriptional responses. This approach helped distinguish changes in the number of regulated genes from changes in the magnitude of regulation. Finally, these quantitative patterns were integrated with gene ontology (GO) enrichment results to infer how transcriptional responses relate to their corresponding pathways. Based on these analyses, the data suggests that H2Bub and H3K36me function as complementary chromatin regulators that modulate transcriptional amplitude and pathway prioritisation, enhancing or restraining gene expression depending on the growth stage of the cell.

6.2 Transcriptional changes between growth phases

6.2.1 Results of analysis of gene expression in wild-type, *htb-K123R*Δ, *hht-K36A*Δ, and the double mutant *K123R-K36A*Δ at the diauxic shift (Dix) compared to transcription of each strain during exponential phase.

To elucidate the transcriptional consequences of specific histone mutations during the time-course of Q-cell development, we conducted differential gene expression analysis in wild-type, *htb-K123R*Δ, *hht-K36A*Δ, and the double mutant *K123R-K36A*Δ at the diauxic shift (Dix) compared to the transcription profile in each strain at exponential phase (Exp), and then compared transcription in each day 7 quiescent cell population to that strains transcription profile in exponential phase cells (see Fig. 6.1). This should offer more insight into how the transcription profile of each mutant changes over time as quiescence develops.

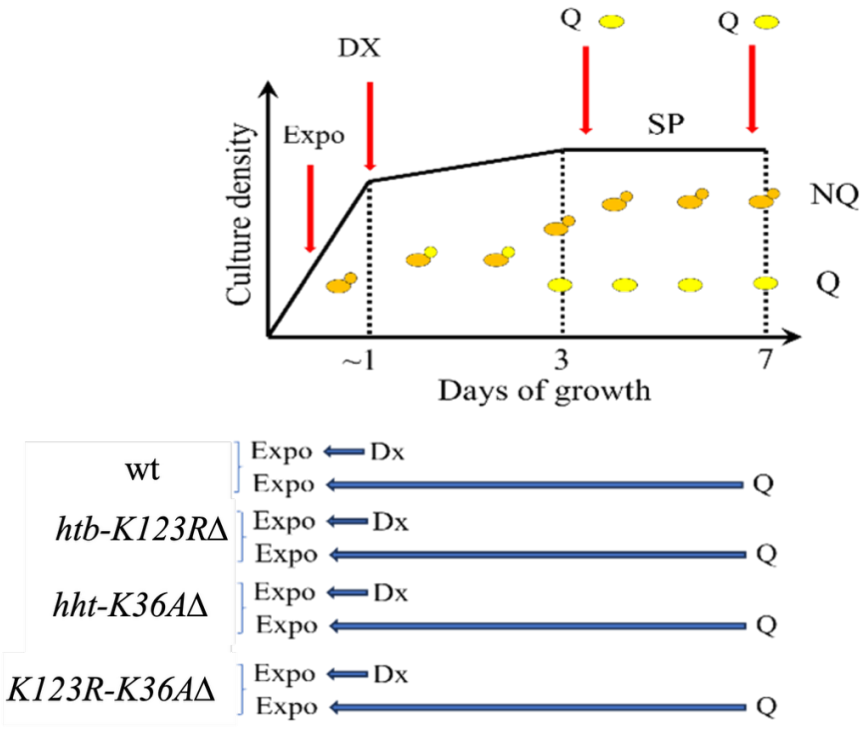


Figure 6.1: Time-course analysis of RNA-Seq data. RNA-Seq data at diauxie and in day 7 quiescent wild-type and mutant cells were compared to their own exponential phase RNase-Seq data.

In the wild-type comparison, 815 genes were differentially expressed, with 728 up-regulated and 87 down-regulated at diauxie compared to transcription in exponentially growing cells. A baseline transcriptional variability is reflected by this modest shift and is consistent with previous observations of dynamic gene expression in yeast under varying growth conditions (Gasch *et al.*, 2000). A substantial transcriptional reprogramming was observed in mutant *htb-K123R*Δ with 1152 differentially expressed genes (524 up-regulated, 628 down-regulated). This was concomitant to previous findings that H2B ubiquitination at K123 is essential for transcriptional elongation and chromatin structure modulation (Henry *et al.*, 2003; Pavri *et al.*, 2006). The most extensive transcriptional alteration was observed in the *hht-K36A*Δ mutant, with 2845 genes differentially expressed (1443 up-regulated, 1402 down-regulated). This dramatic effect was in line with the well-established role of H3K36 methylation in suppressing cryptic transcription and maintaining transcriptional fidelity (Carrozza *et al.*, 2005; Keogh *et al.*, 2005).

The double mutant *K123R-K36A*Δ on the other hand showed an interesting observation of reduced transcriptional response compared to *hht-K36A*Δ alone, with 2191 genes differentially expressed (1227 up-regulated, 964 down-regulated) (Table. 6.1and Fig. 6.2).

This result indicates the potential epistatic interaction between H2B ubiquitination and H3K36 methylation pathways, consistent with models of histone modification crosstalk (Lee *et al.*, 2007). Taken together results obtained highlight the distinct and overlapping roles of H2B K123 and H3 K36 in regulating gene expression. The data highlight the complexity of histone modification networks and their combinatorial influence on transcriptional outcomes.

Strain Comparison	Up-Regulated Genes	Down-Regulated Genes	Total Differentially Expressed Genes
wt Exp vs wt Dix	**728**	**87**	**815**
***htb-K123R*Δ Exp vs Dix**	**524**	**628**	**1152**
***hht-K36A*Δ Exp vs Dix**	**1443**	**1402**	**2845**
***K123R-K36A*Δ Exp vs Dix**	**1227**	**964**	**2191**

Table 6.1: Shows the numbers of genes more than 2-fold up and down-regulated in each strain at diauxie compared to transcription in that same strain at exponential phase.

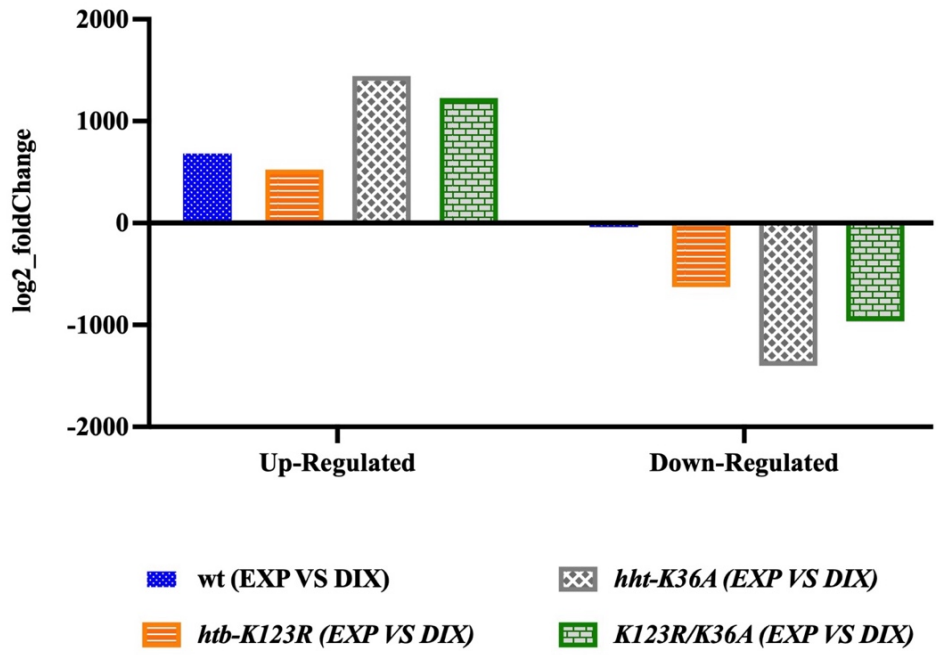


Figure 6.2: Total number of genes up and down regulated at diauxie in each strain compared to when that strain is exponentially growing. Comparisons shown are; genes up and down regulated in wild-type cells at diauxie compared to wild-type exponential phase cells, *htb-K123R*Δ mutants at diauxie compared to *htb-K123R*Δ exponential phase cells, *hht-K36A*Δ mutants at diauxic shift compared to *hht-K36A*Δ exponential phase cells, and *K123R-K36A*Δ double mutants at diauxic shift compared to *K123R-K36A*Δ exponential phase cells

6.2.2 Assessing changes in the levels of gene expression during the diauxic shift (Dix) in wild-type and histone mutant backgrounds relative to exponential phase.

The average fold changes of the genes specifically upregulated in each yeast strain during the diauxic shift compared to the exponential growth phase, were first compared. The wild-type

results served as a baseline of the average gene upregulation occurring during the shift from the exponential phase to post-diauxie. Analysis of gene expression profiles revealed that diauxic *hht-K36A*Δ and *K123R-K36A*Δ mutant strains demonstrated a higher average upregulation of gene transcription as these cells were starved of glucose. The *htb-K123R*Δ mutant (Fig.6.3A) exhibited significantly less average upregulation of gene transcription as these mutant cells were starved of glucose compared to wild-type cells as they transitioned into the stationary phase, consistent with its role in disrupting acetylation dependent transcriptional repression (Millar *et al.*, 2006).

A more pronounced upregulation was seen in the *hht-K36A*Δ mutant, suggesting that loss of H3K36 methylation may lead to de-repression of genes normally silenced during the diauxic shift (Carrozza *et al.*, 2005). The double mutant also exhibited greater average upregulation of genes compared to wild-type , however this was less pronounced than in the *hht-K36A*Δ mutant. In summary, these data revealed differing impacts of the *htb-K123R*Δ*, hht-K36A*Δ and *K123R-K36A*Δ mutants upon upregulation of gene transcription at the diauxic shift relative to transcription in exponentially growing cells. The data therefore suggests H3K36me exerts a greater negative role upon transcription during the diauxic shift whereas H2Bub exerts less of a repressive effect upon gene transcription during the shift from exponential phase to glucose exhaustion.

Conversely, the number of downregulated genes varied significantly across mutants. The *htb-K123R*Δ strain showed a relatively low level of gene repression, while the *hht-K36A*Δ mutant displayed a significant downregulation profile, implicating H3K36 in maintaining transcriptional fidelity during metabolic transitions (Keogh *et al.*, 2005). The double mutant also exhibited the more number of downregulated genes compared to wild-type , however this was less pronounced as *hht-K36A*Δ mutant. In summary, these data revealed differing impacts of the *htb-K123R*Δ*, hht-K36A*Δ and *K123R-K36A*Δ mutants upon downregulation of gene transcription during the diauxic shift. The data suggests *hht-K36A*Δ exerts a greater positive role upon transcription during the diauxic shift whereas *htb-K123R*Δ exerts less of a positive effect upon gene transcription during the shift from exponential phase to glucose exhaustion.

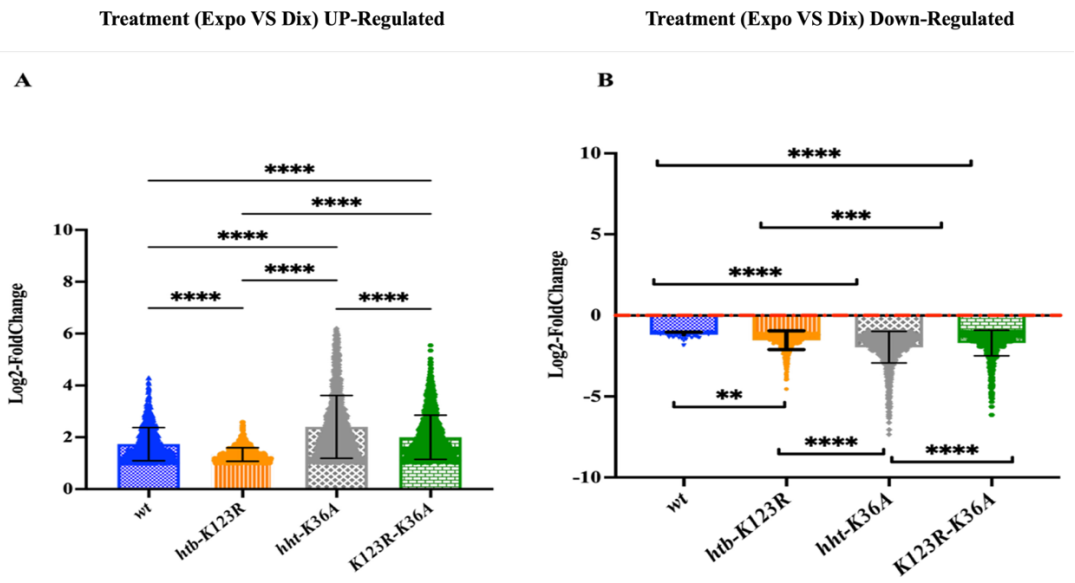


Figure 6.3: Average up and down regulation of gene transcription in wild-type and mutants at diauxie compared to exponential phase. (A) The average log_2 fold change (FC) in genes more than 2-fold upregulated at diauxic shift (Dix) compared to exponential phase (Exp). (B) The average log_2 fold change (FC) in genes more than 2-fold downregulated at diauxic shift (Dix) compared to exponential phase (Exp). (* p = 0.05, ** p = 0.01, **** p = <0.0001).

6.3 Overlap of the upregulated genes in each strain during diauxic shift (Dix)

In *Saccharomyces cerevisiae* the transition from exponential (Exp) growth to the diauxic shift (Dix) represents a critical metabolic reprogramming event. This is characterized by a shift from fermentative to respiratory metabolism (DeRisi *et al.*, 1997; Galdieri *et al.*, 2010). In order to assess the impact of histone modifications on this transition, the overlap of upregulated genes in wild-type , *htb-K123R*Δ, *hht-K36A*Δ, and *K123R-K36A*Δ double mutant strains were analysed (Fig. 6.4).

In wild-type cells, only 5 genes were uniquely upregulated during the diauxic shift (Dix) compared to exponential growing cells. The wild-type specific gene set reflects 'regular' reprogramming in response to nutrient depletion. The *htb-K123R*Δ mutant exhibited 76

uniquely upregulated genes. Conversely, the *hht-K36A*Δ mutant displayed 348 uniquely upregulated genes, indicating a broader transcriptional activation.

The *K123R-K36A*Δ double mutant upregulated 127 unique genes, suggesting a compounded effect of both histone modifications. Interestingly, 321 genes were commonly upregulated across wild-type, *htb-K123R*Δ, *hht-K36A*Δ and *K123R-K36A*Δ double mutant. This overlap implies that H3K36 methylation may partially compensate for the loss of H2B ubiquitination, preserving some transcriptional responsiveness.

6.3.1 Overlap in the downregulated genes of each strains during diauxic shift (Dix)

To assess the impact of histone H2B K123 monoubiquitination and H3 K36 acetylation on gene repression during this transition, we analysed the overlap of downregulated genes in wild-type, *htb-K123R*Δ, *hht-K36A*Δ and *K123R-K36A*Δ double mutant strains (Fig. 6.5). Interestingly, wild-type cells exhibited only 1 uniquely downregulated gene.

The *htb-K123R*Δ mutant downregulated 118 unique genes, while the *hht-K36A*Δ mutant suppressed 489 genes not shared with other conditions. H2B monoubiquitination has been implicated in transcriptional elongation and chromatin compaction (Henry *et al.*, 2003; Pavri *et al.*, 2006), and its loss may lead to aberrant silencing of genes that are normally maintained during metabolic transitions. Similarly, H3K36 acetylation is known to regulate transcriptional fidelity and prevent cryptic initiation (Carrozza *et al.*, 2005; Venkatesh *et al.*, 2012). The broad repression observed in the *hht-K36A*Δ mutant may reflect a loss of transcriptional discrimination, resulting in excessive silencing of genes required for adaptation.

The *K123R-K36A*Δ double mutant downregulated 172 unique genes, indicating a compounded effect of both histone modifications. The double mutant's inability to maintain expression of these genes suggests a failure to engage the transcriptional programs necessary for metabolic

flexibility.. A total of 286 genes were commonly downregulated across all four conditions, representing a core set of transcripts suppressed during the diauxic shift (Dix).

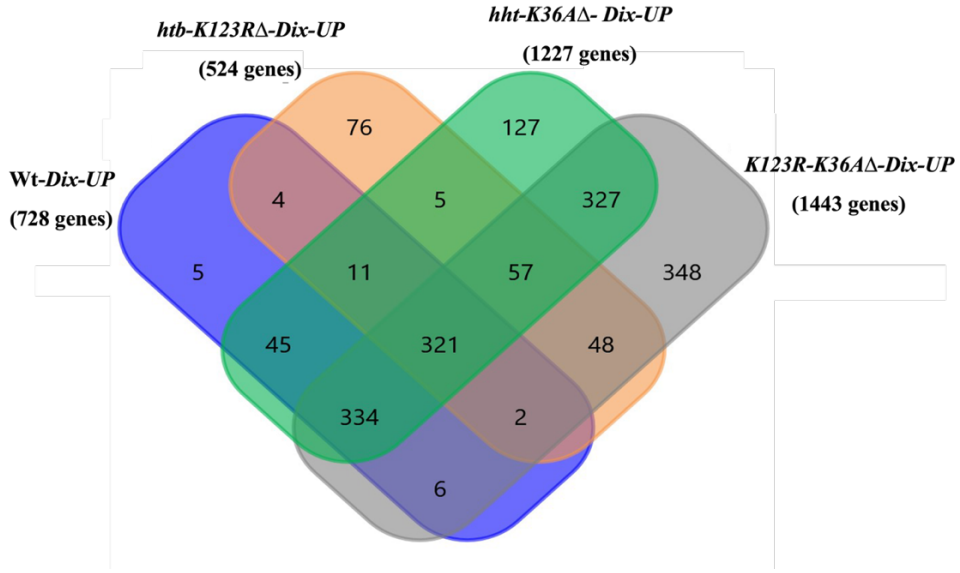


Figure 6.4:Venn diagram of upregulated genes. it shows the number of genes uniquely up-regulated during diauxic shift (Dix) (relative to exponentially growing cells) in the *htb-K123R*Δ mutant (327 genes), uniquely upregulated in the *hht-K36AΔ* mutant (348 genes), and the common set upregulated in both mutants (45 genes). The total number of upregulated genes analysed across the experiment is (524 genes).

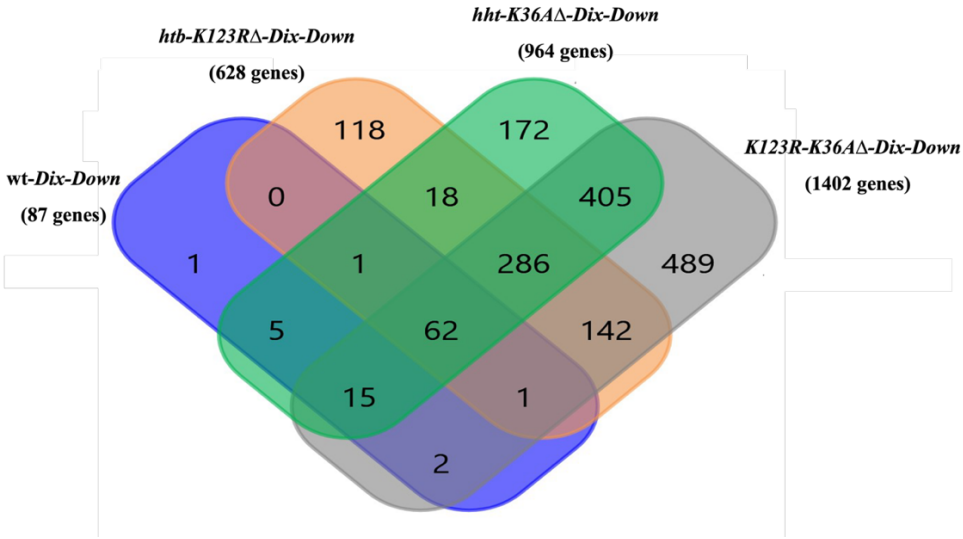


Figure 6.5:Identification of common and unique downregulated genes. The Venn diagram illustrates the overlap between sets of genes significantly down-regulated during diauxic shift (Dix) for (relative to exponentially growing cells). Each number represents the count of genes in that specific segment. The total number of downregulated genes for each primary condition is shown in parentheses.

6.3.2 Analysis of the genes uniquely upregulated and downregulated during the diauxic shift in the *htb-K123RΔ* deletion strains

It has been previously shown that glucose availability directly modulates H2B mono-ubiquitination (H2Bub) such that glucose depletion leads to reduced H2Bub levels and impaired activation of glucose-responsive pathways (Chen *et al.*, 2021). To gain a more clear insight into the impact of H2Bub upon transcription at diauxie, the transcription response of *htb-K123R*Δ mutant cells during the shift from exponential growth to diauxic shift was specifically compared to that observed in wild-type during this shift.

Substantial differences in upregulated and downregulated gene sets was revealed by comparative analysis of gene expression in wild-type cells and *htb-K123R*Δ strains during the diauxic shift as cells exit exponential phase (Fig. 6.6). For those upregulated genes, 576 were commonly upregulated in both strains (overlapped), and 1669 were uniquely upregulated in the *htb-K123R*Δ mutant.

For downregulated genes, 64 were commonly downregulated, and 564 were uniquely downregulated in *htb-K123R*Δ. These results were in line with previous reports that loss of H2Bub-mediated repression of certain gene clusters are exacerbated during metabolic transitions. Taken together it indicates that H2B ubiquitination at K123 fine tunes the diauxic shift (Dix) response by amplifying upregulation in wild-type while mitigating excessive downregulation. This is in line with previous research which showed broader roles of histone modifications in stress adaptation and survival in stationary phase (Sun and Allis, 2002).

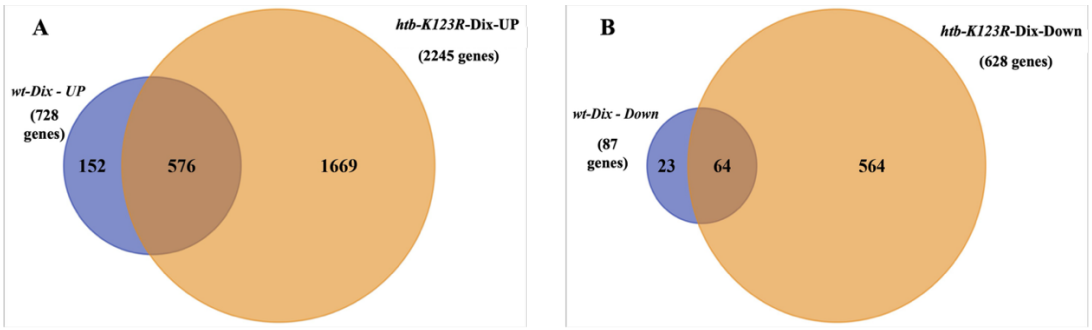


Figure 6.6: Unique and shared transcriptional profiles in *htb-K123R*Δ during diauxic shift compared to exponential phase for upregulated and down regulated.

6.3.3 Analysis of genes uniquely upregulated and downregulated during the diauxic shift in the *hht-K36A*Δ deletion strains

To investigate the impact of the *hht-K36A*Δ mutation on transcriptional regulation under Diauxic shift (Dix), the transcriptional response of *hht-K36A*Δ mutant cells during the shift from exponential growth to diauxic shift was specifically compared to that observed in wild-type during this shift (Fig. 6.7). A substantial divergence in transcriptional activation between exponential phase and diauxie was uncovered in the *hht-K36A*Δ mutant.

Among the upregulated genes at diauxie comparted to exponential phase, 66 were uniquely regulated by wild-type, 780 by *hht-K36A*Δ, and 663 genes were commonly upregulated in both strains. Downregulated genes on the other hand showed a distinct pattern. Only 7 genes were uniquely downregulated in wild-type, while 1322 were uniquely downregulated in *hht-K36A*Δ, with 80 genes shared between the two. This indicates that the *hht-K36A*Δ mutation may potentiate transcriptional silencing mechanisms consistent with prior reports that loss of H3K36 methylation disrupts recruitment of histone deacetylases, thereby altering gene repression dynamics (Carrozza *et al.*, 2005; Venkatesh and Workman, 2015). Altogether these results indicate that the *hht-K36A*Δ mutation exerts a broad and potent influence on gene regulation under Diauxic shift (Dix), enhancing both activation and repression of distinct gene subsets. The overlap in regulated genes between wild-type and mutant strains further implies that while core transcriptional responses are preserved, the magnitude and specificity of regulation are significantly altered in the absence of functional H3K36 methylation.

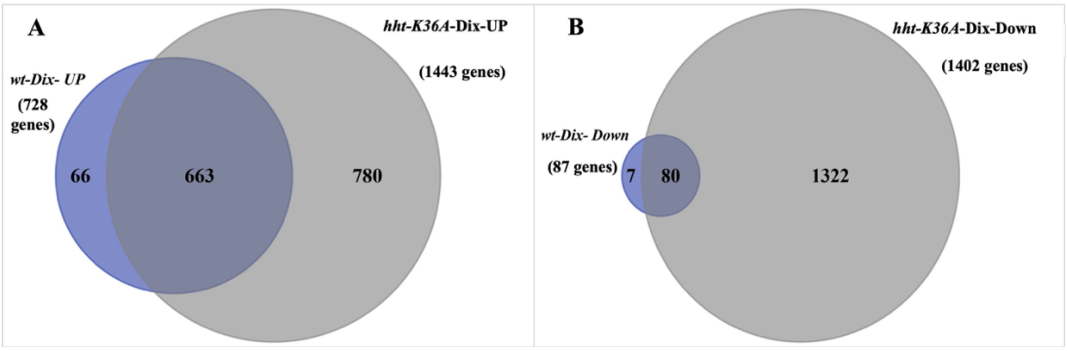


Figure 6.7: Unique and shared transcriptional profiles in yeast deletion mutants during exponential phase compared to diauxic shift in wild-type cells for upregulated and down regulated.

6.3.4 Analysis of the genes uniquely upregulated and downregulated during the diauxic shift in the *K123R-K36A*Δ deletion strains

To understand the transcriptional impact of simultaneous disruption of H3K36 methylation and H2B ubiquitination pathways, the transcriptional response of *K123R-K36A*Δ double mutant cells during the shift from exponential growth to diauxic was specifically compared to that observed in wild-type during this shift. (Fig. 6.8).

A pronounced shift in transcriptional upregulation relative to wild-type was observed in the double mutant. Of the upregulated genes, 18 were uniquely induced in wild-type, 516 were specific to the double mutant, and 711 genes were commonly upregulated in both strains (Fig. 6.8.A). This indicates a hyperactivation phenotype in the double mutant. This is consistent with previous findings that loss of H3K36 methylation leads to aberrant transcriptional elongation and cryptic initiation (Li *et al.*, 2007), while mutation of H3K123 and loss of H2B ubiquitination, further destabilizing transcription (Henry *et al.*, 2003; Weake and Workman, 2008).

The pattern of transcriptional down regulation was similarly amplified in the double mutant (Fig. 6.7B). Only 4 genes were uniquely downregulated in wild-type, compared to 881 in the double mutant, with 83 genes commonly repressed in both.

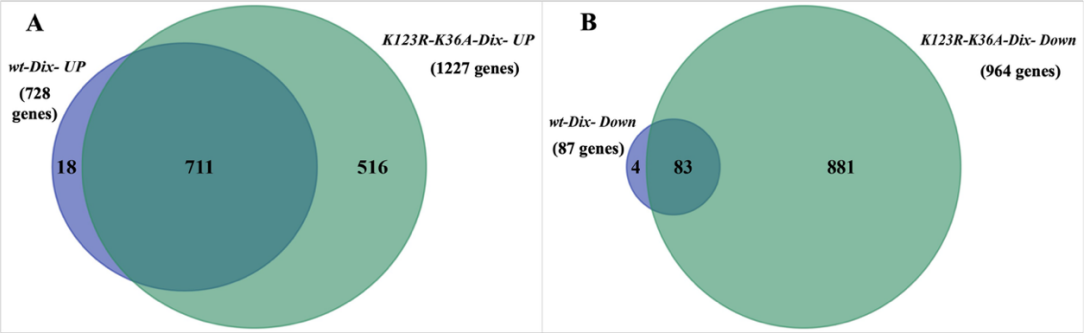


Figure 6.8: Unique and shared transcriptional profiles in yeast deletion mutants during exponential phase compared to diauxic shift in wild-type cells for upregulated and down regulated.

6.4 Gene ontology analysis of upregulated genes in wild-type cells during the transition from Exponential Phase to the Diauxic Shift

To elucidate the functional landscape of the transcriptional changes accompanying the metabolic transition from exponential growth (Exp) to the diauxic shift (Dix) in wild-type , Gene Ontology (GO) enrichment analysis was performed on the genes upregulated at diauxic shift compared to wild-type exponentially growing cells (Appendix Table. 1 and Fig. 6.9). A pronounced enrichment of terms associated with ribosome biogenesis, RNA binding, and biosynthetic processes was seen which reflected the cellular reprogramming that occurs during this metabolic shift. In the Biological Processes category, the most significantly enrichment was in ribosome biogenesis, consistent with studies demonstrating that yeast cells entering the diauxic shift (Dix) undergo a reorganization of translational machinery to adapt to reduced nutrient availability and altered energy demands (Jorgensen *et al.*, 2004; Marks *et al.*, 2008). The notion of metabolic remodelling, as cells shift from fermentative to respiratory metabolism (Roberts and Hudson, 2006), was further supported by the upregulation of small molecule biosynthetic processes and carbohydrate derivative metabolic processes. A heightened emphasis on nucleotide turnover and translational accuracy, which may be critical for ensuring high fidelity protein synthesis prior to the decrease in translation after the glucose-depletion induced stress conditions is supported by enrichment of terms such as purine nucleoside diphosphate metabolic process and maintenance of translational fidelity.

The enrichment of serine biosynthetic process and long-chain fatty acid biosynthetic process might reflect the need for nutrient storage via amino acid and lipid biosynthesis during cellular adaptation to glucose depletion (Tehlivets *et al.*, 2007).

In molecular functions category, sequence-specific mRNA binding and rRNA binding were highly enriched, whilst in the Cellular component category enrichment of terms *cytosolic ribosome* and *cytosolic small ribosomal subunit* further confirms the *transcriptional activation of ribosomal genes involved in governing regulation of translation*. The presence of *RNA polymerase I complex* among enriched components points to increased *rRNA transcription*, a hallmark of *ribosome biogenesis* (Hori *et al.*, 2023). In summary, these changes in gene transcription are consistent with alterations to *translation* and *nutrient storage* which are important factors in the subsequently formed Q cells.

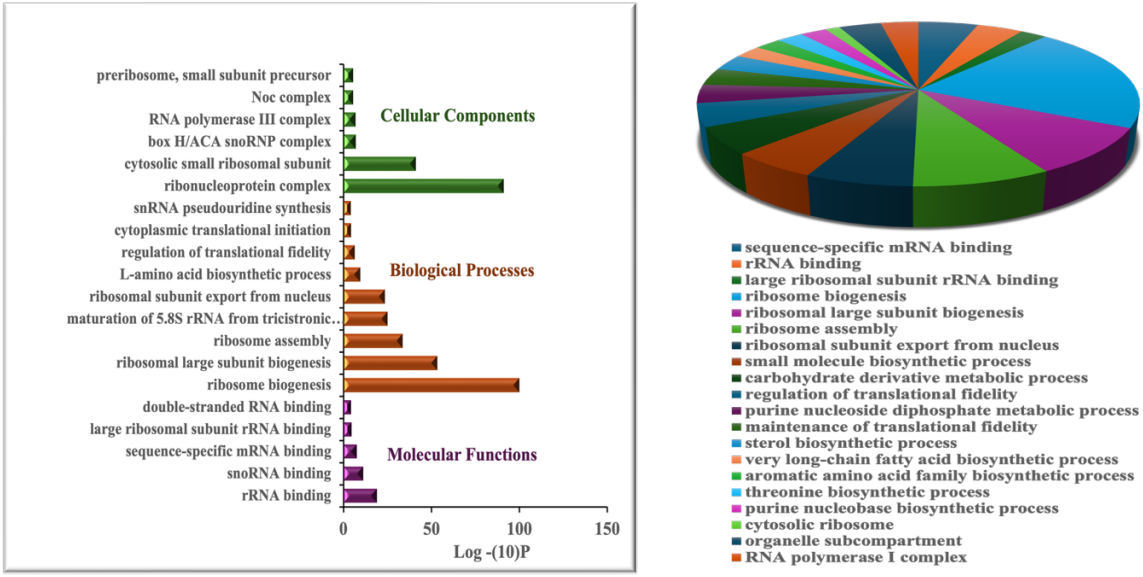


Figure 6.9: GO analysis of genes upregulated in wild-type cells at the diauxic shift compared to exponential phase.

6.4.1 Gene ontology analysis of downregulated genes in wild-type cells during the Exponential Phase to Diauxic Shift

GO analysis on genes downregulated during the transition from exponential growth to the diauxic shift was performed. A targeted suppression of *mitochondrial components, aerobic respiration*, and *key biosynthetic* and *catabolic processes* was revealed (Appendix Table. 2 and Fig. 6.10). This reflected towards the *metabolic recalibration* that is resultant of glucose depletion and the onset of *respiratory metabolism*. In the Biological Processes category, the most significantly downregulated biological process was *aerobic respiration.* This observation was consistent with the *well-documented metabolic* shift from fermentative to oxidative metabolism during the diauxic transition (DeRisi *et al.*, 1997; Galdieri *et al.*, 2010). Other enriched biological process includes *acetyl-CoA metabolic process, regulation of carbohydrate biosynthetic process*, and *small molecule catabolic process*. A broad attenuation of *biosynthetic* and *catabolic activities* is suggestive of these enrichments. This attenuation could be due to reduced nutrient availability and the need to conserve energy (Brauer *et al.*, 2008).

The enrichment of GO terms *purine nucleotide metabolic process* and *carbohydrate biosynthetic process* further supports the notion of a global slowdown in *anabolic metabolism*.

Go term *cellular response to oxidative stress* was also downregulated, this was interesting as it may indicate a temporary reduction in *ROS production* as cells exit rapid growth and enter a more quiescent state (Diaz-Moralli *et al.*, 2013). This contrasts with the upregulation of stress response genes typically observed in later stages of the diauxic shift (Dix), suggesting a phased adaptation to *environmental stressors*. Among molecular functions, *heat shock protein binding* and *protein serine kinase activity* were enriched go terms. The enrichment of these GO terms may reflect a reduced need for *chaperone-mediated folding* and growth-related signalling during metabolic slowdown (Weber, 2020). *Mitochondrial envelope* and *mitochondrial intermembrane space* were the GO terms in cellular components suggesting a temporary restructuring or reduced activity of *mitochondrial architecture*. The *protein phosphatase type 1 complex* involved in cell cycle regulation and metabolic control, was also suppressed, aligning with the reduced proliferation rate during the diauxic shift (Busti *et al.*, 2010).

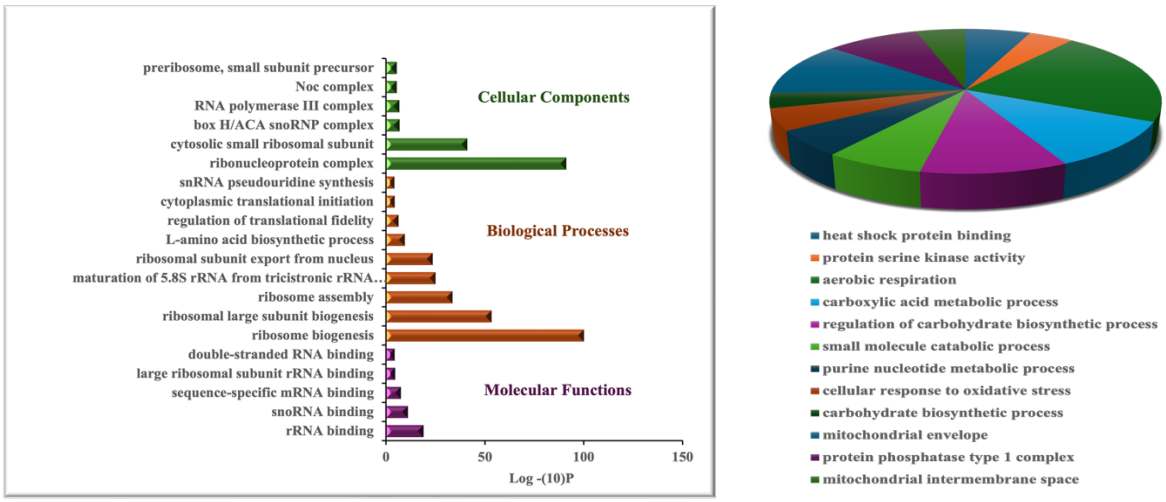


Figure 6.10: GO analysis of genes downregulated in wild-type cells at the diauxic shift compared to exponential phase.

6.4.2 Gene ontology analysis of upregulated genes in the *htb-K123R*Δ Mutant during the transition from Exponential Phase to the Diauxic Shift.

GO analysis on upregulated genes in the *htb-K123R*Δ mutant was performed. A striking enrichment of GO terms associated with *ribosome biogenesis, RNA binding*, and *nucleolar processes* was revealed (Appendix Table. 3 and Fig. 6.11), suggesting that the mutant strain mounts a compensatory *transcriptional response* to maintain translational capacity under metabolic stress. In the Biological Processes category, the most significantly enriched biological process_was *ribosome biogenesis*, followed closely by *ribosomal large subunit biogenesis*, *ribosome assembly*, and *maturation of 5.8S rRNA from tricistronic rRNA transcript*. These enrichments indicate a robust upregulation of genes involved in *ribosomal RNA processing and assembly*. These observation was consistent with previous reports where histone modifications have been shown to influence nucleolar activity and ribosomal gene expression. The enrichment of *ribosomal subunit export from nucleus* further supports the notion of enhanced ribosome production and trafficking, potentially as a compensatory mechanism for impaired chromatin remodelling. Interestingly, moderate enrichment in GO-terms *L-amino acid biosynthetic*

process, *translation*, and *cytoplasmic translation* were observed, suggesting that the mutant strain prioritizes protein synthesis machinery during the diauxic shift.

This is contrary to wild-type cells, which typically downregulate ribosomal genes and shift toward stress response and respiratory metabolism (Gasch et al., 2000; Brauer et al., 2008).

The enrichment of snRNA *pseudouridine synthesis* may reflect increased demand for RNA modification and processing, which are essential for ribosome function and fidelity (Decatur and Fournier, 2002). Among molecular functions, *rRNA binding* and *snoRNA binding* were highly enriched, indicating elevated expression of RNA-binding proteins involved in ribosome maturation. The GO-Term enrichment of *sequence specific mRNA binding* and *double stranded RNA binding* indicates towards a broader regulation of RNA metabolism, possibly linked to altered chromatin accessibility in the mutant background (Ellison et al., 2019). In Cellular Components category the enrichment of *cytosolic large ribosomal subunit*, *preribosome, large subunit precursor*, and *small subunit processed* was observed which further corroborates the transcriptional activation of ribosome-related genes. The appearance of nuclear *HAC1 mRNA ribonucleoprotein complex* and *RNA polymerase III complex* points to increased activity in non-coding RNA transcription and stress-related mRNA processing, potentially reflecting an unfolded protein response or ER stress adaptation (Cox and Walter, 1996).

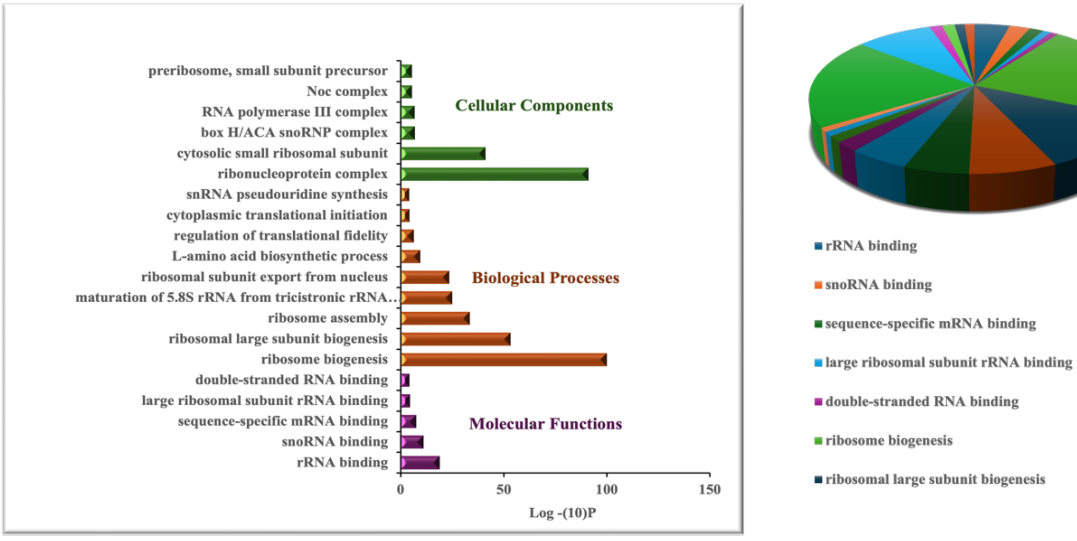


Figure 6.11: GO analysis of genes upregulated in *htb-K123R*Δ cells at the diauxic shift compared to exponential phase.

6.4.3 Gene ontology analysis of downregulated genes in the *htb-K123R*Δ Mutant during the Exponential Phase to Diauxic Shift.

A pronounced suppression of mitochondrial functions, energy metabolism, and oxidative stress responses wild-type revealed by GO enrichment analysis, suggesting that histone ubiquitination plays a critical role in coordinating the transcriptional response to metabolic stress (Appendix Table. 4 and Fig. 6.12). In the biological process category, the most significantly enriched go terms include *generation of precursor metabolites and energy*, *carbohydrate metabolic process*, and *small molecule catabolic process*. A broad repression of central carbon metabolism, including glycolysis and the TCA cycle is indicated by these results, which is further supported by the downregulation of *tricarboxylic acid cycle* and *carbohydrate catabolic process*.

This enrichment is in contrasts with the expected upregulation of respiratory metabolism during the diauxic shift (Dix) in wild-type cells (DeRisi *et al.*, 1997; Galdieri *et al.*, 2010), suggesting that the *htb-K123R*Δ mutant fails to fully activate mitochondrial energy pathways. The enrichment of terms *mitochondrial respiratory chain complex assembly* and *mitochondrial complex I assembly* is indicative of impaired biogenesis of oxidative phosphorylation machinery, which may compromise ATP production and redox balance.

A global attenuation of *alternative carbon utilization* and *NAD^+/NADH cycling*, critical for maintaining *cellular energy homeostasis* can be indicative from the enrichments in terms *alcohol metabolic process*, *lactate metabolic process*, and *nicotinamide nucleotide metabolic process* (Tamburini and Tyler, 2005). Interestingly, *response to oxidative stress* was also enriched pointing towards a failure to mount an adequate antioxidant defence during the metabolic transition. This is notable given that the diauxic shift is typically accompanied by *increased reactive oxygen species (ROS)* and activation of stress response pathways (Shen et al., 2022). Among molecular functions, *oxidoreductase activity* and *secondary active transmembrane transporter activity* were markedly enriched. Their enrichment suggests compromised metabolic flexibility and nutrient sensing in the mutant strain (Bexley et al., 2025). Enriched cellular components were predominantly mitochondrial, including the

mitochondrial envelope, *mitochondrial matrix*, and *intermembrane space*, indicating reduced expression of genes encoding mitochondrial structural proteins.

The enrichment of term *organelle outer membrane* may reflect impaired organelle integrity or biogenesis, consistent with previous reports linking histone modifications to mitochondrial function (Haimovich *et al.*, 2013).

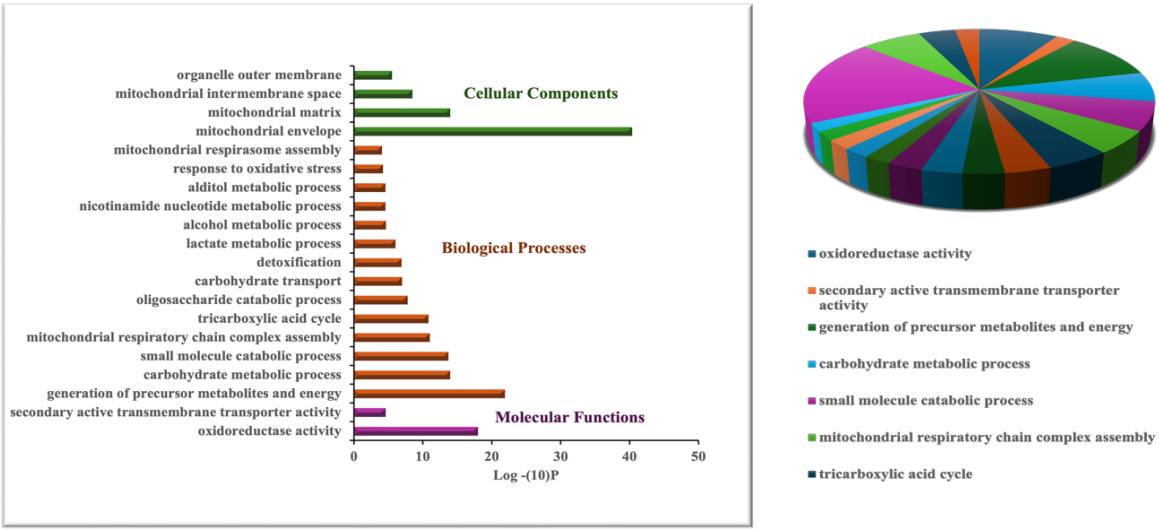


Figure 6.12: GO analysis of genes downregulated in *htb-K123R*Δ cells at the diauxic shift compared to exponential phase.

6.4.4 Gene ontology analysis of upregulated genes in the *hht-K36A*Δ Mutant during the Exponential Phase to Diauxic Shift.

GO enrichment analysis reveals a significant enrichment in terms involved in *ribosome biogenesis, RNA binding*, and *biosynthetic processes*, suggesting that loss of H2B K36 acetylation triggers a compensatory transcriptional program to sustain protein synthesis and cellular growth under nutrient-limited conditions (Table. 5 and Fig. 6.13). In the GO Biological Processes category, the most significantly enriched biological process were *ribosome biogenesis, cytosolic small subunit biogenesis, ribosomal assembly*, and *ribosomal subunit*

export from the nucleus. These enrichments highlight a robust upregulation of genes associated with *ribosomal RNA processing* and *assembly*. This observation is consistent with previous reports linking histone modifications to nucleolar activity and ribosomal gene expression (Warner, 1989). The mutant strain is able to maintains anabolic activity and energy production during the diauxic shift (Dix), potentially bypassing the typical metabolic slowdown observed in wild-type cells can be assumed by the enrichment of energy derivation *metabolic processes* and *small molecule biosynthetic pathways* (Gasch *et al.*, 2000).

The notion of *sustained biosynthetic capacity*, which may reflect a failure to properly repress growth related genes in response to nutrient depletion is further supported by the enrichment of terms *tRNA metabolic processes, glycoprotein biosynthesis*, and *lipid biosynthesis*. This transcriptional profile contrasts with the canonical wild-type response, where *ribosomal* and *biosynthetic* genes are typically downregulated during the diauxic shift (Dix) (Brauer *et al.*, 2008).

Among molecular functions, transferase activity involving one carbon group transfer, sequence specific *mRNA binding*, and *translation factor activity* were highly enriched. This indicated towards an elevated expression of enzymes and *RNA-binding proteins* involved in translation and methylation. The presence of terms snoRNA binding and tRNA binding aligns with the observed upregulation of RNA processing pathways, suggesting enhanced *ribonucleoprotein complex* formation and modification (Decatur and Fournier, 2003). Enrichment of GO terms *cytosolic ribosome components, small* and *large ribosomal subunits and the RNA polymerase I complex* further supports the *transcriptional activation* of ribosome related genes. These components are central to *rRNA transcription* and *ribosome assembly*, and their upregulation may reflect altered chromatin dynamics in the *hht-K36A*Δ mutant that favour nucleolar gene expression (Zhou *et al.*, 2011).

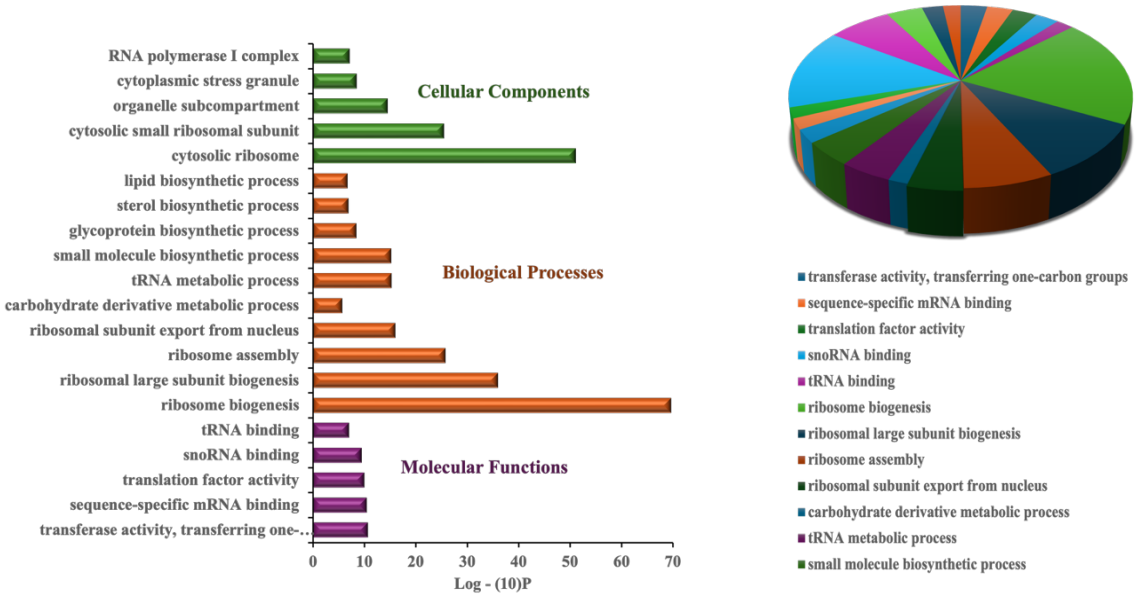


Figure 6.13: GO analysis of genes upregulated in *hht-K36A*Δ cells at the diauxic shift compared to exponential phase.

6.4.5 Gene ontology analysis of downregulated genes in the *hht-K36A*Δ Mutant during the Exponential Phase to Diauxic Shift.

GO enrichment analysis on genes downregulated in the *hht-K36A*Δ mutant during the metabolic transition from exponential growth (Exp) to the diauxic shift (Dix) revealed marked enrichment of genes involved in *mitochondrial respiration*, *small molecule catabolism*, and *stress responses* (Appendix Table. 6 and Fig. 6.14). These enrichments suggest that H2B K36 acetylation is critical for proper transcriptional activation of adaptive pathways under nutrient limited conditions. In the Biological Processes category, the most significantly enriched term was *DNA integration*, which may reflect reduced transposon activity or impaired recombination under stress conditions (Curcio and Derbyshire, 2003). Notably, terms involved in *generation of precursor metabolites and energy*, *small molecule catabolic processes*, and *carbohydrate metabolism* were enriched, indicating a failure to activate key metabolic pathways required for diauxic adaptation (Dix). This aligns with previous findings that histone modifications regulate metabolic gene expression during nutrient shifts (Alam *et al.*, 2016; Evans *et al.*, 2023). The

terms response to oxygen-containing compounds, response to nutrient levels, and response to starvation suggests a dampened stress response in the mutant strain.

These pathways are typically upregulated during the diauxic shift to promote *survival and metabolic flexibility* (Gasch *et al.*, 2000). Additionally, enrichments related to *lipopolysaccharide and interleukin-1 may reflect impaired signalling,* though similar stress responsive genes have been shown to be conserved across eukaryotes (Di Spirito *et al.*, 2025). Among molecular functions, *RNA polymerase II transcription regulatory region sequence specific DNA binding* and *oxidoreductase activity* were significantly enriched suggesting rededication in *transcriptional activation and impaired redox metabolism*. The enrichment of histone H3K4me3 reader activity may indicate disrupted chromatin signalling, as H3K4me3 is associated with active promoters and its recognition is essential for transcriptional fidelity (Zhang *et al.*, 2005; Ruthenburg *et al.*, 2007). A broad suppression of *mitochondrial architecture and function* was highlighted by enrichment of cellular components including the *respiratory chain complex, mitochondrial envelope, mitochondrial membrane*, and *oxidoreductase complex*.

This is consistent with the observed repression of *oxidative metabolism* and suggests that H2B K36 acetylation may facilitate chromatin remodelling at mitochondrial gene loci (Fellas, 2023). The downregulation of the *transcription regulator complex* further supports the *notion of impaired transcriptiona*l control in the mutant strain.

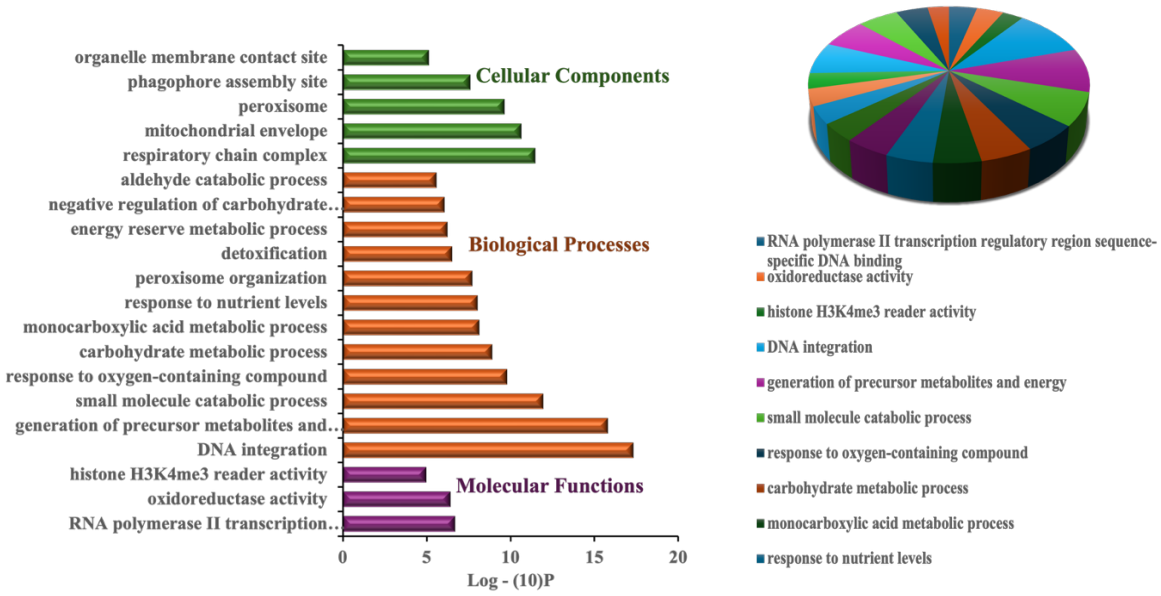


Figure 6.14: GO analysis of genes downregulated in *hht-K36A*Δ cells at the diauxic shift compared to exponential phase.

6.4.6 Gene ontology analysis of upregulated genes in the *K123R-K36A*Δ Double Mutant during the Exponential Phase to Diauxic Shift.

GO enrichment analysis of upregulated genes in the double mutant revealed a striking enrichment of terms *ribosome biogenesis, RNA processing,* and *endoplasmic reticulum (ER) associated biosynthetic pathways* (Appendix Table. 7 and Fig. 6.15). This enrichment is indicating that mutant fails to properly repress growth promoting programs during nutrient limitation. The most significantly enriched biological processes include *ribosome biogenesis, ribosomal large subunit biogenesis, ribosomal subunit export from the nucleus*, and *maturation of 5.8S rRNA*, suggesting sustained *transcriptional drive toward ribosome assembly and rRNA processing.*

These findings are concomitant to prior reports which showed histone modifications regulate *nucleolar activity and ribosomal gene expression* (Warner, 1989; Venema and Tollervey, 1999). The enrichments in terms *carbohydrate derivative metabolic processes, small molecule metabolism, phosphorus metabolism*, and *lipid biosynthesis* points towards the idea that double

mutant is *maintain anabolic activity* during the diauxic shift (Dix), potentially bypassing the typical metabolic reprogramming observed in wild-type cells (Brauer *et al.*, 2008; Liu *et al.*, 2015). Enrichments of *protein localization to the ER and sterol biosynthesis* points to enhanced *ER function and membrane production*. This could be due to a compensatory mechanism to support increased protein synthesis and trafficking (Travers *et al.*, 2000).

Among molecular functions, enrichment of *sequence specific mRNA binding, translation factor activity*, and *snoRNA binding was observed* which indicated towards elevated expression of *RNA binding proteins* and *translation regulators*. Enrichment of unfolded protein binding suggests activation of *chaperone mediated protein folding*. This could be potentially in response to *ER stress or increased translational load* (Ron and Walter, 2007).

Cellular component analysis revealed strong enrichment of the *cytosolic ribosome, cytosolic small ribosomal subunit*, and *RNA polymerase I complex*. This was consistent with elevated *ribosomal gene expression*. Notably, components of the ER, including the *endoplasmic reticulum* and *integral components* of the ER membrane network, were also significantly enriched. This suggests coordinated activation of translation and protein trafficking machinery.

This dual enrichment of ribosomal and ER associated components may reflect a failure to downregulate gro*wt*h related organelles during the diauxic shift, a hallmark of metabolic adaptation in yeast (Galdieri *et al.*, 2010).

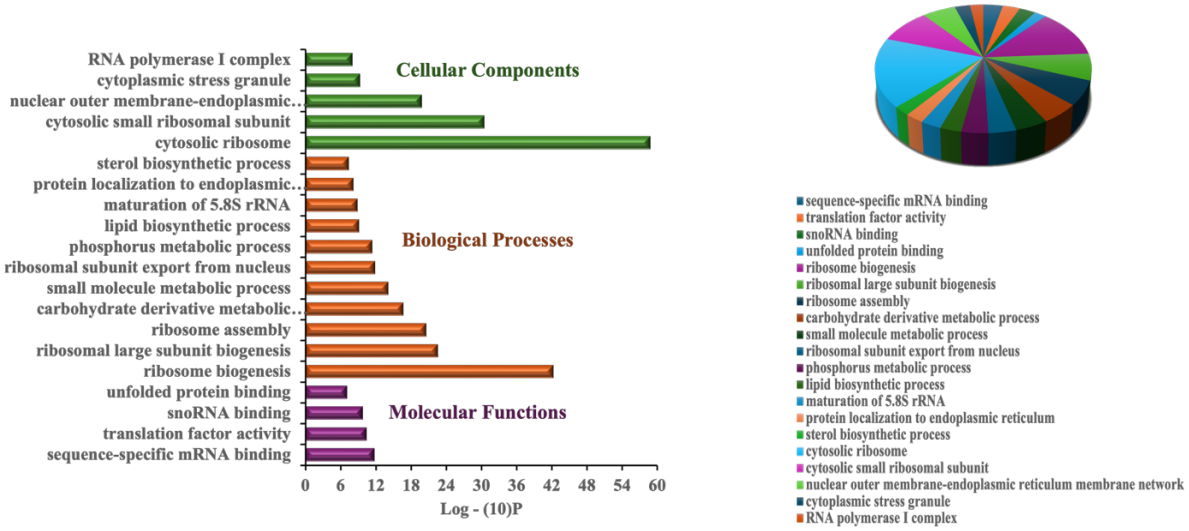


Figure 6.15: GO analysis of genes upregulated in *K123R-K36A*Δ cells at the diauxic shift compared to exponential phase.

6.4.7 Gene ontology analysis of downregulated genes in the *K123R-K36A*Δ Double Mutant during the Exponential Phase to Diauxic Shift.

We performed GO enrichment analysis on genes downregulated in the *K123R-K36A*Δ double mutant during the *metabolic transition* from exponential growth to the diauxic shift (Dix) (Appendix Table. 8 and Fig. 6.16). A coordinated suppression of genes involved in *aerobic respiration* was revealed, *small molecule catabolism*, and *organelle organization*, suggesting that H2B acetylation at K123 and K36 is essential for *activating adaptive metabolic programs* under nutrient limited conditions. Among *molecular functions*, the most significantly downregulated go terms included *oxidoreductase activity, DNA binding transcription factor activity specific to RNA polymerase II*, and *aldehyde dehydrogenase (NAD+) activity*.

These GO terms are related to functions that are central to maintaining redox balance and regulating transcription of metabolic genes. The enrichment of *oxidoreductases and aldehyde dehydrogenases* suggests impaired detoxification and energy conversion.

This was consistent with previous findings that histone modifications modulate mitochondrial gene expression and oxidative stress responses (Brandes *et al.*, 2013; Siauciunaite *et al.*, 2019).

Downregulated biological processes included *aerobic respiration, small molecule catabolism, carbohydrate* and *lipid metabolism*, and *ATP biosynthesis*. These pathways are typically upregulated during the diauxic shift (Dix) to support oxidative phosphorylation and energy production (Gasch *et al.*, 2000; Liu *et al.*, 2015). The enrichment of GO terms involved in *response to nutrient levels* and *cellular response* to oxygen containing compounds indicates a blunted environmental sensing and stress adaptation. This may compromise the mutant's ability to transition into a quiescent state. Interestingly, enrichment of GO terms *peroxisome organization* and *cellular development* were also observed, suggesting broader defects in *organelle remodelling* and *cellular differentiation*. Fatty acid oxidation and *reactive oxygen species detoxification* are the key roles of *peroxisomes* and their repression may *exacerbate metabolic stress* in the mutant (Smith and Shilatifard, 2013). Cellular component analysis revealed significant enrichments of the terms *mitochondrion, peroxisome, aldehyde dehydrogenase complex*, and *mitochondrial outer membrane*.

This pointed to a global suppression of organelles involved in *energy metabolism* and *detoxification*. The enrichment of the Go apparatus and low density lipoprotein particle may reflect impaired lipid trafficking and membrane remodelling, further supporting the notion of disrupted metabolic homeostasis (Mira *et al.*, 2010).

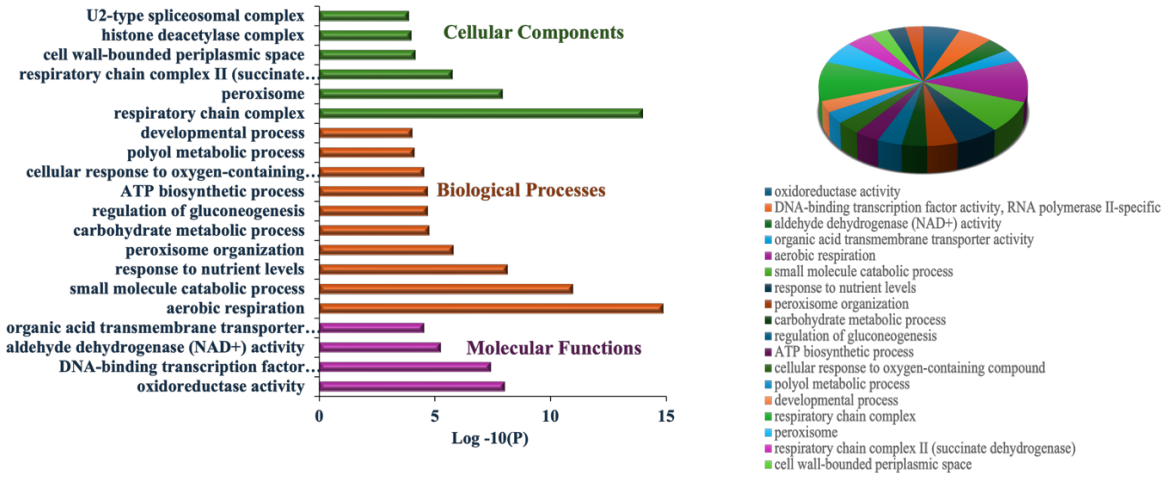


Figure 6.16: GO analysis of genes downregulated in *K123R-K36A*Δ cells at the diauxic shift compared to exponential phase.

6.5 Analysis of gene expression in wild-type, *htb-K123R*Δ*, hht-K36A*Δ*,* and the double mutant *K123R-K36A*Δ in quiescent day 7 (Q-D7) cells compared to transcription during exponential phase

To assess how the histone mutations alter transcription during quiescence, we analysed differential gene expression in wild-type, *htb-K123R*Δ *, hht-K36A*Δ, and the double mutant *K123R-K36A*Δ in quiescent day 7 (Q-D7) cells compared to expression in each strains exponentially (Exp) growing cells. Thus, transcriptional changes were analysed in each strain during the transition from exponential growth into quiescence.

The number of up-regulated and down-regulated genes in day 7 cells was therefore quantified for each strain and compared relative to that seen during its exponential growth. In the wild-type 2001 genes were differentially expressed, with 1128 up-regulated and 837 down-regulated in Q cells compared to transcription in wild-type exponential phase cells. This baseline transcriptional shift reflects the metabolic and regulatory reprogramming associated with entry into quiescence. A substantial transcriptional perturbation was revealed in the *htb-K123R*Δ mutant which exhibited 2426 differentially expressed genes (1241 up-regulated, 1185 down-regulated) as the H2Bub-deficient mutant cells transitioned from exponential growth to quiescence (Table. 6.2 and Fig. 6.17).

The *hht-K36A*Δ mutant showed the most extensive transcriptional disruption, with 3184 genes differentially expressed (1643 up-regulated, 1541 down-regulated). This was in accordance to the established role of H3K36 methylation in suppressing cryptic transcription and maintaining transcriptional fidelity during chromatin transitions (Carrozza *et al.*, 2005; Keogh *et al.*, 2005). Interestingly, the double mutant *K123R-K36A*Δ displayed a reduced transcriptional response compared to *hht-K36A*Δ alone, with 2245 genes differentially expressed (1185 up-regulated, 1060 down-regulated). This attenuation suggests a possible epistatic interaction between H2B K123 and H3 K36 pathways, consistent with chromatin crosstalk models (Lee *et al.*, 2007).

Strain Comparison	Up-Regulated Genes	Down-Regulated Genes	Total Differentially Expressed Genes
wt Exp vs Q-D7	1128	837	2001
*htb-K123R*Δ Exp vs Q-D7	1241	1185	2426
*hht-K36A*Δ Exp vs Q-D7	1643	1541	3184
*K123R-K36A*Δ Exp vs Q-D7	1185	1060	2245

Table 6.2: Shows the numbers of genes more than 2-fold up and down-regulated in each strain in day-7 quiescent cells compared to transcription at exponential phase.

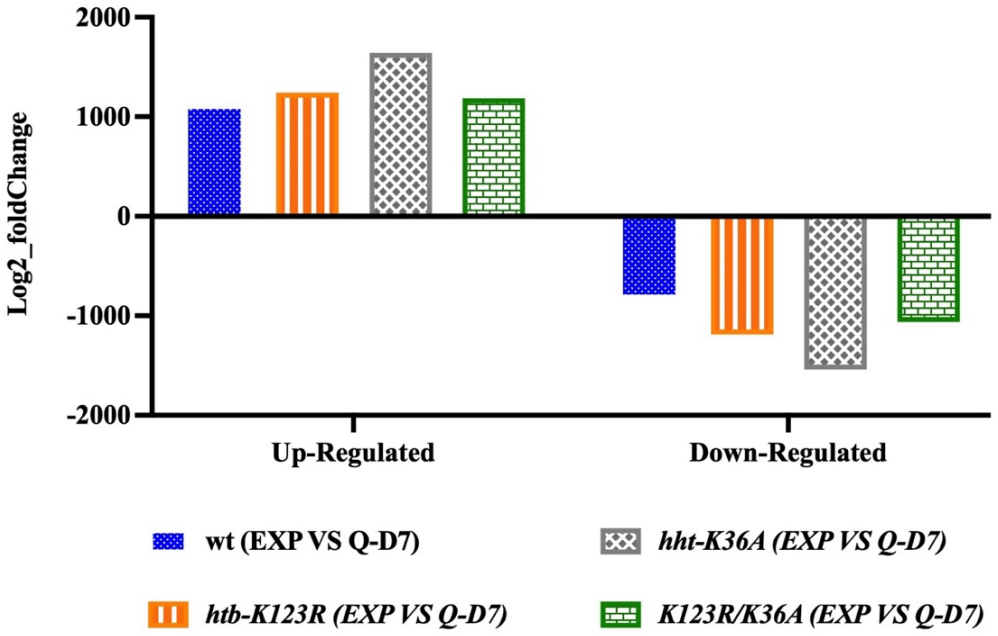


Figure 6.17: Total number of genes for treatment transcriptional profiles in yeast deletion mutants conducted differential gene expression analysis. Across wild-type, *htb-K123R*Δ, *hht-K36A*Δ, and the double mutant *K123R-K36A*Δ in Quiescence cell Day 7 (Q-D7) compared to exponential phase (Exp) for upregulated and down regulated.

6.5.1 Analysing transcription levels of the total number of genes upregulated and downregulated at the Quiescence relative to exponential phase levels of transcription in wild-type and histone mutants.

In Day 7 Q cells, the *htb-K123R*Δ mutant showed (Fig. 6.18A) a modest increase in the average fold increase of the upregulated genes. The K36A mutant displayed a more substantial upregulation, suggesting that loss of H3K36 methylation leads to de-repression of genes normally silenced during quiescence (Carrozza *et al.*, 2005). Notably, in the double mutant *K123R-K36A*Δ the upregulated genes were similar to wild-type, indicating a synergistic disruption of chromatin-mediated repression mechanisms.

A varied downregulated pattern was observed across mutants (Fig. 6.9B). The lowest average down-regulation in transcription was shown by *htb-K123R*Δ mutant. *K36A* exhibited the greatest average gene downregulation which aligned with previous findings that H3K36 methylation maintains transcriptional fidelity and suppresses cryptic transcription (Keogh *et al.*, 2005). However, the double mutant showed less downregulation compared to that seen in the *hht-K36A*Δ single mutant, suggesting potential antagonistic impacts upon gene transcription during this transition by H2Bub and H3K36me. Together these results imply that H2Bub and H3K36me are important for activation and sustaining repression of transcription during quiescence.

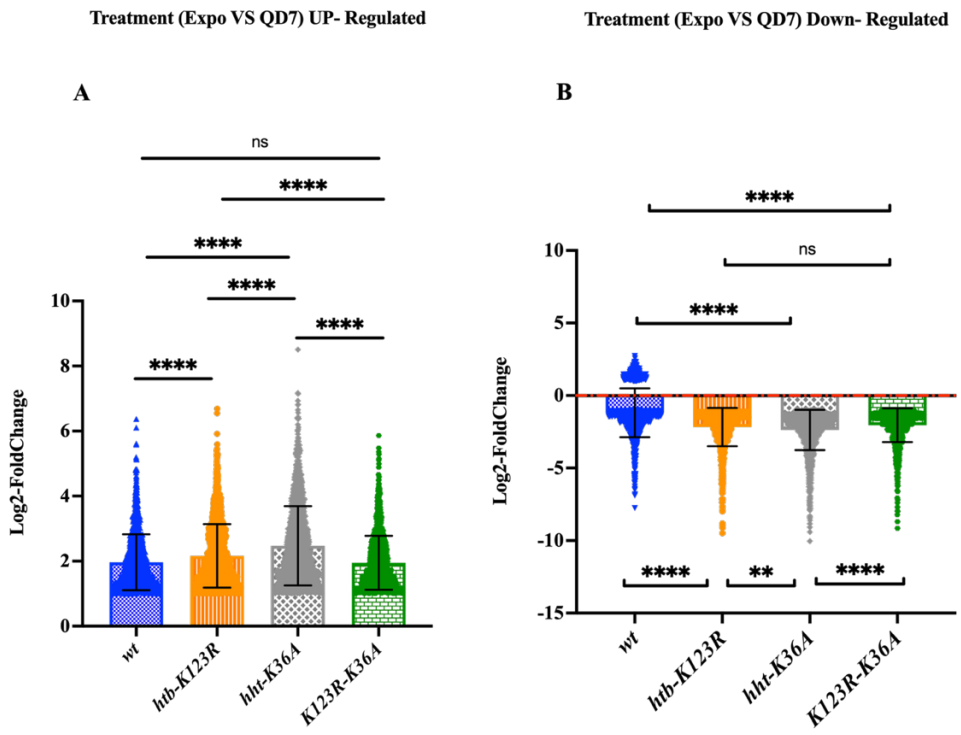


Figure 6.18: Average up and down regulation of gene transcription in wild-type and mutants in day 7 quiescent cells compared to exponential phase cells. The average $\log_2$ fold change (FC) in Quiescent Day 7 (Q-D7) cells compared to exponential phase (Exp) cells. (* p = 0.05, ** p = 0.01, **** p = <0.0001).

6.5.2 Comparison of the upregulated genes of each strain evident in quiescent cells relative to exponentially growing cells

The non-dividing state of quiescence in yeast is induced by nutrient exhaustion, requiring extensive transcriptional reprogramming (Gray *et al.*, 2004; De Virgilio, 2012). To further understand the role played by H2Bub and H3K36me in this transition, we analysed the overlap of genes upregulated in wild-type, *htb-K123R*Δ, *hht-K36A*Δ, and *K123R-K36A*Δ quiescent cells relative to that seen in their exponentially growing cells (Fig. 6.10). A Venn diagram of these upregulated genes revealed that wild-type cells upregulated 69 unique genes, which may reflect those genes whose activation is required to support quiescent cell formation and potential long term survival under nutrient limitation. The *htb-K123R*Δ mutant upregulated 110 unique genes,

while the *hht-K36A*Δ mutant showed a markedly expanded activation profile with 362 unique genes.

The *K123R-K36A*Δ double mutant upregulated 47 unique genes, fewer than either single mutant, suggesting a compensatory or antagonistic interaction between the two histone marks. Notably, 748 genes were commonly upregulated across all four genotypes, representing a conserved core of quiescence-induced transcripts unaffected by H2Bub and H3K36me (Fig. 6.19).

6.6 Comparison of the downregulated genes of each strain evident in quiescent cells relative to exponentially growing cells

To investigate the role of histone H2B K123 monoubiquitination and H3 K36 methylation in activating gene activation during quiescence, we analysed the overlap of downregulated genes in wild-type, *htb-K123R*Δ, *hht-K36A*Δ, and *K123R-K36A*Δ double mutant strains at Day 7 of quiescence compared to that seen in the exponentially growing strains (Fig. 6.11). wild-type cells downregulated 77 unique genes, reflecting a canonical transcriptional response that enables metabolic downscaling and long term survival. The *htb-K123R*Δ mutant downregulated 136 unique genes, while the *hht-K36A*Δ mutant showed a markedly broader profile with 383 uniquely downregulated genes. Interestingly, the *K123R-K36A*Δ double mutant only downregulated 42 unique genes. Furthermore, 532 genes were commonly downregulated across all four strains , representing a conserved core of quiescence-induced transcripts in wild-type that are unaffected by loss of either H2Bub or H3K36me (Fig. 6.11).

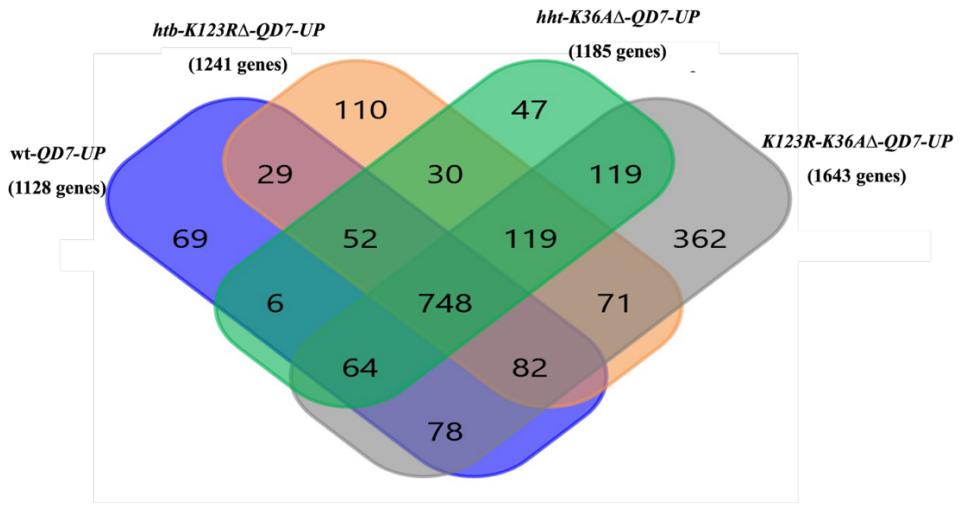


Figure 6.19: Venn diagram of upregulated genes across different quiescent conditions. The diagram shows the overlap of genes significantly upregulated in quiescent cells (relative to exponentially growing cells) under distinct conditions. The numbers in each segment represent the count of unique or shared genes. The total upregulated genes for each condition are indicated in parentheses.

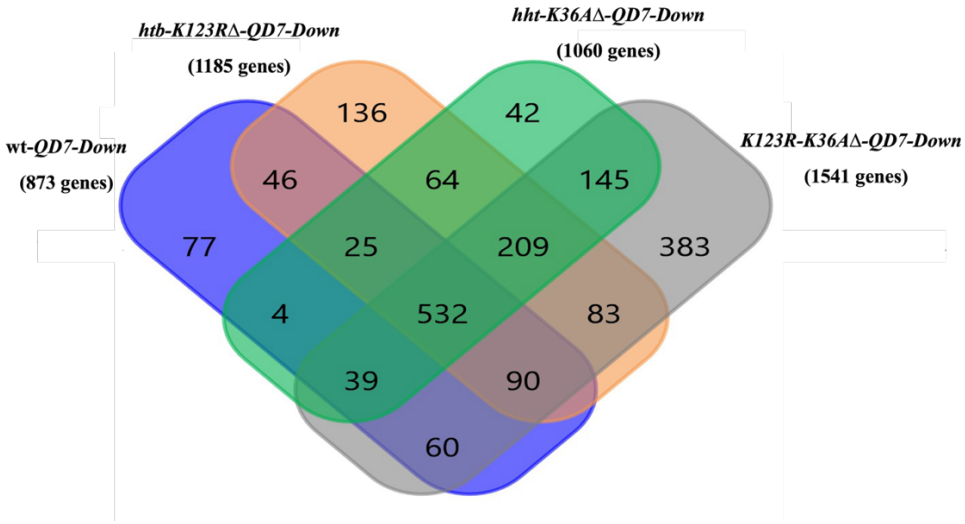


Figure 6.20: Venn diagram of downregulated genes in quiescent cells. The figure shows the overlap of genes significantly downregulated in quiescent cells (relative to exponentially growing cells) across different conditions, including Quiescent Day 7 (QD7). The numbers in each segment represent the count of genes uniquely downregulated in a specific condition or shared between them. The diagram identifies

both the core set of repressed genes common to quiescence and the transcriptional changes specific to individual conditions.

6.6.1 Comparison of the genes uniquely upregulated and downregulated in quiescent *htb-K123R*Δ deletion strains relative to transcription in quiescent wild-type cells .

Among the upregulated genes in quiescent wild-type and *htb-K123R*Δ strains, 217 were uniquely induced in wild-type , 330 were specific to *htb-K123R*Δ and 911 were commonly upregulated in both strains (Fig. 6.21A). This is consistent with loss of H2Bub leading to elevated expression of genes typically repressed during quiescence.

Conversely, when the downregulated genes in Q cells were analysed, 180 genes were uniquely downregulated in wild-type , while 492 were uniquely downregulated in *htb-K123R*Δ with 693 genes shared between the two. Thus, H2Bub is also required for the correct activation of significant numbers of genes in Q cells.

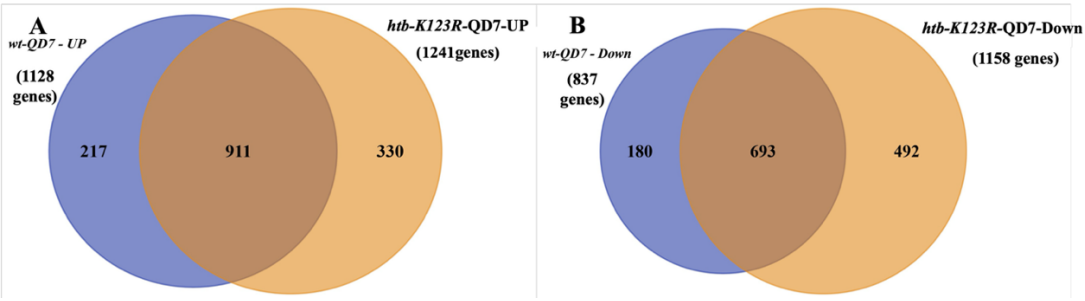


Figure 6.21: Unique and shared transcriptional profiles in yeast deletion mutants during exponential phase compared to Quiescence cell Day 7 in wild-type **cells for upregulated and down regulated.**

6.6.2 Comparison of the genes uniquely upregulated and downregulated in quiescent *hht-K36A*Δ deletion strains relative to transcription in quiescent wild-type cells

To investigate the role of histone H3 lysine 36 methylation in transcriptional regulation during quiescence, we analysed the gene expression data from wild-type and *hht-K36A*Δ mutant strains in day 7 quiescent cells compared to their transcription in exponential phase. (Fig. 6.22). Among

the upregulated genes, 156 were uniquely upregulated in wild-type , 671 were specifically up in *hht-K36A*Δ, and 972 were commonly upregulated in both strains (Fig. 6.22A). This result is consistent with H3K36 methylation playing a role in repression of genes in Q cells.

The downregulated gene set showed a similarly number of genes altered in wild-type and the *hht-K36A*Δ mutant (Fig. 6.22), with 152 genes uniquely downregulated in wild-type , while 820 were uniquely downregulated in *hht-K36A*Δ with 721 genes shared between the two.

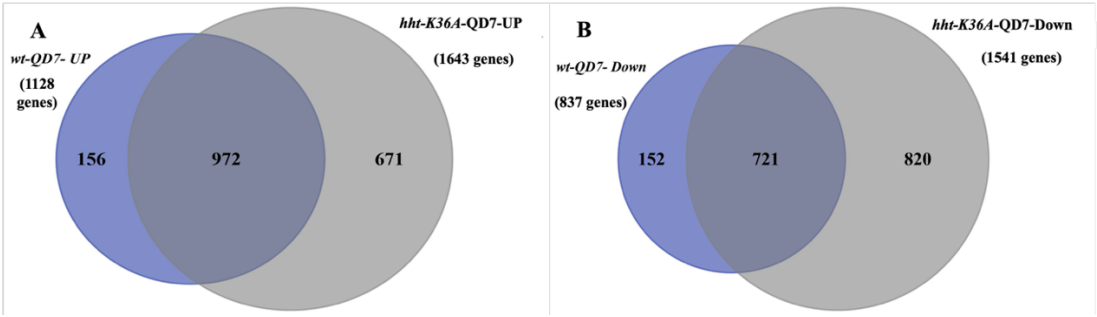


Figure 6.22: Unique and shared transcriptional profiles in yeast deletion mutants during exponential phase compared to Quiescence cell Day 7 in wild-type **cells for upregulated and down regulated.**

6.6.3 Comparison of the genes uniquely upregulated and downregulated in quiescent *K123R-K36A*Δ deletion strains relative to transcription in quiescent wild-type cells

In this analysis, among the upregulated genes, 258 were uniquely upregulated in wild-type , 315 were specific to the *K123R-K36A*Δ double mutant, and 870 were commonly upregulated in both strains (Fig. 6.23.A). The upregulated 315 genes aligns with prior studies showing that loss of H3K36 methylation leads to increased transcriptional noise and cryptic initiation (Li *et al.*, 2007), while the additional mutation of H2B ubiquitination further compromises transcriptional repression (Henry *et al.*, 2003; Weake and Workman, 2008).

Conversely, 273 genes were uniquely downregulated in wild-type , compared to 460 in the double mutant, with 600 genes commonly downregulated in both (Fig. 6.23). The combined mutation therefore leads to mis-regulation of both activating and repressive chromatin states.

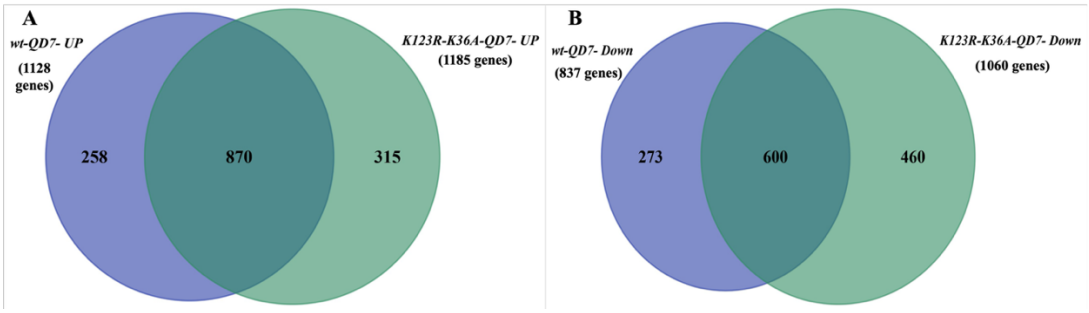


Figure 6.23: Unique and shared transcriptional profiles in yeast deletion mutants during exponential phase compared to Quiescence cell Day 7 in wild-type **cells for upregulated and down regulated.**

6.7 Gene ontology analysis of upregulated genes in the wild-type cells during the transition from Exponential Phase to cell Quiescence.

To characterize the transcriptional landscape of *Saccharomyces cerevisiae* during the transition from exponential growth to long term quiescence, we performed GO enrichment analysis on genes upregulated in wild-type cells at Day 7 of nutrient depletion, Our analysis revealed a robust upregulation of genes associated with *ribosome biogenesis, RNA binding*, and *translational regulations* (Appendix Table. 9 and Fig. 6.24). This suggests that even in deep quiescence, wild-type cells maintain a poised translational apparatus, potentially to enable rapid reactivation upon nutrient repletion.

In biological process category the enrichments were observed in GO terms *ribosome biogenesis, small ribosomal subunit biogenesis, ribosome assembly*, and *ribosomal subunit* export from nucleus. These enrichments suggest that ribosomal gene expression remains active or is reactivated during quiescence. This was consistent with prior study showing that quiescent yeast cells retain *functional ribosomes and nucleolar integrity* (Enenkel, 2014).

The enrichment of *nucleotide metabolic process, ribonucleoside diphosphate metabolic process*, and *small molecule metabolic process* suggests that quiescent cells maintain a basal level of *metabolic activity*. This is likely to support maintenance and survival functions.

High enrichment in term *DNA integration* was also observed, indicating towards increased transposon activity or chromatin remodelling during quiescence, a phenomenon previously observed in stress induced genomic reorganization (Gasch *et al.*, 2000; Curcio and Derbyshire, 2003). The enrichment of *regulation of translational fidelity* and *protein localization* to plasma membrane further corroborates the notion of a controlled, responsive translational environment in quiescent cells. Sequence specific *mRNA binding, translation factor activity*, and *rRNA binding* were significantly enriched among molecular functions. This indicated towards elevated expression of *RNA binding proteins* and *translation regulators*. The enrichment of amide binding may reflect increased *activity of enzymes involved in amino acid metabolism or protein modification*. These molecular signatures suggest that quiescent cells maintain a translationally competent state, poised for rapid entry into the cell cycle upon nutrient availability (De Virgilio, 2012).

A strong enrichment of *cytosolic ribosome, cytosolic large* and *small ribosomal subunits*, and *preribosome precursors* (large and small subunits) were observed in the cellular component analysis category. These findings are in line with previous reports that ribosomal components are preserved during quiescence and may be selectively translated to maintain proteostasis (Laporte *et al.*, 2017).

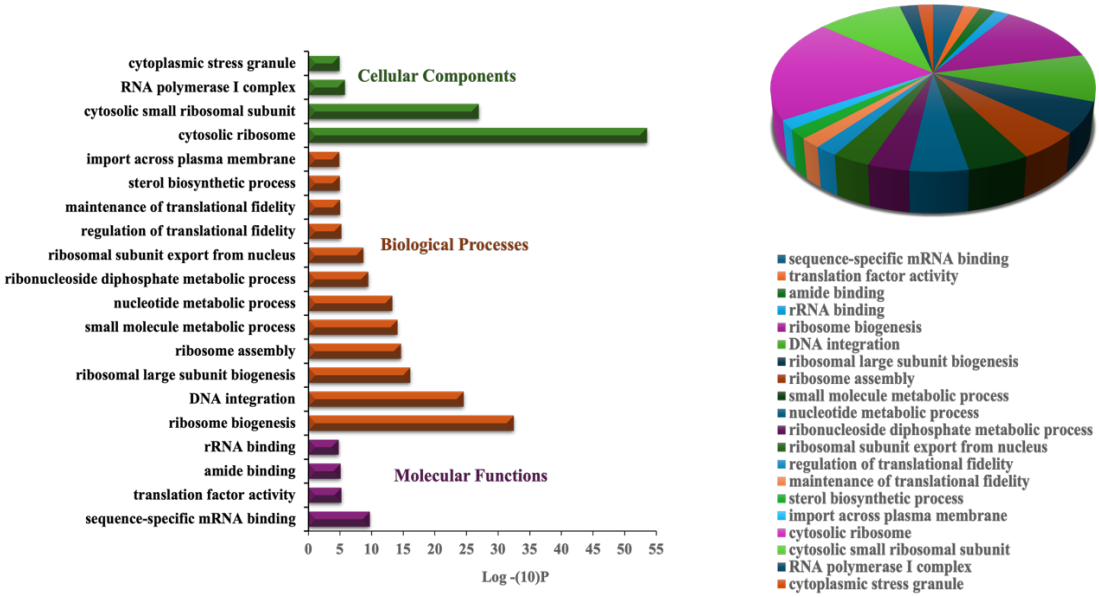


Figure 6.24: GO analysis of genes upregulated in wild-type **cells at the exponential phase compared to Quiescence day 7 (Q-D7).**

6.7.1 Gene ontology analysis of downregulated genes in the wild-type cells during the Exponential Phase to Quiescence Day 7 (Q-D7).

To investigate the transcriptional reprogramming associated with entry into long term quiescence, we performed GO enrichment analysis on genes downregulated in wild-type cells in Quiescence day 7 (Appendix Table. 10 and Fig. 6.25). Our analysis reveals a broad suppression of genes involved in *oxidative metabolism, stress responses*, and *organelle function*, consistent with the physiological shift from growth to maintenance. The most significantly enriched biological processes include response to *nutrient levels, response to chemical stimulus, response to stress*, and *detoxification*. Enrichments of these terms suggest that quiescent cells reduce their transcriptional responsiveness to environmental fluctuations. This is likely to conserve energy and stabilize internal conditions (Gasch *et al.*, 2000).

The enrichment of *protein modification by small protein conjugation* or removal may reflect reduced ubiquitin mediated turnover.

This aligned with the decreased proteolytic activity observed in quiescent cells (Laporte *et al.*, 2017). Enrichments of terms *carbohydrate metabolic process, gluconeogenesis*, and *tricarboxylic acid cycle* suggests a marked suppression of central carbon metabolism. This aligns with previous studies showing that quiescent yeast cells rely on stored carbohydrates and downregulate *energy intensive biosynthetic pathways* (Klosinska *et al.*, 2011; Liu *et al.*, 2015). The enrichments in response to reactive *oxygen species* and *aldehyde metabolic process* suggests reduced *oxidative stress* and *detoxification activity*. This could be due to lower *mitochondrial respiration* and *ROS production*. *DNA binding transcription factor activity* was enriched notably in molecular functions category, indicating a *global reduction in transcriptional regulation*. This was concomitant to previous study where chromatin

compaction and transcriptional silencing observed during quiescence (McKnight *et al.*, 2015). The enrichments in *oxidoreductase activity and ligase activity forming carbon sulfur* bonds further supports the downregulation of redox *metabolism and sulfur containing compound biosynthesis*, both of which are energetically demanding processes.

In cellular component category significant enrichments of *peroxisome, phagophore assembly site membrane*, and *outer membrane* were observed. Peroxisomes are involved in *fatty acid oxidation* and *ROS detoxification*, and their repression may reflect reduced *lipid metabolism* and *oxidative stress* in quiescent cells (Smith and Shilatifard, 2013).

The downregulation of autophagy related structures such as the *phagophore membrane* suggests a shift away from *active organelle turnover*, consistent with the stabilization of cellular architecture during dormancy.

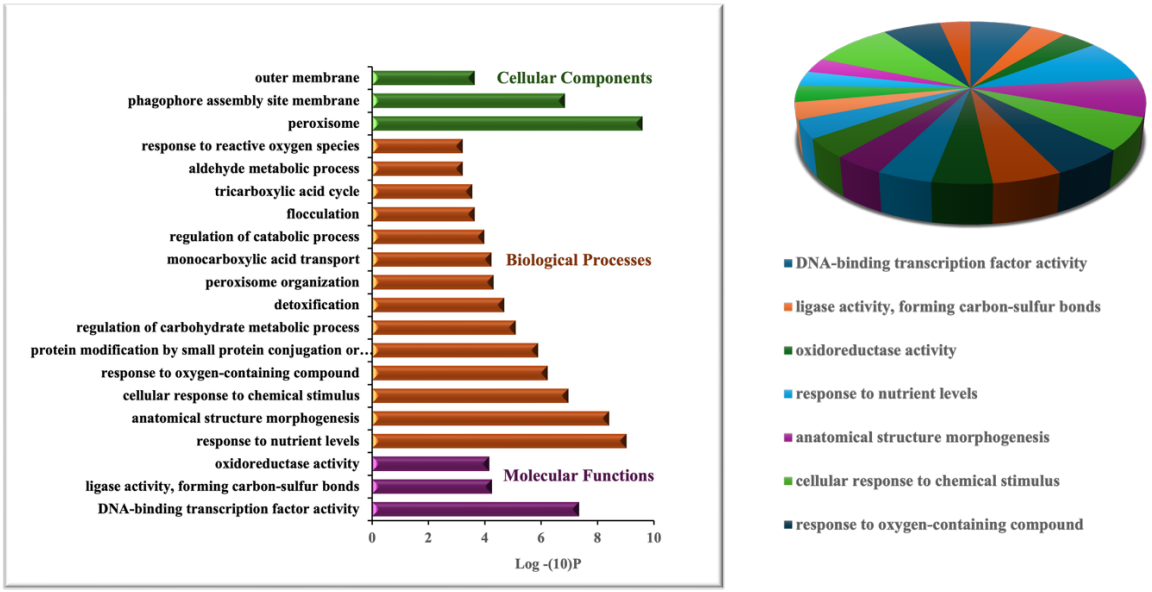


Figure 6.25: GO analysis of genes downregulated in wild-type **cells at the exponential phase compared to Quiescence day 7 (Q-D7).**

6.7.2 Gene ontology analysis of upregulated genes in the *htb-K123R*Δ Mutant during the Exponential Phase to Quiescence Day 7 (Q-D7).

We performed GO enrichment of genes upregulated in the *htb-K123R*Δ mutant after seven days of Quiescence. Mutation of this residue disrupts normal chromatin remodelling, potentially altering the gene expression landscape during cellular dormancy (Appendix Table. 11 and Fig. 6.26).The most enriched biological processes among upregulated genes include *ribosome biogenesis, ribosome assembly*, and *ribosomal large subunit biogenesis*. These enrichments indicate that the *htb-K123R*Δ mutant fails to suppress ribosomal gene expression during quiescence. This was in contrast to wild-type cells which typically downregulate these pathways to conserve energy (De Virgilio, 2012; Laporte *et al.*, 2017). The enrichment of *amino acid metabolic processes* and *carbohydrate derivative metabolism* further indicates sustained *biosynthetic activity*, which may reflect a failure to fully enter the quiescent state.

Additionally, enrichments of genes involved in nucleoside monophosphate metabolism and ribosomal subunit export from the nucleus suggests persistent nucleotide turnover and ribosome trafficking.

Both these functions are typically repressed during quiescence (McKnight *et al.*, 2015). Enrichments in molecular functions include *aspartic type endopeptidase activity, purine ribonucleotide binding*, and *translation factor activity*. These enrichments point to *active protein synthesis and RNA processing*, which are normally attenuated in quiescent cells (Liu *et al.*, 2015). The increased expression of sequence specific *mRNA binding* and *amidic binding* further supports the notion of sustained post transcriptional regulation and translational readiness. In the cellular component category significant enrichment of *ribosomal subunits, cytosolic ribosomes*, and *large ribosomal subunits* were observed, indicating elevated ribosome abundance. Enrichments of terms *mitochondrial inner membrane* and *mitochondrial proton transporting V-type ATPase complex* suggests enhanced *mitochondrial activity*, which may increase energy expenditure and ROS production factors detrimental to quiescent stability (Gray *et al.*, 2004; Smith and Shilatifard, 2013). The enrichment of nuclear components may reflect increased transcriptional activity and chromatin accessibility which further supports the notion of impaired quiescent remodelling.

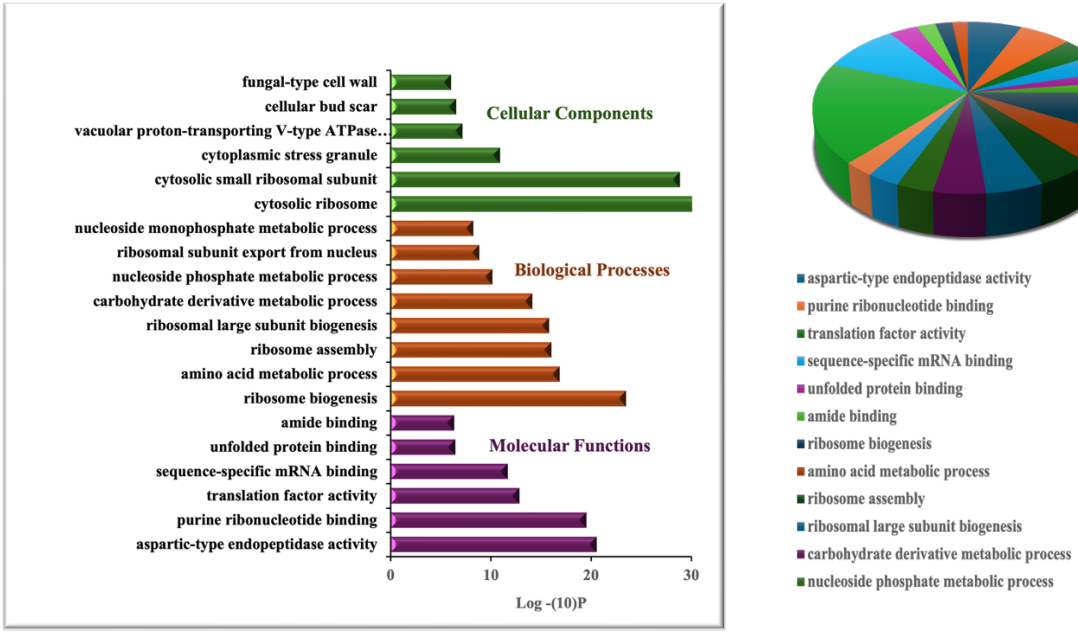


Figure 6.26: GO analysis of genes upregulated in *htb-K123R*Δ cells at the exponential phase compared to Quiescence day 7 (Q-D7).

6.7.3 Gene ontology analysis of downregulated genes in the *htb-K123R*Δ Mutant during the Exponential Phase to Quiescence Day 7 (Q-D7).

GO enrichment of genes downregulated in the *htb-K123R*Δ mutant after day 7 of Quiescence was performed. The most significantly enriched biological processes include *sporulation, small molecule catabolic process, tricarboxylic acid cycle*, and *detoxification* (Appendix Table. 12 and Fig. 6.27). Enrichments of these GO terms suggest a broad suppression of *metabolic flexibility* and *stress adaptation mechanisms*. The enrichment of term *mitochondrial electron transport* from succinate to ubiquinone and *aldehyde metabolic process* in the mutant strain indicates compromised *mitochondrial respiration* and detoxification capacity. These enrichments indicate that cells may be more vulnerable to oxidative damage during dormancy. The enrichment in terms cellular response to *xenobiotic stimulus* and response to oxygen containing compounds further supports the hypothesis that the *htb-K123R*Δ mutant fails to mount adequate stress responses.

These pathways are typically upregulated in quiescent cells to ensure survival under nutrient-limited and oxidative conditions (Gasch *et al.*, 2000; Gray *et al.*, 2004). Among *molecular functions, DNA binding transcription factor activity* was significantly enriched, suggesting a

global reduction in transcriptional regulation. This is consistent with previous studies showing that H2B monoubiquitination facilitates transcriptional elongation and chromatin accessibility (Zhang *et al.*, 2005; Pavri *et al.*, 2006). The enrichments in terms acyltransferase activity and secondary active transmembrane transporter activity may reflect diminished lipid remodelling and nutrient transport, both of which are critical for metabolic adaptation during quiescence.

Cellular component category revealed strong enrichments of terms *peroxisome, peroxisomal membrane*, and *phagophore assembly site membrane*. Peroxisomes play a key role in *fatty acid oxidation* and *ROS detoxification*, and their suppression may compromise cellular resilience during quiescence (Smith and Shilatifard, 2013). The enrichment of piccolo histone acetyltransferase complex and nuclear ubiquitin ligase complex terms suggests impaired chromatin remodelling and protein turnover, processes that are tightly regulated during the transition to dormancy (McKnight *et al.*, 2015).

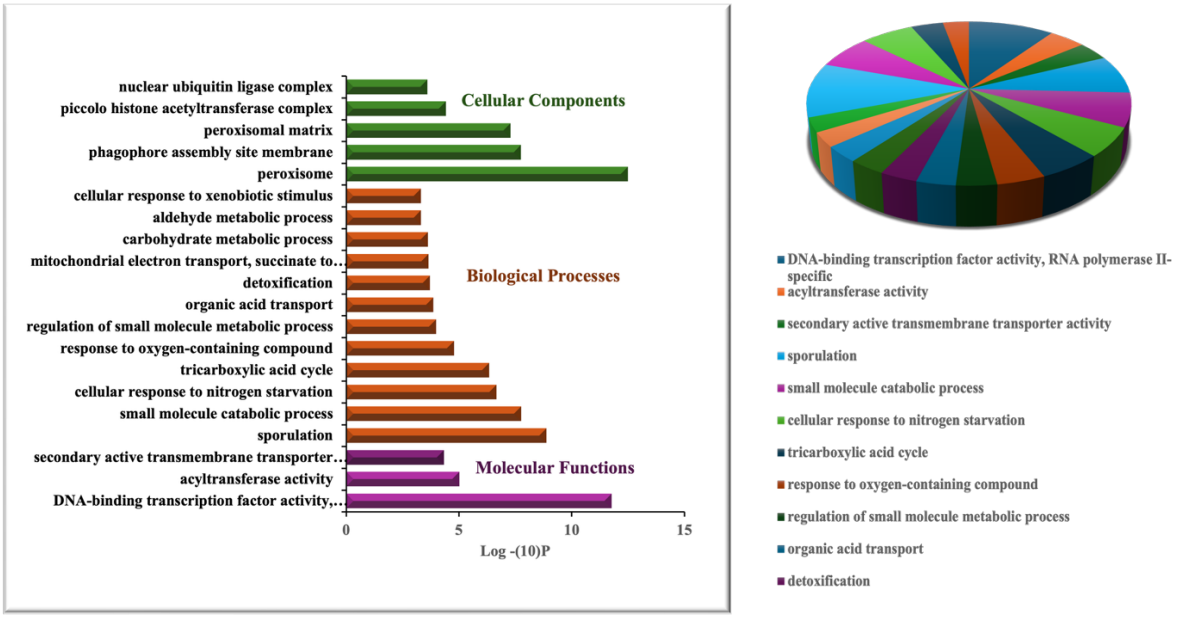


Figure 6.27: GO analysis of genes downregulated in *htb-K123R*Δ cells at the exponential phase compared to Quiescence day 7 (Q-D7).

6.7.4 Gene ontology analysis of upregulated genes in the *hht-K36A*Δ Mutant during the Exponential Phase to Quiescence Day 7 (Q-D7).

We performed GO enrichment analysis on genes upregulated in the *hht-K36A*Δ mutant after 7 day of quiescence (Appendix Table. 13 and Fig. 6.28). The most significantly enriched biological processes among upregulated genes include *ribosome biogenesis, ribosomal large subunit biogenesis, ribosome assembly*, and *rRNA processing*. Enrichments of these GO terms suggest that the *hht-K36A*Δ mutant fails to repress ribosomal gene expression during quiescence, a hallmark of wild-type dormancy programs (De Virgilio, 2012; McKnight *et al.*, 2015). The enrichments of *carbohydrate derivative metabolic processes* and *nucleoside phosphate metabolism* further indicates sustained biosynthetic activity, indicating an incomplete transition into the quiescent state. Notably, enrichments in terms protein targeting to the endoplasmic reticulum and maturation of 5.8S rRNA were also observed, suggesting persistent translation and ribosome trafficking. These processes are typically downregulated in quiescent cells to conserve energy and reduce proteotoxic stress (Gray *et al.*, 2004; Liu *et al.*, 2015).

Enrichments in molecular functions category include *catalytic activity acting on RNA, translation factor activity*, and *snoRNA binding,* all of which are central to *ribosome biogenesis* and *RNA maturation*. The enrichment of *nucleotidyltransferase activity* and *tRNA binding* further supports the idea of persistent translational preparedness. These results are consistent with previous findings that histone acetylation promotes transcriptional activation of growth-related genes (Millar *et al.*, 2006).

Cellular component category enrichments included *cytosolic ribosome, cytosolic small ribosomal subunit,* and *cytosolic large ribosomal subunit*, indicating *elevated ribosome abundance*. The enrichment of term *vacuolar proton transporting V-type ATPase complex* may reflect altered vacuolar function, which plays a role in pH homeostasis and autophagy during nutrient stress (Breton and Brown, 2013).

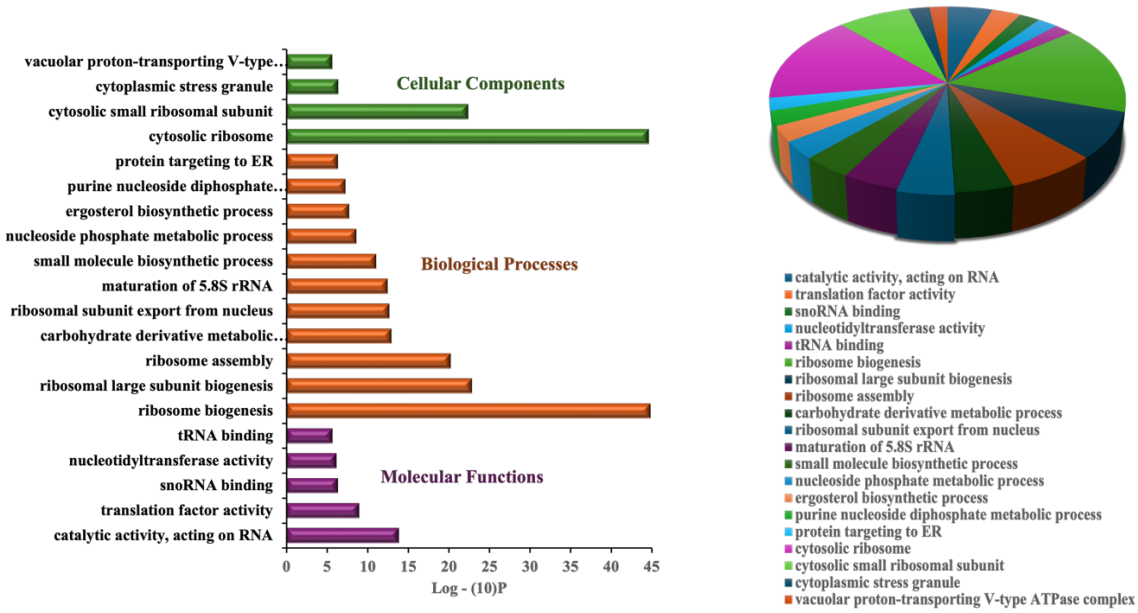


Figure 6.28: GO analysis of genes upregulated in *hht-K36A*Δ cells at the exponential phase compared to Quiescence day 7 (Q-D7).

6.7.5 Gene ontology analysis of downregulated genes in the *hht-K36A*Δ Mutant during the Exponential Phase to Quiescence Day 7 (Q-D7).

The most significantly enriched biological processes include *developmental process, response to oxygen-containing compounds, response to nutrient levels*, and *detoxification* (Appendix Table. 14 and Fig. 6.29). Enrichments in these terms suggest that the *hht-K36A*Δ mutant fails to activate stress responsive and adaptive pathways that are typically upregulated during quiescence (Gasch *et al.*, 2000; De Virgilio, 2012). The enrichment of terms *autophagy of mitochondrion* and *regulation of autophagy of carbohydrate metabolic process* indicates *impaired organelle turnover* and *metabolic remodelling, hallmarks* of quiescent stage (Breton and Brown, 2013; Laporte *et al.*, 2017). Additionally, enrichments in GO terms *small molecule catabolic process, carbohydrate metabolic process*, and *generation of precursor metabolites*

and *energy reflects a failure to reprogram central metabolism*. Quiescent cells typically shift toward energy conservation and redox homeostasis, relying on tightly regulated catabolic pathways (Liu *et al.*, 2015).

Among molecular functions, *DNA binding transcription factor activity (RNA polymerase II-specific), ubiquitin-like protein ligase activity*, and *oxidoreductase activity* were significantly downregulated GO terms. These results suggest a global reduction in *transcriptional regulation* and *protein turnover*, consistent with impaired chromatin remodelling and stress adaptation. Histone acetylation has been shown to facilitate transcriptional activation of stress responsive genes (Millar *et al.*, 2006), and its absence in the *hht-K36A*Δ mutant may lead to transcriptional silencing of key survival pathways. The repression of GO term *serine/threonine kinase activity* and *secondary active transmembrane transporter activity* further corroborates the notion of diminished signalling and nutrient uptake. These functions are critical for sensing environmental changes and coordinating metabolic responses during quiescence (Gray *et al.*, 2004). Cellular component category revealed strong enrichment of *peroxisome*. Peroxisomes play a key role in *fatty acid oxidation* and *ROS detoxification*, and their suppression may compromise cellular resilience during quiescence (Smith and Shilatifard, 2013).

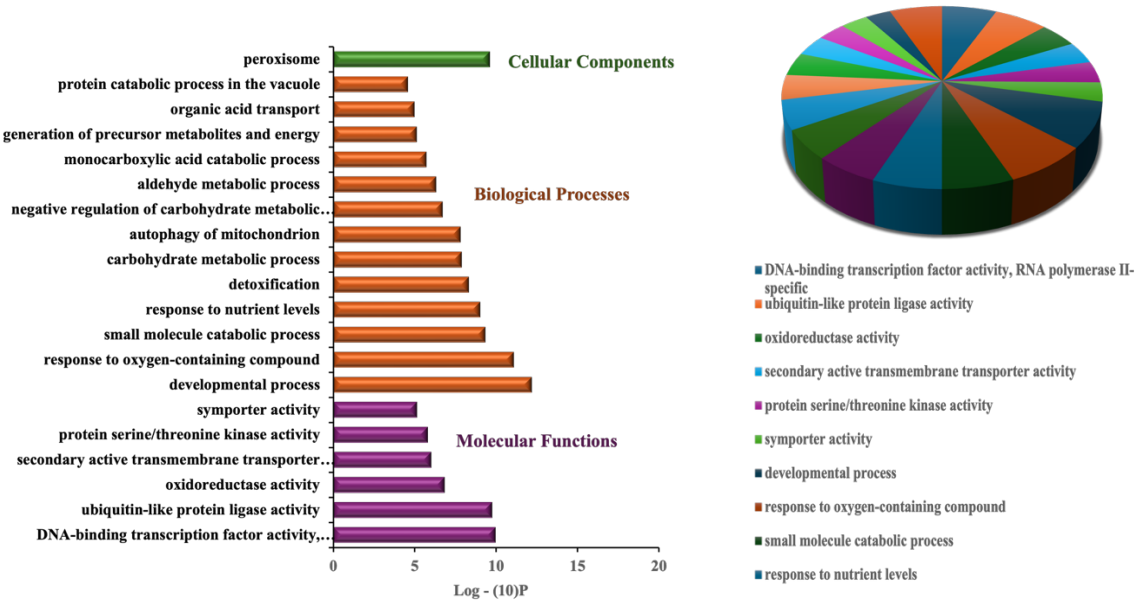


Figure 6.29: GO analysis of genes downregulated in *hht-K36A*Δ cells at the exponential phase compared to Quiescence day 7 (Q-D7).

6.7.6 Gene ontology analysis of upregulated genes in the *K123R-K36A*Δ Double Mutant during the Exponential Phase to Quiescence Day 7 (Q-D7).

To investigate the transcriptional consequences of combined disruption of histone H2B lysine 123 monoubiquitination and lysine 36 acetylation, we performed GO enrichment analysis on genes upregulated in the *K123R-K36A*Δ double mutant during the transition from exponential growth to Day 7 of quiescence (Appendix Table. 15 and Fig. 6.30). The most significantly enriched biological processes among upregulated genes include *DNA integration, ribosome assembly, ribosomal large subunit biogenesis*, and *small molecule metabolic process*. These enrichments indicate that the double mutant fails to repress ribosomal and biosynthetic gene expression during quiescence. This observation is a deviation from the canonical wild-type response, where *ribosome biogenesis* is tightly suppressed to conserve energy (De Virgilio, 2012; McKnight *et al.*, 2015).

Upregulation of GO terms *carbohydrate derivative metabolic process, nucleoside metabolic process,* and *nucleoside triphosphate metabolic process* indicates sustained *nucleotide turnover* and energy consuming *biosynthetic activity*.

These enrichments profile mirrors a growth like state, signifying that the double mutant is not fully employing the metabolic reprogramming required for quiescent survival (Liu *et al.*, 2015). Among molecular functions, *purine ribonucleoside triphosphate binding, sequence specific mRNA binding*, and *translation factor activity* were highly enriched. These terms reflect persistent activation of translation and RNA processing machinery. These processes are typically downregulated in quiescent cells to reduce proteotoxic stress and conserve resources (Gray *et al.*, 2004).

The enrichment of amide binding further supports the notion of active protein synthesis and metabolic engagement. Cellular component analysis revealed enrichment of *cytosolic ribosome, cytosolic ribosomal subunit,* and *RNA polymerase II transcription factor holoenzyme complex, indicating elevated ribosome abundance* and *transcriptional activity*. The presence of *proteasome regulatory particle ATPase complex* suggests increased protein turnover, which

may reflect a compensatory mechanism to manage misfolded proteins resulting from sustained translation under stress (Breton and Brown, 2013).

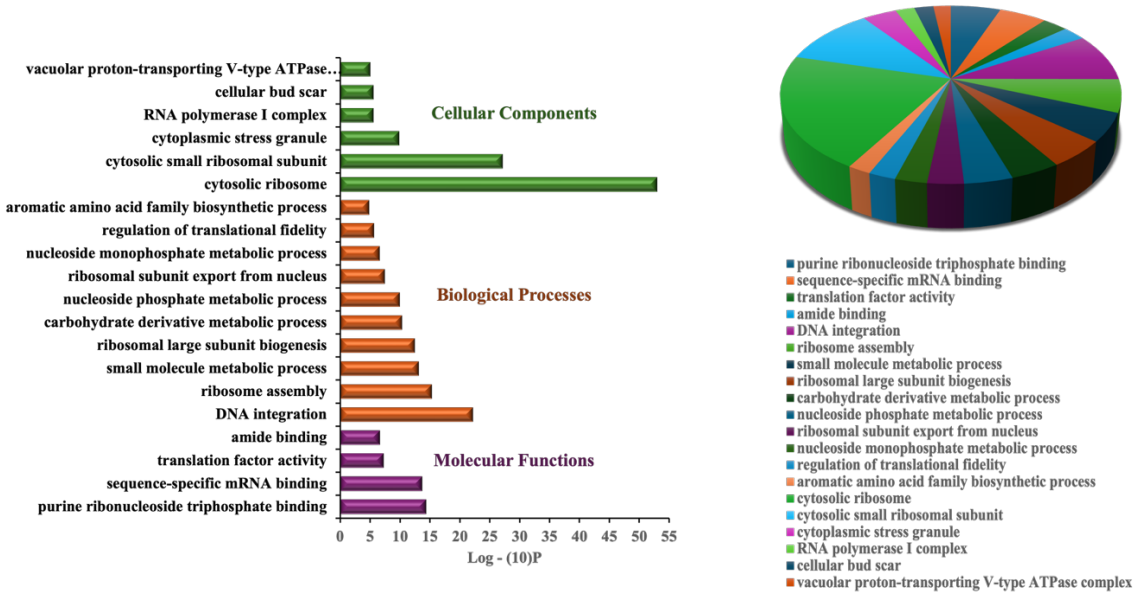


Figure 6.30: GO analysis of genes upregulated in *K123R-K36A*Δ cells at the exponential phase compared to Quiescence day 7 (Q-D7).

6.7.7 Gene ontology analysis of downregulated genes in the *K123R-K36A*Δ Double Mutant during the Exponential Phase to Quiescence Day 7 (Q-D7).

We analysed the GO enrichment of genes downregulated in the *K123R-K36A*Δ double mutant during the transition from exponential growth to quiescence (Appendix Table. 16 and Fig. 6.31). The most significantly downregulated GO terms biological processes category include *transmembrane transport, small molecule catabolic process, organic acid catabolic process*, and *fatty acid catabolic process*. These pathways are central to energy generation and nutrient recycling during quiescence (Zaman *et al.*, 2008; De Virgilio, 2012). The suppression of GO terms *sporulation and autophagy of mitochondrion* further suggests impaired cellular remodelling and organelle turnover, which are critical for long term survival under nutrient

limitation (Kanki and Klionsky, 2008). Downregulation of GO terms *tricarboxylic acid (TCA) cycle genes* and *oxoacid metabolic processes* indicates a broad suppression of mitochondrial respiration.

This aligns with previous findings that quiescent yeast cells rely on tightly regulated *mitochondrial activity* to balance energy production and ROS management (Laporte *et al.*, 2017). Among molecular functions, *DNA binding transcription factor activity (RNA polymerase II-specific)* and *oxidoreductase activity* were significantly downregulated GO terms. A global reduction in transcriptional initiation and redox metabolism are indicatives of these reductions, both of which are tightly modulated during quiescence to minimize damage and conserve resources (Gray *et al.*, 2004). The suppression of GO terms symporter activity and acyltransferase activity reflects reduced nutrient uptake and lipid remodelling. These processes are typically upregulated in wild-type cells entering quiescence (Gasch *et al.*, 2000).

Cellular component analysis revealed strong downregulation of GO terms *peroxisome, mitochondrion, mitochondrial membranes*, and *respiratory chain complex II (succinate dehydrogenase).* A profound suppression of *organelles central to energy metabolism* and *oxidative stress* regulation can be indicative of these repressions. In wild-type yeast, peroxisomes and mitochondria are dynamically remodelled during quiescence to support fatty acid oxidation and maintain redox balance. The failure to maintain these components in the double mutant suggests a compromised metabolic state that may impair long term viability.

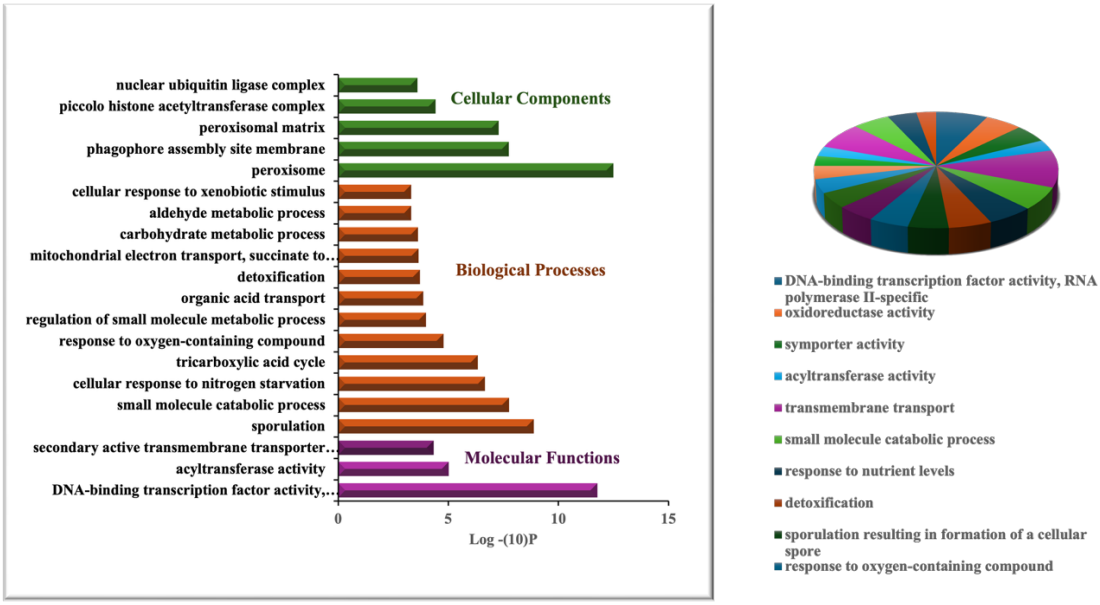


Figure 6.31: GO analysis of genes downregulated in *K123R-K36A*Δ cells at the exponential phase compared to Quiescence day 7 (Q-D7).

6.8. Discussion

6.8.1 Transcriptional Reprogramming in Histone Mutants During the Diauxic Shift and quiescence (Q-D7)

To characterize genome-wide transcriptional changes induced by histone mutations during metabolic transition, we compared gene expression profiles of wild-type and mutant yeast strains, *htb-K123R*Δ*, K123R-K36A*Δ*,* and *hht-K36A*Δ*,* under diauxic shift (Dix) conditions relative to exponential phase (Figure 6.32). Substantially variation in the number of regulated genes was seen across genotypes, with *hht-K36A*Δ showing the most extensive transcriptional response (2845 genes), followed by *htb-K123R*Δ (2426 genes), *K123R-K36A*Δ (2191 genes), and wild-type (815 genes). The overlap of 618 genes across all five conditions suggests a conserved core response to the diauxic shift, independent of specific histone tail modifications. In *htb-K123R*Δ*,* 573 unique genes were seen, indicating broad transcriptional activation linked to H2B K123 acetylation mimicry. *K123R-K36A*Δ showed 154 unique genes, reflecting a more selective regulatory footprint. In hht-K36A 650 unique genes were seen, consistent with its role

in chromatin remodelling and transcriptional de-repression. In wild-type only 7 unique genes were seen highlighting the mutation-driven divergence in transcriptional output. Combinatorial overlaps revealed shared regulatory programs among mutants.

Notably, 661 genes were co-regulated in *htb-K123R*Δ and *hht-K36A*Δ, suggesting functional convergence between H2B and H3 tail modifications. Similarly, 367 genes were shared between *htb-K123R*Δ and *K123R-K36A*Δ, pointing to potential functional interplay. These findings demonstrate that histone tail mutations induce both shared and mutation-specific transcriptional programs during the diauxic shift, with implications for chromatin-mediated metabolic adaptation and gene regulation.

Differential gene expression analysis in wild-type and mutant yeast strains, *htb-K123R*Δ**,** *K123R-K36A*Δ**, a**nd *hht-K36A*Δ**,** on day 7 of quiescence (Q-D7) relative to exponential phase was also performed (Figure 6.33). The magnitude of transcriptional repression varied across genotypes, *hht-K36A*Δ exhibited the most extensive downregulation (3184 genes), consistent with the role of H3K36 in transcriptional elongation and chromatin-mediated silencing. *K123R-K36A*Δ and wild-type followed with 2245 and 2001 downregulated genes, respectively. *htb-K123R*Δ showed a more modest repression profile (1152 genes), suggesting a subtler contribution of H2B K123 to quiescence-associated transcriptional control. A conserved set of 542 genes was downregulated across all five conditions, indicating a core transcriptional program associated with quiescent maintenance. In contrast, each genotype also displayed distinct subsets of uniquely repressed genes. 1046 unique genes were seen in *hht-K36A*Δ**,** reflecting its broad impact on chromatin accessibility and transcriptional shutdown. *K123R-K36A*Δ showed 314 unique genes**,** suggesting targeted repression linked to combined H2B and H3 tail alterations. In *htb-K123R*Δ 165 unique genes were seen, indicative of selective modulation. In wild-type 245 unique genes were observed, representing baseline quiescence-induced repression. 661 genes were co-repressed in *htb-K123R*Δ and *hht-K36A*Δ, suggesting functional interplay between H2B and H3 tail modifications. Similarly, 367 genes were jointly downregulated in *htb-K123R*Δ and *K123R-K36A*Δ, pointing to convergent transcriptional control mechanisms. These data highlight both conserved and mutation-specific transcriptional repression programs during deep quiescence, with H3K36A mutations exerting the most pronounced effect on global gene silencing.

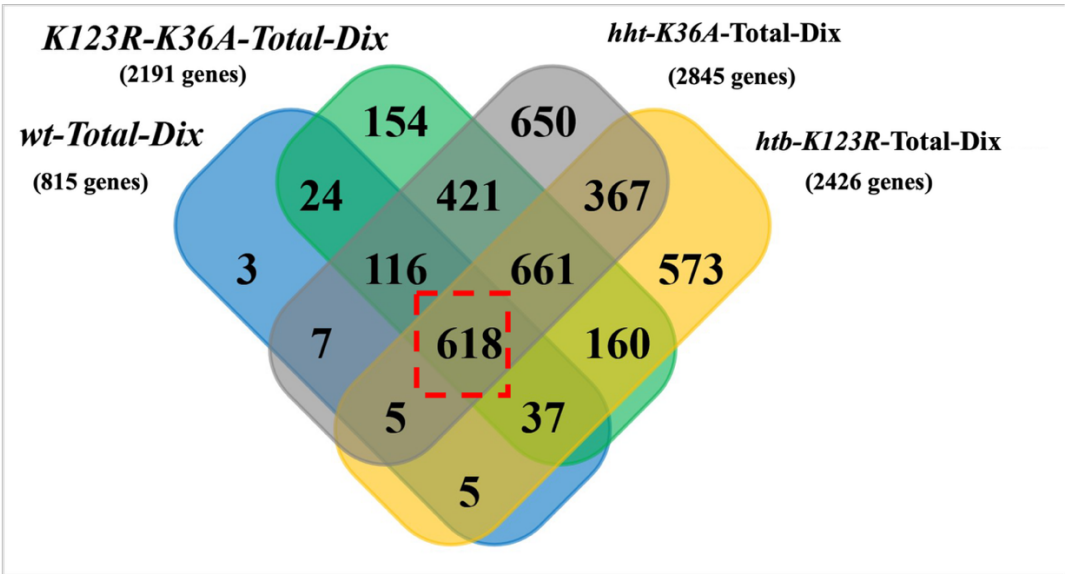


Figure 6.32: Venn diagram showing the total number of genes treatment bound in various yeast strains under Total-Dix treatment. wild-type -Total-Dix: wild-type -strain (815 genes). *K123R-K36A*Δ-Total-Dix (2191 genes). *htb-K123R*Δ-Total-Dix (2426 genes). *hht-K36A*Δ-Total-Dix (2845 genes). The numbers in the overlapping sections represent the count of genes common to the respective groups.

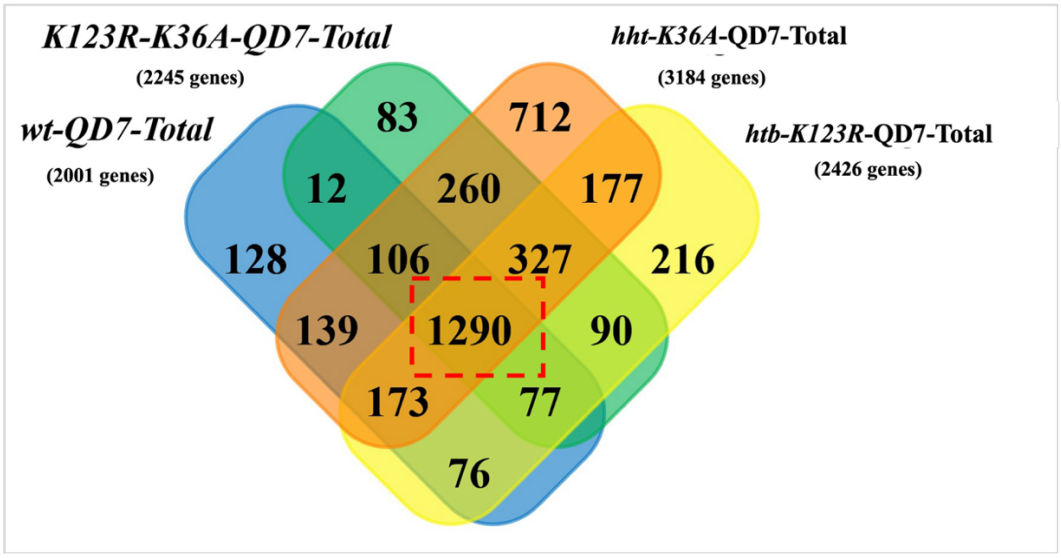


Figure 6.33: Venn diagram showing the total number of genes treatment bound in various yeast strains under QD7-Total treatment. wild-type -QD7-Total: wild-type -strain (2001 genes). *K123R-K36A*Δ-QD7-Total (2245 genes). *htb-K123R*Δ-QD7-Total (2426 genes). *hht-K36A*Δ-QD7-Total (3184 genes). The numbers in the overlapping represent the count of genes common to the respective groups.

6.9 Differential Gene Expression Reveals Stage-Specific Adaptations

6.9.1 Comparative Analysis of Upregulated and Downregulated Genes in wild-type Yeast During Diauxic Shift and quiescent day 7 (Q-D7)

To investigate the transcriptional response of yeast under different metabolic states, we compared the differentially expressed genes in wild-type t cells during the diauxic (Dix) and quiescent day 7 (Q-D7) phases. The Venn diagrams (Fig. 6.34) illustrate the overlap and specificity of upregulated and downregulated genes across these conditions.

During the transition from exponential to diauxic growth quiescent day 7 (Q-D7) phase, we observed 728 and 1128 genes upregulated**,** of which 551 were shared, while 177 genes were uniquely induced in (Dix) and 577 genes uniquely induced in (Q-D7). Similarly, 137 and 873 downregulated genes were detected, with 49 overlapping and 38 being unique to (Dix). 824 genes were found to be uniquely downregulated (Q-D7). These results are consistent with the major transcriptional reprogramming reported during the diauxic shift (Dix), where yeast cells switch from fermentative to respiratory metabolism and induce genes involved in mitochondrial function, stress response, and alternative carbon source utilization (DeRisi *et al.*, 1997; Breeden and Tsukiyama, 2022). The strong repression of genes during prolonged quiescence is consistent with the global transcriptional downscaling described in nutrient depleted cells (Gasch *et al.*, 2000; Young *et al.*, 2017). Many of these downregulated genes are enriched in cell cycle progression and biosynthetic pathways, supporting the establishment of a low metabolic, stress resistant state characteristic of quiescent yeast populations (Gray *et al.*, 2004). Overall, these results highlight the progressive restructuring of the yeast transcriptome as cells transition from exponential (Exp) growth through the diauxic shift (Dix) and into quiescence (Q).

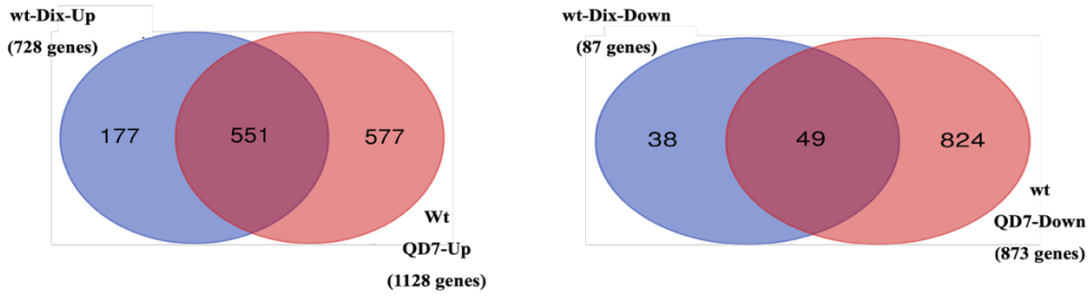


Figure 6.34: Gene regulation wild-type **-Exp-Dix VS Exp-Q-D7 Up and Downregulated**

6.9.2 Comparative Analysis of Upregulated and Downregulated Genes in *htb-K123R*Δ mutant Yeast During Diauxic Shift and quiescent day 7 (Q-D7)

To assess the impact of histone H2B ubiquitination deficiency on transcriptional dynamics, we compared gene expression in the *htb-K123R*Δ mutant strain across diauxic (Dix) and quiescent day 7 (Q-D7) phases (Fig. 6.35). The *htb-K123R*Δ mutant displayed 524 and 1241 upregulated genes, of which 364 were shared between (Dix) and (Q-D7), while 160 and 877 were uniquely expressed in (Dix) and (Q-D7), respectively. Similarly, we identified 628 and 1185 downregulated genes, with 351 overlapping between (Dix) and (Q-D7), and 277 and 834 being unique to each phase, respectively. These results indicate that although a significant portion of gene regulation is conserved between phases, the *htb-K123R*Δ mutant shows a broader set of uniquely regulated genes compared to wild-type , reflecting altered metabolic adaptation at the diauxic shift (Dix). This largescale downregulation is consistent with previous observations that chromatin remodelling and histone modifications play a central role in establishing transcriptional silencing during quiescence (Q) (McKnight *et al.*, 2015; Young *et al.*, 2017).

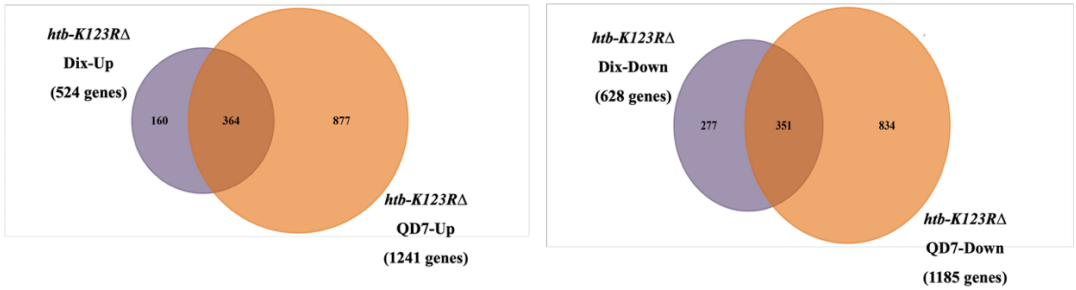


Figure 6.35: Gene regulation *htb-K123R*Δ -Exp-Dix VS Exp-Q-D7 Up and Downregulated

6.9.3 Comparative Analysis of Upregulated and Downregulated Genes in *hht-K36A*Δ mutant Yeast During Diauxic Shift and quiescent day 7 (Q-D7)

We analysed gene expression profiles of the *hht-K36A*Δ mutant during diauxic (Dix), and quiescent day 7 (Q-D7) phases to examine the role of histone H3 lysine 36 (H3K36) methylation in transcriptional regulation (Fig. 6.36). During the transition from exponential to diauxic growth and quiescent day 7 (Q-D7), the *hht-K36A*Δ mutant displayed a large set of differentially regulated genes.

A total of 1433 and 1643 upregulated genes were detected, with 1,110 shared between (Dix) and (Q-D7), while 333 and 533 were uniquely upregulated in (Dix) and (Q-D7), respectively. Similarly, 1402 and 1541 genes were downregulated, including 944 shared between the two phases, with 458 and 597 uniquely suppressed in (Dix) and (Q-D7), respectively. These results indicate that loss of H3K36 methylation does not abolish diauxic reprogramming but expands the set of uniquely regulated genes compared to wild-type . This is consistent with earlier findings showing that H3K36 methylation is essential for restricting inappropriate transcription and for buffering transcriptional noise during metabolic transitions (Youdell *et al.*, 2008; Venkatesh *et al.*, 2012).

This suggests that the *hht-K36A*Δ mutant fails to establish a distinct transcriptional program upon entry into quiescence (Q), instead maintaining an aberrant transcriptional state reminiscent of growth phases. Overall, these findings demonstrate that the *hht-K36A*Δ mutation profoundly alters gene regulation across growth states.

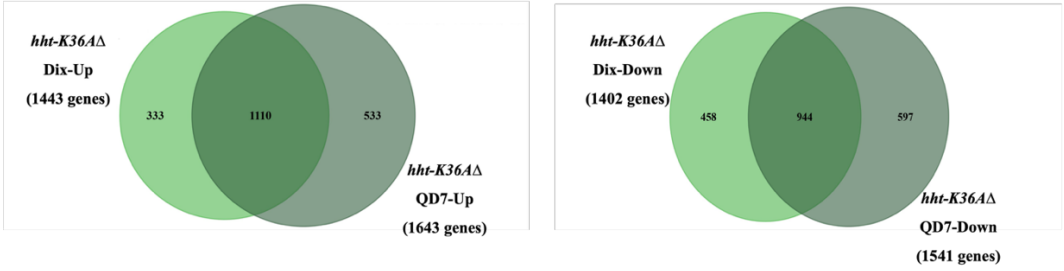


Figure 6.36: Gene regulation *hht-K36A*Δ -Exp-Dix VS Exp-Q-D7 Up and Downregulated

6.9.4 Comparative Analysis of Upregulated and Downregulated Genes in *K123R-K36A*Δ double *mutant* Yeast During Diauxic Shift and quiescent day 7 (Q-D7)

To investigate the transcriptional impact of histone mutations, we compared global gene expression profiles in *K123R-K36A*Δ mutant strains across different metabolic states. Specifically, we analysed transcriptomes during the diauxic shift (Dix) and quiescence (Q-D7) (Fig. 6.37).

During the transition from exponential to diauxic growth and quiescent day 7 (Q-D7), the *K123R-K36A*Δ mutant displayed a large set of differentially regulated genes.

A total of 1227 and 1185 upregulated genes were detected, with 840 shared between (Q-D7) and (Dix), while 387 and 345 were uniquely upregulated in (Dix) and (Q-D7), respectively. A total of 964 and 1060 downregulated genes were detected, with 602 shared between (Q-D7) and (Dix), while 362 and 458 were uniquely upregulated in (Dix) and (Q-D7), respectively. The *K123R-K36A*Δ mutant exhibited extensive transcriptional changes.

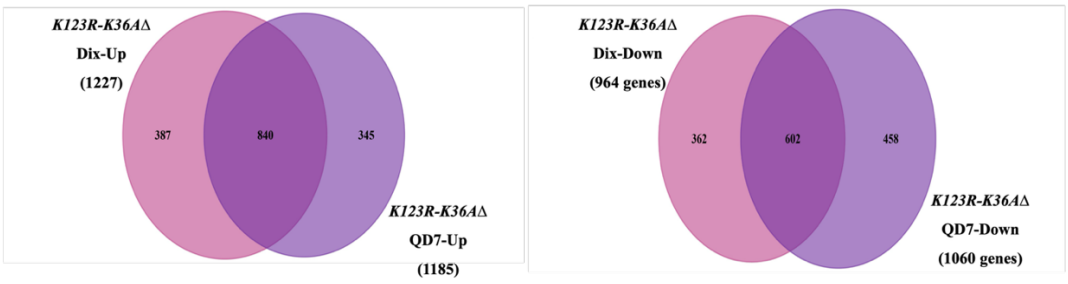


Figure 6.37: Gene regulation *K123R-K36A*Δ -Exp-Dix VS Exp-Q-D7 Up and Downregulated

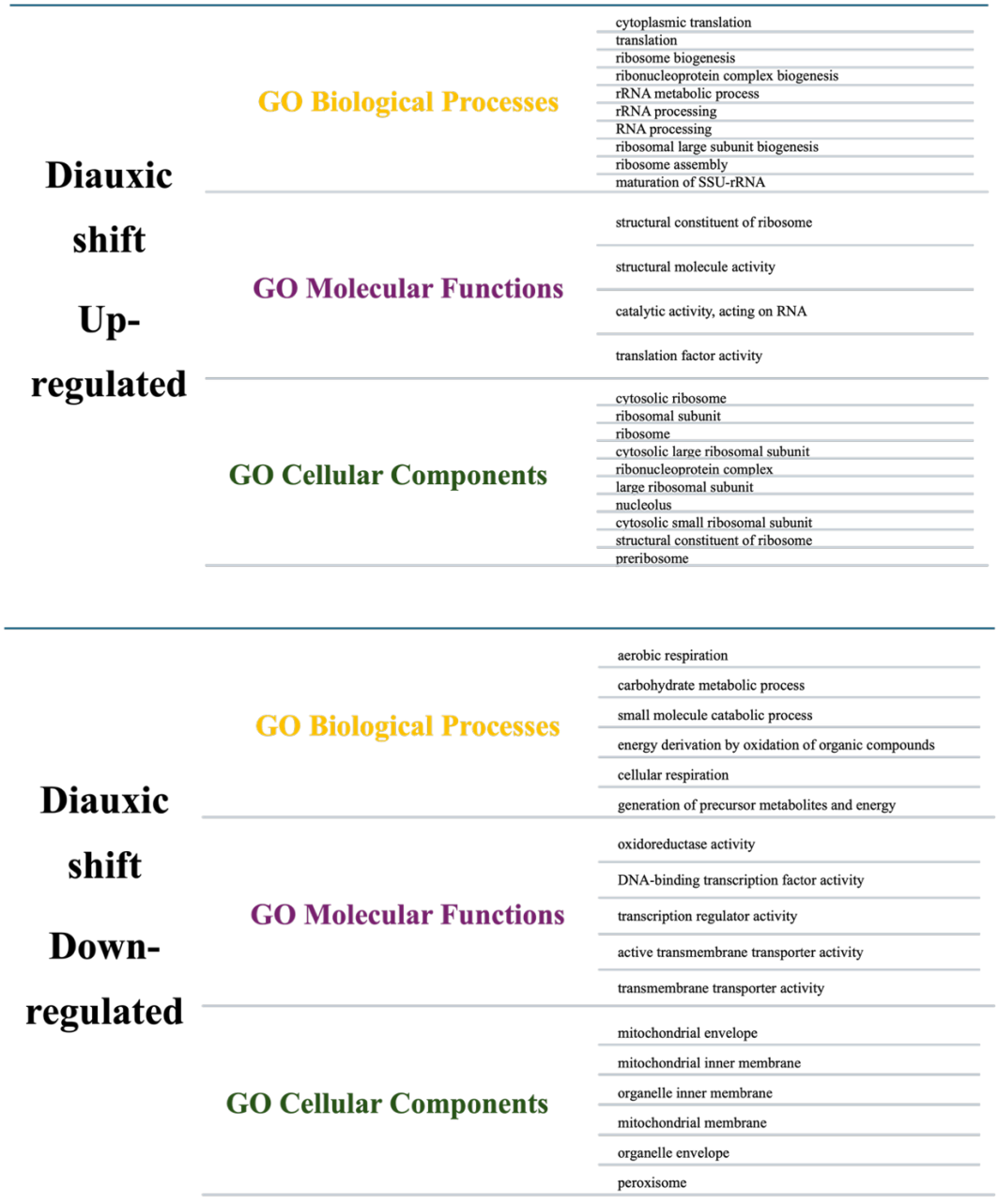


Figure 6.38: Gene Ontology (GO) analysis of genes differentially expressed in the comparison of Exp vs. Dix for up and downregulated. The analysis categorizes genes based on three GO terms: Biological Process, Molecular Function, and Cellular Component. It shows upregulated and

downregulated genes in wild-type and single mutants, highlighting both shared and unique genes across all mutants for each of the three categories.

Quiescence Day 7 Up-regulated	**GO Biological Processes**	cytoplasmic translation DNA integration ribosome biogenesis ribonucleoprotein complex biogenesis rRNA metabolic process rRNA processing RNA processing ribosomal large subunit biogenesis ribosome assembly maturation of SSU-rRNA small molecule metabolic process ribosomal small subunit biogenesis amino acid metabolic process small molecule biosynthetic process
	GO Molecular Functions	structural constituent of ribosome structural molecule activity catalytic activity, acting on RNA aspartic-type endopeptidase activity
	GO Cellular Components	cytosolic ribosome cytosolic large ribosomal subunit ribosome cytosolic small ribosomal subunit ribosomal subunit large ribosomal subunit nucleolus small ribosomal subunit ribonucleoprotein complex Preribosome, 90S cytoplasmic translation

Quiescence Day 7 Down-regulated	**GO Biological Processes**	small molecule catabolic process carboxylic acid metabolic process response to nutrient levels anatomical structure morphogenesis sporulation resulting in formation of a cellular spore anatomical structure formation involved in morphogenesis sporulation developmental process cellular response to chemical stimulus
	GO Molecular Functions	DNA-binding transcription factor activity transcription regulator activity ubiquitin-like protein transferase activity aminoacyltransferase activity oxidoreductase activity transmembrane transporter activity transporter activity
	GO Cellular Components	peroxisome

Figure 6.39: Gene Ontology (GO) analysis of genes differentially expressed in the comparison of Exp vs. QD7 for up and downregulated. The analysis categorizes genes based on three GO terms: Biological Process, Molecular Function, and Cellular Component. It shows upregulated and downregulated genes in wild-type and single mutants, highlighting both shared and unique genes across all mutants for each of the three categories.

6.10 Summary of Main Findings

6.10.1 Widespread Transcriptional Deregulation in Histone Mutants.

A modest and precise transcriptional response to the diauxic shift was shown by wild-type strain. The histone mutant strains (especially the *hht-K36A*Δ mutant), exhibit a massive and widespread deregulation of gene expression. The wild-type cells undergo a major transcriptional shift during Quiescence re-entry. The mutants however were severely impaired, with the *K123R-K36A*Δ double mutant showing the most profound failure to regulate gene expression.

6.10.2 Unique and Overlapping Gene Regulation.

A minimal number of uniquely regulated genes was shown by wild type cells during diauxic Shift, indicating a conserved and finely tuned response. The *hht-K36A*Δ mutant on the other hand showed a large number of uniquely up-regulated genes, providing strong evidence that H3K36 methylation is crucial for suppressing inappropriate transcription. A core set of 321 genes is commonly regulated across all strains, suggesting a fundamental response independent of these specific histone modifications. *K123R-K36A*Δ double mutant during Quiescence Entry exhibits a severe and unique deregulation with a large number of uniquely up-regulated genes and down-regulated genes, highlighting a breakdown of transcriptional control that goes beyond what is seen in the single mutants.

6.10.3 Functional and Metabolic Dysregulation.

A failure to repress "ribosome biogenesis" and other growth-related pathways during both the diauxic shift and quiescence entry was seen by the Gene Ontology (GO) analysis of all three mutant strains. This suggests a fundamental failure to transition out of a growth-like state. The impaired proper activation of key metabolic pathways was seen in mutants. For example, failure to fully up-regulate mitochondrial energy pathways during the diauxic shift was seen in the *htb-K123R*Δ mutant, and the double mutant shows a compromised metabolic state during quiescence re-entry, with a failure to activate nutrient recycling and energy generation.

6.10.4 Intricate Functional Relationship Between Histone Modifications

A complex functional connection between H2B K123 ubiquitination and H3 K36 methylation was revealed in this study. A reduced transcriptional response during the diauxic shift was seen in double mutant, *K123R-K36A*Δ*,* compared to the *hht-K36A*Δ single mutant, suggesting that the partial mitigation of some of the aberrant transcriptional activity caused by the loss of H3K36 methylation is obtained by the loss of H2B ubiquitination. This points to a synergistic, non-redundant role for these two modifications.

6.10.5 Chromatin state evidence

Although locus-specific chromatin occupancy was not directly assessed in the present study, the chromatin state alterations observed during quiescence entry are supported by complementary qPCR and ATAC-Seq data. qPCR analysis of H3K14ac, H4ac4, Hho1p, and Htz1p confirmed transcriptional changes consistent with chromatin-mediated repression, while ATAC-Seq revealed genome-wide shifts in accessibility during the transition into quiescence in *S. cerevisiae* FY-406. To directly validate the occupancy and distribution of these specific histone modifications and chromatin factors, future work should incorporate locus-specific chromatin occupancy assays (e.g., ChIP-qPCR or ChIP-Seq) targeting H3K14ac, H4ac4, Hho1p, and Htz1p at the same quiescence-associated promoters and regulatory elements. Such

analyses would enable precise mapping of mark- and factor-specific enrichment, strengthening the mechanistic link between chromatin remodelling and transcriptional silencing during quiescence.

Chapter 7

Final Discussion

7.1 Global Transcriptional Reprogramming in Response to Metabolic Transition

A comprehensive overview of the global transcriptional changes that accompany two critical metabolic transitions in *Saccharomyces cerevisiae*: the diauxic shift and quiescence entry is provided in this study. The findings from our study in wild-type strain in agreement to established literature (De Virgilio, 2012), showing that yeast undergoes a finely tuned and dynamic transcriptional response to adapt to nutrient scarcity. During the diauxic shift in wild-type cells the modest number of differentially expressed genes observed (815) is a testament to the cell's efficient and specific regulatory machinery. A conserved survival strategy that allows yeast to transition from rapid, glucose-based growth to a more sustainable, respiratory state is represented by the response, characterized by the upregulation of genes involved in respiratory metabolism and the repression of fermentative genes.

7.2 The Diauxic Shift

A profound and widespread deregulation of gene expression was observed during the diauxic shift in the histone mutant strains, with the most pronounced effects seen in the *hht-K36AΔ* mutant. This strain exhibited 2,845 differentially expressed genes, highlighting the essential role of H3K36 methylation in maintaining transcriptional fidelity and genomic stability. The scale of this mis-regulation supports a model in which H3K36 methylation normally functions as a transcriptional brake, and its loss leads to a global disruption of gene expression rather than aberrant regulation of a limited number of pathways. Both upregulated and downregulated gene sets were affected, indicating a broad collapse of transcriptional control.

Comparison of the single and double mutant strains revealed a non-additive interaction between H2B K123 ubiquitination and H3K36 methylation during the diauxic shift. The *K123R-K36AΔ* double mutant displayed a reduced transcriptional response relative to the *hht-K36AΔ* single mutant, with (2,191 versus 2,845) differentially expressed genes, respectively. This attenuation indicates that loss of H2B ubiquitination suppresses, at least in part, the transcriptional dysregulation associated with loss of H3K36 methylation.

In classical genetic terms, this relationship is consistent with partial epistasis, in which the *htb-K123RΔ* mutation modifies and dampens the H3K36 methylation loss phenotype rather than enhancing it. The data therefore argue against a simple additive model and instead support a functional dependency between these histone modification pathways.

Consistent with established models of histone modification crosstalk (Youdell et al., 2008), H2B ubiquitination appears not only to facilitate transcriptional activation but also to condition the chromatin environment in which the absence of H3K36 methylation exerts its effects during metabolic state transitions.

During the diauxic shift, loss of H2B K123 ubiquitination partially suppresses the transcriptional deregulation caused by loss of H3K36 methylation, revealing a non-additive, partially epistatic interaction between these chromatin pathways.

7.3 Quiescence entry (Day 7)

A massive transcriptional shift upon entry into quiescence (Day 7) was seen in wild-type cells, corroborating the extensive reprogramming required to establish the quiescent state (Laporte et al., 2017). Severe impairment was seen in this reprogramming in histone mutants. A striking phenotype, particularly in the *K123R-K36A*Δ double mutant was seen, with 3,184 differentially expressed genes relative to wild type, indicating a profound failure to properly engage the transcriptional programs needed for robust quiescence establishment.

This deregulation involved both hyper-activation and amplified repression across broad gene sets, with a substantial number of uniquely regulated genes compared to wild type.

For the single compared to double mutants the distinct transcriptional profiles observed during quiescence entry highlight the non-redundant and synergistic roles of H2B K123 ubiquitination and H3 K36 methylation in maintaining a transcriptionally balanced state required for long-term survival during quiescence.

7.4 Unique and Overlapping Gene Regulation: Dissecting the Roles of H2B K123ub and H3 K36me

7.4.1 Diauxic Shift

A powerful lens through which the specific, non-redundant functions of H2B K123ub and H3 K36me can be obtained by the analysis of unique and shared gene expression patterns.

The wild-type strain demonstrated a highly specific response during the diauxic shift, with a minimal number of uniquely regulated genes, indicative of a precise and finely tuned regulatory program (Gasch et al., 2000). This was in sharp contrast to what was seen in the mutant strains, which showed a vast number of unique genes, suggesting a failure to properly execute the wild-type transcriptional response.

With a striking 348 uniquely up-regulated genes the *hht-K36A*Δ mutant, a strong evidence for the role of H3K36 methylation in suppressing cryptic and inappropriate transcription is obtained. A cascade of transcriptional de-repression was unleashed by the loss of this repressive mark, leading to the activation of genes that are normally silenced during this metabolic transition. This is consistent with previous research demonstrating that H3K36 methylation prevents spurious transcription initiation within gene bodies and at inappropriate promoters (Carrozza et al., 2005; Keogh et al., 2005; Venkatesh et al., 2012). The broad transcriptional deregulation observed in this mutant provides strong support for the notion that H3K36 methylation is essential for maintaining transcriptional fidelity and precision.

With a smaller number of uniquely up-regulated genes (76), the *htb-K123R*Δ mutant, on the on the other hand, supports the notion that H2B ubiquitination is more critical for amplifying the activation of a limited number of essential genes rather than a broad transcriptional switch. This corroborates the established role in promoting transcriptional elongation and maintaining a proper chromatin structure (Henry et al., 2003; Pavri et al., 2006). The observation that H2B ubiquitination is crucial for ensuring the proper and efficient activation of a key set of genes required for metabolic adaptation is evident from the shift towards repression and the smaller number of uniquely up-regulated genes in this mutant.

One of the significant finding is the presence of a core set of 321 genes commonly up-regulated across all four strains.

This suggests that the regulation of the subset of genes essential for the diauxic shift is independent of the H2B K123ub and H3 K36me pathways. Other non-histone-based regulatory mechanisms, such as transcription factors or other chromatin remodeler may be the controllers of these genes. An important reference point for understanding the robustness of the diauxic shift program is provided by this core set of shared genes. It also highlights the possibility of compensatory regulatory mechanisms that maintain a baseline level of responsiveness even in the absence of key histone modifications. For example, the shared up-regulation of certain genes could be partially compensated by H3K36 acetylation, which is known to promote transcriptional activation.

These observations were further reinforced by the analysis of down-regulated genes. Only one unique down-regulated gene was demonstrated by the wild-type strain, suggesting that gene repression during the diauxic shift is a highly conserved process. A failure of transcriptional discrimination was demonstrated by the *hht-K36A*Δ mutant, with 489 uniquely down-regulated genes.

The widespread Deregulation may resultant of the broad repression observed in this mutant, leading to the excessive silencing of genes that are necessary for proper adaptation. H2B ubiquitination, implicated in transcriptional elongation and chromatin compaction, appears to be essential for mitigating this excessive down-regulation and ensuring that genes required for metabolic transitions are not aberrantly silenced (Weake and Workman, 2008).

7.4.2 Quiescence entry (Day 7)

A distinct and highly-deregulated transcriptional landscape in the histone mutant strains compared to the diauxic shift was observed during quiescence entry through the analysis of unique and overlapping genes. A massive and coordinated response was exhibited by the wild-type strain, indicating a robust and tightly regulated program for quiescence entry. The histone

mutants, on the other hand, displayed a failure to properly execute this entry program, leading to a large number of uniquely regulated genes. A particular severe phenotype was shown by the *K123R-K36A*Δ double mutant, with a high number of uniquely regulated genes (1,532 up-regulated and 1,652 down-regulated genes). This highlight a towards a failure to properly utilize the transcriptional programs required for a controlled transition in to quiescence.

In this mutant significant number of uniquely regulated genes were observed suggesting that the combined loss of both H2B K123ub and H3 K36me abolishes a critical layer of transcriptional control. The result corroborates a model where these two histone marks function synergistically to maintain a state of transcriptional balance during quiescence, ensuring that genes can be properly activated and repressed upon entry into quiescence (Lee et al., 2007).

The analysis further demonstrates that, although deregulation is evident in the single mutants, a strongly amplified phenotype is exhibited by the double mutant, underscoring a critical synergistic role for these histone modifications in sustaining transcriptional fidelity and chromatin robustness during prolonged quiescence.

The combined loss of these marks results in a collapse of both activating and repressive chromatin states, leading to a loss of precise gene expression control necessary for long-term stress tolerance, metabolic adaptation, and the capacity for efficient cell-cycle re-entry upon nutrient repletion. This interpretation is consistent with previous studies demonstrating that coordinated H2B ubiquitylation and H3K36 methylation are required to maintain transcriptional fidelity (Youdell et al., 2008).

7.5 Gene Ontology Analysis: A Detailed Functional Interpretation

A functional context for the observed transcriptional changes is provided by the Gene Ontology (GO) analysis, which revealed profound metabolic and regulatory dysfunctions in the histone mutant strains.

7.5.1 GO Analysis of the Diauxic Shift

The diauxic shift in wild-type cells is characterized by orchestrated metabolic shift from fermentation to respiration resultant of a sophisticated transcriptional program.

A clear picture of this transition is painted by the GO enrichment of terms such as "ribosome biogenesis" and "RNA binding" in up-regulated genes, and "aerobic respiration" and "mitochondrial components" in down-regulated genes (Jorgensen et al., 2004).

This is consistent with the cell's strategy to re-organize its protein synthesis machinery and downscale energy-intensive processes to conserve resources.

This orchestrated response is severely disrupted in the histone mutant strains. Failure to fully activate mitochondrial energy pathways, was evident by the significant suppression of terms like "generation of precursor metabolites and energy" and "mitochondrial respiratory chain complex assembly" in the *htb-K123R*Δ mutant. This contrasts sharply with the expected upregulation of respiratory metabolism in wild-type cells during the diauxic shift. A similar failure to activate key metabolic pathways was exhibited by the *hht-K36A*Δ mutant. This was seen along with a dampened stress response, suggesting an inability to properly adapt to the nutrient-limited environment.

The persistent and extensive upregulation of "ribosome biogenesis" and other growth-related pathways in all three mutant strains, *htb-K123R*Δ, *hht-K36A*Δ, and the *K123R-K36A*Δ double mutant, across both the diauxic shift and quiescence entry was the most striking observation from the GO analysis. This observation represents a significant contrast from the wild-type response, where these anabolic pathways are typically repressed to conserve energy. A fundamental failure of the mutants to properly transition out of a growth-like state is suggestive of this finding. An aberrant, energy-intensive transcriptional program that is inappropriate for a nutrient-deprived environment is indicative of the sustained upregulation of "ribosome biogenesis," "ribosomal subunit export," and "nucleotide metabolism".

7.5.2 GO Analysis of Quiescence entry (Day 7)

The GO analysis of quiescence entry further highlights the essential role of these histone alterations in preserving a transcriptionally stable state for long-term survival (Gray et al., 2004). A massive transcriptional shift, activating programs related to the cell cycle, DNA replication, and protein synthesis to support a return to proliferation was exhibited by wild type cells upon entering quiescence.

Severe impairment in this process was seen in the histone mutants. One of the critical findings is the persistent upregulation of "ribosome biogenesis" and other biosynthetic pathways in the double mutant during quiescence cells entry to indicates that the mutant fails to properly repress these growth related programs during quiescence itself, leading to a state of inappropriate metabolic activity. It is metabolically wasteful to have this persistent "idling" of the translational machinery which can likely compromises the cell's long-term viability.

A failure to activate pathways central to energy generation and nutrient recycling (transmembrane transport and fatty acid catabolic process) during quiescence was revealed by the GO analysis of the double mutant. This suggests a compromised metabolic state that may impair the cell's ability to survive prolonged periods of nutrient limitation.

7.6 Implications for Quiescence and Long-Term Viability

A non-redundant and synergistic role of H2B K123ub and H3 K36me was highlighted by the distinct transcriptional profiles observed in the single and double mutants during quiescence entry. Although maintaining transcriptional fidelity is important roles of both modifications, their combined loss leads to a breakdown of both activating and repressive chromatin states, resulting in a profound loss of control over gene expression.

A model where H3K36 methylation is essential for suppressing transcriptional noise, while H2B ubiquitination is crucial for ensuring proper transcriptional elongation and chromatin accessibility is supported by our data. A severe misregulation of the transcriptome, impairing the cell's ability to properly enter and exit quiescence is resultant of the synergistic loss of these

two functions. This is consistent with previous research that a complex of H2B ubiquitylation and H3K36 methylation is required for transcriptional elongation (Lee et al., 2007).

7.7 Conclusions and Future Directions

This study provides a detailed analysis of how disrupting two key histone modifications H2B K123 ubiquitination and H3 K36 methylation affects global transcription and cellular function during metabolic transitions in *Saccharomyces cerevisiae*. While these histone marks are commonly associated with transcriptional regulation, our results indicate that they are also essential for maintaining transcriptional accuracy. Additionally, they are required for orchestrating the precise gene expression programs needed for adaptation to nutrient stress.

Extensive transcriptional deregulation was observed in the histone mutants, and the failure to repress growth-promoting pathways suggests that cellular regulation was significantly disrupted, limiting adaptation and survival under nutrient-poor conditions.

Furthermore, our findings reveal a complex functional relationship between H2B K123ub and H3 K36me, indicating that different histone modification pathways interact in a coordinated manner. This suggests that further research is needed to clarify the molecular mechanisms underlying this interaction. Detailed analysis of genes that are uniquely or commonly affected by each modification could reveal new regulatory networks that depend on, or operate independently of, these histone marks.

The implications of this work extend beyond yeast biology. Both H2B K123ub and H3 K36me are highly conserved across eukaryotes, and disruptions in these modifications have been linked to human diseases such as cancer and developmental disorders. Therefore, yeast remains a valuable model for understanding fundamental principles of chromatin based regulation of gene expression and metabolic state. However, the long-term effects of the observed transcriptional deregulation on cell viability and physiology remain unclear. Future studies should include long-term viability assays and single cell RNA sequencing to capture the full range of cellular responses and population heterogeneity.

To further validate and expand these findings, several complementary experimental approaches are recommended. First, chromatin immunoprecipitation (ChIP) assays targeting H3K14ac, H4ac4, Htz1, and Hho1p should be performed to identify genomic regions where chromatin misregulation occurs. This will provide direct evidence linking altered chromatin states to specific transcriptional changes. Second, time-course RT-qPCR analysis of representative genes should be conducted to confirm RNA-Seq observations and to monitor dynamic changes during the transition from exponential growth to quiescence. Third, quantification of RNAPII CTD phosphorylation (Ser2 and Ser5) is needed to establish a mechanistic link between histone modification changes and transcriptional activity. Finally, viability and metabolic profiling of quiescent versus non-quiescent cells in double mutants should be performed to determine whether chromatin and transcriptional defects affect long-term survival and metabolic adaptation. Overall, further investigation into the interplay between histone modifications, gene expression, and metabolism will deepen our understanding of how cells adapt to environmental stress and may reveal conserved regulatory mechanisms relevant to human disease.

References

Alam, MT, Zelezniak, A, Mülleder, M, Shliaha, P, Schwarz, R, Capuano, F, Vowinckel, J, Radmaneshfar, E, Krüger, A, and Calvani, E (2016). The metabolic background is a global player in Saccharomyces gene expression epistasis. Nature Microbiology 1, 1–10.

Allen, BL, and Taatjes, DJ (2015). The Mediator complex: a central integrator of transcription. Nature Reviews Molecular Cell Biology 16, 155–166.

Allen, C, Büttner, S, Aragon, AD, Thomas, JA, Meirelles, O, Jaetao, JE, Benn, D, Ruby, SW, Veenhuis, M, and Madeo, F (2006). Isolation of quiescent and nonquiescent cells from yeast stationary-phase cultures. The Journal of Cell Biology 174, 89–100.

Allis, CD, and Jenuwein, T (2016). The molecular hallmarks of epigenetic control. Nature Reviews Genetics 17, 487–500.

Aricthota, S, Rana, PP, and Haldar, D (2022). Histone acetylation dynamics in repair of DNA double-strand breaks. Frontiers in Genetics 13, 926577.

Baek, SH, and Kim, KI (2017). Epigenetic control of autophagy: nuclear events gain more attention. Molecular Cell 65, 781–785.

Bagchi, DN (2016). The interplay between transcription, histone variants, and chromatin structure in Eukaryotes.

Baxter, J, and Diffley, JFX (2008). Topoisomerase II Inactivation Prevents the Completion of DNA Replication in Budding Yeast. Molecular Cell 30, 790–802.

Bexley, K, Ristova, M, Sharma, S, Spanos, C, Chabes, A, and Tollervey, D (2025). Metabolic tuning enables immediate adaptation to energy stress in yeast. bioRxiv, 2025–06.

Bilokapic, S, and Halic, M (2019). Nucleosome and ubiquitin position Set2 to methylate H3K36. Nature Communications 10, 3795.

Björklund, S, and Gustafsson, CM (2005). The yeast Mediator complex and its regulation. Trends in Biochemical Sciences 30, 240–244.

Bonitto, K, Sarathy, K, Atai, K, Mitra, M, and Coller, HA (2021). Is there a histone code for cellular quiescence? Frontiers in Cell and Developmental Biology 9, 739780.

Brandes, N, Tienson, H, Lindemann, A, Vitvitsky, V, Reichmann, D, Banerjee, R, and Jakob, U (2013). Time line of redox events in aging postmitotic cells. Elife 2, e00306.

Brauer, MJ, Huttenhower, C, Airoldi, EM, Rosenstein, R, Matese, JC, Gresham, D, Boer, VM, Troyanskaya, OG, and Botstein, D (2008). Coordination of growth rate, cell cycle, stress response, and metabolic activity in yeast. Molecular Biology of the Cell 19, 352–367.

Breeden, LL, and Tsukiyama, T (2022). Quiescence in Saccharomyces cerevisiae. Annual Review of Genetics 56, 253–278.

Breton, S, and Brown, D (2013). Regulation of luminal acidification by the V-ATPase. Physiology 28, 318–329.

Briggs, SD, Bryk, M, Strahl, BD, Cheung, WL, Davie, JK, Dent, SY, Winston, F, and Allis, CD (2001). Histone H3 lysine 4 methylation is mediated by Set1 and required for cell growth and rDNA silencing in Saccharomyces cerevisiae. Genes & Development 15, 3286–3295.

Brivanlou, AH, and Darnell Jr, JE (2002). Signal transduction and the control of gene expression. Science 295, 813–818.

Buratowski, S (2009). Progression through the RNA polymerase II CTD cycle. Molecular Cell 36, 541–546.

Buratowski, S, Hahn, S, Guarente, L, and Sharp, PA (1989). Five intermediate complexes in transcription initiation by RNA polymerase II. Cell 56, 549–561.

Busti, S, Coccetti, P, Alberghina, L, and Vanoni, M (2010). Glucose signaling-mediated coordination of cell growth and cell cycle in Saccharomyces cerevisiae. Sensors 10, 6195–6240.

Cairns, BR, Lorch, Y, Li, Y, Zhang, M, Lacomis, L, Erdjument-Bromage, H, Tempst, P, Du, J, Laurent, B, and Kornberg, RD (1996). RSC, an essential, abundant chromatin-remodeling complex. Cell 87, 1249–1260.

Carrozza, MJ, Li, B, Florens, L, Suganuma, T, Swanson, SK, Lee, KK, Shia, W-J, Anderson, S, Yates, J, and Washburn, MP (2005). Histone H3 methylation by Set2 directs deacetylation of coding regions by Rpd3S to suppress spurious intragenic transcription. Cell 123, 581–592.

Cencioni, C, Spallotta, F, Martelli, F, Valente, S, Mai, A, Zeiher, AM, and Gaetano, C (2013). Oxidative stress and epigenetic regulation in ageing and age-related diseases. International Journal of Molecular Sciences 14, 17643–17663.

Chen, F, Liu, B, Guo, L, Ge, X, Feng, W, Li, D-F, Zhou, H, and Long, J (2021). Biochemical insights into Paf1 complex–induced stimulation of Rad6/Bre1-mediated H2B monoubiquitination. Proceedings of the National Academy of Sciences 118, e2025291118.

Cheng, C, Tang, R-Q, Xiong, L, Hector, RE, Bai, F-W, and Zhao, X-Q (2018). Association of improved oxidative stress tolerance and alleviation of glucose repression with superior xylose-utilization capability by a natural isolate of Saccharomyces cerevisiae. Biotechnology for Biofuels 11, 1–19.

Chou, KY, Lee, J-Y, Kim, K-B, Kim, E, Lee, H-S, and Ryu, H-Y (2023). Histone modification in Saccharomyces cerevisiae: a review of the current status. Computational and Structural Biotechnology Journal 21, 1843–1850.

Chu, X, Qin, X, Xu, H, Li, L, Wang, Z, Li, F, Xie, X, Zhou, H, Shen, Y, and Long, J (2013). Structural insights into Paf1 complex assembly and histone binding. Nucleic Acids Research 41, 10619–10629.

Clapier, CR, and Cairns, BR (2009). The biology of chromatin remodeling complexes. Annual Review of Biochemistry 78, 273–304.

Claude, K-L (2022). Regulation of histone proteins with cell volume and genome content in Saccharomyces cerevisiae.

Clements, A, Poux, AN, Lo, W-S, Pillus, L, Berger, SL, and Marmorstein, R (2003). Structural basis for histone and phosphohistone binding by the GCN5 histone acetyltransferase. Molecular Cell 12, 461–473.

Collart, MA, and Oliviero, S (1993). Preparation of yeast RNA. Current Protocols in Molecular Biology 23, 13–12.

Conaway, RC, and Conaway, JW (2011). Function and regulation of the Mediator complex. Current Opinion in Genetics & Development 21, 225–230.

Corden, JL (2013). RNA polymerase II C-terminal domain: tethering transcription to transcript and template. Chemical Reviews 113, 8423–8455.

Corona, DF, and Tamkun, JW (2004). Multiple roles for ISWI in transcription, chromosome organization and DNA replication. Biochimica et Biophysica Acta (BBA)-Gene Structure and Expression 1677, 113–119.

Cox, JS, and Walter, P (1996). A novel mechanism for regulating activity of a transcription factor that controls the unfolded protein response. Cell 87, 391–404.

Cullen, PJ, and Sprague Jr, GF (2000). Glucose depletion causes haploid invasive growth in yeast. Proceedings of the National Academy of Sciences 97, 13619–13624.

Curcio, MJ, and Derbyshire, KM (2003). The outs and ins of transposition: from mu to kangaroo. Nature Reviews Molecular Cell Biology 4, 865–877.

De Virgilio, C (2012). The essence of yeast quiescence. FEMS Microbiology Reviews 36, 306–339.

Decatur, WA, and Fournier, MJ (2002). rRNA modifications and ribosome function. Trends in Biochemical Sciences 27, 344–351.

Decatur, WA, and Fournier, MJ (2003). RNA-guided nucleotide modification of ribosomal and other RNAs. Journal of Biological Chemistry 278, 695–698.

DeRisi, JL, Iyer, VR, and Brown, PO (1997). Exploring the metabolic and genetic control of gene expression on a genomic scale. Science 278, 680–686.

Di Spirito, F, Di Palo, MP, De Benedetto, G, Piedepalumbo, F, Galdi, M, Cannatà, D, Cafà, N, and Contaldo, M (2025). Periodontal Microbial Profiles Across Periodontal Conditions in Pediatric Subjects: A Narrative Review. Microorganisms 13, 1813.

Diaz-Moralli, S, Tarrado-Castellarnau, M, Miranda, A, and Cascante, M (2013). Targeting cell cycle regulation in cancer therapy. Pharmacology & Therapeutics 138, 255–271.

Draizen, EJ, Shaytan, AK, Mariño-Ramírez, L, Talbert, PB, Landsman, D, and Panchenko, AR (2016). HistoneDB 2.0: a histone database with variants—an integrated resource to explore histones and their variants. Database 2016, baw014.

Ellison, MA, Lederer, AR, Warner, MH, Mavrich, TN, Raupach, EA, Heisler, LE, Nislow, C, Lee, MT, and Arndt, KM (2019). The Paf1 complex broadly impacts the transcriptome of Saccharomyces cerevisiae. Genetics 212, 711–728.

Enenkel, C (2014). Nuclear transport of yeast proteasomes. Biomolecules 4, 940–955.

Evans, CR, Smiley, MK, Asahara Thio, S, Wei, M, Florek, LC, Dayton, H, Price-Whelan, A, Min, W, and Dietrich, LE (2023). Spatial heterogeneity in biofilm metabolism elicited by local control of phenazine methylation. Proceedings of the National Academy of Sciences 120, e2313208120.

Fellas, A (2023). Investigating the molecular mechanism of caffeine and antifungal resistance in Schizosaccharomyces pombe epimutants.

Fink, MF (2007). Contribution of histones to nucleosome stability, DNA accessibility, and higher order chromatin structures in yeast.

Fleming, AB, Kao, C-F, Hillyer, C, Pikaart, M, and Osley, MA (2008). H2B ubiquitylation plays a role in nucleosome dynamics during transcription elongation. Molecular Cell 31, 57–66.

Francette, AM, Tripplehorn, SA, and Arndt, KM (2021). The Paf1 complex: a keystone of nuclear regulation operating at the interface of transcription and chromatin. Journal of Molecular Biology 433, 166979.

Fuchs, G, Hollander, D, Voichek, Y, Ast, G, and Oren, M (2014). Cotranscriptional histone H2B monoubiquitylation is tightly coupled with RNA polymerase II elongation rate. Genome Research 24, 1572–1583.

Galdieri, L, Mehrotra, S, Yu, S, and Vancura, A (2010). Transcriptional regulation in yeast during diauxic shift and stationary phase. Omics: A Journal of Integrative Biology 14, 629–638.

Gallagher, S, Winston, SE, Fuller, SA, and Hurrell, JG (2011). Immunoblotting and immunodetection. Current Protocols in Cell Biology 52, 6–2.

Gasch, AP, Spellman, PT, Kao, CM, Carmel-Harel, O, Eisen, MB, Storz, G, Botstein, D, and Brown, PO (2000). Genomic expression programs in the response of yeast cells to environmental changes. Molecular Biology of the Cell 11, 4241–4257.

Goffeau, A, Barrell, BG, Bussey, H, Davis, RW, Dujon, B, Feldmann, H, Galibert, F, Hoheisel, JD, Jacq, C, and Johnston, M (1996). Life with 6000 genes. Science 274, 546–567.

Gray, JV, Petsko, GA, Johnston, GC, Ringe, D, Singer, RA, and Werner-Washburne, M (2004). “Sleeping beauty”: quiescence in Saccharomyces cerevisiae. Microbiology and Molecular Biology Reviews 68, 187–206.

Grigoreva, TA, Romanova, AA, Tribulovich, VG, Pestov, NB, Oganov, RA, Kovaleva, DK, Korneenko, TV, and Barlev, NA (2024). p53: The Multifaceted Roles of Covalent Modifications in Cancer. Pharmaceuticals 17, 1682.

Grunstein, M (1997). Histone acetylation in chromatin structure and transcription. Nature 389, 349–352.

Haimovich, G, Medina, DA, Causse, SZ, Garber, M, Millán-Zambrano, G, Barkai, O, Chávez, S, Pérez-Ortín, JE, Darzacq, X, and Choder, M (2013). Gene expression is circular: factors for mRNA degradation also foster mRNA synthesis. Cell 153, 1000–1011.

Halley, JE, Kaplan, T, Wang, AY, Kobor, MS, and Rine, J (2010). Roles for H2A. Z and its acetylation in GAL1 transcription and gene induction, but not GAL1-transcriptional memory. PLoS Biology 8, e1000401.

Han, AK (1987). Non-parametric analysis of a generalized regression model: the maximum rank correlation estimator. Journal of Econometrics 35, 303–316.

Hansen, TB, Wiklund, ED, Bramsen, JB, Villadsen, SB, Statham, AL, Clark, SJ, and Kjems, J (2011). miRNA-dependent gene silencing involving Ago2-mediated cleavage of a circular antisense RNA. The EMBO Journal 30, 4414–4422.

Harlen, KM, and Churchman, LS (2017). The code and beyond: transcription regulation by the RNA polymerase II carboxy-terminal domain. Nature Reviews Molecular Cell Biology 18, 263–273.

Hartzog, GA (2003). Transcription elongation by RNA polymerase II. Current Opinion in Genetics & Development 13, 119–126.

Hauer, MH, and Gasser, SM (2017). Chromatin and nucleosome dynamics in DNA damage and repair. Genes & Development 31, 2204–2221.

Henry, KW, Wyce, A, Lo, W-S, Duggan, LJ, Emre, NT, Kao, C-F, Pillus, L, Shilatifard, A, Osley, MA, and Berger, SL (2003). Transcriptional activation via sequential histone H2B ubiquitylation and deubiquitylation, mediated by SAGA-associated Ubp8. Genes & Development 17, 2648–2663.

Herman, PK (2002). Stationary phase in yeast. Current Opinion in Microbiology 5, 602–607.

Hintermair, C, Heidemann, M, Koch, F, Descostes, N, Gut, M, Gut, I, Fenouil, R, Ferrier, P, Flatley, A, and Kremmer, E (2012). Threonine-4 of mammalian RNA polymerase II CTD is targeted by Polo-like kinase 3 and required for transcriptional elongation. The EMBO Journal 31, 2784–2797.

Hori, Y, Engel, C, and Kobayashi, T (2023). Regulation of ribosomal RNA gene copy number, transcription and nucleolus organization in eukaryotes. Nature Reviews Molecular Cell Biology 24, 414–429.

Howe, F (2012). Crosstalk between histone modifications in Saccharomyces cerevisiae.

Isern, JA, Carlucci, R, Labadie, GR, and Porta, EO (2025). Progress and prospects of triazoles in advanced therapies for parasitic diseases. Tropical Medicine and Infectious Disease 10, 142.

Jaehning, JA (2010). The Paf1 complex: platform or player in RNA polymerase II transcription? Biochimica et Biophysica Acta (BBA)-Gene Regulatory Mechanisms 1799, 379–388.

Jorgensen, P, Rupeš, I, Sharom, JR, Schneper, L, Broach, JR, and Tyers, M (2004). A dynamic transcriptional network communicates growth potential to ribosome synthesis and critical cell size. Genes & Development 18, 2491–2505.

Kaabache, T, Barraud, B, Feldmann, G, Bernuau, D, and Lardeux, B (1995). Direct solution hybridization of guanidine thiocyanate-solubilized cells for quantitation of mRNAs in hepatocytes. Analytical Biochemistry 232, 225–230.

Kanki, T, and Klionsky, DJ (2008). Mitophagy in yeast occurs through a selective mechanism. Journal of Biological Chemistry 283, 32386–32393.

Kari, S, Subramanian, K, Altomonte, IA, Murugesan, A, Yli-Harja, O, and Kandhavelu, M (2022). Programmed cell death detection methods: a systematic review and a categorical comparison. Apoptosis 27, 482–508.

Karkowska-Kuleta, J, and Kozik, A (2015). Cell wall proteome of pathogenic fungi. Acta Biochimica Polonica 62.

Keogh, M-C, Kurdistani, SK, Morris, SA, Ahn, SH, Podolny, V, Collins, SR, Schuldiner, M, Chin, K, Punna, T, and Thompson, NJ (2005). Cotranscriptional set2 methylation of histone H3 lysine 36 recruits a repressive Rpd3 complex. Cell 123, 593–605.

Kim, J, Hake, SB, and Roeder, RG (2005). The human homolog of yeast BRE1 functions as a transcriptional coactivator through direct activator interactions. Molecular Cell 20, 759–770.

Kim, M, Krogan, NJ, Vasiljeva, L, Rando, OJ, Nedea, E, Greenblatt, JF, and Buratowski, S (2004). The yeast Rat1 exonuclease promotes transcription termination by RNA polymerase II. Nature 432, 517–522.

Klosinska, MM, Crutchfield, CA, Bradley, PH, Rabinowitz, JD, and Broach, JR (2011). Yeast cells can access distinct quiescent states. Genes & Development 25, 336–349.

Komarnitsky, P, Cho, E-J, and Buratowski, S (2000). Different phosphorylated forms of RNA polymerase II and associated mRNA processing factors during transcription. Genes & Development 14, 2452–2460.

Kornberg, RD (1974). Chromatin Structure: A Repeating Unit of Histones and DNA: Chromatin structure is based on a repeating unit of eight histone molecules and about 200 DNA base pairs. Science 184, 868–871.

Koutelou, E, Hirsch, CL, and Dent, SY (2010). Multiple faces of the SAGA complex. Current Opinion in Cell Biology 22, 374–382.

Kouzarides, T (2007). Chromatin modifications and their function. Cell 128, 693–705.

Krogan, NJ, Dover, J, Wood, A, Schneider, J, Heidt, J, Boateng, MA, Dean, K, Ryan, OW, Golshani, A, and Johnston, M (2003). The Paf1 complex is required for histone H3 methylation by COMPASS and Dot1p: linking transcriptional elongation to histone methylation. Molecular Cell 11, 721–729.

Kuranda, K, Leberre, V, Sokol, S, Palamarczyk, G, and François, J (2006). Investigating the caffeine effects in the yeast Saccharomyces cerevisiae brings new insights into the connection between TOR, PKC and Ras/cAMP signalling pathways. Molecular Microbiology 61, 1147–1166.

Lan, X, Atanassov, BS, Li, W, Zhang, Y, Florens, L, Mohan, RD, Galardy, PJ, Washburn, MP, Workman, JL, and Dent, SY (2016). USP44 is an integral component of N-CoR that contributes to gene repression by deubiquitinating histone H2B. Cell Reports 17, 2382–2393.

Laporte, D, Jimenez, L, Gouleme, L, and Sagot, I (2017). Yeast quiescence exit swiftness is influenced by cell volume and chronological age. Microbial Cell 5, 104.

Lawrence,MBD (2019). HISTONE ACETYLATION, NOT STOICHIOMETRY, REGULATES LINKER HISTONE BINDING IN SACCHAROMYCES.

Lee, J-S, Shukla, A, Schneider, J, Swanson, SK, Washburn, MP, Florens, L, Bhaumik, SR, and Shilatifard, A (2007). Histone crosstalk between H2B monoubiquitination and H3 methylation mediated by COMPASS. Cell 131, 1084–1096.

Lewin, B (2004). Genes Viii.

Li, B, Carey, M, and Workman, JL (2007). The role of chromatin during transcription. Cell 128, 707–719.

Li, Y, Ma, T, Jiang, J, Hahn, M, and Yin, Y (2024). The dynamics and functional mechanisms of H2B mono-ubiquitination. Crop Health 2, 1.

Liu, G, Zheng, X, Guan, H, Cao, Y, Qu, H, Kang, J, Ren, X, Lei, J, Dong, M-Q, and Li, X (2019). Architecture of Saccharomyces cerevisiae SAGA complex. Cell Discovery 5, 25.

Liu, L, Zhang, Y, Liu, Z, Petranovic, D, and Nielsen, J (2015). Improving heterologous protein secretion at aerobic conditions by activating hypoxia-induced genes in Saccharomyces cerevisiae. FEMS Yeast Research 15, fov070.

Mäder, AW, Richmond, RK, Sargent, DF, and Richmond, TJ (1997). Crystal structure of the nucleosome core particle at 2.8 Å resolution. Nature 389, 251–260.

Malik, S, and Roeder, RG (2005). Dynamic regulation of pol II transcription by the mammalian Mediator complex. Trends in Biochemical Sciences 30, 256–263.

Marks, VD, Ho Sui, SJ, Erasmus, D, Van Der Merwe, GK, Brumm, J, Wasserman, WW, Bryan, J, and Van Vuuren, HJ (2008). Dynamics of the yeast transcriptome during wine fermentation reveals a novel fermentation stress response. FEMS Yeast Research 8, 35–52.

McDaniel, SL, Hepperla, AJ, Huang, J, Dronamraju, R, Adams, AT, Kulkarni, VG, Davis, IJ, and Strahl, BD (2017). H3K36 methylation regulates nutrient stress response in Saccharomyces cerevisiae by enforcing transcriptional fidelity. Cell Reports 19, 2371–2382.

McKnight, JN, Boerma, JW, Breeden, LL, and Tsukiyama, T (2015). Global promoter targeting of a chromatin remodeling complex during quiescence entry and exit. Molecular Cell 59, 318–331.

Millar, CB, Xu, F, Zhang, K, and Grunstein, M (2006). Acetylation of H2AZ Lys 14 is associated with genome-wide gene activity in yeast. Genes & Development 20, 711–722.

Mira, NP, Teixeira, MC, and Sá-Correia, I (2010). Adaptive response and tolerance to weak acids in Saccharomyces cerevisiae: a genome-wide view. Omics: A Journal of Integrative Biology 14, 525–540.

Morgan, M, and Shepherd, L (2017). AnnotationHub: Client to access AnnotationHub resources. R Package Version 2, 2017.

Nechaev, S, and Adelman, K (2011). Pol II waiting in the starting gates: Regulating the transition from transcription initiation into productive elongation. Biochimica et Biophysica Acta (BBA)-Gene Regulatory Mechanisms 1809, 34–45.

Negesse, MY (2024). Investigation of the Role of the PhD Domain of SET4 in Stress-Mediated Chromatin Regulation in Saccharomyces cerevisiae.

Ng, HH, Xu, R-M, Zhang, Y, and Struhl, K (2002). Ubiquitination of histone H2B by Rad6 is required for efficient Dot1-mediated methylation of histone H3 lysine 79. Journal of Biological Chemistry 277, 34655–34657.

Orphanides, G, LeRoy, G, Chang, C-H, Luse, DS, and Reinberg, D (1998). FACT, a factor that facilitates transcript elongation through nucleosomes. Cell 92, 105–116.

Pavri, R, Zhu, B, Li, G, Trojer, P, Mandal, S, Shilatifard, A, and Reinberg, D (2006). Histone H2B monoubiquitination functions cooperatively with FACT to regulate elongation by RNA polymerase II. Cell 125, 703–717.

Petrenko, N, and Struhl, K (2021). Comparison of transcriptional initiation by RNA polymerase II across eukaryotic species. Elife 10, e67964.

Petty, EL, Lafon, A, Tomlinson, SL, Mendelsohn, BA, and Pillus, L (2016). Promotion of cell viability and histone gene expression by the acetyltransferase Gcn5 and the protein phosphatase PP2A in Saccharomyces cerevisiae. Genetics 203, 1693–1707.

Phatnani, HP, and Greenleaf, AL (2006). Phosphorylation and functions of the RNA polymerase II CTD. Genes & Development 20, 2922–2936.

Polanco, FM (2019). mRNA granules focus the production of glycolytic enzymes to fuel glucose fermentation, The University of Manchester (United Kingdom).

Porrua, O, and Libri, D (2015). Transcription termination and the control of the transcriptome: why, where and how to stop. Nature Reviews Molecular Cell Biology 16, 190–202.

Redon, C, Pilch, D, Rogakou, E, Sedelnikova, O, Newrock, K, and Bonner, W (2002). Histone H2a variants H2AX and H2AZ. Current Opinion in Genetics & Development 12, 162–169.

Roberts, GG, and Hudson, AP (2006). Transcriptome profiling of Saccharomyces cerevisiae during a transition from fermentative to glycerol-based respiratory growth reveals extensive metabolic and structural remodeling. Molecular Genetics and Genomics 276, 170–186.

Robzyk, K, Recht, J, and Osley, MA (2000). Rad6-dependent ubiquitination of histone H2B in yeast. Science 287, 501–504.

Rogakou, EP, Pilch, DR, Orr, AH, Ivanova, VS, and Bonner, WM (1998). DNA double-stranded breaks induce histone H2AX phosphorylation on serine 139. Journal of Biological Chemistry 273, 5858–5868.

Ron, D, and Walter, P (2007). Signal integration in the endoplasmic reticulum unfolded protein response. Nature Reviews Molecular Cell Biology 8, 519–529.

Roy, DG, Chen, J, Mamane, V, Ma, EH, Muhire, BM, Sheldon, RD, Shorstova, T, Koning, R, Johnson, RM, and Esaulova, E (2020). Methionine metabolism shapes T helper cell responses through regulation of epigenetic reprogramming. Cell Metabolism 31, 250–266.

Ruthenburg, AJ, Allis, CD, and Wysocka, J (2007). Methylation of lysine 4 on histone H3: intricacy of writing and reading a single epigenetic mark. Molecular Cell 25, 15–30.

Ryu, H-Y (2024). Histone Modification Pathways Suppressing Cryptic Transcription. Epigenomes 8, 42.

Schäfer, G, McEvoy, CR, and Patterton, H-G (2008). The Saccharomyces cerevisiae linker histone Hho1p is essential for chromatin compaction in stationary phase and is displaced by transcription. Proceedings of the National Academy of Sciences 105, 14838–14843.

Schulze, JM, Jackson, J, Nakanishi, S, Gardner, JM, Hentrich, T, Haug, J, Johnston, M, Jaspersen, SL, Kobor, MS, and Shilatifard, A (2009). Linking cell cycle to histone modifications: SBF and H2B monoubiquitination machinery and cell-cycle regulation of H3K79 dimethylation. Molecular Cell 35, 626–641.

Serrano-Quílez, J, Roig-Soucase, S, and Rodríguez-Navarro, S (2020). Sharing marks: H3K4 methylation and H2B ubiquitination as features of meiotic recombination and transcription. International Journal of Molecular Sciences 21, 4510.

Shen, D, He, X, Weng, P, Liu, Y, and Wu, Z (2022). A review of yeast: High cell-density culture, molecular mechanisms of stress response and tolerance during fermentation. FEMS Yeast Research 22, foac050.

Shi, X, Finkelstein, A, Wolf, AJ, Wade, PA, Burton, ZF, and Jaehning, JA (1996). Paf1p, an RNA polymerase II-associated factor in Saccharomyces cerevisiae, may have both positive and negative roles in transcription. Molecular and Cellular Biology.

Siauciunaite, R, Foulkes, NS, Calabrò, V, and Vallone, D (2019). Evolution shapes the gene expression response to oxidative stress. International Journal of Molecular Sciences 20, 3040.

Silcocks, E (2022). The effect of mitochondrial deficiency on DNA damage response mutants of Saccharomyces cerevisiae.

Singh, S, Sahu, RK, Sugathan, A, and Tomar, RS (2021). The H2A N-terminal tail is required to alleviate copper-induced stress in Saccharomyces cerevisiae. FEMS Yeast Research 21, foab061.

Smith, E, and Shilatifard, A (2013). Transcriptional elongation checkpoint control in development and disease. Genes & Development 27, 1079–1088.

Smith, MD (2020). Investigating the Role of TORC1 and the Transcription Factor SFP1P in the Regulation of HMO1 Gene in Saccharomyces Cerevisiae, Louisiana State University and Agricultural & Mechanical College.

Squazzo, SL, Costa, PJ, Lindstrom, DL, Kumer, KE, Simic, R, Jennings, JL, Link, AJ, Arndt, KM, and Hartzog, GA (2002). The Paf1 complex physically and functionally associates with transcription elongation factors in vivo. The EMBO Journal.

Steinmetz, EJ, Conrad, NK, Brow, DA, and Corden, JL (2001). RNA-binding protein Nrd1 directs poly (A)-independent 3′-end formation of RNA polymerase II transcripts. Nature 413, 327–331.

Strahl, BD, and Allis, CD (2000). The language of covalent histone modifications. Nature 403, 41–45.

Struhl, K (1998). Histone acetylation and transcriptional regulatory mechanisms. Genes & Development 12, 599–606.

Struhl, K, and Segal, E (2013). Determinants of nucleosome positioning. Nature Structural & Molecular Biology 20, 267–273.

Sun, Z-W, and Allis, CD (2002). Ubiquitination of histone H2B regulates H3 methylation and gene silencing in yeast. Nature 418, 104–108.

Szymanski, EP, and Kerscher, O (2013). Budding yeast protein extraction and purification for the study of function, interactions, and post-translational modifications. Journal of Visualized Experiments: JoVE, 50921.

Tamburini, BA, and Tyler, JK (2005). Localized histone acetylation and deacetylation triggered by the homologous recombination pathway of double-strand DNA repair. Molecular and Cellular Biology 25, 4903–4913.

Tehlivets, O, Scheuringer, K, and Kohlwein, SD (2007). Fatty acid synthesis and elongation in yeast. Biochimica et Biophysica Acta (BBA)-Molecular and Cell Biology of Lipids 1771, 255–270.

Travers, KJ, Patil, CK, Wodicka, L, Lockhart, DJ, Weissman, JS, and Walter, P (2000). Functional and genomic analyses reveal an essential coordination between the unfolded protein response and ER-associated degradation. Cell 101, 249–258.

Venema, J, and Tollervey, D (1999). Ribosome synthesis in Saccharomyces cerevisiae. Annual Review of Genetics 33, 261–311.

Venkatesh, S, Smolle, M, Li, H, Gogol, MM, Saint, M, Kumar, S, Natarajan, K, and Workman, JL (2012). Set2 methylation of histone H3 lysine 36 suppresses histone exchange on transcribed genes. Nature 489, 452–455.

Venkatesh, S, and Workman, JL (2015). Histone exchange, chromatin structure and the regulation of transcription. Nature Reviews Molecular Cell Biology 16, 178–189.

Wagner, EJ, and Carpenter, PB (2012). Understanding the language of Lys36 methylation at histone H3. Nature Reviews Molecular Cell Biology 13, 115–126.

Wan, Y, Saleem, RA, Ratushny, AV, Roda, O, Smith, JJ, Lin, C-H, Chiang, J-H, and Aitchison, JD (2009). Role of the histone variant H2A. Z/Htz1p in TBP recruitment, chromatin dynamics, and regulated expression of oleate-responsive genes. Molecular and Cellular Biology 29, 2346–2358.

Warner, JR (1989). Synthesis of ribosomes in Saccharomyces cerevisiae. Microbiological Reviews 53, 256–271.

Weake, VM, and Workman, JL (2008). Histone ubiquitination: triggering gene activity. Molecular Cell 29, 653–663.

Weber, CA (2020). SiROP-Regulation of the cytosolic and metabolic response to glucose starvation.

Weiner, A, Chen, HV, Liu, CL, Rahat, A, Klien, A, Soares, L, Gudipati, M, Pfeffner, J, Regev, A, and Buratowski, S (2012). Systematic dissection of roles for chromatin regulators in a yeast stress response.

Werner-Washburne, M, Braun, E, Johnston, GC, and Singer, RA (1993). Stationary phase in the yeast Saccharomyces cerevisiae. Microbiological Reviews 57, 383–401.

Werner-Washburne, M, Roy, S, and Davidson, GS (2011). Aging and the survival of quiescent and non-quiescent cells in yeast stationary-phase cultures. Aging Research in Yeast, 123–143.

Werner-Washburne, M, Roy, S, and Davidson, GS (2012). Aging and the survival of quiescent and non-quiescent cells in yeast stationary-phase cultures. Aging Research in Yeast, 123–143.

Wickham, H (2016). Data analysis. In: Ggplot2: Elegant Graphics for Data Analysis, Springer, 189–201.

Wood, A, Schneider, J, Dover, J, Johnston, M, and Shilatifard, A (2003). The Paf1 complex is essential for histone monoubiquitination by the Rad6-Bre1 complex, which signals for histone methylation by COMPASS and Dot1p. Journal of Biological Chemistry 278, 34739–34742.

Xu, S, Hu, E, Cai, Y, Xie, Z, Luo, X, Zhan, L, Tang, W, Wang, Q, Liu, B, and Wang, R (2024). Using clusterProfiler to characterize multiomics data. Nature Protocols 19, 3292–3320.

Youdell, ML, Kizer, KO, Kisseleva-Romanova, E, Fuchs, SM, Duro, E, Strahl, BD, and Mellor, J (2008). Roles for Ctk1 and Spt6 in regulating the different methylation states of histone H3 lysine 36. Molecular and Cellular Biology 28, 4915–4926.

Young, CP, Hillyer, C, Hokamp, K, Fitzpatrick, DJ, Konstantinov, NK, Welty, JS, Ness, SA, Werner-Washburne, M, Fleming, AB, and Osley, MA (2017). Distinct histone methylation and transcription profiles are established during the development of cellular quiescence in yeast. BMC Genomics 18, 107.

Zaman, S, Lippman, SI, Zhao, X, and Broach, JR (2008). How Saccharomyces responds to nutrients. Annual Review of Genetics 42, 27–81.

Zeng, S (2025). Investigation of epigenome changes in quiescent fission yeast cells.

Zhang, H, Roberts, DN, and Cairns, BR (2005). Genome-wide dynamics of Htz1, a histone H2A variant that poises repressed/basal promoters for activation through histone loss. Cell 123, 219–231.

Zhang, T, Cooper, S, and Brockdorff, N (2015). The interplay of histone modifications–writers that read. EMBO Reports 16, 1467–1481.

Zhang, W, Bone, JR, Edmondson, DG, Turner, BM, and Roth, SY (1998). Essential and redundant functions of histone acetylation revealed by mutation of target lysines and loss of the Gcn5p acetyltransferase. The EMBO Journal.

Zhang, Y, and Reinberg, D (2001). Transcription regulation by histone methylation: interplay between different covalent modifications of the core histone tails. Genes & Development 15, 2343–2360.

Zhou, VW, Goren, A, and Bernstein, BE (2011). Charting histone modifications and the functional organization of mammalian genomes. Nature Reviews Genetics 12, 7–18.

Appendix

Table 1: List of genes commonly Up-regulated in wild-type at the diauxic shift (Dix) compared to transcription in exponential phase (Exp).

Category	Function	Number of Genes	Example Genes
GO Biological Processes	cytoplasmic translation	1439	RPS14A,RPL22B,RPL2A,RPL29,RPL15A
	translation		RPS14A,RPL22B,FRS2,RPL2A
	ribosome biogenesis		KRR1,SPB1,SRD1,RPS14A,YCR087C-A
	ribonucleoprotein complex biogenesis		KRR1,SPB1,SRD1,RPS14A,YCR087C-A
	rRNA metabolic process		KRR1,SPB1,SRD1,RPS14A,YCR087C-A
	rRNA processing		KRR1,SPB1,SRD1,RPS14A,YCR087C-A
	RNA processing		KRR1,SPB1,SRD1,MAK31,RPS14A,YCR087C-A
	ribosomal large subunit biogenesis		SPB1,RPL2A,RIX7,RPL10,RPL37A
	ribosome assembly		RPS14A,SDO1,RPS0B,RPL10,RPS31
GO Cellular Components	cytosolic ribosome	245	RPS14A,RPL22B,RPL2A,RPL29
	ribosomal subunit		RPS14A,RPL22B,RPL2A,RPL29,RPL15A,
	ribosome		RPS14A,RPL22B,RPL2A,RPL29,RPL15A,
	cytosolic large ribosomal subunit		RPL22B,RPL2A,RPL29,RPL15A,RPL22A,
	ribonucleoprotein complex		KRR1,SPB1,MAK31,RPS14A,RPL22B,RPL2A
GO Molecular Functions	structural constituent of ribosome	344	RPS14A,RPL22B,RPL2A,RPL29
	structural molecule activity		RPS14A,RPL22B,RPL2A,RPL29

	sequence-specific mRNA binding		FRS1,SES1,YDR341C,ILS1,GRS1

Table 2: List of genes commonly Down-regulated in wild-type during (Exp) compared to (Dix) treatment.

Category	Function	Number of Genes	Example Genes
GO Biological Processes	organic acid metabolic process		CIT2,IDP2,GDH2,DLD1,ARO10,ACH1
	carbohydrate metabolic process		CIT2,IDP2,KNH1,PYC1,NQM1,GAC1
	small molecule catabolic process		GDH2,DLD1,ARO10,UGA2,GUT2
	regulation of transcription by RNA polymerase II		FUN19,SEF1,EDS1,GSM1,SIP4
GO Cellular Components	mitochondrial envelope	**82**	MRX19,DLD1,COR1,COX13,CLD1
	mitochondrial inner membrane		MRX19,DLD1,COR1,COX13,CLD1
	organelle inner membrane		MRX19,DLD1,COR1,COX13,CLD1,
	mitochondrial membrane		MRX19,DLD1,COR1,COX13,CLD1,
GO Molecular Functions	oxidoreductase activity		IDP2,GDH2,DLD1,UGA2,COX13,SDH9
	DNA-binding transcription factor activity		SEF1,EDS1,GSM1,SIP4,HMS1,SFL1,CAT8,ROX1
	heat shock protein binding	**40**	SSA3,GAC1,APJ1

	transcription regulator activity		FUN19,SEF1,EDS1,GSM1,SIP4,HMS1
	protein serine kinase activity		KNS1,VHS1,NNK1,MEK1,SKS1,GUT1,YHR033W

Table 3: List of genes commonly UP-regulated in *htb-K123R*Δ during (Exp) compared to (Dix) treatment.

Category	Function	Number of Genes	Example Genes
GO Biological Processes	ribosome biogenesis	**1242**	KRR1, SPB1, RBP95, RPS14A, LOC1
	ribonucleoprotein complex biogenesis		KRR1, SPB1, RBP95, RPS14A, LOC1
	rRNA metabolic process		KRR1, SPB1, RBP95, RPS14A, LOC1
	RNA processing		KRR1, SPB1, RBP95, RPS14A, LOC1
	rRNA processing		KRR1, SPB1, RBP95, RPS14A, LOC1
GO Molecular Function	structural molecule activity	**288**	RPS14A, RPL22B, RPL2A, RPL29, RPL15A
	structural constituent of ribosome		RPS14A, RPL22B, RPL2A, RPL29, RPL15A
	catalytic activity, acting on RNA		SPB1, LOC1, CBF5, EMG1, DBP9
GO Cellular Component	ribosome	**603**	RPS14A, RPL22B, RPL2A, RPL29, RPL15A
	ribosomal subunit		RPS14A, RPL22B, RPL2A, RPL29, RPL15A
	nucleolus		KRR1, SPB1, RBP95, RPS14A, LOC1

	preribosome		KRR1, SPB1, RPS14A, LOC1, DRS1

Table 4: List of genes commonly Down-regulated in *htb-K123R*Δ during (Exp) compared to (Dix) treatment.

Category	Function	Number of Genes	Example Genes
GO Biological Process	energy derivation by oxidation of organic compounds		GLK1, CIT2, IGD1, HXK1, SDH2
	cellular respiration		GLK1, CIT2, HXK1, SDH2, COX12
	oxidative phosphorylation		COX12, SHH4, COX8, SDH4, ATP5
	mitochondrial translation		RSO55, RSM10, MRPL1, RSM24, MRPL7
	mitochondrial gene expression		RPO41, RSO55, RSM10, MRPL1, RSM24
	mitochondrial organization		RPO41, COX19, COX17, DNM1, COX12
GO Cellular Component	mitochondrial envelope	**742**	PTC6, COX19, COX17, SDH2, DNM1
	mitochondrial membrane		SDH2, DNM1, COX12, XDJ1, SHH4
	mitochondrial inner membrane		SDH2, COX12, SHH4, UPS1, COQ9

	organelle inner membrane		SDH2, COX12, SHH4, UPS1, COQ9
	mitochondrial matrix		CHA1, CIT2, PTC6, RPO41, PUT1
	mitochondrial intermembrane space		PTC6, COX19, COX17, COX12, UPS1
GO Molecular Function	oxidoreductase activity	**293**	MXR2, JLP1, SDH2, COX12, PUT1
	active transmembrane transporter activity		ERS1, HXT10, COX12, COX8, YDL199C
	transmembrane transporter activity		VBA3, ADY2, ERS1, AQY3, ALR2
	transporter activity		VBA3, ADY2, ERS1, AQY3, ALR2

Table 5: List of genes commonly up-regulated in *hht-K36A*Δ during (Exp) compared to (Dix) treatment.

Category	Function	Number of Genes	Example Genes
GO Biological Process	ribosome biogenesis	**2016**	KRR1, SPB1, RBP95, SRD1, RPS14A
	ribonucleoprotein complex biogenesis		KRR1, SPB1, RBP95, SRD1, RPS14A
	RNA processing		KRR1, SPB1, RBP95, SRD1, MAK31
	rRNA metabolic process		KRR1, SPB1, RBP95, SRD1, RPS14A
	rRNA processing		KRR1, SPB1, RBP95, SRD1, RPS14A
	ribosomal small subunit biogenesis		KRR1, RPS14A, BUD23, PWP2, LOC1
	maturation of SSU-rRNA		KRR1, RPS14A, BUD23, PWP2, LOC1
GO Molecular Function	structural molecule activity	**580**	CDC10, RPS14A, TUB2, RPL22B, PAU5
	structural constituent of ribosome		RPS14A, RPL22B, RPL2A, RPL29, RPL15A

	catalytic activity, acting on RNA		SPB1, BUD23, FRS2, SPB4, DEG1
	catalytic activity, acting on a tRNA		FRS2, DEG1, FRS1, SEN2, TAD3
	methyltransferase activity		SPB1, BUD23, BMT6, DPH5, EMG1
GO Cellular Component	ribosome	**926**	RPS14A, RPL22B, GCN20, RPL2A, RPL29
	ribosomal subunit		RPS14A, RPL22B, RPL2A, RPL29, RPL15A
	nucleolus		KRR1, SPB1, RBP95, RPS14A, BUD23
	endoplasmic reticulum membrane		EMC1, CWH43, ELO2, PER1, ARE1
	cytosolic large ribosomal subunit		RPL22B, RPL2A, RPL29, RPL15A, RPL22A
	large ribosomal subunit		RPL22B, RPL2A, RPL29, RPL15A, RPL22A

Table 6: List of genes commonly Down-regulated in *hht-K36A*Δ during (Exp) compared to (Dix) treatment.

Category	Function	Number of Genes	Example Genes
GO Biological Process	DNA integration	**831**	YFL002W-A, YLR035C-A, YLR157C-B
	generation of precursor metabolites and energy		GLK1, CIT2, SOL2, IGD1, QCR6
	energy derivation by oxidation of organic compounds		GLK1, CIT2, IGD1, QCR6, KGD4
	response to oxygen-		ZNF1, GPB2, SNF3, GPR1, NTH1

	containing compound		
GO Molecular Function	oxidoreductase activity	**486**	GRX1, MXR2, YCP4, KGD4, JLP1
	aspartic-type endopeptidase activity		YFL002W-A, YLR035C-A, YLR157C-B,
	peptidase activity		RRT12, OTU1, YFL002W-A, FRA1, YLR035C-A
GO Cellular Component	mitochondrial envelope		PTC6, MIC19, QCR6, VPS13, SDH2
	mitochondrial membrane	**656**	MIC19, QCR6, VPS13, SDH2, DNM1
	peroxisome		CIT2, AGX1, VPS13, DNM1, PCD1
	phagophore assembly site		ATG38, VPS34, ATG39, ATG17, ATG23

Table 7: List of genes commonly up-regulated in *K123R-K36A*Δ during (Exp) compared to (Dix) treatment.

Category	Function	Number of Genes	Example Genes
GO Biological Process	cytoplasmic translation	**1484**	RPS14A, RPL22B, RPL2A, RPL29
	ribosome biogenesis		KRR1, SPB1, RBP95, SRD1, RPS14A
	ribonucleoprotein complex biogenesis		KRR1, SPB1, RBP95, SRD1, RPS14A
	rRNA processing		KRR1, SPB1, RBP95, SRD1, RPS14A

	ribosome assembly		RPS14A, PWP2, RSA4, DRS1, RLP24
GO Cellular Component	cytosolic ribosome	**1384**	RPS14A, RPL22B, RPL2A, RPL29
	ribosomal subunit		MRPL32, RPL22B, RPL2A, RPL29
	structural constituent of ribosome		MRPL32, RPS14A, RPL22B, RPL2A, RPL29
	ribosome		MRPL32, RPS14A, RPL22B, RPL2A
	cytosolic large ribosomal subunit		RPL22B, RPL2A, RPL29, RPL15A, RPL22A
	preribosome		KRR1, SPB1, RPS14A, PWP2, RIX7
	cytosolic small ribosomal subunit		RPS14A, RPS0B, RPS31, RPS28B
GO Molecular Function	structural molecule activity	**428**	CDC10, MRPL32, RPS14A, ACT1
	structural constituent of ribosome		MRPL32, RPS14A, RPL22B, RPL2A, RPL29
	translation factor activity		HCR1, YEF3, FUN12, EFB1, RLI1
	transporter activity		VBA3, ADY2, ERS1, AQY3, ALR2

Table 8: List of genes commonly Down-regulated in *K123R-K36A*Δ during (Exp) compared to (Dix) treatment.

Category	Function	Number of Genes	Example Genes
GO Biological Process	aerobic respiration	**480**	CIT2, QCR6, KGD4, PUF3, SDH2
	generation of precursor metabolites and energy		CIT2, IGD1, QCR6, KGD4, PUF3

	energy derivation by oxidation of organic compounds		CIT2, IGD1, QCR6, KGD4, PUF3
	cellular respiration		CIT2, QCR6, KGD4, PUF3, SDH2
	small molecule catabolic process		CHA1, JLP1, PUT1, ASP3-1, ASP3-2
	monocarboxylic acid metabolic process		IDP2, ECI1, ACS1, YAT1, DLD1
GO Cellular Component	respiratory chain complex	**655**	QCR6, SDH2, COX12, SHH4, ATP14
	mitochondrial inner membrane		QCR6, SDH2, COX12, PET309, SHH4
	mitochondrial membrane		QCR6, PUF3, SDH2, DNM1, COX12
	organelle inner membrane		QCR6, SDH2, COX12, PET309, SHH4
	mitochondrial envelope		QCR6, COX19, PUF3, SDH2, DNM1
	peroxisome		PEX34, CIT2, AGX1, DNM1, PCD1
GO Molecular Function	oxidoreductase activity	**335**	ADH7, KGD4, JLP1, YLL056C, SDH2
	transmembrane transporter activity		AGP1, ADY2, GIT1, ALR2, YFL040W
	inorganic cation transmembrane transporter activity		ADY2, ALR2, YFL040W, HXT10, QCR6
	active transmembrane transporter activity		YFL040W, HXT10, QCR6, COX12, COX8

Table 9: List of genes commonly Up-regulated in wild-type during (Exp) compared to Quiescence day 7 (Q-D7) treatment.

Category	Function	Number of Genes	Example Genes
GO Biological Processes	**cytoplasmic translation**	**3328**	RPS14A,RPL2A,RPL 29,RPL15A

	ribosome biogenesis		KRR1,SPB1,RBP95, SRD1,RPS14A
	ribonucleoprotein complex biogenesis		KRR1,SPB1,RBP95, SRD1,RPS14A
	DNA integration		YCL019W,YFL002 W-A,YLR035C-A,YLR227W-B,YLR410W-B
	rRNA processing		KRR1,SPB1,RBP95, SRD1,RPS14A
	ribosomal small subunit biogenesis		KRR1,RPS14A,RPS0 B,RPS31,EMG1
GO Cellular Components	**cytosolic ribosome**	**1148**	RPS14A,GCN20,RP L2A,RPL29
	cytosolic large ribosomal subunit		RPL2A,RPL29,RPL1 5A,RPL22A,RPL10
	ribosomal subunit		RPS14A,RPL2A,RPL 29,RPL15A,RPS0B
	ribosome		RPS14A,GCN20,RP L2A,RPL29,RPL15A
GO Molecular Functions	**structural constituent of ribosome**	**842**	RPS14A,RPL2A,RPL 29,RLP24,RPL15A
	structural molecule activity		CDC10,RPS14A,AC T1,TUB2,RPL2A
	catalytic activity, acting on RNA		SPB1,YCL019W,FR S2,YFL002W-A,YLR035C-A
	nucleotidyltransfera se activity		APA1,YCL019W,YF L002W-A,YLR035C-A,YLR227W-B,
	sequence-specific mRNA binding		FRS1,SES1,YDR341 C,ILS1,GRS1,SHE3, SUP45,GUS1

Table 10: List of genes commonly Down-regulated in wild-type during (Exp) compared to Quiescence day 7 (Q-D7) treatment.

Category	Function	Number of Genes	Example Genes
GO Biological Processes	small molecule catabolic process	1687	XYL2,ECI1,CAR2, ACS1,GCV3
	monocarboxylic acid metabolic process		ISA1,IDP2,ECI1,AC S1,YAT1
	carboxylic acid metabolic process		ISA1,IDP2,ECI1,CA R2,ACS1,GCV3
	response to nutrient levels		ADY2,PAT1,PUF3, TIS11,TAG1,DCS1, ATG39
	cellular response to nutrient levels		PAT1,PUF3,TAG1, DCS1,ATG39,DHH 1
GO Cellular Components	peroxisome	338	GID7,UBI4,AYT1,P CD1,ECI1,MDH3
	microbody		GID7,UBI4,AYT1,P CD1,ECI1,MDH3
	phagophore assembly site membrane		ATG10,ATG38,AT G39,ATG9,ATG20
	phagophore assembly site		ATG10,ATG38,AT G39,ATG9,ATG20
	ubiquitin ligase complex		GID7,LUG1,UBX3, SLX5,CDC34,SWM 1
GO Molecular Functions	DNA-binding transcription factor activity	738	PPR1,SFP1,PHO2,R PN4,NRG1
	transcription regulator activity		AHC2,TEN1,PPR1, SFP1,FUN19
	DNA-binding transcription factor activity, RNA polymerase II-specific		PPR1,SFP1,PHO2,R PN4,NRG1
	transcription regulatory region nucleic acid binding		PPR1,SFP1,PHO2,R PN4,NRG1
	transcription cis-regulatory region binding		PPR1,SFP1,PHO2,R PN4,NRG1

Table 11: List of genes commonly Up-regulated in *htb-K123R*Δ during (Exp) compared to Quiescence day 7 (Q-D7) treatment.

Category	Function	Number of Genes	Example Genes
GO Cellular Components	cytosolic ribosome	**768**	RPS14A, RPL22B, GCN20, RPL2A, RPL29
	cytoplasmic translation		RPS14A, RPL22B, RPL2A, RPL29, RPL15A
	cytosolic large ribosomal subunit		RPL22B, RPL2A, RPL29, RPL15A, RPL22A
	ribosome		RPS14A, RPL22B, GCN20, RPL2A, RPL29
	ribosomal subunit		RPS14A, RPL22B, RPL2A, RPL29, RPL15A
GO Biological Processes	ribosome biogenesis	**1193**	KRR1, SPB1, RBP95, SRD1, RPS14A
	ribonucleoprotein complex biogenesis		KRR1, SPB1, RBP95, SRD1, RPS14A
	amino acid metabolic process		HIS4, LEU2, ILV6, THR4, FRS2
	ribosome assembly		RPS14A, DRS1, RLP24, SDO1, RPS0B
	small molecule biosynthetic process		HIS4, LEU2, ILV6, PGK1, ELO2
	small molecule metabolic process		APA1, HIS4, LEU2, ILV6, PGK1
	ribosomal small subunit biogenesis		KRR1, RPS14A, RPS0B, RPS31, HCR1
GO Molecular Functions	structural constituent of ribosome	**1317**	RPS14A, RPL22B, RPL2A, RPL29, RLP24
	aspartic-type endopeptidase activity		YCL019W, YFL002W-A,

			YLR035C-A, YPS3, YLR227W-B

Table 12: List of genes commonly Down-regulated in *htb-K123R*Δ during (Exp) compared to Quiescence day 7 (Q-D7) treatment.

Category	Function	Number of Genes	Example Genes
GO Biological Processes	generation of precursor metabolites and energy	**1132**	GLK1,CIT2,IGD1,HXK1,SDH2
	aerobic respiration		GLK1,CIT2,HXK1,SDH2,COX12
	energy derivation by oxidation of organic compounds		GLK1,CIT2,IGD1,HXK1,SDH2,COX12
	cellular respiration		GLK1,CIT2,HXK1,SDH2,COX12
	carbohydrate metabolic process		GLK1,CIT2,IGD1,HXK1
GO Cellular Components	mitochondrial envelope	**786**	PTC6,COX19,COX17,SDH2,COX20
	mitochondrial membrane		SDH2,DNM1,COX12,XDJ1,SHH4
	organelle envelope		PTC6,POM33,COX19,COX17,SDH2
	mitochondrial inner membrane		SDH2,COX12,SHH4,UPS1,COQ9,MSS51
	organelle inner membrane		SDH2,COX12,SHH4,UPS1,COQ9,MSS51
GO Molecular Functions	oxidoreductase activity	**478**	MXR2,JLP1,SDH2,COX12,PUT1,SHH4,

	active transmembrane transporter activity		ERS1,HXT10,COX12,COX8, YDL199C
	transmembrane transporter activity		VBA3,ADY2,ERS1,AQY3,ALR2,HXT10
	transporter activity		VBA3,ADY2,ERS1,AQY3,ALR2,HXT10

Table 13: List of genes commonly Up-regulated in *hht-K36A*Δ during (Exp) compared to Quiescence day 7 (Q-D7) treatment.

Category	Function	Number of Genes	Example Genes
GO Biological Process	ribosome biogenesis	**1616**	KRR1, SPB1, RRP43, RPL2A, RPS14A
	cytoplasmic translation		RPS14A, RPL2A, RPL29, RPL15A, RPS0B
	ribonucleoprotein complex biogenesis		KRR1, SPB1, RRP43, RPL2A, RPS14A
	rRNA processing		KRR1, SPB1, RRP43, RPL2A, RPS14A
	rRNA metabolic process		KRR1, SPB1, RRP43, RPL2A, RPS14A
	ribosomal small subunit biogenesis		KRR1, RPS14A, RPS0B, RPS31, EMG1
	ribosome assembly		RPS14A, RPL10, RPS31, RPL12B, RPS17B
GO Cellular Component	cytosolic ribosome	**1302**	RPS14A, RPL2A, RPL29, RPL15A, RPS0B
	cytosolic large ribosomal subunit		RPL2A, RPL29, RPL15A, RPL22A, RPL10
	ribosomal subunit		RPS14A, RPL2A, RPL29, RPL15A, RPS0B
	ribosome		RPS14A, RPL2A, RPL29, RPL15A, RPS0B
	ribonucleoprotein complex		KRR1, SPB1, RRP43, RPL2A, RPS14A

	preribosome		KRR1, SPB1, RPS14A, RPL2A, RPL37A
GO Molecular Function	structural constituent of ribosome	**367**	RPS14A, RPL2A, RPL29, RPL15A, RPL22A
	structural molecule activity		RPS14A, RPL2A, RPL29, RPL15A, RPL22A
	translation factor activity		HCR1, YEF3, FUN12, EFB1, RLI1

Table 14: List of genes commonly Down-regulated in *hht-K36A*Δ during (Exp) compared to Quiescence day 7 (Q-D7) treatment.

Category	Function	Number of Genes	Example Genes
GO Biological Processes	developmental process	**895**	HMLALPHA2, SPS22, RRT12, FIG2, HMRA1
	sporulation		SPS22, RRT12, PES4, SPO75, OSW2
	response to oxygen-containing compound		RIM15, GPB2, SNF3, SFA1, RGT2
	anatomical structure morphogenesis		SPS22, RRT12, FIG2, SPO75, OSW2
	sporulation resulting in formation of a cellular spore		SPO75, OSW2, ATG26, CRR1, RED1
	anatomical structure formation involved in morphogenesis		SPO75, OSW2, ATG26, CRR1, RED1
	cellular response to oxygen-containing compound		SOD1, CUP1-1, CUP1-2, TRR2, YCK1

GO Cellular Components	peroxisome	**76**	PEX5, PEX10, PEX14, PEX19, FOX2
GO Molecular Functions	DNA-binding transcription factor activity, RNA Pol II	**665**	PHO2, RPN4, LYS14, MIG1, YAP1
	ubiquitin-like protein ligase activity		UBR1, CDC34, TOM1, SKP1, SLX5
	acyltransferase activity		POT1, DGA1, ATG3, CIT3, FOX2
	ubiquitin-like protein transferase activity		UBC5, UBR1, CDC34, TOM1, SLX5
	aminoacyltransferase activity		UBC5, UBR1, CDC34, TOM1, SLX5

Table 15: List of genes commonly Up-regulated in *K123R-K36A*Δ during (Exp) compared to Quiescence day 7 (Q-D7) treatment.

Category	Function	Number of Genes	Example Genes
GO Cellular Components	cytosolic ribosome	**1353**	RPS14A, GCN20, RPL2A, RPL29, RPL15A
	cytosolic large ribosomal subunit		RPL2A, RPL29, RPL15A, RPL22A, RPL10
	ribosome		MRPL32, RPS14A, GCN20, RPL2A, RPL29
	ribosomal subunit		MRPL32, RPS14A, RPL2A, RPL29, RPL15A
	cytosolic small ribosomal subunit		RPS14A, RPS0B, RPS31, RPS28B, RPS30A
	large ribosomal subunit		MRPL32, RPL2A, RPL29, RPL15A, RPL22A
	small ribosomal subunit		RPS14A, RPS0B, RPS31, RPS28B, RPS30A
	ribonucleoprotein complex		KRR1, SPB1, MRPL32, RPS14A, SAD1

GO Biological Processes	cytoplasmic translation	**1180**	RPS14A, RPL2A, RPL29, RPL15A, RPS0B
	DNA integration		YCL019W, YFL002W-A, YLR035C-A, YLR227W-B, YLR410W-B
	ribosome biogenesis		KRR1, SPB1, RBP95, SRD1, RPS14A
	ribonucleoprotein complex biogenesis		KRR1, SPB1, RBP95, SRD1, RPS14A
GO Molecular Functions	structural constituent of ribosome	**482**	MRPL32, RPS14A, RPL2A, RPL29, RLP24
	structural molecule activity		CDC10, MRPL32, RPS14A, TUB2, RPL2A
	RNA-directed DNA polymerase activity		YCL019W, YFL002W-A, YLR035C-A, YLR227W-B, YLR410W-B
	RNA-DNA hybrid ribonuclease activity		YCL019W, YFL002W-A, YLR035C-A, YLR227W-B, YLR410W-B

Table 16: List of genes commonly Down-regulated in *K123R-K36A*Δ during (Exp) compared to Quiescence day 7 (Q-D7) treatment.

Category	Function	Number of Genes	Example Genes
GO Biological Processes	transmembrane transport	**348**	PEX34, CIT2, AGX1, UBI4, AYT1
	small molecule catabolic process		ATG22, DFP3, ADY2, FEN2, ATG15
	response to nutrient levels		PEX34, PEX13, PEX22, PEX5, PEX10
	detoxification		ATG22, DFP3, FEN2, CPR4, GIT1
	response to oxygen-		ATG10, ATG38, ATG39, ATG9, ATG20

	containing compound		
GO Cellular Component	peroxisome	**328**	PEX34, CIT2, AGX1, UBI4, AYT1
	vacuole		ATG22, DFP3, ADY2, FEN2, ATG15
	peroxisomal membrane		PEX34, PEX13, PEX22, PEX5, PEX10
	storage vacuole		ATG22, DFP3, FEN2, CPR4, GIT1
GO Molecular Function	transmembrane transporter activity	**689**	AGP1, ADY2, FEN2, PHO87, GIT1
	transporter activity		AGP1, ADY2, FEN2, PHO87, GIT1
	DNA-binding transcription factor activity		HMLALPHA2, MATALPHA2, HMRA1, GAT1, PDR8
	DNA-binding transcription factor activity		HMLALPHA2, MATALPHA2, HMRA1, GAT1, PHO4